Molecular-level ion-specific effects in aqueous salt solutions and on thermoresponsive polymers

Dissertation

by

Ellen Elisabet Bruce, M.Sc.

from Örtofta

submitted in fulfillment of the requirements
for the degree of doctor rerum naturalium (Dr. rer. nat.)

at the Department of Chemistry
of the Technical University of Darmstadt

Examiner: Prof. Dr. Nico F. A. van der Vegt
Co-examiner: Prof. Dr. Paul S. Cremer

Date of submission: March 16, 2021
Date of oral exam: April 30, 2021

Darmstadt 2021

Ellen Elisabet Bruce
Molecular-level ion-specific effects in aqueous salt solutions and on thermoresponsive polymers

Darmstadt, Technische Universität Darmstadt
Published online on TUprints in 2021
Date of submission: March 16, 2021
Date of oral exam: April 30, 2021

URN: urn:nbn:de:tuda-tuprints-197582
URL: https://tuprints.ulb.tu-darmstadt.de/id/eprint/19758

Preface

This dissertation is the result of my work as a doctoral student in the Computational Physical Chemistry research group of the Department of Chemistry at the Technical University of Darmstadt. I would like to take the opportunity to thank everyone who contributed to the success of this work.

I am grateful for the support of my supervisor Prof. Dr. Nico F. A. van der Vegt and for the freedom he has given me to pursue my own scientific work. His openness to discussions, his engagement, and particularly his passion for science have both inspired me and contributed to the success of my research.

I thank Prof. Dr. Paul S. Cremer for reviewing this thesis, for the months I spent in his research group, his interest in my work, and for challenging me with questions that pushed my research further.

I want to express my gratitude to Prof. Dr. Markus Biesalski and Prof. Dr. Wolfgang Ensinger as members of my examination board.

Many thanks to all collaborators, colleagues, students, and friends for the exciting projects we have worked on together and for the good times.

Abstract

Aqueous salt solutions are omnipresent and central to countless processes in chemical, biological and physical systems. Examples of such phenomena are protein stability, molecular self-assembly, surface effects, and membrane permeability, among others. Despite their ubiquitous importance, scientific understanding of salt effects is incomplete. One particular field of interest is the alteration of the solubility of nonpolar molecules, such as polymers, by various salt solutions.

Salt ions can be ordered according to the so-called Hofmeister series, an empirical and qualitative classification ranking the relative influence of ions on protein stability and polymer solubility. Although the concept of ion-specific effects has been known since the late 19th century, many aspects are unclear. For instance, while a general anionic Hofmeister series is established, a molecular level mechanism for a cationic Hofmeister series with polymers is missing. In addition, the impact of mixtures of salts on the polymer solubility is poorly explored.

This work addresses these knowledge gaps by combining molecular dynamics simulations with experimental data. Intriguing phase transition temperature (lower critical solution temperature, LCST) trends of the polymer, poly(*N*-isopropylacrylamide) (PNIPAM), obtained from thermodynamic measurements, are elucidated on a molecular level using computer simulations. The present work investigates the complex interplay of polymer–ion, polymer–water, ion–water, and particularly ion–counterion interactions.

It is shown that the individual consideration of anion effects provides an incomplete picture of polymer solubility. Instead, the anions' nonadditive interplay with countercations and, hence, concurrent Hofmeister effects must be considered. The LCST of PNIPAM is governed by the balance between electrostatic polymer–ion interactions, which increase the LCST, and ion hydration in the bulk solution, which decreases it. Cation–anion contact pair formation of weakly hydrated ions in the bulk causes a loss in the usually favorable electrostatic interactions for weakly hydrated anions, and, hence, leads to a LCST decrease. Strongly hydrated ions accumulate locally at the polymer surface owing to the formation of solvent shared cation–anion pairs and favorable electrostatic polymer–cation interactions. Hence, these contributions affect the behavior of the usually depleted strongly hydrated anions and increase the LCST.

Abstract

Unintuitively, mixing strongly and weakly hydrated salts does not balance both their influences, but instead leads to nonadditive ion effects and a complex concentration-dependent behavior of the LCST. In particular, it is shown that ion hydration benefits from a flexible hydration shell, a unique ability of the weakly hydrated anion. It is caused by cation partitioning from the weakly to the strongly hydrated anion, leading to an increase of the water affinity of the weakly hydrated anion and, hence, to a decrease of the LCST. At higher concentrations of the weakly hydrated salt instead, the LCST increases. Here, the polymer–anion interaction contribution dominates. This is caused by a decrease of the solubility of the weakly hydrated anion induced by the strongly hydrated salt.

The present work extends the realms of Hofmeister chemistry adding understanding of the role of cations on the solubility of polymers, both in combination with a weakly and a strongly hydrated anion. Moreover, the current Hofmeister series is updated accounting for the bifurcated behavior of weakly hydrated anions in mixed salt solutions. Contradicting earlier mechanisms, it is demonstrated that ion effects are not strictly additive but can be nonadditive. The implications of the discoveries of the present work go beyond polymer solubility and are vital for a vast number of processes in salt solutions in disciplines of chemistry and related fields.

Kurzfassung

Wässrige Salzlösungen sind allgegenwärtig und von zentraler Bedeutung für unzählige Prozesse in chemischen, biologischen und physikalischen Systemen. Beispiele für solche Phänomene sind u.a. Proteinstabilität, molekulare Selbstorganisation, Oberflächeneffekte und Membranpermeabilität. Trotz ihrer weitreichenden Bedeutung ist der wissenschaftliche Kenntnissstand zu Salzeffekten unvollständig. Von besonderem Interesse ist die Veränderung der Löslichkeit unpolarer Moleküle, wie z.B. Polymere, durch verschiedene Salzlösungen.

Salzionen können nach der sogenannten Hofmeister-Reihe geordnet werden, einer empirischen und qualitativen Klassifikation, die den relativen Einfluss von Ionen auf die Stabilität von Proteinen und die Löslichkeit von Polymeren ordnet. Obwohl das Konzept ionenspezifischer Effekte seit dem späten 19. Jahrhundert bekannt ist, sind viele Aspekte unklar. Beispielsweise existiert eine allgemeine Hofmeister-Reihe für Anionen, jedoch fehlt für eine Kationen-Hofmeister-Reihe mit Polymeren ein Wirkprinzip auf molekularer Ebene. Darüber hinaus ist der Einfluss von Salzmischungen auf die Löslichkeit von Polymeren weitgehend unerforscht.

Diese Arbeit widmet sich den obigen Wissenslücken durch die Kombination von Molekulardynamiksimulationen mit experimentellen Daten. Das ungewöhnliche Verhalten der Phasenübergangstemperatur (untere kritische Lösungstemperatur, *engl.:* lower critical solution temperature, LCST) von Poly(*N*-Isopropylacrylamide) (PNIPAM), das in thermodynamischen Messungen bestimmt wurde, wird auf molekularer Ebene mit Hilfe von Computersimulationen aufgeklärt. Die vorliegende Arbeit untersucht das komplexe Zusammenspiel von Polymer-Ionen-Wechselwirkungen, die Hydratation von Ionen und Polymeren, oberflächenähnliche Phänomene und insbesondere Ionen-Gegenionen-Wechselwirkungen.

Es wird gezeigt, dass die isolierte Betrachtung von Anioneneffekten ein unvollständiges Bild der Polymerlöslichkeit zeichnet. Stattdessen muss die nichtadditive Wechselwirkung von Anionen mit Kationen, also gleichzeitige Hofmeister-Effekte, berücksichtigt werden. Die LCST von PNIPAM hängt vom Gegenspiel von elektrostatischen Polymer-Ionen-Wechselwirkungen, die die LCST erhöhen, und Ionenhydratisierung in der Lösung, die die LCST senken, ab. Die Bildung von Kationen-Anionen-Kontaktpaaren aus schwach hydratisierten Ionen in Lösung führt zur Reduktion der sonst anziehenden

elektrostatischen Wechselwirkung schwach hydratisierter Anionen und damit zu einer Abnahme der LCST. Stark hydratisierte Ionen reichern sich lokal an der Polymeroberfläche an, was auf die Bildung von lösungsmittelgetrennten Kationen-Anionen-Paaren und bevorzugte elektrostatische Polymer-Kationen-Wechselwirkungen zurückzuführen ist. Diese Effekte beeinflussen das Verhalten der sonst abgestoßenen stark hydratisierten Anionen und steigern die LCST.

Entgegen der Intuition führt das Mischen von stark und schwach hydratisierten Salzen nicht zum Ausgleich beider Einflüsse, sondern stattdessen zu nicht-additiven Ionen-Effekten und einem komplexen konzentrationsabhängigen Verhalten der LCST. Insbesondere wird gezeigt, dass Ionenhydratation von einer flexiblen Hydratationshülle begünstigt wird, eine einzigartige Fähigkeit des schwach hydratisierten Anions. Sie wird durch Kationenanreicherung weg vom schwach hin zum stark hydratisierten Anion verursacht, was zu einer Erhöhung der Wasseraffinität des schwach hydratisierten Anions und damit zu einer Senkung der LCST führt. Bei höheren Konzentrationen des schwach hydratisierten Salzes steigt stattdessen die LCST an. Hier dominiert der Beitrag der Polymer-Anion-Wechselwirkung. Dies wird durch eine durch das stark hydratisierte Salz induzierte Abnahme der Löslichkeit des schwach hydratisierten Anions verursacht.

Die vorliegende Arbeit erweitert die Hofmeister-Chemie und trägt zum Verständnis der Rolle von Kationen hinsichtlich der Löslichkeit Polymere bei, sowohl in Kombination mit einem schwach als auch mit einem stark hydratisierten Anion. Darüber hinaus wird die aktuelle Hofmeister-Reihe unter Berücksichtigung des zweifaltigen Verhaltens schwach hydratisierter Anionen in gemischten Salzlösungen aktualisiert. Entgegen zuvor angenommener Mechanismen wird gezeigt, dass Ionen-Effekte nicht streng additiv sind, sondern nicht-additiv sein können. Die Implikationen der Entdeckungen der vorliegenden Arbeit gehen über die Polymerlöslichkeit hinaus und sind für eine Vielzahl von Prozessen in Salzlösungen in Disziplinen der Chemie und verwandten Gebieten von entscheidender Bedeutung.

Table of contents

Nomenclature

Abbreviations

2SIP	Solvent-separated ion pair
AMBER	Assisted model building with energy refinement
C	Collapsed state
CIP	Contact ion pair
DRS	Dielectric relaxation spectroscopy
E	Extended state
ECC	Electronic continuum correction
ELP	Elastin-like polypeptide
KB	Kirkwood–Buff
KBI	Kirkwood–Buff integral
IR	Infrared
LCST	Lower critical solution temperature
LJ	Lennard–Jones
LMWA	Law of matching water affinities
MD	Molecular dynamics
μVT	Grand canonical ensemble
NMA	*N*-methylacetamide
NMR	Nuclear magnetic resonance
NPT	Isothermal–isobaric ensemble
NVE	Microcanonical ensemble
NVT	Canonical ensemble
OS	Oscillator strength
PBC	Periodic boundary conditions
PDEA	Poly(*N*,*N*-diethylacrylamide)
PDMA	Poly(*N*,*N*-dimethylacrylamide)
PEG	Polyethylene glycol
PME	Particle mesh Ewald
PMF	Potential of mean force
PNIPAM	Poly(*N*-isopropylacrylamide)
PDI	Polydispersity
RDF	Radial distribution function

RESP	Restrained electrostatic potential
SF	Sum frequency
SFG	Sum frequency generation
SIP	Solvent-shared ion pair
SPM	Solute partitioning model
SPC/E	Extended simple point-charge
TMAO	Trimethylamine *N*-oxide
UCST	Upper critical solution temperature
VIS	Visible
VSFS	Vibrational sum frequency spectroscopy
W1	First solvation-shell water
W2	Second solvation-shell water

Indices and notations

$\bigcirc^{0}$	Bulk
$\bigcirc^{E\rightarrow C}$	Transition from extended to collapsed polymer state
$\bigcirc^{N}$	Number of particles
$\bigcirc^{res}$	Residual
$\bigcirc_{\pm}$	Salt
$\bigcirc_{\infty}$	Infinitely diluted solution
$\bigcirc_{0}$	Equilibrium, pure water
$\bigcirc_{1}$	Polymer, solvent/water
$\bigcirc_{2}$	Polymer, solvent/water
$\bigcirc_{3}$	Ions
$\bigcirc_{a}$	Attractive
$\bigcirc_{an}$	Anion
$\bigcirc_{b}$	Bonded
$\bigcirc_{BB}$	Backbone
$\bigcirc_{bend}$	Bending
$\bigcirc_{bulk}$	Bulk
$\bigcirc_{c}$	Contour, cosolute, critical solution
$\bigcirc_{C}$	Collapsed polymer conformation state
$\bigcirc_{cat}$	Cation
$\bigcirc_{cav}$	Cavity
$\bigcirc_{conf}$	Conformational
$\bigcirc_{DOF}$	Degrees of freedom
$\bigcirc_{E}$	Extended polymer conformation state

$\bigcirc_{\mathrm{eff}}$	Effective
$\bigcirc_{\mathrm{el}}$	Electrostatic
$\bigcirc_{\mathrm{GDS}}$	Gibs dividing surface
$\bigcirc_{\mathrm{id}}$	Ideal solution
$\bigcirc_{i}$	Species i
$\bigcirc_{ij}$	Atom/particle i and j
$\bigcirc_{ijk}$	Atom/particle i, j and k
$\bigcirc_{ijkl}$	Atom/particle i, j, k and l
$\bigcirc_{\mathrm{in}}$	Inner limit
$\bigcirc_{\mathrm{intra}}$	Intramolecular
$\bigcirc_{\mathrm{ion}}$	Ion property
$\bigcirc_{j}$	Species j
$\bigcirc_{\mathrm{l}}$	Liquid
$\bigcirc_{\mathrm{m}}$	Mixing
$\bigcirc_{\mathrm{n}}$	N-th resonant mode
$\bigcirc_{\mathrm{nb}}$	Nonbonded
$\bigcirc_{\mathrm{NR}}$	Non-resonant
$\bigcirc_{\mathrm{out}}$	Outer limit
$\bigcirc_{\mathrm{pv}}$	Polymer–solvent
$\bigcirc_{\mathrm{r}}$	Repulsive
$\bigcirc_{\mathrm{R}}$	Resonant
$\bigcirc_{\mathrm{rotation}}$	Rotation
$\bigcirc_{\mathrm{s}}$	Salt, solvation
$\bigcirc_{\mathrm{S}}$	Solute
$\bigcirc_{\mathrm{salt}}$	Salt
$\bigcirc_{\mathrm{ss}}$	Salt–salt
$\bigcirc_{\mathrm{stretch}}$	Stretching
$\bigcirc_{\mathrm{T}}$	Trimethylamine N-oxide (TMAO)
$\bigcirc_{\mathrm{tot}}$	Total terms
$\bigcirc_{\mathrm{TW}}$	TMAO–water
$\bigcirc_{\mathrm{U}}$	Property of urea
$\bigcirc_{\mathrm{uv}}$	Solute–solvent
$\bigcirc_{\mathrm{UW}}$	Urea–water
$\bigcirc_{\mathrm{v}}$	Vapor
$\bigcirc_{\mathrm{vdW}}$	van der Waals
$\bigcirc_{\mathrm{vv}}$	Solvent–solvent
$\bigcirc_{\mathrm{w}}$	Water
$\bigcirc_{\mathrm{ws}}$	Water–salt
$\bigcirc_{\mathrm{x,y,z}}$	Direction x, y, z

Latin symbols

a	Activity
A	Area, oscillator strength
$\boldsymbol{a}$	Acceleration vector
$B_{\max}$	Maximum increase in lower critical solution temperature
c	Concentration
E	Energy
F	Force
$\boldsymbol{F}$	Force vector
g	Radial distribution function
G	Gibbs free energy, Kirkwood-Buff integral
H	Enthalpy, hamiltonian
I	Intensity
K	Equilibrium constant, kinetic energy
k^{θ}	Force constant for angles
k^{r}	Force constant for torsions
k^{ϕ}	Force constant for angles
$\mathrm{k_B}$	Boltzmann constant
K_{D}	Dissociation constant
L	Length
m	Mass, molality
M	Molar mass, number of integration steps
$\overline{M}_{\mathrm{n}}$	Number-average molar mass
$\overline{M}_{\mathrm{w}}$	Weight-average molar mass
n	Local number of particles/molecules, moles
N	Number of particles/pairs/blocks
ΔN	Affinity, excess coordination number, excess ion pairing
$\boldsymbol{p}$	Vector of linear momentum
P	Pressure, probability
$\boldsymbol{P}$	Nonlinear polarization vector
q	Ionic charge
r	Distance, coordinate/position
$\boldsymbol{r}$	Position vector
R	Gas constant
R_{g}	Radius of gyration
S	Entropy
t	Time
T	Temperature
T_{c}	Lower critical solution temperature
T_{EC}	Transition temperature from extended to collapsed polymer state

u	Direct interactions between solutes
U	Force field potential
v	Velocity
$\boldsymbol{v}$	Velocity vector
V	Volume, pair potential, potential energy
w	Pairwise potential of mean force
Δw	Solvent-mediated contribution to w
W	Potential of mean force
x	Molar fraction
y	Mean activity coefficient
z	Distance/position in z-direction

Greek symbols

γ	Activity coefficient, surface tension
ε	Dispersion interaction strength
ε_0	Vacuum electric permittivity
ε_{el}	High-frequency dielectric permittivity
θ	Angle
κ	Force constant
κ_T	Compressibility
μ	Chemical potential
μ^*	Excess chemical potential
ν	Number of components, stoichiometric coefficient,
ω	Frequency, resonance frequency
ϕ	Phase angle, potential energy, osmotic coefficient, volume fraction
ρ	Number density
σ	Lennard–Jones size parameter, sample standard deviation
τ	Coupling time
$\chi^{(2)}$	Second-order nonlinear Susceptibility
Δ	Change, difference
Γ	Peak width, preferential binding coefficient, preferential adsorption coefficient, surface access
Π	Osmotic pressure
Ξ	Inner virial

Chapter 1

Introduction

Aqueous salt solutions (i.e., electrolyte solutions) are ubiquitous. They are of universal importance in chemistry, biology and life science, where they are significant to myriad chemical, biological and physical processes. Among others, aqueous solvated ions are found in solutions in living cells, in body fluids, in brine solutions of ocean waters, in aerosol droplets in the atmosphere, in food and drinks, in pharmaceuticals, in solutions in electrochemical setups, and in hydrogels and other soft functional materials. Salts affect properties of bulk water and nonelectrolytes, such as polymers or other macromolecules dissolved in the solutions. How salts modulate properties of polymers, such as the solubility, has been the focus of an intensively studied research field over the last decades.

1.1 Motivation

An aqueous salt solution is one of the simplest systems one can imagine and, yet, essential knowledge is missing. With the introduction of an interface, e.g., a polymer in aqueous solution, the system's complexity increases drastically because a vast number of crucial chemical interactions take place at these surfaces. Therefore, it is important to understand ion effects in both bulk solutions and in the vicinity of hydrophobic surfaces, such as air–water or polymer–water interfaces. For polymer solutions, this task is challenging because the addition of different types and concentrations of ions leads to direct or indirect ion-specific effects, where all solution components are involved. Specifically, polymer–ion, ion–ion, ion–water, polymer–water, and polymer–polymer interactions need to be understood for a complete understanding of polymer solubility. These interactions will affect surface-related phenomena, ion pair formation, hydration of ions, hydration of the polymer, intra- and inter-chain forces, and the hydrogen bonding network.

One particular class of polymers, namely thermoresponsive polymers, exhibits a solubility change and undergo a phase transition when exposed to a temperature shift. This

corresponds to a conformational change of the polymer chain. Depending on the proportions of the components of a polymer–solvent mixture, the solubility change happens at a certain temperature called phase transition temperature. The critical temperature below which a complete miscibility of the components is observed, independent of the proportions, is referred to as the lower critical solution temperature (LCST). It is well-known that specific ions cause conformational changes of water-soluble thermoresponsive polymers since they affect the phase transition temperature. However, the chemistry behind the addition of salt to aqueous solutions containing thermoresponsive polymers is far from simple. How does a specific salt affect the polymer conformation and thereby the polymer solubility? The answer is a complex interplay of various ion-specific effects in aqueous solutions. However, certain trends among ions are observed. How different salts affect the solubility of macromolecules, such as polymers and proteins and other properties, have been ranked according to the so-called Hofmeister series. Until today, neither the entire underlying mechanism of the Hofmeister series, nor the effects of salts are understood completely.

Hofmeister series. The Hofmeister series ranks ions systematically according to their ability to affect polymer solubility and protein stability (Fig. 1.1).[1–3] Ions on the left-hand side are classified as strongly hydrated, while ions on the right-hand side are denoted weakly hydrated. The boundary between the two classes is typically drawn at the chloride ion. Strongly hydrated anions decrease polymer solubility, i.e., they decrease the LCST, a process called salting out.[4] They interact repulsively with and are depleted from the polymer–water interface. The addition of these ions to an aqueous polymer solution leads to a strengthening of the hydrophobic effect, i.e., a force leading to the minimization of the solvent-exposed surface. Weakly hydrated anions have a preference for nonpolar environments instead, such as air–water[5] and polymer–water[4,6,7] interfaces. The addition of these ions to an aqueous polymer solution leads to a weakening of the hydrophobic effect. This causes a moderate increase of the polymer solubility, i.e., a moderate increase of the LCST, a process called salting in.[4] The terminology of salting out and salting in originates from the phenomenologically observed clouding during precipitation of macromolecules. A corresponding universal description of the cationic Hofmeiser series is not available today because a thorough understanding of cation-specific effects is missing. The salting-out and salting-in ranking of cations in Fig. 1.1 applies to proteins and should not be seen as a general classification. However, Fig. 1.1 shows that the salting-out and salting-in behavior of cations relative to the hydration capacity is opposite compared to anions.

How ions that follow the Hofmeister series change various physical behaviors is usually referred to as the Hofmeister effect. One of the most commonly studied Hofmeister effects is thermoresponsive polymer solubility. However, the Hofmeister series also ranks other physical properties such as surface tension, catalysis of chemical reactions,

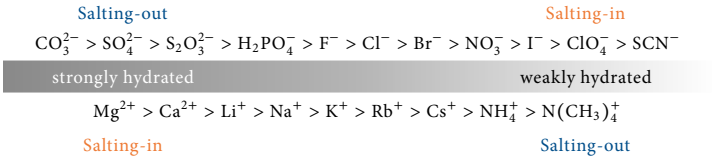

Fig. 1.1 The anionic (top) and cationic (bottom) Hofmeister series, ranking ions from strongly to weakly hydrated and the corresponding salting-out and salting-in abilities.

solubility of gasses and of colloids, equilibrium constants, cavity formation and protein denaturation.[8,9] Therefore, an understanding of the Hofmeister series does not only help to understand ion effects on the solubility of polymers and other macromolecules, but also to understand ion effects on other interfacial phenomena and on bulk solution properties. In addition, the Hofmeister series has been observed for bulk properties in nonaqeuous solutions.[10]

Scientific questions. For certain well-studied systems, the effect of anions on the direct and indirect contributions to the polymer solubility is known.[4,7,9,11–21] However, two fields that are insufficiently explored are the role of cations and the role of a second salt in polymer solubility. Extending the knowledge of ion-specific effects to cations is important since biological systems naturally contain cations, which play key roles in such systems. For instance, sodium and potassium ions are vital for the regulation of (bio)macromolecular processes. Understanding the role of cations would allow for explaining, and even tuning, biological phenomena. For long, cation and anion effects have been assumed to be independent and additive, due to earlier studies[22,23] of thermodynamic bulk solution properties. This has been followed up by other studies[24–26] that applied the idea to partitioning of ions to air–water interfaces and protein–water interfaces. However, it is unclear whether polymer solubility is related to the sum of cationic and anionic effects (additive behavior), or if the behavior of an ion depends on the type of counterion (nonadditive behavior). This raises several specific questions.

1. What role do cations play for the phase transition temperature of polymers?
2. How dominant are such cation effects?
3. Does the type of anion influence the cation effect and vice versa?
4. Are cation–anion combinations additive or nonadditive?

Extending the understanding of ion-specific effects to mixed electrolyte solutions is important since, naturally, multiple ions are present in biological systems. Hofmeister effects in systems comprising a mixture of different ions must be investigated in order to understand this ion specificity. It is especially intriguing to explore if mixed salt

effects are additive or nonadditive, i.e., whether the sum of the effects from separate salts solutions, e.g., on the LCST behavior, is similar to the effect of the mixture (additive behavior), or if it differs (nonadditive behavior). Hence, the interplay between multiple ions must be investigated, which raises the following questions:

5. Are ion effects in aqueous electrolyte mixtures additive or nonadditive?
6. How does this impact bulk thermodynamic properties of mixed electrolyte solutions?
7. Do the ion effects lead to an additivity or nonadditivity of phase transition temperature behaviors?
8. Additionally, can the knowledge of salt mixtures be transferred to other complex mixtures such as osmolyte (organic compounds of low-molecular weight) mixtures?

Anion effects are universal and chemistry independent, i.e., apply to different types of polymers, and uncharged or charged systems. Systems of interest do not only contain mixtures of salts, they can also contain mixtures of polymers. Further, until today, studies concerning ion-specific effects have mainly focused on structural properties. The Hofmeister effects are heretofore unexplored in terms of dynamic properties. In general, ion effects on polymer solubility have been investigated in bulk solutions, but not in confined spaces. All these observations raise the following additional questions.

9. Are cation and mixed salt effects general in a similar way to anion effects?
10. What happens with observed ion effects when the polymer solution consist of a mixture of polymers?
11. Is the Hofmeister ordering also observed for dynamic properties?
12. What happens with ion effects in confined environments?

An understanding of these questions will bring physical chemistry even closer to biochemistry . However, a combined theoretical and experimental effort is needed. Here, the ability of computer simulations to examine systems of interest on a molecular level plays a crucial role. A key point for computer simulations are appropriate models (i.e., force fields). For the investigation of ion-specific effects, all-atom force fields are needed. In particular, nonpolariazble force fields are well-suited because of their low computational cost and their comparatively simple development compared to polarizable force fields. However, nonpolarizable force fields are usually suffering from artifacts such as too strong ion pairing, which raises the following question:

13. How can polarizable effects be counted for, especially for multivalent ions, in a smart way in nonpolarizable force fields?

Applications. Understanding the ion-specific effects in polymer solutions has become of interest across many fields concerned with such systems. Some examples are smart polymer materials, chemical sensors, chemo-mechanical actuators, biochemical processes in the living cell, controlled drug delivery and bioseparation. This has lead to major advances in polymer applications used in both specialized fields and everyday products. For example, the thermoresponsive polymers possess a number of properties well-suited for use in a new generation of analytical and sensory devices with improved performance over existing products. Especially the ion-specific conformational change occurring at the phase transition temperature, can be utilized to functionalize inner walls of nanopores and thereby control the pore diameter in an ion-specific manner. Among others, this is useful for medical diagnostics (e.g., measurement of body fluids and for people with diabetes), environmental analytics (e.g., measurement of drink and ground water), and process sensors (e.g., within pharmaceutical and food industry).

1.2 State of the art

For as long as 130 years, studies have shown that ion effects are specific. Ion effects are important for a vast range of biological and chemical phenomena and physical properties such as polymer collapse,[4,11,27] protein stability,[1,2,28–31] protein–protein interactions,[30,32,33] protein crystallization,[34,35] molecular self-assembly,[36–39] colloidal stability,[40] surface effects,[41–43] hydrophobic interactions,[44] enzyme activity,[34,45–49] DNA–protein interactions,[34] membrane permeability,[50] ion-channel function,[34] bubble coalescence,[51–53] water structure[54] and bacterial growth.[55,56] Explanations of these phenomena and how ions influence them go beyond classical theories for electrolyte solutions.[57] Instead, the concept of Hofmeister effects is needed.

History of Hofmeister effects. Hofmeister effects have a long history in the literature. The following summary of important publications on Hofmeister effects in the context of salts' influence on polymer solubility takes inspiration from impactful review articles in the field.[13,17] The idea of ion-specific effects goes back to the late 1800s when Hofmeister discovered that the ability of salts to precipitate egg white proteins from aqueous solutions could be ordered.[1] His rankings of individual anions and cations have later been referred to as the anionic and cationic Hofmeister series as described above. The series have been broadened beyond the ranking of the precipitation ability of proteins and are still relevant today, even if Hofmeister was limited in his choice of proteins and salts. The first findings were directly followed up and extended to additional proteins and colloidal particles.[2] The ordering of the ions were also related to their hydration strength.[2] Back then, this was referred to as the "water-absorbing effects of salts".[2] The

devised ideas were based on the theory by Arrhenius and Ostwald about electrolytic dissociation.[17,20]

For the following decades, the concept of the change of bulk water properties being crucial for salt effects on nonelectrolytes, e.g., polymers and proteins, remained. Presumably, this originated from researchers being limited to bulk solution studies. Some of the studies conclusive for the bulk water idea are briefly presented here. Jones and Dole formulated a model describing the salt concentration dependence of the viscosity of aqueous salt solutions.[58] Cox and Wolfenden expanded the theory by emphasizing that the ion-specificity (expressed by the Jones–Dole viscosity coefficient) and the temperature coefficient of an ion's electrical mobility are correlated.[59] This mobility was further correlated with the water structure of ions' hydration shells, i.e., their degree of ion hydration.[59] Small ions with strong hydration strength have the ability to increase the water viscosity. Large ions with weaker hydration strength have the ability to decrease the water viscosity. Gurney followed up and classified ions as either capable of ordering or disordering water molecules.[60] All these studies in the 1930s to 1950s lead to a theory referring to ions as "water structure makers" or "water structure breakers".[59–61] The terms correspond to how ions modify the hydrogen bonding network of the surrounding water. The terms kosmotropes and chaotropes were introduced, too.[24,62] Initially, they were used to characterize ions depending on their effect on biomolecules,[24,62] but came to be employed to provide information about the ability of ions to affect the hydrogen bonding network, and were later used as synonyms for "water structure maker" and "water structure breaker".[63] Kosmotropes increase structuring of adjacent water molecules and stabilize proteins and other macromolecules.[64–66] Chaotropes instead decrease the water structure, and destabilize proteins and other macromolecules.[64–66] These terms lead to a focus on ions' ability to affect the bulk water structure, instead of how they affect the nonelectrolyte. For many decades, the prevailing ideas were that nonelectrolytes were indirectly affected by salts through bulk water properties[24,59–62] as illustrated in Fig. 1.2a.

From the late 1950s to the early 1980s the interest in the Hofmeister series was renewed. The focus shifted to investigations of interactions between ions and surfaces of proteins. Typically, these interactions were examined by using small model systems (e.g., *N*-methylacetamide (NMA)) and thermodynamic techniques (e.g., calorimetry and viscosity measurements).[67,68] Investigations including solubility studies of larger systems (e.g., polyglycine oligomers[69–71] and proteins[72]) and chromatography studies of model polyacrylamide–water interfaces[73] followed after. The outcome from these decades, dominated by the thermodynamic measurements, was that weakly hydrated anions (e.g., SCN^- and I^-) and strongly hydrated cations (e.g., Mg^{2+} and Li^+) interact with (macro)molecules.[67–73] The preferential interaction site was the peptide backbone. However, no interactions were observed for strongly hydrated anions (e.g., SO_4^{2-} and F^-) and weakly hydrated cations (e.g., NH_4^+ and Cs^+).[67–73] Except for some initial tries,[24,34]

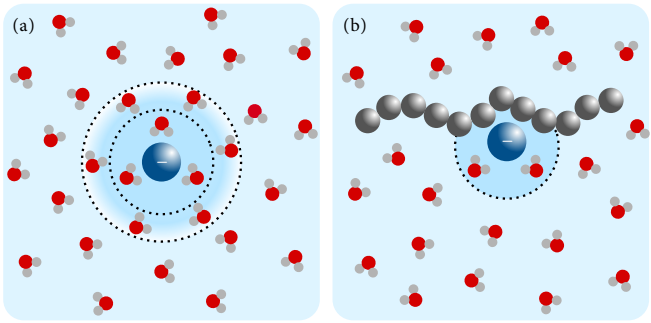

Fig. 1.2 (a) The concept of "water structure makers" and "water structure breakers" implies that water molecules beyond an ion's first hydration shell are organized. (b) Direct polymer–ion interactions and random organized water molecules in the bulk solution. Blue represents anions, red and white represent water molecules, and the chain of gray spheres represents the polymer. Ion hydration shells are depicted with black dashed circles.

spectroscopy techniques were not exploited yet, owing to their immaturity. This made atomistic level investigations of (macro)molecules–ion interactions and corresponding ion-specific effects difficult. Therefore, the attention to "Hofmeister effects" cooled off for the following two decades.

First in the beginning of the 2000s, the attention resurfaced, mainly owing to a Hofmeister conference (including an associated published special issue[74]). Hofmeister's ideas also became more accessible to the whole community, since the issue also contained English translations of the above two original papers from Hofmeister.[3] New experimental techniques (e.g., sensitive spectroscopy techniques) and new computational methods due to more powerful computers now allowed for re-examination of the underlying source for the Hofmeister effects. During the succeeding years the amount of studies dealing with Hofmeister effects exploded,[15,17,26,29,75–84] which is known as the "Renaissance for Hofmeister".[85] The idea of explaining the Hofmeister ordering by ions as structure makers and structure breakers was now critically challenged.[86–97] The main reasons were that i) evidence speaking against the ability of ions to affect long-range bulk water structure was found,[86,98] ii) it was questioned if the effect of ions on proteins and other nonelectrolytes could actually be investigated without looking at the nonelectrolyte itself,[17] and iii) cations' opposite behavior (i.e., strongly hydrated cations cause salting-in and weakly hydrated cations cause salting-out) compared to anions implies that the idea about water structure breakers and makers cannot explain polymer solubilities. Further, the preferred classification of ions as strongly or weakly hydrated is a consequence of distancing oneself from the concepts of kosmotropes and chaotropes. Multiple researchers have contributed to the disproval of the hydration

behavior of ions in bulk solutions as an explanation for the Hofmeister ordering and to discarding the structure breaker and maker terminology by investigating a large variety of different ions.[86–97] Using spectroscopic measurements and investigating rotational dynamics of water molecules, Bakker et al. showed that there is no influence of ions on the hydrogen bonding network outside the first hydration shell.[86–89] Spectroscopic measurements, in combination with computer simulations, were also used by Saykally et al. to demonstrate that the perturbation observed in OH vibrational spectra of aqueous salt solutions originates from the electric field of the ions solely on the closest water molecules.[95] That water molecules within the first hydration shell are perturbed and that no significant perturbation is observed for the ones outside, was also demonstrated by neutron diffraction measurements conducted by Soper et. al.[96,97] Simultaneously, thermodynamic analysis and pressure perturbation calorimetry was used by Pielak et al. to show that there is no correlation between the effect of salts (and solutes such as sugars, trimethylamine N-oxide (TMAO) and urea) on the water structure and on protein stability.[90] In addition, a modified theory taking the dispersion interactions into account (model is discussed below) was introduced by Ninham et al to study ions-specific interactions with charged particles and other ion-specific phenomena.[91–94] This also contributed to the disproval of ions' long-range effect on bulk water.

An alternative explanation was developed and the idea of specific ion interactions with surfaces was established.[99] The shift of attention to interfaces, in particular to air–water interfaces and macromolecule–water interfaces (e.g., polymers, proteins and lipids), originates from key contributions from multiple researchers.[4–6,25,26,42,100–113] Molecular dynamics (MD) simulations, performed by Jungwirth, Tobias et al., showed a preferred absorption of weakly hydrated halide ions at the air–water interface.[5,100–103] These findings were proved by Hemminger et al. using spectroscopy.[104] In agreement with the two studies, by applying a salt ion-partitioning model (model is discussed below), Pegram and Record showed a higher tendency for weakly hydrated anions to accumulate at interfaces such as air–water and protein–water interfaces.[25,26,113] The weakly hydrated anion propensity for air–water interfaces has also been confirmed by others.[42,105,106] Jungwirth et al. demonstrated interactions between ions and protein–water interfaces, especially with charged and polar groups, by means of MD simulations.[107–109] Just before that, Cremer et al. showed that ions affect water molecules in the hydration shell of macromolecules at an ion–water–macromolecule interface according to the Hofmeister series using thermodynamic and spectroscopic techniques (model is discussed below).[4,6,12] A correlation between the size of an ion and anion effects on monolayers of lipids at the air–water interface was found by Leontidis et al. using spectroscopy, and theoretical modeling.[110–112] Thereby, thermodynamic, spectroscopic and molecular simulation techniques have proven that the underlying explanation for the Hofmeister series originates from ion interactions as illustrated in Fig. 1.2b. These are, interactions of ions and ion pairs with specific molecular groups of the backbone and side chains of nonelectrolytes,

such as polymers and proteins, and with their hydration shell.[9,13] The complete change of the view of the crucial mechanism for the Hofmeister effects is remarkable, but can be explained with the accessibility of developed techniques. However, this does not imply that ion interactions with water molecules are irrelevant.

In recent years, interactions between all components in the examined solutions, i.e., salts (cations and anions), water and nonelectrolytes (charged and uncharged) have been recognized to contribute to the Hofmeister effects.[17,21,114] The Hofmeister community has therefore started to explore the following: The cationic Hofmeister series,[43,75,78,84,115–118] combined anionic and cationic Hofmeister effects,[19,119–121] and a phenomenon called reversed (or inverse) Hofmeister series.[20,21,43,78,118,122–127]

The vast number of publications concerning Hofmeister effects and ion-specific effects every year signifies the substantial research effort within the field. The interested reader can refer to summaries and reviews for more information.[13,17,21,57,74,103,107,114,128–132] Further, Hofmeister effects have been investigated within the supramolecular community,[133–135] which is not covered in this work. Below follows a description of Hofmeister effects and some examples of characteristic ion interactions for anions and cations.

Anionic Hofmeister effects and anion interactions. So far, studies concerning the influence of salts on polymer solubilities have mainly focused on anions, while cations have usually only been assigned a charge balancing role in the solution. This has lead to an improved understanding of anionic Hofmeister effects and how they tune physical behavior in aqueous solutions. The focus on anions has many different reasons: i) biomacromolecules with positively charged groups are typical targets for Hofmeister studies, i.e., studies between these groups and anions,[20,21] ii) easier access to weakly hydrated inorganic anions has led studies of direct interactions between anions and macromolecules,[20,21] and iii) the larger size of anions and, hence, their weaker hydration shell stimulated studies of noncovalent interactions with macromolecules.[20]

Two mechanisms are considered Hofmeister effects that explain the two phenomena: salting-out and salting-in that take place when salt is added to aqueous solutions. First, the so-called excluded-volume mechanism leads to salting-out of nonelectrolytes.[136] A complete picture on the molecular level is still missing. However, it is understood that strongly hydrated anions bind water molecules and the nonelectrolyte is pushed out of the solution owing to a lack of water molecules that can solvate the nonelectrolyte.[21] Second, direct binding between ions and nonelectrolytes, when replacing water molecules at the surface, leads to salting-in of the latter.[21] A third mechanism, the reverse (or inverse) Hofmeister effect, exists. Compared to the traditional Hofmeister effects mentioned above, the precise mechanism of the reverse Hofmeister effect is not well understood today.[20,21] However, it has been proposed that the effect is caused by ion pairing with charged groups of proteins (or other molecules) leading to charge neutralization.[20] Ions

are commonly not fully hydrated and do not compose a statistical mixture.[126,137] Instead, ion pairing and ion clustering are usual phenomena in aqueous solutions. Owing to ion pairing, weakly hydrated anions can cause a reduction of the net charge of the solute and, thereby, aggregation and precipitation instead of, as expected, an increase of the solubility.[20,21] Furthermore, strongly hydrated anions that are usually depleted from macromolecules can lead to salting-in behavior through the interaction with the charged groups.[138] It is important to point out that this effect caused by Coulombic interactions is different from both the excluded-volume effect (leading to salting-out), and from ion binding with nonpolar groups (leading to salting-in). Additionally, a problem arises regarding the nomenclature of salting-out and salting-in, since some salts can be both.[21] The concept of reverse Hofmeister effects contributed to discarding the structure breaker and maker terminology, since the same ion can lead to both a reverse and a direct Hofmeister effect, but cannot be both a water structure maker and breaker.[20]

To develop an understanding of the preferential interaction (or exclusion) of anions with nonelectrolytes, the following systems have been investigated: Small organic molecules,[15,139] amino acids,[79] model amides,[15,81] peptides,[138,140] model polypeptide system,[6,82] proteins,[109,141] and polymers.[4,7,15,16] Consensus has been formed regarding anion interactions.[13] Weakly hydrated anions (e.g., SCN^- and I^-) preferentially bind to (bio)polymers. Strongly hydrated anions (e.g., SO_4^{2-}, F^- and Cl^-) do not bind preferentially. The interaction sites on the (bio)polymer are the nitrogen of the polar amide moieties (e.g., amide moieties on side chains or along backbones) and nonpolar CH groups (e.g., alpha-carbons on the backbones).[4,6,7,16,82,141] This has been demonstrated for poly(*N*-isopropylacrylamide) (PNIPAM),[4,7,16] poly(*N,N*-diethylacrylamide (PDEA)[7] and elastin-like polypeptides (ELPs),[6,82,141] using MD simulations,[82] phase transition temperature,[4,6,7,82] nuclear magnetic resonance (NMR) spectroscopy,[7,82] and other spectroscopic measurements.[7,16,141] A comparison of a polymer without an amide hydrogen (i.e., PDEA) and polymers with (i.e., PNIPAM and ELP) demonstrated that the NH site is not necessary for anion binding.[7,16] Investigations of smaller molecules, i.e., NMA and *t*-butyl alcohol, by means of MD simulations and spectroscopic measurements, respectively, have pointed out the hydrophobic methyl groups as interaction sites for weakly hydrated anions but not for strongly hydrated anions.[81,139] Indeed, the chemical environment of amide moieties has an influence on the binding affinity of anions and should be taken into account.[15] Additionally, predictions of ion interactions with proteins have been made since ELP is seen as a model for protein[6] and NMA as a model for peptide bonds.[70,81] Interactions with charged groups have also been investigated.[79,109,138] Strongly hydrated anions (e.g., SO_4^{2-}, F^- and Cl^-) interact with positively charged groups, while an accumulation of weakly hydrated anions (e.g., SCN^- and I^-) is observed close to nonpolar groups.[79,109,138] This is a reverse behavior compared to the uncharged nonelectrolytes presented above showing a repulsion of strongly

hydrated anions. This has been shown for lysozyme[109] and for basic amino acids,[79] both by means of MD simulations and for an uncapped triglycine by performing MD simulations and NMR measurements.[138] The uncapped triglycine was used as a model system protein and, thus, the behavior is expected to be the same for positively charged amino acids.

Cationic Hofmeister effects and cation interactions. Salt effects on nonelectrolytes, e.g., causing changes in the polymer solubility, are a cumulative result of both anions and cations. This means that i) anion effects are specific for one cation, and ii) different cation must be examined for a full picture of Hoffmeister effects. Although cations are important, the difficulties in observing cation-specific effects presumably explain why they have been studied to a lesser extent than anions. For instance, the influence of cations on thermodynamic properties is weaker than for anions.[115] Further, the nonelectrolytes typically used when investigating cation effects are proteins, and interactions between cations and peptide backbones are interfered by side chain and secondary structure effects.[73,142,143] Therefore, a picture as general as for anions does not exist, yet. That strongly hydrated cations lead to a salting-in behavior and weakly hydrated cations to a salting-out behavior, i.e., opposite compared to anions (Fig. 1.1), originates from considerably different binding sites for anions and cations.[118] Cations interact with polar groups and charges on proteins.[118] Exact interactions with the protein depend on the specific ion and on the charge distribution on the protein.[115] Cations interact favorably with negatively charged carboxylate moieties.[75–78,115,144–146] This has been observed experimentally[76,77,115,146] and with MD simulations[75,78,144–146] by investigating small carboxylate ions,[78,144,146] amide acids containing a carboxylate group in the side chain,[76,77] ELP consisting of amino acids with carboxylate groups,[115] or protein surfaces.[75] The experimental techniques were phase transition temperature,[115] spectroscopic,[76,77] and conductivity measurements.[76] Additionally, the backbone plays a smaller role, but for the backbone the amide carbonyl oxygen stands for the ion specificity.[75] Uncharged systems have been investigated as well, but to a smaller extent than for anions. As for the anions, the driving force for uncharged and charged macromolecules is very different. The cation effect is weaker for uncharged systems. NMA[67,68,81,147] and other amides[147] have also been used as models for cations. Alkali and alkaline earth metal ions exhibit an affinity for the amide carbonyl group (amide carbonyl oxygen).[67,68,81,147] This has been shown by using thermodynamic techniques,[67,68] spectroscopy,[147] and MD simulations.[81] However, spectroscopy studies of butyramide show that only divalent and not monovalent cations bind to the amide carbonyl oxygen.[84] Larger uncharged nonelectrolytes have not been used for cation interaction investigations to the same extent as protein (or as for the anions). However, the same behavior as for NMA (cation interaction with carbonyl oxygen) has been observed with peptides[148] and PNIPAM when using MD simulations.[149] More studies, both experiments and simulations, are needed for a clearer picture of cation interactions and their effect on macromolecule

solubility. Especially, contradictions about the ion interaction of sodium and potassium ions with the amide carbonyl oxygen, both if there is a favorable interaction at all and how strong it is, must be resolved.[15,81,82,84,148,149]

Anion versus cation interactions and their relative strength. A description of the interaction strength and preferential interaction sites of cation and anions with macromolecules can be found in the literature.[118] Here, a brief summary of the aforementioned ion interactions for anions and cations follows. Strongly hydrated anions and cations interact the strongest with charged groups, while weakly hydrated anions and cations show a weaker interaction. For uncharged groups (e.g., backbones of proteins), weakly hydrated anions and strongly hydrated cations show interaction. The former interacts stronger than the latter, and its interaction strength is between strongly and weakly hydrated ions with charged groups. All mentioned ion interactions and their relative strengths are summarized in Fig. 1.3.

Owing to the different binding sites and the different sensitiveness of used methods, it is difficult to compare the binding strength of cations and anions. It has actually been shown that cation interactions with the amide moieties are quite strong.[81,148,149] Some even claim that cation interactions with the carboxylate group are stronger than anion interactions with the NH group.[81,138,140,149] This is, however, highly questionable since other studies suggest the opposite.[15,82,84]

Hofmeister effects on the aqueous solubility of thermoresponsive polymers. During the last two decades, much attention was devoted to explaining interactions between ions and polymers (and other nonelectrolytes) affecting the stability of the solution. Three different models that attempt to explain the ion-specific effects in polymer solutions are introduced here. For a more detailed summary of the models the reader can refer to Moghaddam and Thormann.[114]

Cremer et al. proposed a molecular perspective approach for ion-specific effects on polymers. The effects are described using a mechanism consisting of three contributions: direct ion binding, surface tension and polarization.[4,6,82] The first mechanism describes anion interactions with the polymer surface, while the other two consider anion interactions with the hydration shell of the polymer. With this, the phase transition temperature as a function of salt concentration can be explained for macromolecules such as PNIPAM and ELP in sodium salts.[4,6] A linear decrease of the LCST (salting-out behavior) as a function of the salt concentration is observed for strongly hydrated anions, while weakly hydrated anions show a nonlinear behavior with a slight increase of the phase transition temperature (salting-in behavior) at low concentrations followed by a decrease (salting-out behavior) at higher concentrations.[4,6,82] This is illustrated in Fig. 1.4. The model describes the linear decrease for salts containing a strongly hydrated anion with the polarization contribution. More specifically, it is assumed that these

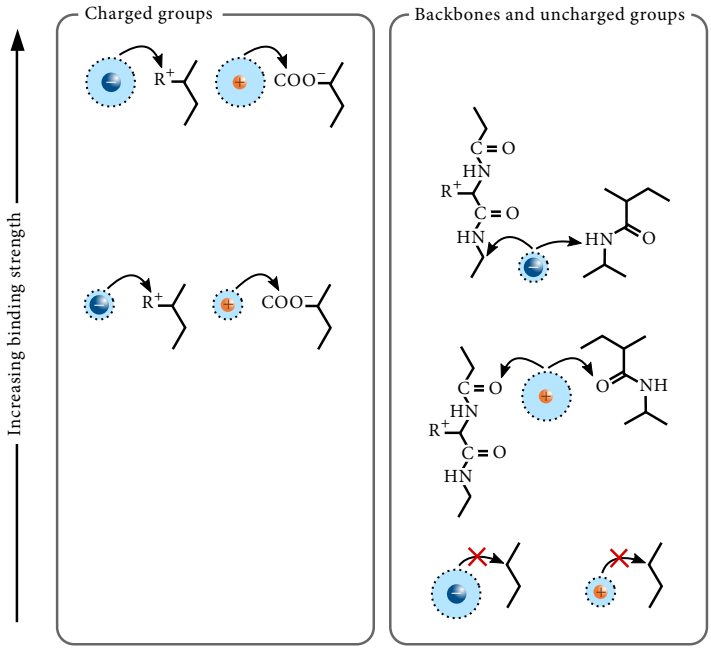

Fig. 1.3 Relative ion binding strengths of anions (blue) and cations (orange) with charged groups, uncharged groups and backbones. Hydration shells are shown by dashed lines and the large or small size indicates strongly or weakly hydrated ions, respectively.

anions induce polarization of neighboring water molecules that are hydrogen-bonded to the amide group of the PNIPAM or ELP. The degree of a strongly hydrated anion's polarization ability has been shown to be correlated with its entropy of hydration.[4] Therefore, a larger anion hydration results in a stronger salting-out behavior. The model describes the nonlinear LCST for salts containing a weakly hydrated anion by the balance between direct ion binding to the polymer and the surface tension contribution. The former leads to an increase and the latter to a decrease of the LCST. More specifically, it is assumed that ion binding is caused by direct polyamide–anion interactions (details have been discussed above), while the surface tension contribution includes a rise in the surface tension of the cavity around the polymer's nonpolar parts (i.e., backbone and isopropyl side chain) affecting the hydrophobic hydration. The degree of a weakly hydrated anion's ability to salt out a polymer has been shown to be correlated with its change in surface tension (per mole of added salt) at an air–water interface. A larger surface tension gradient corresponds to a stronger salting-out behavior. The ion binding is

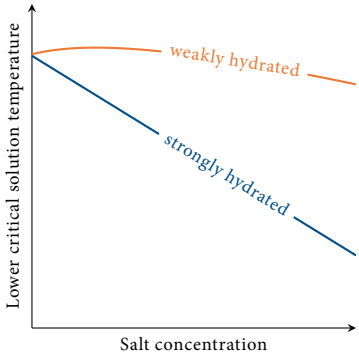

Fig. 1.4 Illustration of the lower critical solution temperature of PNIPAM in solutions containing a weakly hydrated anion (orange) and a strongly hydrated anion (blue), respectively, as a function of the salt concentration.

not observed for strongly hydrated anions since they do not easily shed their innermost hydration shell and, hence, do not show significant binding with polyamide groups.[73,150] Ion-specific effects on a range of various systems such as PNIPAM,[4,9,11,12,27] proteins,[141] polypeptides,[6,82,115,138] lysozyme,[122] negatively charged hydrophilic surfaces,[151] fatty amine monolayers,[14] water hydrogen bonding, and interfacial structure[124] have been investigated with this model.

Cremer et al. typically fit the phase transition temperature of macromolecules in aqueous salt solutions as a function of the salt concentration with three terms: pure water contribution, a linear term corresponding to the salting-out ability, and a Langmuir binding isotherm corresponding to the salting-in ability.[4] Some systems also need an extra term corresponding to electrostatic interactions between ions and charged groups on the macromolecule.[115]

The model enables investigations of polymer solubilities, where polymers themselves are involved. However, the model is empirical and provides no direct information about the underlying physical mechanism. The empirical model is supposedly consistent with associated proposed mechanisms (and is also validated with a thermodynamic model by Dzubiella, Heyda et al.[18]). However, ambiguous interpretations can be made when making inference about a mechanism only from variables and coefficients since some of them are not based on thermodynamic models. The model can also not be used to predict behaviors, since it is based on fitting to experimental data. However, a qualitative assessment of a salting-in and salting-out behavior can be given. Finally, the model assesses ion effects by the anion type, although the cation plays a role as well. The total salt, and not as usually phrased, only the anions, explains the observed behaviors.

Ion-specific effects can also be described by a model specifying ion accumulation and ion depletion relative to surfaces developed by Pegram and Record. Their model is based on the solute partitioning model (SPM).[152] Specifically, the spatial ion partitioning in the bulk water versus the hydration water at surfaces were evaluated in terms of partition coefficients. Salt effects on air–water surface tension[25,153] and on biopolymer stability in aqueous solutions[26,152,154–158] have been investigated. Strongly hydrated anions posses low ion partition coefficients, indicating exclusion from the air–water interface. Weakly hydrated anions posses larger values, indicating partitioning to the interface. Most cations posses partition coefficients close to zero indicating exclusion. Further, the first-order conformational transition between two assumed thermodynamic states of macromolecules (coil and globule for polymers, and unfolded and native for proteins) can be analyzed as a function of the salt concentration. The salt-specific effects are expressed in terms of the first-order transition standard free energy and quantified with a so-called m_{SPM} value. Both interpretations and predictions of noncoulombic interactions with a surface and of m_{SPM} values can be made using the SPM.[155,157,158] The model can also be used to interpret and predict changes in water-exposed surface area[155,157,158] since this property is proportional to m_{SPM} values. Some trend (e.g., the larger or less negative m_{SPM} value, the less hydrated the salt), are observed in general. However, when ranking strongly and weakly hydrated salts according to the Hofmeister series, the series only partly agree.

The SPM-obtained partition coefficients for individual cations and anions have been ranked for various surfaces (e.g., air–water interfaces and surfaces containing hydrocarbons and polar amide groups),[154] and compared with the Hofmiester series based on processes such as protein surface exposure. The Hofmeister series agrees, both in ordering and magnitude, with the ranking of the air–water partition coefficients of anions. For cations, there is a clear discrepancy. Cations takes a neutral position in the Hofmeister series and have large partition coefficients when considering polar amide surfaces, while being excluded (partition coefficient close to zero) from air–water interfaces.

The model provides a tool that can both interpret and predict surface accumulation in a qualitative way. It is, however, limited to systems showing linear changes in the transition free energy. This is, for instance, problematic for weakly hydrated salts showing a nonlinear salting-in behavior. Additionally, the model assumes additivity of the cation and anion effects, which is questionable for certain systems.

Another approach to investigate ion-specific effects on the conformational transition of polymers and proteins is the thermodynamic model developed by Dzubiella, Heyda et al.[18,19,159–161] This model, derived from the second-order expansion of the free energy with respect to temperature and concentration, assumes two states, i.e., coil and globule, as well. For a specific salt, the model can be used to fit experimental LCST data of

polymers to get the thermodynamic parameters. For instance, very good agreement with experimentally obtained LCST data from Cremer et al.[18] was shown. This confirms Cremer's model. A so-called *m* value describes how the two-state free energy function is affected by the salt concentration. Two mechanisms are proposed for the behavior of the phase transition temperature of polymers in electrolyte solutions. A not monotonic change of the free energy with increasing salt concentration is observed for weakly hydrated salts and a monotonic change for strongly hydrated salts. The not monotonic behavior is modeled by including second-order correction terms in the model. Direct polymer–ion interactions cause this nonlinear behavior. A preferential adsorption to the coil conformation is observed at low salt concentrations and to the globule conformation at higher salt concentrations. For the monotonic linear behavior, the second-order correction terms vanish and the salt effect is described purely from a free energy concentration dependent function. The thermodynamic *m* value itself can describe the linear salting-out behavior, where the strongest hydrated salts correspond to the largest negative values. This salting-out behavior is caused by the collapse of the macromolecule leading to a larger salt-accessible volume.

Compared to the model by Cremer et al., this thermodynamic model consists of parameters that all have a distinct physical meaning. It also complements the SPM by Pegram and Record by additionally capturing nonlinear LCST behavior. The scope of systems that can be investigated has thus been expanded.

Conclusions about the driving forces for ion-specific interactions in polymer solutions can also been drawn from models explicitly not involving polymers. Two exemplary models are introduced below.

Ions' affinity to bind to counterions or to charged groups, in relation to their relative behavior in the Hofmeister series, was explained by Collins by introducing the law of matching water affinities (LMWA).[162–164] This affinity follows the rule "like seeks like" where ions are classified according to their hydration strength. The LMWA was deduced from alkali–halide salts by taking the solubility, standard heat of solution and the Jones–Dole coefficients, and the Gibbs free energy of hydration into account.[165] It is an empirical hypothesis capable of describing observed trends from experiments and is supported by activity coefficients[166] and data from MD simulations.[167] However, it is unable to explain the observations theoretically. The idea is relevant for ion binding to proteins where Coulombic interactions exist. It can also be used for neutral polymers with partially charged atoms. However, it cannot explain ions' affinity for uncharged surfaces (e.g., air–water interfaces). Owing to its simplified concept, the LMWA should not be taken as a strict law but be examined critically, instead. For multivalent ions, molecular ions and ionic moieties of biological macromolecules, it is especially interesting to ask if the LMWA provides the correct picture of ion pairing.

Ninham et al. suggested that in addition to electrostatic and hydration contributions, dispersion interactions should contribute to ion specificity for surfaces.[37,57,91,92,94,168–181] This is based on that both ions of the same size but opposite charge, and ions of the same charge but different size and shape show different affinities. The chemical and geometrical nature of the ions affect many-body dipole–dipole, dipole–induced dipole and induced dipole–induced dipole forces, as well as image forces. These are all taken into account in the dispersion interaction model. This fundamental model contributes to the understanding of ion-specific tendencies. The theory includes the role of surfaces and solvents. Additionally, it provides, compared to the LMWA, explanations of ion affinities to uncharged hydrophobic surfaces.

Additive and nonadditive effects in single and mixed electrolyte solutions. So far, most studies concerning Hofmeister effects on the macromolecular solubility or on ion interactions with nonelectrolytes have focused on the type of anion or the type cation, but not a combination of both. This is somewhat surprising since the total salt effect depends on both ion types. Presumably, this is a consequence of earlier ideas on additivity for anions and cations based on thermodynamic bulk properties described above.[22,23] However, there has been a growing interest for ion–counterion interactions in bulk solution and close to macromolecular surfaces as an additional contributing factor to the change in phase transition temperatures.[17,182] The specific combination of cation and anion can potentially indirectly affect macromolecule–ion interactions. A deviation from the commonly believed additive behavior is, therefore, possible in single salts. Indeed, this has been observed for guanidinium salts.[19,121] In one study, salt effects on the rotational mobility of NMA were investigated using spectroscopy,[121] where a nonadditive effect in the interaction of guanidinium with NMA was observed. When guanidinium was paired with a weakly hydrated anion, weaker than expected interactions were observed. Other ion combinations with weakly hydrated anions (e.g., NaI, NaBr, and MgI_2) showed additive effects. In another study, salt effects on the conformation of ELP were investigated using phase transition temperature measurements and spectroscopy.[19] The counteranion to guanidinium can lead to quite contrary behavior. Either polymer swelling or collapse can occur. The effect deviates from pure anion effects and are nonadditive. One explanation is that the counteranion is decisive for guanidinium's ability to form ion pairs at the macromolecule surface.[19] These two studies show that a separation into cationic and anionic Hofmeister series is insufficient for a complete understanding of salt effects.

Other systems, where the question about additivity or nonadditivity is of interest, are mixed electrolyte solutions. These types of systems have not been studied to the same extent as single electrolyte solutions. Actually, only few studies related to ion interactions and macromolecule solubilities are reported in the literature. However, they include polymers,[183–185] polyelectrolytes,[186,187] proteins,[48] and micelles.[188] The phase

transition temperature of poly(propylene oxide) in mixtures of sodium salts (anions equal to Cl^-, Br^-, I^- or SCN^-) have been measured.[184] A mixture of two salts of the same behavior, either both salting-in or both salting-out salt, showed nonadditivity. A combination of two salts with different behavior, salting-in and salting-out, showed additivity. Charged PNIPAM particles, cationic and anionic, in sodium sulfate and sodium thiocyanate solutions, and in a mixed solution containing the two salts have been investigated to obtain information on electrophoretic mobility.[183] Here, additive effects were observed for the mixture. Another type of charged system that has been investigated is charged micelles in mixtures of sodium chloride and sodium bromide.[188] As long as the ratio between the two salts was the same, the interfacial counterion exchange decisive for the aggregate structure was insensitive. However, for a constant total salt concentration, the fraction of bromide had an impact. Different types of polymer and polyelectrolyte brushes have also been examined in mixed electrolyte solutions. In mixtures of potassium acetate and potassium thiocyanate, the influence of the salts on the swelling–collapse balance of poly(oligoethylene glycol methacrylate) brushes was temperature-dependent.[185] An additive effect was observed at temperatures below the LCST, while a nonadditive effect was observed at temperature above the LCST. Polymer swelling was also investigated by measuring the height of polyelectrolyte brushes in solutions containing hydrophilic and hydrophobic salts using a theoretical model.[186] A nonadditive effect was observed, since the total effect was stronger than expected based on the individual contributions. The height of polyelectrolyte brushes has also been investigated in mixed electrolyte solutions of potassium chloride combined with thiocyanate or nitrate using optical measurements and theory.[187] An additive behavior was observed for chloride mixed with nitrate, while a complex behavior is observed when mixed with thiocyanate. Noteworthy, ion-specific effects have been observed to be different for grafted polymer brushes than for polymer chains free in salt solutions,[189] and are likely to apply for polymer brushes in mixed salt effects as well. Further, the adsorption of sodium, choline, chloride, and sulfate ions at two protein surfaces have been investigated using MD simulations.[48] Additive effects were observed in mixtures containing all four ions. In addition, mixed electrolyte solutions in the presence of an air–water interface have been studied.[190] By means of MD simulations and spectroscopic measurements, a further accumulation of weakly hydrated anions in the vicinity of the interface caused by the presence of strongly hydrated anions was demonstrated. The above studies merely represent the beginning of the investigation of mixed electrolyte solutions. Interesting observations are made, but, so far, only parts of the Hofmeister series and limited combinations of ions have been investigated.

Theories for the investigation of polymer solvation and ion affinity. To investigate the solvation of polymers and the effect of salts, proper tools and theories are necessary. On one hand, the attention has lead to further development of techniques including molecular-level thermodynamic measurements (e.g., phase transition measurements),

molecular spectroscopy (e.g., vibrational sum frequency spectroscopy (VSFS)) and advanced molecular simulations (e.g., umbrella sampling and thermodynamic integration). On the other hand, the interest for the theory of solutions, considered to be the number one in terms of being both general and simultaneously powerful, published in 1951 by Kirkwood and Buff[191] has been renewed. They linked molecular (microscopic) details in the form of pair correlation functions to bulk (macroscopic) properties in what is known today as Kirkwood–Buff (KB) theory. The crucial quantity is the so-called Kirkwood–Buff integral (KBI) specifying the distribution deviation of a molecule around another central molecule from a bulk solution with random distribution.[192] However, due to the lack of knowledge regarding pair correlation functions, little attention was paid to the theory back then. This changed because of the work of Ben-Naim in the 1970s. In 1972, the first break through lead to the ability of using the KB theory for interpretations of aqueous solutions by viewing the solutions as a one-component mixture of quasi-components.[193] In 1978, the second break through included the inversion of the KB theory.[194] This enabled the determination of molecular details (pair correlation functions) from bulk (macroscopic) measurements, such as small-angle X-ray and neutron scattering.[195–201]. After this, the KB theory got a lot more attention and the amount of publications of the topic increased drastically. Theory and microscopically obtained information from computer simulations can be used to explain experimentally determined bulk properties. Additionally, experimentally obtained thermodynamic quantities can be used to define molecular details in models (force fields) for computer simulations. However, calculating KBIs with accurate values is challenging.[202,203] Inconsistency between calculated values of KBIs are observed when comparing[204] different studies.[205–208]

The KB theory opened up for studies of, for example, salt and osmolyte effects on biomolecules, where simple binding models[209,210] were used before. Using KB theory, a better understanding of these solution mixtures can be provided through information about interactions between salts or osmolytes and biomolecules. The preferential interactions can be given with exact expressions.[211] Usually the preferential binding is reported, a purely thermodynamic quantity. However, the exact interactions are still to be studied for many systems. Among others, the wish to understand the Hofmeister series[1,2] has motivated the preferential binding theory including the preferential interactions concept.[212,213] Electrolyte solutions cannot be treated as ternary systems (solvent, cations and anions) due to the problem with the electroneutrality condition.[214,215] Instead, all ions need to be considered as indistinguishable ions and the system can then be treated as a binary system.[214,216–218] The KB theory accessible preferential binding concept is especially well-suited for salts and osmolytes weakly binding to macromolecules. Information about these systems obtained from experimental structure techniques, such as X-ray crystallography and NMR spectroscopy, is usually limited.[211] Instead, the use of computer simulations increased the interest for KB theory. Additionally, multiple

approaches of applying KB theory to calculate the preferential binding interactions have evolved over the years.[219–224]

Force fields for electrolyte solutions. All-atom MD simulations of polymer–salt solutions require elaborate models, both for interactions in between all involved atoms and the atoms themselves. Accurate force fields are crucial for the quality of simulations. Typically, a force field cannot correctly reflect all possible properties. Instead, key properties important for the specific application must be identified and tuned during the development of force fields. This has lead to various force fields for specific purposes over the years.[225–228] Investigations of interactions in aqueous salt–polymer solutions demand all-atom force fields. Furthermore, electrolyte solutions require accurate force fields for differentiations of ions and for capturing ion-specific effects. Hence, coarse grained force fields grouping atoms to larger units and thereby using fewer numbers of interaction sites to make it possible to extend the simulation time is not desirable. Furthermore, nonpolarizable force fields are extensively used because of their good performance originating from a parameter reduction and their simplicity during the parameterization process compared to polarizable force fields.[229] The partial charge of ions together with their Lennard-Jones (LJ) diameters, i.e., excluded volume diameters, and dispersion interaction strengths define these force fields. However, compared to polarizable force field, they can show artifacts such as too strong ion pairing and even ion clustering originating from overestimated ion interactions.[230,231] The development of ion force fields is not straight forward and has been, and still is, an ongoing task. Various approaches to compensate for polarization effects have been used for the parameterization of force fields for electrolyte solutions over the years. In the 1970s and 1980s, models used for simulations of electrolyte solutions usually utilized an implicit water description.[232] Instead of accounting for water molecules explicitly, a scaling factor equal to the dielectric constant of water was used for coulombic interactions.[232] With increasing computer power during the last 30 years, models that describe water, which constitutes the largest part of an electrolyte solution, explicitly have become affordable.

In the early days, when the computational performance was poor, ion force fields were typically optimized by considering single-ion properties (e.g., ion–water structure, ionic solvation free energy or ionic hydration structure).[233] For electrolyte solutions with finite ion concentrations, this lead to an unrealistic ion–ion structure and bad thermodynamics. This was observed for sodium chloride, for example.[234,235] It has been shown that interactions between ions are heavily dependent on ion pairing[165,167] and solution thermodynamics.[236–238] In addition, using one experimental quantity when defining two force field parameters (LJ size parameters and dispersion interaction strengths) is insufficient. Therefore, two separate studies[239,240] probed the single ion hydration free energy as a function of the two force field parameters, while optimizing a second

independent property (i.e., crystal lattice energy[239] or effective solution ion size).[240] It was partly successful, but finding a combination that fulfills multiple properties simultaneously proved challenging for some salts. Therefore, parameterization against collective thermodynamic properties (e.g., osmotic or activity coefficients) are desired. This approach has been used by Weersinghe, Smith et al.[241,242], Hess and van der Vegt[78], and Fyta, Netz et al.[243,244].

Weersinghe, Smith et al.[241,242] optimized ion force fields for alkali halides against electrolyte solution activities by comparing simulations with fits from experiments using KBIs.[191,192] Hess and van der Vegt[78] used the same method when optimizing a LiCl force field. After either parameterization of the force field parameters for all ions, or the use of already existing force field parameters, both groups scaled the interactions between the cation and water oxygens by using a scaling factor for the dispersion interaction mixing term. An advantage of the KB approach is its sensitivity to small changes in the molecular distribution. However, its disadvantage is that the integral is not unique. That is, different molecular distributions may yield the same integral. Additionally, a scaling of the interactions between an ion and the water molecules leads to a not preserved single ion solvation free energy.

Fyta, Netz et al.[243,244], therefore, developed an approach for force field optimization where both single ion properties (e.g., solvation free energy) and ion pairing properties are simultaneously defined. This was simply done by first optimizing the combination of the two force field parameters (i.e., LJ size parameters and dispersion interaction strengths). Second, the mixing rule between cations and anions were scaled when not sufficient, while keeping ion interactions with water molecules constant. The force fields were optimized against osmotic coefficient[243] or activity derivatives,[243,245] both determined from KB integrals and compared to experimentally obtained values. This approach has shown to be successful for both monovalent[243,244] and divalent ions.[245] It can also be readily transferred to additional ions, where salts consisting of size-asymmetric ions are in a greater need of scaled mixing rules. However, the drawback is that no general solution exist for all electrolyte solutions. That is, every ion pair needs to be optimized individually.

Another way to avoid too strong ion pairing is to include electronic polarization in a mean-field approach, for instance by using the theory of electronic continuum correction (ECC), an implicit model of electronic polarizability.[246–252] It is implicit since the electronic interactions in an otherwise nonpolarizable force field are modified to include electronic polarization effects. This is done by using a pre-determined charge rescaling factor (0.75) for ions. The motivation for this approach is to account for the screening between two close ions caused by the electronic contribution to the water dielectric permittivity missing for ions described with integer charges and nonpolarizable water models. After Leontyev, Stuchebrukhov et al. proposed ECC, Jungwirth et al.

has been following up and promoting it. Multiple studies have shown the ECC to be successful for electrolyte solutions. The approach has been used for a range of different salts, such as K_2CO_3,[253,254] KNO_3,[253] Na_2SO_4,[255] Gdm_2CO_3,[256] LiCl,[257,258] Li_2SO_4,[257] $CaCl_2$,[259] NaCl,[260] $NaNO_3$,[254] $LiNO_3$,[254] $MgCl_2$,[261] $ZnCl_2$,[261] and calcium chloride and calcium paired with formate and acetate,[262] respectively. ECC force fields are usually benchmarked against neutron scattering data[253,256–259,261,262] and lately also against free energy profiles of ion pairing obtained with *ab initio* MD simulations.[255,261,262] Some ECC force fields utilize an additional ionic size rescaling, and is referred to as ECCR.[259] The advantage of ECC is that polarizability is accounted for efficiently, without additional computational cost. Because of the reduction of interactions between ions and/or charged molecules, the force fields show better performance concerning the structure of electrolyte solutions. The largest improvement is achieved for high charge density ions, since they strongly polarize their surrounding water molecules. It has even shown better performance than other models (e.g., explicit solvent shell model).[255] Even if the rescaling of charges in the ECC approach leads to accurate short-range ion–ion interactions, an open question is still if long-range electrostatic ion interactions are represented accurately, as well. The disadvantage of ECC is that the amount of available ECC force fields is still very limited. Ions from ECC force fields can only be combined with counterions using the same scaling factor. This applies for the nonelectrolytes in the solution, too. Since the approach is based on an empirical scaling factor, it is not clear how properties of nonelectrolytes are affected, rendering the application not straight forward. However, very recently relevant biological systems, such as protein moieties[263,264] and phospholipid molecules[265] have been started to be simulated with ECC force fields.

Many researchers have followed the idea of charge rescaling proposed by Leontyev, Stuchebrukhov et al. Carlos Vega et al. have developed a force field for alkali and alkaline earth halides combined with chloride or sulfate, with a scaling factors of 0.85 and 1.7 for monovalent and divalent ions, respectively.[232] Fuentes-Azcatl and Barbosa suggested a scaling factor of 0.885 for aqueous NaCl solutions,[266] while Li and Wang suggested a scaling factor of 0.804 for monovalent ions.[267,268]

1.3 Objectives and structure

This work aims at extending the current understanding of the Hofmeister series. For this purpose, it investigates ion-specific effects in aqueous solutions and ions' influences on the solubility of thermoresponsive polymers. By extending the scope of the Hofmeister series to include the effect of cations and mixtures of salts, it provides a comprehensive picture of the behavior of ions in simple aqueous salt solutions, complex aqueous macromolecule solutions, and of the phase transition temperature of polymers

in these solutions. This requires addressing two main questions: i) what role do the exact cation–anion combination play, and ii) are the ion-effects in single and mixed salt solutions additive or nonadditive? The phenomena of interest have been observed in thermodynamic data (i.e., phase transition temperatures) collected by collaborative partners. Then, using MD simulations, the underlying molecular level mechanism is investigated, elucidated and described. Analyses of additional spectroscopic measurements have sometimes been used to confirm the proposed mechanisms and provide additional physical and chemical insights. An overview of available knowledge on the topic, objectives of the present work, and yet unresolved issues is given in Fig. 1.5.

The text is organized as follows: Chapter 2 summarizes relevant chemical and physical concepts, and introduces a consistent notation. Basic principles of experimental techniques carried out by collaborators are also described. Chapter 3 is dedicated to the method of MD simulations used throughout the present work. Chapters 4 to 8 present the findings of the present work. Using the known behavior of weakly hydrated anions in polymer solutions, Chapter 4 investigates the effect of the cation. Cation-specific effects on the phase transition temperature of polymer solutions, including iodide salts, are observed. This study emphasizes the role of the cation in the underlying molecular-level mechanism of polymer solubility. Chapter 5 contributes with findings and a novel study on the cationic Hofmeister series. A molecular-level mechanism for the phase transition temperature of polymer solutions, including chloride salts, is presented. The specific ion type and the cation–anion combination prove key for the mechanism, and explain the deviant behavior from the typical consensus about the cationic Hofmeister series. Chapter 6 extends the understanding of the Hofmeister series regarding not only single electrolyte solutions but also mixed electrolyte solutions. Specific combinations of ions influence the phase transition temperature of polymers in unique ways. Nonadditive behavior of the ions distinguish the behavior from well-known effects in single electrolyte solutions. Chapter 7 assesses the current status of solvation in mixed salt and mixed osmolyte solutions and identifies needed key advances to direct efforts of future research. Similar nonadditive effects are observed for the two types of mixed solutions, both for salts and osmolytes. Hence, they can be assumed to originate from a more general effect. In Chapter 8, the method of charge rescaling to count for polarizable effects in nonpolarizable force fields is extended to multivalent ions. With this mean-field approach of including electronic polarization artifacts, such as too strong ion pairing, is avoided. Accurate force fields are of importance to allow for the computational examination of systems and, hence, for obtaining insights on underlying mechanism. Force fields for salts developed within this work is not only presented in Chapter 8, but also in Chapter 4 and in Chapter 6. The present work is summarized in Chapter 9 and suggestions for further studies are presented.

Since Chapters 4 to 8 are based on (peer-reviewed) journal articles, some information and concepts introduced in Chapter 2 are repeated throughout the different chapters.

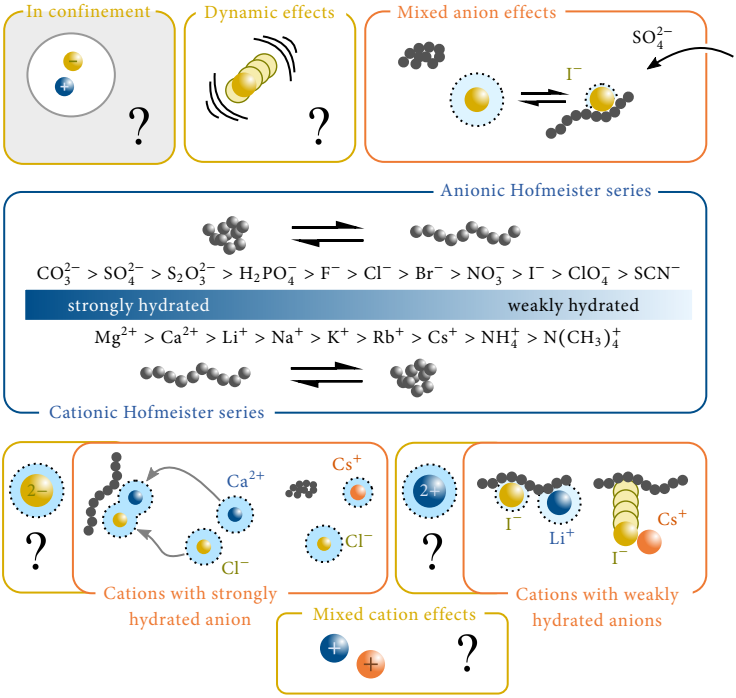

Fig. 1.5 Illustration of the state of the art (blue box), new findings of the present work (orange boxes), and some of the noteworthy remaining questions in the field of Hofmeister effects (yellow boxes). Blue box: i) general anionic Hofmeister series including salting-in and salting-out behavior of polymer, ii) typical consensus cationic Hofmeister series for proteins. Orange boxes: i) effect of the cation when combined with weakly hydrated anions (e.g., iodide ions), ii) effect of cations when combined with strongly hydrated anions (e.g., chloride ions), and iii) effect of mixed salt solutions, all on the polymer solubility. Yellow boxes: i) effect on the polymer solubility when weakly hydrated anions are combined with divalent cations (e.g., Ca^{2+}), ii) effect on the polymer solubility when cations are combined with strongly hydrated divalent anions (e.g., SO_4^{2-}), iii) effects in mixed salt solutions consisting of two different cations, iv) Hofmeister effects in confined environments (with and without grafted polymer chains on the walls), and v) dynamic Hofmeister effects.

Nonetheless, all information is provided concisely in Chapter 2 in order to provide a complete picture of the concepts relevant to the understanding of Chapters 4 to 8. In addition, some of the peer-reviewed journal articles include Supporting Information or an Appendix, leading to figures and tables not always presented in chronological order.

Chapter 2

Chemical and physical concepts

The present work is concerned with the effects of ions on polymer solubility in aqueous solutions. To allow for an understanding of the influence of the different components such as solvent, ions, and polymer, relevant chemical and physical concepts are introduced in this chapter. The following sections present fundamentals of solvation, concepts concerning ions in aqueous solutions, a brief introduction to stimuli-responsive polymers, methods for the description of the influence of ions on hydrophobic polymers, and basic principles of experimental techniques. The chapter also introduces a consistent notation and relevant mathematical concepts.

2.1 Solvation

Solvation refers to a reorganization process of the components in a solution (solutes and solvent), to form solvation shells surrounding the solutes, i.e., solvation complexes. The process and shells are referred to as hydration and hydration shells, respectively, when the solvent is water. Not only solute–solvent, but also solvent–solvent and solute–solute interactions and their strengths affect the solubility of solutes. The solvation process is crucial for any experiment performed in solutions. This process together with the hydrophobic effect (force acting to minimize solvent exposed surface of solutes) play key roles in the understanding of polymer solubility. In a ternary solution, a third component, except solvent (e.g., water) and solute (e.g., polymer), is present. It is referred to as a cosolute when a second solute is added (e.g., salt) or as a cosolvent when a second solvent is added (e.g., alcohol or osmolyte).

A decrease of the Gibbs free energy of the solution relative to the sum of individual contributions of the solvent and the solutes is necessary for the solvation process to be thermodynamically favorable.[269] The Gibbs free energy refers to the maximum additional (not expanding) work accompanying a process performed by a thermodynamic system at constant temperature and pressure.[269] Solvation thermodynamics aids in calculating solubilities and equilibrium constants.

2.1.1 Solvation thermodynamics

The change in Gibbs free energy G between ideal gas and liquid phase is denoted Gibbs free energy of solvation (s) and can be expressed by[192]

$$\Delta G_s = \Delta H_s - T\Delta S_s, \tag{2.1}$$

where ΔH_s and ΔS_s denote the corresponding changes in thermodynamic enthalpy and thermodynamic entropy, respectively. The solvation process of small molecules is dependent on solute–solvent (uv), as well as solvent–solvent (vv), interactions. These interactions taken into account, the thermodynamic enthalpy and entropy can be defined as[136]

$$\Delta H_s = E_{uv} + \Delta E_{vv}, \tag{2.2}$$

and

$$\Delta S_s = S_{uv} + \Delta S_{vv}, \tag{2.3}$$

respectively. Here, E_{uv} and S_{uv} denote the solute–solvent energy and solute–solvent fluctuation entropy, respectively. Even though S_{uv} is not entropy in the sense of a temperature derivative of ΔG_s, it is referred to as entropy because it captures the role of fluctuations.[136] ΔE_{vv} denotes the change in solvent reorganization energy and ΔS_{vv} the change in equivalent entropy upon dissolution. At 1 atm ambient pressure, the otherwise necessary pressure–volume term $P\Delta V$ on the right-hand side of Eq. (2.2) is negligible.

The experimentally determined Gibbs free energy of solvation ΔG_s equals the excess chemical potential of the solute according to

$$\mu^* = \Delta G_s, \tag{2.4}$$

at constant temperature T and pressure P. Solvation effects on the chemical potential have been presented by van der Vegt and Nayar and will be repeated here.[136] If the molality scale is used, μ^* quantifies the effects of solvation on the chemical potential and is equal to the difference between the chemical potentials in liquid (l) and in vapor (v), $\mu^* = \mu_l - \mu_v$.[194] The inverse form of the Widom potential distribution theorem[270] yields

$$\exp\left(\frac{\mu^*}{RT}\right) = \left\langle \exp\left(\frac{\phi}{RT}\right)\right\rangle, \tag{2.5}$$

where R denotes the gas constant, ϕ the potential energy corresponding to the interactions between the solute and the surrounding solvent molecule, and $\langle\cdot\rangle$ a configuration ensemble average. Using Eq. (2.5), the excess chemical potential of the solute can also

be expressed as

$$\mu^* = \langle \phi \rangle + \mathrm{R}T \ln \left\langle \exp\left(\frac{\delta\phi}{\mathrm{R}T} \right) \right\rangle, \tag{2.6}$$

where $\langle \phi \rangle$ denotes the average solute–solution interaction energy. It is identical to the solute–solvent energy, $E_{\mathrm{uv}} \equiv \langle \phi \rangle$. The other term on the right-hand side, where $\delta\phi \equiv \phi - \langle \phi \rangle$, is entropic, and is determined by fluctuations of ϕ. It is identical to the solute–solvent fluctuation entropy $S_{\mathrm{uv}} \equiv -\mathrm{R} \ln\langle \exp(\delta\phi/\mathrm{R}T) \rangle$. Using these definitions and Eqs. (2.4) and (2.6), yields

$$\Delta G_{\mathrm{s}} = E_{\mathrm{uv}} - TS_{\mathrm{uv}}. \tag{2.7}$$

As can be seen from Eq. (2.7), ΔG_{s} does not explicitly depend on E_{vv} nor on S_{vv}. They cancel out since they are equal to each other, $\Delta E_{\mathrm{vv}} = T\Delta S_{\mathrm{vv}}$. The cancellation is referred to as the energy–entropy compensation [271] and is valid for all solvation processes. That is, solvation free energy can be calculated solely from the solute–solvent terms. However, even if E_{vv} and S_{vv} cancel out, they are important to quantify because of their large variations in presence of cosolutes (or cosolvents), where they have an implicit impact. This has been shown with computer simulations, [271–273] as well as with experiments. [274] When investigating solvation of solutes, and especially the driving forces, it has been shown that using Eq. (2.7) gives a better microscopic view of solvation than using Eq. (2.1). [271] The reason is the energy–entropy compensation [271] and the difficulties in defining the driving force for ΔG_{s} when using ΔH_{s} and ΔS_{s}.

To provide a complete picture of solvation, consider the following thought process where all solute–solvent and solvent–solvent interactions are taken into consideration, while solute–solute interactions are neglected due to an assumed low concentration. [20] The solvation process is split into two separate steps. First, a cavity with the size and shape of the solute is formed. Second, attraction forces are switched on. This includes van der Waals and electrostatic interactions. The potential energy of all solute–solvent interactions can be split by the two steps, $\phi = \phi_{\mathrm{r}} + \phi_{\mathrm{a}}$. [192] The index r denotes the repulsive parts (step 1) and the index a attractive parts (step 2). The excess chemical potential can then be exactly written as

$$\mu^* = \mu_{\mathrm{cav}} + \langle \phi_{\mathrm{a}} \rangle + \mathrm{R}T \ln \left\langle \exp\left(\frac{\Delta\phi_{\mathrm{a}}}{\mathrm{R}T} \right) \right\rangle, \tag{2.8}$$

where μ_{cav} denotes the cavity (also known as solvent-excluded volume, Section 2.4.4) contribution, a completely entropic term. The second term on the right-hand side is the average attraction originating from solute–solvent interactions and is enthalpic. The third term is fluctuations in the attractive interactions, where $\Delta\phi_{\mathrm{a}} \equiv \phi_{\mathrm{a}} - \langle \phi_{\mathrm{a}} \rangle$ and is entropic. This term is crucial when investigating the hydrophobic effect (Sec-

tion 2.1.2). The Gibbs–Bogoliubov inequality $\Delta G_s \geq \langle \phi \rangle$ yields $S_{uv} \leq 0$.[275,276] A negative solute–solvent fluctuation entropy indicates a loss in entropy. The reorganization of solvent molecules until both the position and the orientation of the solvent molecules are in equilibrium to host the chemical moieties of the solute, explains why S_{uv} is negative. The reorganization includes contributions from both the first and third term in Eq. (2.8).

2.1.2 Hydrophobic effect

Nonpolar (hydrophobic) solutes aggregate in aqueous solutions caused by an effective force and, hence, segregate from water molecules. This tendency is called the hydrophobic effect.[277–289] More specifically, the insertion of a nonpolar solute is referred to as hydrophobic effect, while the association of two of these solutes is referred to as hydrophobic hydration. The hydrophobic interactions arise from hydrophobic hydration.[289] The exposed surface area of nonpolar solutes to the surrounding aqueous solvent environment is minimized when clusters (aggregates) of nonpolar solutes are formed.[282,290] The difference between the hydration free energy of an aggregate and of all individual molecules together corresponds to the water-mediated interaction free energy of this aggregate.[289] In order to understand the hydrophobic effect, it is important to understand the behavior of nonpolar solutes in water, including solubility, and the association and folding/collapsing of the solutes. The effect plays a central role in chemistry and biology. That is, it regulates processes such as aggregation, polymer collapse, protein stability, membrane and micelle formation, drug partitioning, emulsion stabilization and detergent facilitation.

Size dependence. The physics of hydration at a macroscopic scale is different from the molecular scale.[286,291–297] While the hydrophobic effect on the macroscopic scale can be understood in terms of surface tension, the hydrophobic effect on the molecular scale is related to local density fluctuations and the compressibility of bulk water. The local structure of water is a tetrahedral hydrogen network. Depending on the solute size, the thermal fluctuations of the water are sufficient or insufficient to host the solute. For the solute to dissolve in the water, the formation of a cavity is needed. The accommodation of small solutes takes place without breaking the hydrogen-bonding network.[298] This leads to a noticeable entropic penalty and a restriction of water molecule configurations. A denser hydration shell around the solute than in the bulk is observed, and the small solutes are said to be wetted.[286,294] The release of the restricted water molecules when small solutes associate, leads to an increase of water entropy. This entropy is the driving force for the solvation of small solutes, and the solvation free energy scales with the solute volume.[286,294] Large ($\approx$ 1 nm or larger) solutes cause the hydrogen-bonding network to break.[286,291] This leads to a

less dense hydration shell compared to the bulk structure and a dewetting of the solute surface occurs.[286,294] Solvation of larger solute is dominated by enthalpy, and the solvation free energy scales with the solute surface area.[286,294] The entropy–enthalpy crossover takes place as the solute size of approximately 1 nm (ambient conditions). For the understanding of protein folding and polymer collapse, an understanding of the hydrophobic effect in the crossover region is necessary. The length scales in these processes are in the range from subnanometer to nanometer. Besides the size, the curvature (convex, concave or zero) of the solute has an impact on the hydrophobic effect.[299] The specific size and curvature yield specific behavior, due to the extent of breaking the hydrogen-bonding network, and the enthalpic or entropic driving force.

Thermodynamics of the hydrophobic effect. The thermodynamics of the hydrophobic effect are temperature dependent. The probability to solvate the solute is proportional to[286]

$$P_s \propto \exp\left(-\frac{\Delta G_s}{k_B T}\right), \tag{2.9}$$

where k_B denotes the Boltzmann constant and T the temperature. While ΔG_s is only weakly temperature dependent, its two contributions ΔH_s and ΔS_s (Eq. (2.1)) are highly temperature dependent.[289] For the (entropy driven) small solute case at ambient conditions, ΔG_s increases with increasing temperature.[286] For the (enthalpy driven) large solute case at ambient conditions, $\Delta G_s/T$ decreases with increasing temperature.[286] ΔS_s describes how the different solutes are ordered relative to each other or how they are correlated, while the average potential energy of interaction between solutes is described by ΔH_s.[300]

Hydrophobic interactions. The hydrophobic interactions explained on a pairwise level[289,301] can be described with a potential of mean force (PMF). A PMF describing the pairwise interaction between two nonpolar solutes in an aqueous solution is defined by[289]

$$w(r) = u(r) + \Delta w(r), \tag{2.10}$$

where $u(r)$ denotes the direct interactions between solutes in the absence of solvent (e.g., water), $\Delta w(r)$ the solvent-mediated contribution and r the distance between the two solutes (center if solutes are spherical). The type of solute–solvent interactions affect both the sign and magnitude of $\Delta w(r)$. Even if the direct interactions are repulsive, the total PMF can be attractive because of solvent-mediated interactions. Depending on the strength of van der Waals interactions between solute and solvent (e.g., water), $u(r)$ can either favor aggregation or breakup of the solutes.

2.2 Electrolyte solutions

An aqueous electrolyte solution is composed of water and ions. In a ternary solution, the salt acting as the cosolute can modulate the hydrophobic effect and, hence, affect the solvation process. This modulation is ion specific. It depends on the ions' properties, their behavior in bulk solutions, at interfaces and their pairing characteristics.

2.2.1 Electrolyte solution properties in bulk and at air–water interfaces

The simplest system for studying ion effects is ions in bulk water. Ions with low charge density (e.g., Cs^+ and I^-) are referred to as soft or, as hereinafter, weakly hydrated.[162] Ions with high charge density (e.g., Li^+ and SO_4^{2-}) are referred to as hard or, as hereinafter, strongly hydrated.[162] The ion-specific solution composition affects different properties. Relevant properties are described in the following.

Classical electrolyte solution theories. Salts dissociate to ions in water. The orientation of water molecules surrounding the ions is influenced by the electric field of the ion. As a consequence, the water structure in the vicinity of an ion is different from that in the bulk solution. It has been demonstrated that cation–water and anion–water interactions are dissimilar and, hence, they influence the water structuring around the ions differently.[66,302] However, classical electrolyte solution theories, such as the Debye–Hückel theory, ignore the solvent structure and solvent properties.[303] Instead, the solvent is seen as a continuum medium, often described with a dielectric constant.[304] Hence, these models do not capture the different water molecule arrangements close to ions. Ions are all assumed point charges and interactions are purely electrostatic in the Debye–Hückel model.[305] With the electric charge as the only decisive parameter, ions with the same charge but different size or shape cannot be distinguished. That is, all alkali metal ions and halides are treated identically. Such a model cannot explain ion-specific phenomena, such as ion pairing propensity (Section 2.2.2). Further, the model leads to an overestimation of the electrostatic interactions and is only applicable to low salt concentrations. Classical electrolyte solution models also struggle to capture the ion-specific behavior at interfaces (Section 2.2.1) since according to the image charge effect[306] repulsion between all ions and nonpolar surfaces is expected.

Electrostriction. Ions in aqueous solutions modulate the dipole of the surrounding water molecules through their strong electric field. A rearrangement of water molecules occurs and the binding to ions restricts their freedom. This leads to a reduction in the translational entropy and is called solvent binding or electrostriction.[307] Different ions affect the entropy of their surrounding water molecules differently. The addition of

strongly hydrated ions to water leads to a decrease of entropy of the water near the ion, while the addition of weakly hydrated ions increases the entropy.[165] Ions of opposite electrical charge associate in aqueous solutions to form chemical species, such as ion pairs (Section 2.2.2) and diminish the electric field of individual ions. This loosens the electrostriction of water. Hence, less water is restricted, some molecules are even released in a desolvation process, and the entropy of the system increases.

Activity coefficients and osmotic coefficients. For a binary system containing salt (s) and water (w), the chemical potential of each component, $\mu_s(P, T)$ and $\mu_w(P, T)$, is expressed as the Gibbs free energy change of each component with the molar amount of the component at constant P and T.[303] The chemical potentials are defined as

$$\mu_s(P,T) = \left(\frac{\partial G}{\partial n_s}\right)_{P,T,n_s} = \mu_s^{\infty}(P,T) + \mathrm{R}T\ln(x_s\gamma_s) = \mu_s^{\infty}(P,T) + \nu\mathrm{R}T\ln(x_{\pm}\gamma_{\pm}), \tag{2.11}$$

and

$$\mu_w(P,T) = \left(\frac{\partial G}{\partial n_w}\right)_{P,T,n_w} = \mu_w^{\infty}(P,T) + \mathrm{R}T\ln(x_w\gamma_w), \tag{2.12}$$

where n_i denotes the moles of species i, ∞ the infinitely diluted solution, R the gas constant, $\nu = \nu_+ + \nu_-$ the stoichiometric coefficient (e.g., 2 for NaCl), and x_i and γ_i the molar fraction and activity coefficient for species i, respectively. Note, $\gamma_{\pm}$ is the mean activity coefficient for the salt, while γ_s is the activity coefficient for the salt. The activity coefficient γ characterizes the differences between a solution and an ideal solution.

The Gibbs–Duhem equation,[269] stating that the chemical potentials of the components i in a mixture cannot change independently, can be expressed as

$$\sum_i n_i \mathrm{d}\mu_i = n_w \mathrm{d}\mu_w + n_s \mathrm{d}\mu_s = 0, \tag{2.13}$$

for binary salt and water systems. Additionally, the salt activity a_s and water activity a_w are defined as[269]

$$a_s = x_s\gamma_s, \qquad \text{and} \qquad a_w = x_w\gamma_w, \tag{2.14}$$

respectively. The mean activity coefficient $\gamma_{\pm}$ can be converted to the molarity or molality scale. If the molality scale is used, the Gibbs–Duhem equation (2.13) gives a relation between the salt activity and the water activity according to

$$\nu m M_w \,\mathrm{d}\ln a_s + \mathrm{d}\ln a_w = 0, \tag{2.15}$$

where m denotes the molality and M_w the molar mass of water. By using Eqs. (2.13) and (2.15) together with Eqs. (2.11) and (2.12), the mean activity coefficient of salt can be expressed in terms of the water activity through

$$\ln \gamma_{\pm} = -\frac{1}{\nu M_w} \int_0^m \frac{\ln a_w - \nu M_w}{m} \mathrm{d}m. \tag{2.16}$$

Furthermore, the osmotic coefficient is a measure of the water activity and can be calculated from[303]

$$\phi = \frac{\Pi}{\Pi_{id}} = \frac{-\ln a_w}{\nu m M_w}, \tag{2.17}$$

where Π and Π_{id} denote the osmotic pressures of a nonideal and ideal solution, respectively. Hence, ϕ characterizes the difference between a solvent and an ideal solvent. Eq. (2.16) can be rewritten to relate the salt activity coefficient to the osmotic coefficient by using Eq. (2.17). The relation is[303]

$$\ln \gamma_{\pm} = (\phi - 1) - 2 \int_0^m \frac{(1-\phi)}{m^{\frac{1}{2}}} \mathrm{d}m^{\frac{1}{2}}. \tag{2.18}$$

The type of ion affects both the mean salt activity coefficient and the osmotic coefficient.[303] For a specific salt concentration, the coefficients increase with increasing ion radii due to the excluded radii effect. Additionally, a high coefficient corresponds to a strong ion solvation and/or weak ion association. This originates from strong ion-solvent interactions affecting more water molecules.

Surface tension. A property characterizing the behavior of ions at the simplest interface, the air–water interface, is surface tension.[303] Surface tension can be described as the tendency of minimizing the number of boundary molecules and, thereby, shrinking the water surface into the minimum surface area possible.[308] This originates from water molecules at the boundary having fewer neighbors compared to the ones in the bulk solution and, thereby, having a higher energy. The minimal surface area minimizes the energy state of the liquid.

The addition of salts to water affects the surface tension.[24,309] According to the Gibbs binding isotherm, a decrease of the surface tension can be associated with an affinity of ions for the interface, while an increase can be associated with a depletion of ions from the interface.[303] The change of the surface tension in the presence of ions can be calculated from the Gibbs adsorption equation[303]

$$\Delta\gamma = -\mathrm{k_B} T \int_0^{c^{\mathrm{bulk}}} \frac{\sum_i \Gamma_i(c)}{c} \mathrm{d}c, \tag{2.19}$$

where k_B denotes the Boltzmann constant, T the temperature and c the concentration. Γ_i denotes the surface access and is defined as

$$\Gamma_i = \int_{-\infty}^{z_{GDS}} c_i(z)\mathrm{d}z + \int_{z_{GDS}}^{\infty} \left[c_i(z) - c_i^{bulk}\right]\mathrm{d}z, \tag{2.20}$$

where z_{GDS} denotes the Gibbs-dividing-surface position, $c_i(z)$ the concentration profile, and c_i^{bulk} the bulk concentration of the ith ion. Nearly all electrolyte solutions show a linear behavior of surface tension versus concentration.[25] Weakly hydrated ions have a lower surface tension increment (and sometimes negative) relative to water than strongly hydrated ions and, thereby, approach the surface closer.[25] This spatial molecular picture originates from the interpretation of the Gibbs binding isotherm. The molecular interpretation is, however, not straightforward. For instance, ion adsorption can also result in an increase of the surface tension.[103] This can be explained by a local ion adsorption closest to the interface even if the overall effect in the whole surface region, i.e., from interface to pure bulk solution, given by the Gibbs binding isotherm consisting of an integral, indicates depletion. That is, a molecular picture of surface tension goes beyond Eq. (2.19).[103] In addition, it is also difficult to differentiate the polarizability effect of ions from the size and charge effect on the surface tension.[303] Further, anions have a larger impact on the surface tension than cations.[25,309] Ion effects on surface tension are, however, small. Hence, exact experiments and quantitative predictions by means of theories and simulations are challenging.[303]

2.2.2 Ion pairing and ion hydration in bulk aqueous solutions

Ions of opposite charge show attraction. Ions' relative interactions with other counterions and with the surrounding water molecules affect the tendency for ions to pair or to stay solvated.

Ion pairing. The concept of ion pairing including association of two ions specified by an equilibrium constant was originally introduced in order to describe bulk properties containing associating ions. Ion pairs can be classified according to the nature of their interaction, which depends on the type of ions involved and the interactions between all solution components (ion–ion, ion–water and water–water interactions)[163,165] This applies for small distances, where the ion–counterion attraction and the thermal energy $k_B T$ are comparable. In contrast, at large ion–counterion distances the attraction is reduced by a factor corresponding to the dielectric constant (78 at 298 K) and is not dependent on the specific types of ions.[304] The different types are here called[1]: contact

[1] In Chapter 4, the ion pairs are instead referred to as contact ion pair (CIP), solvent-separated ion pair (SIP), and double solvent-separated ion pair (2SIP).

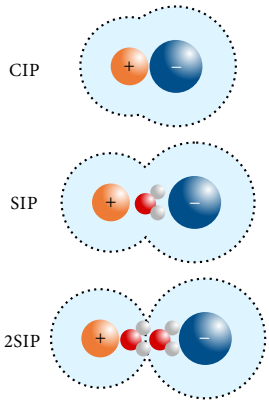

Fig. 2.1 Types of ion pairs. Contact ion par (CIP), solvent-shared ion pair (SIP) and solvent-separated ion pair (2SIP). Black dashed circles around the ions represent hydration shells. Only characteristic water molecules are explicitly shown.

ion pair (CIP), solvent-shared ion pair (SIP) and solvent-separated ion pair (2SIP) (Fig. 2.1). CIP ions are in direct contact with each other. For SIP ions, the first hydration shells overlap. In the case of 2SIP ions, the first hydration shells are maintained, but the second hydration shells overlap. Ion pairs can be studied using the radial distribution function (RDF)[229,310,311] by means of computer simulations. The RDF between particles of types i and j is defined as

$$g_{ij}(r) = \frac{\langle \rho_j(r) \rangle}{\langle \rho_j^0 \rangle} = \frac{1}{\langle \rho_j^0 \rangle N_i} \sum_{\alpha=1}^{N_i} \sum_{\beta=1}^{N_j} \frac{\zeta(r_{\alpha\beta} - r)}{4\pi r^2}, \tag{2.21}$$

where $\langle \rho_j(r) \rangle$ is the particle density of type j at a distance r around particles i, and $\langle \rho_j^0 \rangle$ is the particle bulk density of type j. The $\langle \cdot \rangle$ symbol denotes the ensemble average. Denoting the distances between two particles α and β of types i and j, respectively, as $r_{\alpha\beta}$, the particle density of type j at a distance r can be calculated using the surface area normalized counter function

$$\zeta(x) = \begin{cases} 1 & x = 0, \\ 0 & x \neq 0, \end{cases} \tag{2.22}$$

and summing over all particles of type j. Repeating this summation for every particle of type i, and normalizing to the total number N_i of particles i, then yields the RDF. If i and j denote the same type of particles, i.e., $i = j$, the second sum must be adjusted

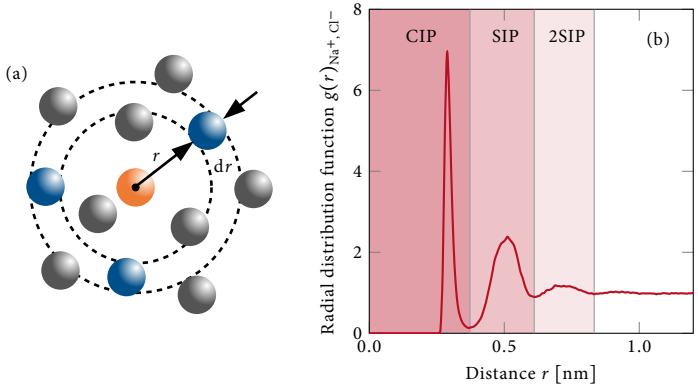

Fig. 2.2 Radial distribution function. (a) Illustration of the variation of the density of a particle j (blue) with radial distance r from the reference particle i (orange). (b) Radial distribution function $g(r)$ between Na^+ and Cl^- as a function of the distance r. The shaded red areas indicate the different ion pairs: contact ion pair (CIP), solvent-shared ion pair (SIP) and solvent-separated ion pair (2SIP).

to begin at $\beta > \alpha$. The function describes the particle density variation of particles of type j in a spherical volume around particles of type i, as a function of the distance r (Fig. 2.2a). An exemplary anion–cation RDF for NaCl is shown in Fig. 2.2b. The area under the first peak corresponds to the number of CIPs, the second to the number of SIPs and the third to the number of 2SIPs. Only three distinct peaks are observed for this salt example. Ions in a larger distance than the third peak are usually referred to as free ions. They are totally solvated and their hydration shells neither overlap nor come in contact with hydration shells from other ions. Further, thermodynamic and dynamic properties of aqueous electrolyte solutions are affected by ion pairs. Properties such as osmotic and activity coefficients follow ion-specific series.[312]

The RDF $g(r)$ allows for investigating the PMF defined as

$$W(r) = -\ln g(r) + \ln g(r \to \infty), \tag{2.23}$$

where the RDF is determined either via MD simulations (2.21),[229,310,311] other theoretical concepts[237] or experiments[310] (neutron and X-ray scattering). A typical PMF curve for ions features local minima corresponding to the CIP, SIP and 2SIP states.[167,235,237,313–321] PMFs represent the free-energy landscape along the distance between two ions. Hence, they reveal free energy differences, energy barriers and the relative population between different types of ion pairs.

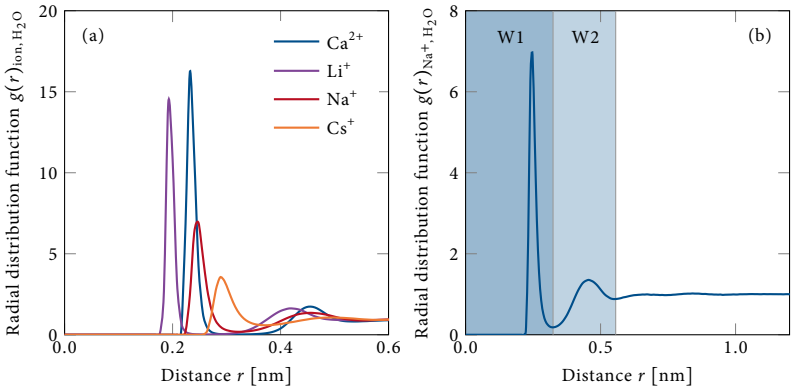

Fig. 2.3 (a) Radial distribution function $g(r)$ between various ions and water oxygen as a function of the distance r compared to a $g(r)$ between water oxygens in pure water. (b) Radial distribution function $g(r)$ between Na^+ and water oxygen as a function of the distance r. The shaded blue areas indicate the different solvation-shell waters: first (W1) and second (W2).

Ion hydration. Most ions, including the large monovalent ones, possess a first hydration shell.[164,322] Strongly hydrated ions also possess a second hydration shell.[322,323] Fig. 2.3a shows some examples of RDFs between various ions and water molecules. Some ions show a strong hydration (e.g., Li^+), which can be seen from a tighter hydration shell than an oxygen–oxygen RDF in pure water. Other ions show a weaker hydration (e.g., Cs^+). Ion hydration numbers can be obtained from computer simulations as the area under the ion–water RDF[324] (Fig. 2.3b) and provide information about the number of water molecules in a specific shell. In analogy to the ion pairs explained above, the first peak corresponds to the primary (first) hydration number and the second peak to the second hydration number. Hydration numbers can also be obtained from diffraction measurements.[324] Hydration numbers indicate thermodynamic affinities but do not provide information about the underlying mechanism driving it. Namely, they provide neither information about the strength of ion–water interactions nor about the movement of the water molecules is given. The hydration number can also be defined from operational methods such as the standard partial molar compressibility of the ion, the fitting of standard Gibbs free energies and enthalpies of hydration to the size of the ions, or from the ionic Stokes radii defining a "Stokes volume" of the hydrated ion.[324]

By taking the hydration shell(s) into account, the effective ion radius in aqueous solutions is affected. Experiments, e.g., conductivity measurements, have proved this.[325] Effective

radii instead of ion radii should be considered, otherwise some properties would show surprising trends. For instance, strongly hydrated ions have a lower mobility than weakly hydrated ions even though they are smaller because of their larger hydration shell.[326]

Law of matching water affinities. Collins formulated the LMWA stating that CIPs are formed spontaneously only between oppositely charged ions when their water affinities are equal.[165] The idea is based on the picture of ions as spheres with centered point charges. The classification of ions depends on their charge density and, hence, their size. Point charges associated with small ions are close to water molecules' point charges of the opposite sign, and distant for large ions. The former leads to a tight hydration shell, i.e., strongly hydrated ions, while the latter leads to a loose hydration shell, i.e., weakly hydrated ions. In addition, the classification depends on the strength of ion–water interactions compared to water–water interactions. The various ion–ion and ion–water interactions can be ranked according to Fig. 2.4. For the same charge density, an anion is more strongly hydrated than a cation.[162,165] This originates from the asymmetric charge distribution of water in the hydration shell.[327–329]

The distance between point charges is crucial for the existence of ion pairing.[165] Owing to strong ion–water interactions for small ions, it is energetically unfavorable to remove water molecules from their hydration shell. However, when replaced with a small ion, the favorable ion–ion interactions overcompensate for it. For large ions, water is released and pairing takes place since the weak ion–ion interactions are overcompensated by stronger water–water interactions. The formation of both types of CIP is energetically favorable. The formation of a CIP between a small and a large ion of opposite charge is energetically unfavorable. A small and a large ion remain soluble since distant point charges lead to weak ion–ion interactions. These interactions can especially not compensate for loss of strong ion–water interactions for the small ion. In summary, two ions of opposite charge and of similar size are prone to form CIPs, since they posses similar hydration energies and have similar water affinities. Two weakly hydrated ions have loosely bound hydration spheres leading to expulsion of the hydration spheres between them. Two strongly hydrated ions show a mutual attraction leading to expulsion of the hydration spheres between them. Ions of dissimilar size remain solvent separated.

2.3 Polymers in aqueous solutions

The properties of polymers, such as solubility, and their behavior in aqueous solutions depends on the chemical structure. In addition, polymer solvation is influenced by the polymer solution composition and temperature.

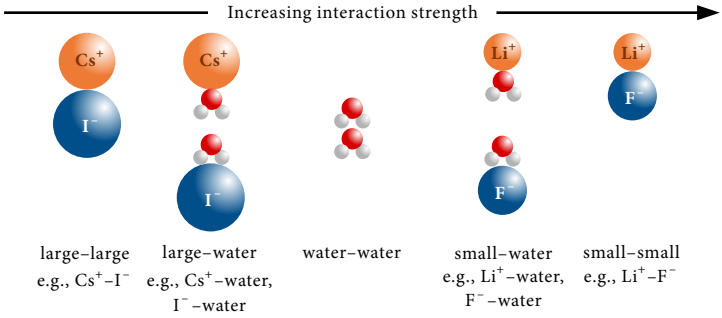

Fig. 2.4 Relative interaction strength of ion–ion, ion–water and water–water interactions for large and small ions.

2.3.1 Basic polymer physics

A polymer is a molecule consisting of repeating units assembling a chain-like structure, long enough such that adding or removing one repeating unit does not effect its properties.[330] The units are referred to as monomers and consist of one group of atoms (homopolymers) or different groups of atoms (copolymers).[330] The process of polymerization is linking the monomers by covalent bonds. Some examples of skeletal structures are linear, cyclic, and nonlinear, such as branched and network.[330] All have in common that their molar mass are large. Therefore, polymers are commonly also referred to as macromolecules. The number-average molar mass is defined as[330]

$$\overline{M}_\mathrm{n} = \frac{\sum N_i M_i}{N_i}, \tag{2.24}$$

where N_i denotes the number and M_i the molar mass of molecule i, while the weight-average molar mass is defined as[330]

$$\overline{M}_\mathrm{w} = \frac{\sum N_i M_i^2}{N_i M_i}. \tag{2.25}$$

The ratio $\overline{M}_\mathrm{w}/\overline{M}_\mathrm{n}$, describes the polydispersity (PDI).[330] It specifies the molar mass distribution range, where a PDI equal to 1 corresponds to a monodisperse polymer and a value of 1.5–2 is common. Polymers, due to long chain structure and flexible nature, can exist in different spatial arrangements (conformations). Stretched chains, i.e., coil conformations, and collapsed chains, i.e., globular conformations are two examples depicted in Fig. 2.5.

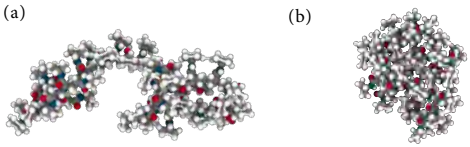

Fig. 2.5 Examples of polymer conformation types, (a) coil and (b) globular conformation.

2.3.2 Thermodynamics of polymer solutions

A binary polymer solution is a mixture where the two components, polymer and solvent (e.g., water), are mixed on a molecular scale.[330] According to the thermodynamic requirement, the formation of a solution takes place when the Gibbs free energy of mixing $\Delta G_\mathrm{m} < 0$.[330] That is, the Gibbs free energy of the mixed solution must be smaller than the sum of the two components' Gibbs free energy. This can be expressed as

$$\Delta G_\mathrm{m} = G_{12} - \left(G_1 + G_2\right), \tag{2.26}$$

where 1 and 2 denote polymer and solvent (water), respectively. Using Eq. (2.1), Eq. (2.26) may also be written as

$$\Delta G_\mathrm{m} = \Delta H_\mathrm{m} - T\Delta S_\mathrm{m}, \tag{2.27}$$

where Δ denotes the change from pure components to mixture, T the temperature, ΔH_m the enthalpy of mixing, and ΔS_m the entropy of mixing.

Experimentally, the thermodynamic stability of states of a binary polymer–solvent mixture can be measured and graphically represented in a phase diagram that shows the phase transition temperature, also known as cloud point, as a function of polymer concentration. An illustration of a temperature-induced phase separation for a binary polymer–solvent mixture is shown in Fig. 2.6. Fig. 2.6a represents systems where the solubility increases with increasing temperature. This behavior results in a concave coexistence curve, a so-called binodal curve, on which two phases may co-exist. It corresponds to the condition where the chemical potentials of the solution components in the polymer-rich and solvent-rich phase are equal. The curve representing the conditions where the second derivative of the free energy is equal to zero is called the spinodal curve. The joint maximum of the two curves corresponds to an upper critical solution temperature (UCST).[330] Above the UCST, polymer and solvent are miscible at any mixture composition and present as a one-phase system. Fig. 2.6b represents systems where the solubility decreases with increasing temperature. This behavior results in a convex coexistence curve with the joint minimum of binodal and spinodal corresponding to a lower critical solution temperature (LCST).[330] Here, polymer and

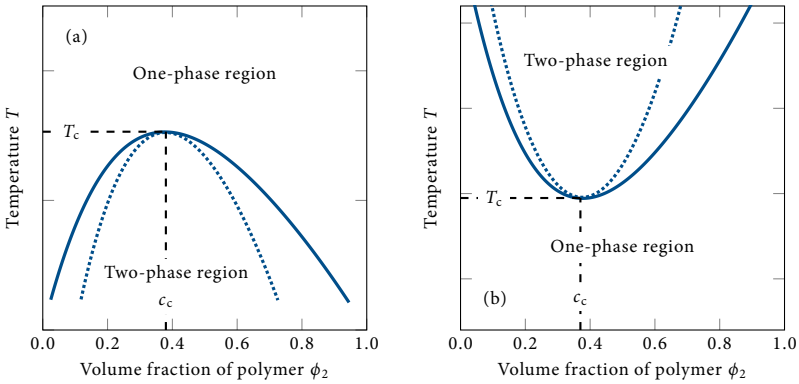

Fig. 2.6 Illustration of polymer solution phase diagrams (temperature T versus the volume fraction of polymer ϕ_2) showing (a) an upper critical solution behavior and (b) a lower critical solution behavior. The solid lines are the binodals, while the dotted lines are spinodals. T_c denotes the upper and lower critical solution temperatures, and c_c the upper and lower critical solution concentrations.

solvent are miscible at any mixture composition below the LCST. Polymers showing an LCST behavior usually indicate polymer–solvent interactions, such as hydrogen bonding or charge transfer.[330]

2.3.3 Stimuli-responsive polymers

Stimuli-responsive (also known as stimuli-sensitive, environmentally sensitive, smart, or intelligent) polymers are polymers that are sensitive to external stimuli.[331–334] Their responsiveness triggers changes in their physical or chemical properties. Usually a small environmental change is enough to cause a large property change because of a highly nonlinear response. External stimuli cover a great variety and are usually divided into three categories: physical, chemical and biological stimuli.[331,333–335] Physical stimuli include changes in temperature, light, magnetic and electric fields, and mechanical forces.[331,333–335] Chemical stimuli include changes in pH, ions, redox and solvent.[331,333–335] Biological stimuli include changes in glucose, enzyme and inflammation.[331,333–335] The responses are manifold, ranging from structural changes, such as shape, volume and size, to conductivity, permeability, opacity and color change.[331,333–335] Polymers being responsive to two or more stimuli are classified as dual and multi stimuli-responsive polymers, respectively.[333,336,337]

Stimuli-responsive polymers are broadly applied in chemistry and material science.

Examples of materials utilizing stimuli-responsive polymers are polymer brushes, films of polymer networks, colloids, micelles, nanogels and membranes.[338] Applications within medical devices,[339] (bio)sensors,[340] drug delivery,[341–344] environmental remediation,[345] and chemo-mechanical actuators[346,347] are other examples. The reader can refer to a number of reviews for more details on stimuli-responsive polymers, their applications and syntheses.[333,334,338,348–352]

Thermoresponsive polymers. The most studied stimulus, and also the best understood, is temperature. Temperature can be varied and tracked easily, which, presumably, is a decisive reason for the intensive examination of thermoresponsive polymers. Thermoresponsive polymers[333,337,353] exhibit a drastic change in solubility when exposed to a temperature variation. Within a small to modest temperature change at the critical solution temperature, the thermoresponsive polymers undergo a phase transition. The LCST is governed by the entropy of the system, i.e., water molecules being less ordered,[354] while the UCST is governed by the enthalpy of the system, i.e., polymer–water hydrogen bonding.[284] In the following, the focus will be on polymers exhibiting an LCST.

At the cloud point, a molecular transition from a coil conformation to a globular conformation takes place minimizing the free energy of the system. Assuming a two-state process (i.e., first order transition) as depicted in Fig. 2.7a, the coil-to-globule equilibrium process can be illustrated as shown in Fig. 2.7b. Macroscopically, the decrease of the polymer solubility with increasing temperature can be observed through a change in the turbidity of the solution (Fig. 2.7c). When increasing the temperature from the cloud point, a transition from a stable one-phase to an unstable two-phase system is observed (Fig. 2.6b). This transition is reversible. Examples of thermoresponsive polymers exhibiting an LCST are poly(*N*-substituted acrylamides), poly(vinyl alcohol) and poly(ethylene oxide).[330,331]

Besides temperature, parameters such as chain length,[355–357] tacticity,[358–361] pressure[362] and the exact nature of the polymer, such as the incorporation of co-monomers[363] and the chemistry of the end group[364,365] affect the LCST of a polymer. Tacticity describes the relative steroechemistry of neighboring monomers' chiral centers.[330] Polymers can be classified as isotactic (all repeating units placed on the same side of the polymer backbone), syndiotatic (alternating placement of repeating units relative the polymer backbone) or atactic (random placement of repeating units).[330]

Poly(*N*-isopropylacrylamide) as a model thermoresponsive polymer. One of the polymers in the poly(*N*-acrylamide) family is PNIPAM. The chemical structure of the NIPAM-monomer is shown in Fig. 2.8. It consists of a backbone of a poly-ethylene chain and of a side chain containing both an amide group and an isopropyl group. PNIPAM contains both hydrophobic moieties (backbone and isoprorpyl group) and a hydrophilic moiety (amide group).[366]

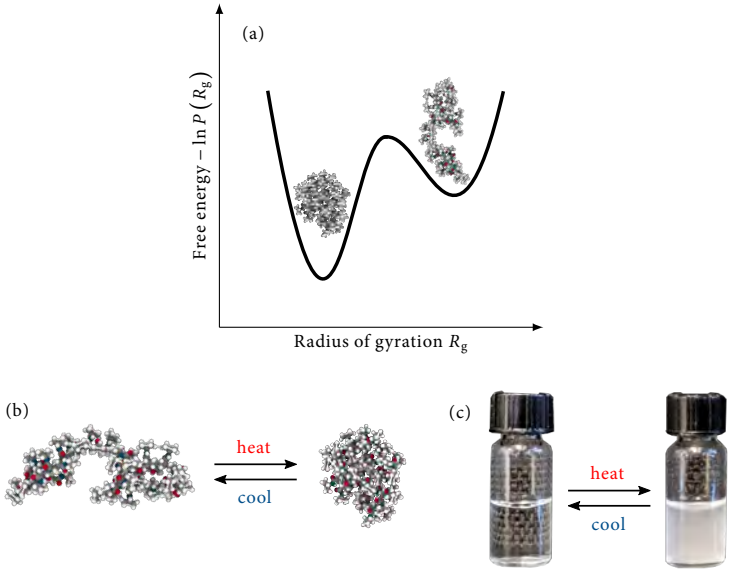

Fig. 2.7 (a) Free energy as a function of the radius of gyration R_g indicating the probability (P) for conformations. (b) Two-state phase equilibrium of a thermoresponsive polymer exhibiting a lower critical solution temperature T_c. Heating the polymer solution above the cloud point temperature shifts the equilibrium to the right, cooling it down shifts it to the left. (c) Equilibrium between soluble (left) and precipitated (right) polymer solution.

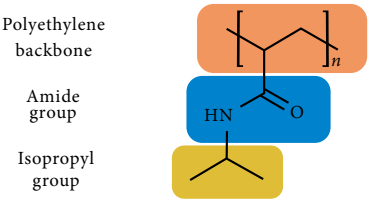

Fig. 2.8 Chemical structure of poly(*N*-Isopropylacrylamide).

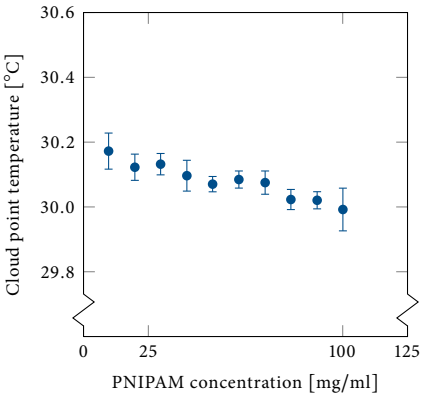

Fig. 2.9 Phase diagram of PNIPAM in water showing the phase transition temperature, i.e., cloud point, as a function of the of PNIPAM. The diagram is reconstructed from Furyk et al. [364].

PNIPAM can be produced by linking monomers using different polymerization techniques such as ionic polymerization,[367] redox polymerization,[368] radiation polymerization,[369] free radical polymerization[370] and living radical polymerization.[371]

The polymer is soluble in cold water and shows an inverse solubility (precipitation) upon heating.[372,373] The transition is reversible, meaning that the polymer becomes soluble again when the temperature decreases below its LCST of 32 °C.[374,375] The phase transition temperature of PNIPAM as a function of the solution composition in pure water is shown in Fig. 2.9. It is characterized by a flat binodal curve, and the LCST is also independent of the molecular weight of PNIPAM.[364,376] PNIPAM is widely used as a prototype polymer with coil-to-globule transition.[377,378] Its coil-to-globule equilibrium process E ⇌ C is illustrated in Fig. 2.7b and is thermodynamically driven by the free energy change. The coil conformation is enthalpically favored, while the globular conformation is entropically favored, and will be discussed below. PNIPAM is also a commonly used polymer for investigations of Hofmeister effects.[4,9,11,13,364,379] Its solubility is ion specific and the modulation of its LCST by anions follows the Hofmeister series.[4]

There is no precise explanation for why PNIPAM collapses in water (i.e., the self-assembly mechanism) above its LCST, but the following is assumed:[375] hydrogen-bonding formation between adjacent water molecules and the amide group and the carbonyl group of PNIPAM aid the solvation of the polymer below its LCST. The nitrogen atom of the amide group acts as a hydrogen bond donor (one hydrogen bond), while the oxygen of the carbonyl group acts as a hydrogen bond acceptor (two hy-

drogen bonds).[374] Meanwhile, water molecules at the polymer–water interface show restricted mobility and, hence, a loss in configurational entropy.[278] However, the enthalpic gain of water molecules through hydrogen bonds dominates below the LCST. During the coil-to-globule transition (Fig. 2.7b and Section 2.4.2), the exposed surface area decreases reducing the hydrogen bonds between water molecules and PNIPAM. This minimization of the polymer (hydrophobic) surface interactions can be explained by the hydrophobic effect (Section 2.1.2). Water molecules around the hydrophobic isopropyl part of the side chain dissociate and, instead, intra-chain hydrogen bonds are formed.[375] In addition to this loss of favorable polymer–water hydrogen-bonding interactions, the conformational entropy of the polymer chain also reduces with the polymer collapse.[380] Despite this loss, and despite the bigger influence of entropy at higher temperature (2.27), the polymer chain still collapses at higher temperature. This can be explained by a solvent-related entropy contribution.[136,380] The polymer chain reduces its excluded volume (Section 2.4.4) by collapsing, leading to a translational entropy gain for the surrounding water molecules.[136] This effect is larger in water than in other solvents due to the small, and hence many, water molecules. This favorable entropy contribution, together with the increase of water entropy originating from the loss of polymer–water hydrogen bonds, overcompensate the counter effects (i.e., conformational entropy reduction of the chain and enthalpic loss of water molecules), when increasing the temperature above the LCST. The hydrophobic interactions between polymer segments are believed to be of importance for the coil-to-globule transition, as well.[374,381,382]

The LCST of PNIPAM in aqueous solutions is sharp and within the physiological temperature range, making it eligible for biological and medical applications.[334,375] Some examples of applications for PNIPAM are in sensors,[340] membranes,[383] polymer brushes[384] and thin films.[385] PNIPAM is also used as a biomaterial in bioseparation, and in drug and gene delivery applications.[375]

2.4 Influence of electrolytes on the solubility of hydrophobic polymers

The collapse of hydrophobic polymers such as PNIPAM is related to polymer solvation and thermodynamic properties associated with it. Salts can affect the phase transition temperature (i.e., polymer collapse) through, for instance, enthalpic (preferential binding) or entropic (solvent-excluded volume) contributions. The KB theory provides information on cosolute effects and their interactions with macromolecules like polymers.

2.4.1 Kirkwood–Buff theory and preferential binding

The relationships between macroscopic and microscopic properties for solutions can be explained using the KB theory.[191] The application of the KB theory is suited for computer simulations investigating cosolute effects on macromolecules, since it is straightforward to apply.

Kirkwood–Buff theory. Pair correlation functions (i.e., molecular distribution functions) can be used to derive thermodynamic properties. The relation is given by the so-called KBI,[191] defined as

$$G_{ij} = G_{ji} = 4\pi \int_0^\infty \left[g_{ij}^{(\mu \mathrm{VT})}(r) - 1 \right] r^2 \mathrm{d}r, \tag{2.28}$$

where $g_{ij}^{(\mu \mathrm{VT})}(r)$ denotes the center of mass based RDF of species i and j defined in the open (T, V, μ) system (Section 3.2). The KBI quantifies the distribution deviation of particles j around the central particles i from a random bulk distribution. From $g_{ij}^{(\mu \mathrm{VT})}(r)$, thermodynamic properties such as compressibility, partial molar volumes and derivatives of chemical potentials can be computed. The resulting expressions for compressibility, partial molar volumes and derivatives of chemical potentials can be written in terms of G_{ij}. The reader is referred to the original paper by Kirkwood and Buff[191] or to books[192] for these expressions. This applies for the derivation of the KB theory, as well. The opposite is possible, too, and is referred to as inversion of the KB theory. Thermodynamic properties can be used to generate G_{ij}, which provides local information even though it is not a molecular property. Primarily, the KB theory, including its inversion, has been applied to two-component systems, since the expressions for multicomponent systems are involved. Another consequence of the complexity of the KB theory for systems with three or more components, is that it has mainly been applied to dilute solutions. When a solute S is very diluted in a mixture of the two components, the KB theory for three components can be applied and examined in the limit of $\rho_S \to 0$.

The KB theory is general and powerful.[192,211] That is, it is exact, it is valid for all types of particles (independent of size and shape), it can be applied to all stable solutions independent of the number of components, it does not assume pairwise additivity of interactions, and it can be be applied to classical and quantum systems.

For the application of the KB theory to aqueous electrolyte solutions, two different approaches can be taken.[192] i) The dissociation of the salt to individual ions (e.g., $\mathrm{NaCl} \to \mathrm{Na}^+ + \mathrm{Cl}^-$) can be ignored and the system is a two-component system consisting of water and salt.[214,218] ii) The dissociation is taken into account leading to a three-component system consisting of water, cations and anions. In case i), the ion–ion correlations are

not taken into account in the KB theory. In case ii), they are, but the thermodynamic properties (e.g., partial molar volumes) are not available.

Preferential binding. The preferential binding of solvent and cosolute with the macromolecule are commonly reported as the preferential binding coefficient. It specifies the relation between the excess number of cosolutes in proximity to the macromolecule and the statistical number for the bulk composition. Multiple approaches have been applied over the years for the derivation of preferential binding coefficients based on the KB theory.[219–224] Herein, the approach by Pierce[211] will be described. From now on, macromolecule refers to a polymer, the solvent to water and the cosolute to a salt. The standard thermodynamic convention for ternary mixtures will be followed: 1 denotes water, 2 the polymer chain, and 3 the salt, i.e., indistinguishable salt ions. The preferential binding coefficient of salt to the polymer Γ_{23} is defined as

$$\Gamma_{23} = \rho_3 \left(G_{23} - G_{21} \right), \tag{2.29}$$

where $\rho_3 = n_3/V$ denotes the bulk number density of the salt ions, n_3 the number of salt ions, and V the volume. G_{23} and G_{21} denote the polymer–salt and polymer–water KBIs, respectively. To underline the nature of the preferential binding coefficient to be an excess quantity, Eq. (2.29) can be rewritten to

$$\Gamma_{23} = N_{23} - \frac{\rho_3}{\rho_1} N_{21}, \tag{2.30}$$

where $N_{ij} = \rho_j G_{ij}$ denotes the excess coordination number. $\Gamma_{23} < 0$ implies an excess of solvent molecules over cosolute molecules, and $\Gamma_{23} > 0$ an excess of cosolute molecules over solvent molecules. Eq. (2.29) expresses the relation between the preferential binding coefficient and the cosolute concentration. A constant $G_{23} - G_{21}$ yields a linear dependence of Γ_{23} on the salt concentration ρ_3.[18] Thus, a salt concentration independent behavior for the difference between the water–salt and the polymer–water affinity is seen. This will be reflected in a linear LCST as a function of salt concentration. In contrast, for a value of $G_{23} - G_{21}$ that changes with salt concentration, a nonlinear LCST is expected. Depending on larger or smaller affinity of ions over water molecules, a favorable partitioning to or depletion of the ions from the polymer chain is observed.

In order to apply Eq. (2.29) to computer simulations, some approximations are necessary. The reason is that simulations are usually carried out in closed systems. KBIs need to be truncated at a distance where the RDF converges to unity and surface referenced RDFs need to be used. The second approximation deals with the convergence issue.[386] Additionally, a correction to the bulk solution distribution is required when investigating the preferential binding coefficient as a function of the distance from the polymer.[387] Molecules (water and ions) that are counted to the bulk distribution will be counted

to the local distribution as the distance to the polymer is increasing. Therefore, the approach of Pierce[211] is used to calculate the preferential binding coefficient from computer simulations. It reads

$$\Gamma_{23} = \left\langle n_3(r) - \frac{N_3 - n_3(r)}{N_1 - n_1(r)} n_1(r) \right\rangle, \tag{2.31}$$

where N_1 and N_3 denote the total numbers of water molecules and salt ions in the system, respectively, and $n_1(r)$ and $n_3(r)$ denote the local numbers of water molecules and salt ions within a specific distance r to the polymer, respectively. The angle brackets $\langle\cdot\rangle$ denote time averaging. That is, the sign of Γ_{23} at large values of r specifies favorable partitioning (positive preferential binding) or a depletion (negative preferential binding) of ions. On account of the r^2 weighting term in Eq. (2.28), the KBIs become increasingly sensitive to deviations from bulk at larger distances from the polymer and are, thus, prone to noise.[388] The convergence at large distances from the polymer is, therefore, commonly a challenge when computing preferential binding coefficients.[389]

The preferential binding coefficient provides information about the polymer's collapse process and is commonly used when investigating the solubility of macromolecules (polymers and proteins). Wyman[209] proposed and Tanford[390] extended the relation linking the preferential binding coefficient to cosolute effects on the polymer collapse equilibrium. The change in the preferential binding coefficient together with the conformation change from an extended (E) to a collapsed (C) state is investigated. The equilibrium constant K of the polymer collapse equilibrium and the cosolute activity a_3 at a given temperature, pressure and solution composition is related to the change in the preferential binding through

$$\left(\frac{\partial \ln K}{\partial \ln a_3}\right)_{T,P} = \Delta\Gamma_{23}^{\mathrm{E}\to\mathrm{C}}, \tag{2.32}$$

where $\Delta\Gamma_{23}^{\mathrm{E}\to\mathrm{C}} = \Gamma_{23}^{\mathrm{C}} - \Gamma_{23}^{\mathrm{E}}$. To account for solvent nonideality

$$\left(\frac{\partial \ln a_3}{\partial \ln c_3}\right)_{T,P} = \frac{1}{1 + \rho_3 \left(G_{33} - G_{31}\right)}, \tag{2.33}$$

can be used to rewrite Eq. (2.32) to

$$\left(\frac{\partial \ln K}{\partial \ln c_3}\right)_{T,P} = \frac{\Delta\Gamma_{23}^{\mathrm{E}\to\mathrm{C}}}{1 + \rho_3 \left(G_{33} - G_{31}\right)}. \tag{2.34}$$

Here, G_{33} and G_{31} denote the salt–salt and salt–water KBIs, respectively, and the denominator is positive.[192] If the numerator is positive as well, ions prefer the collapsed state over the extended state. Conversely, ions prefer the extended state if it is negative.

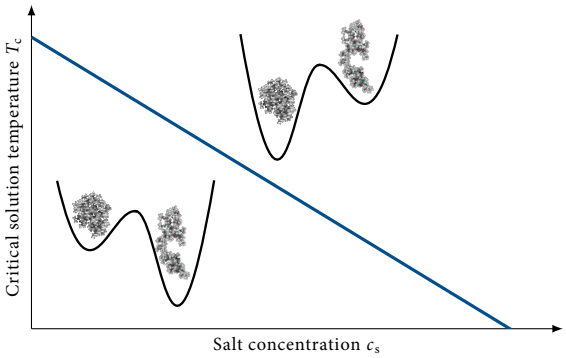

Fig. 2.10 Critical solution temperature T_c as a function of the salt concentration c_s depicting the salt effect on the first-order coil-to-globule transition. The insets on each side of the lower critical solution temperature line illustrate the conformation probability indicated by the free energy as a function of radius of gyration.

Hence, by means of MD simulations and employing Eq. (2.34), predictions of salt effects on the polymer collapse equilibrium can be made.

2.4.2 Thermodynamics of hydrophobic polymer collapse

Water-soluble polymers like PNIPAM can be described by a two-state consideration similar to proteins.[391,392] The coil-to-globule transition (Fig. 2.7b) describes the transition between the two states. A first-order and discontinuous transition is illustrated in the insets in Fig. 2.10, showing a decrease of the LCST of a polymer as a function of salt concentration. The line represents the 50:50 probability for the two states. The probability for the collapsed state is higher above the LCST, and higher for the extended state below the LCST. Note, neither the extended nor the collapsed state are uniquely defined for flexible polymers. However, in order to differentiate the two states structurally, degenerated states can be distinguished by using an appropriate size metric, such as the radius of gyration (i.e., mean position of monomers with respect to the center of mass).[393–395] For the example illustrated in Fig. 2.10, an addition of salts (or other cosolutes) will shift the equilibrium to the collapsed state. This is reflected in a lower free energy minimum for a smaller radius of gyration. Opposite effects may be observed (Section 2.4.3).

The equilibrium constant K controls the ratio between the extended and collapsed conformations. It is related to the free energy difference between the collapsed (globular

conformation) and extended (coil conformation) state through

$$K = \exp\left(-\frac{\Delta G^{\mathrm{E}\to\mathrm{C}}}{\mathrm{R}T}\right), \tag{2.35}$$

where R denotes the ideal gas constant and T the temperature. While a change in the solvation free energy for small molecules can be explained by Eqs. (2.4) and (2.7), the solvation of polymer chains include additional terms. That is, the free energy difference for the polymer equilibrium process E ⇌ C accounts for the difference in the solvation free energies (chemical potential) of the collapsed and extended chains, as well as for an intramolecular part. This can be written as[380]

$$\Delta G^{\mathrm{E}\to\mathrm{C}} = \Delta\mu^{*\mathrm{E}\to\mathrm{C}} + \Delta G^{\mathrm{E}\to\mathrm{C}}_{\mathrm{intra}}, \tag{2.36}$$

with

$$\Delta\mu^{*\mathrm{E}\to\mathrm{C}} = \mu^{*}_{\mathrm{C}} - \mu^{*}_{\mathrm{E}}, \tag{2.37}$$

and

$$\Delta G^{\mathrm{E}\to\mathrm{C}}_{\mathrm{intra}} = \Delta E^{\mathrm{E}\to\mathrm{C}}_{\mathrm{intra}} - T\Delta S^{\mathrm{E}\to\mathrm{C}}_{\mathrm{conf}}. \tag{2.38}$$

Here, μ^{*}_{C} and μ^{*}_{E} denote the excess chemical potential for the collapsed and extended conformations, respectively, $\Delta E^{\mathrm{E}\to\mathrm{C}}_{\mathrm{intra}}$ denotes the change in polymer intramolecular (intra) potential energy upon chain collapse, and $\Delta S^{\mathrm{E}\to\mathrm{C}}_{\mathrm{conf}}$ the corresponding change in the polymer conformational (conf) entropy. The interested reader can refer to the literature[380] for details on Eq. (2.36).

Using Eqs. (2.4) and (2.7) by inserting Eq. (2.38), Eq. (2.36) can be rewritten as

$$\Delta G^{\mathrm{E}\to\mathrm{C}} = \Delta E^{\mathrm{E}\to\mathrm{C}}_{\mathrm{intra}} + \Delta E^{\mathrm{E}\to\mathrm{C}}_{\mathrm{uv}} - T\left(\Delta S^{\mathrm{E}\to\mathrm{C}}_{\mathrm{conf}} + \Delta S^{\mathrm{E}\to\mathrm{C}}_{\mathrm{uv}}\right). \tag{2.39}$$

Here, the definitions

$$\Delta E^{\mathrm{E}\to\mathrm{C}}_{\mathrm{pv}} \equiv \Delta E^{\mathrm{E}\to\mathrm{C}}_{\mathrm{intra}} + \Delta E^{\mathrm{E}\to\mathrm{C}}_{\mathrm{uv}}, \tag{2.40}$$

and

$$\Delta S^{\mathrm{E}\to\mathrm{C}}_{\mathrm{pv}} \equiv \Delta S^{\mathrm{E}\to\mathrm{C}}_{\mathrm{conf}} + \Delta S^{\mathrm{E}\to\mathrm{C}}_{\mathrm{uv}}, \tag{2.41}$$

which have been introduced for frozen polymer chains,[380] are used to simplify the expression. The pv-terms include contributions from both internal polymer changes and polymer–solvent interactions. For frozen polymer chains, Eq. (2.39) can now be rewritten as

$$\Delta G^{\mathrm{E}\to\mathrm{C}} = \Delta E^{\mathrm{E}\to\mathrm{C}}_{\mathrm{pv}} - T\Delta S^{\mathrm{E}\to\mathrm{C}}_{\mathrm{pv}}. \tag{2.42}$$

The polymer solubility is studied at the LCST where the polymer and solvent start to phase separate. At this critical temperature the system is in equilibrium and $\Delta G^{\mathrm{E}\to\mathrm{C}} = 0$.

The critical temperature T_c can therefore be defined as

$$T_c = \frac{\Delta E_{pv}^{E\to C}}{\Delta S_{pv}^{E\to C}} = \frac{\Delta H^{E\to C}}{\Delta S^{E\to C}}, \tag{2.43}$$

where Eq. (2.1) is used to obtain the second equality. Here, $\Delta H^{E\to C}$ and $\Delta S^{E\to C}$ denote the collapse enthalpy and collapse entropy, respectively. Salts suppress T_c causing polymer collapse. This suppression upon addition of salt can originate from an enthalpic change ($\Delta\Delta E_{uv}^{E\to C}$), an entropy change ($\Delta\Delta S_{uv}^{E\to C}$), or from a combination of both contributions. This will be explained in the following sections.

2.4.3 Salt effects on the lower critical solution temperature

The critical solutions temperature T_s of a polymer in an aqueous salt solution is a function of the salt concentration c_s. The addition of a salt leads to a decrease or increase of the polymer solubility, owing to whether the added salt alters the transition temperature upward or downward relative the experimental temperature. A decrease of the LCST as a function of salt concentration is depicted in Fig. 2.11a, while an increase of the LCST as a function of salt concentration is depicted in Fig. 2.11b. For polymers with an LCST, $\Delta E_{pv}^{E\to C}$ and $\Delta S_{pv}^{E\to C}$ are both positive. A change in either one or both upon the addition of salt leads to a change of the LCST (2.43). Strongly hydrated anions affect $\Delta S_{pv}^{E\to C}$, but typically have a negligible impact on $\Delta E_{pv}^{E\to C}$. The decrease in T_c for these ions originates from an increase in $\Delta S_{pv}^{E\to C}$ caused by the so-called solvent-excluded volume effect (Section 2.4.4) as the underlying driving force. Weakly hydrated anions interact with the polymer and, therefore, affect not only $\Delta S_{pv}^{E\to C}$ but also $\Delta E_{pv}^{E\to C}$. That is, T_c is affected by both $\Delta E_{pv}^{E\to C}$ and $\Delta S_{pv}^{E\to C}$. A counterbalance between the two contributions, favorable polymer–ion interactions and solvent-excluded volume effect, leads to the salt concentration-dependent behavior for weakly hydrated ions.

PNIPAM in an aqueous solution with a strongly hydrated salt, e.g., NaCl or Na_2SO_4,[4] as a cosolute is an example of a system with linear salting-out behavior (Fig. 2.11a). PDEA in an aqueous solution with urea as a cosolvent[396] is an example of a system with linear salting-in behavior (Fig. 2.11b). T_c can also have a nonlinear trend with an inversion of the solubility behavior. This behavior usually originates from polymer–ion interactions.[4,118] For example, PNIPAM in an aqueous solution with a weakly hydrated salt, e.g., NaI, as a cosolute[4] shows a slight increase of the LCST (salting-in) at low salt concentrations followed by a decrease (salting-out) at higher concentrations after the maximum in the LCST was reached.

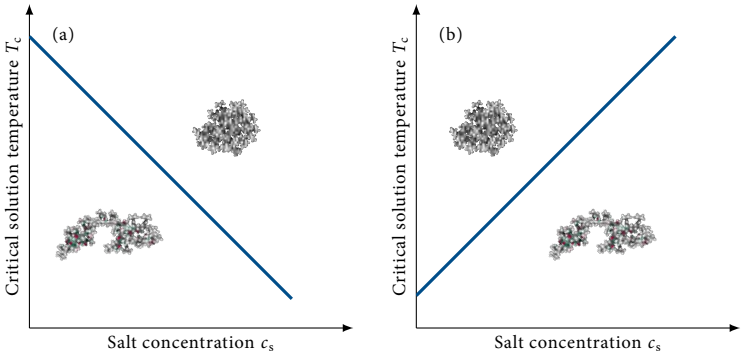

Fig. 2.11 (a) Decrease and (b) increase of the critical solution temperature T_c as a function of the salt concentration c_s. Snapshots of extended and collapsed polymer chains represent typical conformations at the respective salt concentration and temperature.

2.4.4 Effect of solvent-excluded volume on polymer solubility

The concept of solvent-excluded volume effects is crucial for a molecular understanding of how $\Delta S_{pv}^{E\to C}$ affects the LCST (2.43), both for strongly and weakly hydrated salts. For a bulk solvent to host a solute (e.g., polymer), local solvent density fluctuations creating an empty space (a cavity) of the size of the solute are necessary. This is referred to as the solvent-excluded volume effect.[136] It is solely an entropic contribution and is a part of the excess chemical potential (Eq. (2.8)). The excluded volume of a molecule is equal to the volume inaccessible for other molecules due to the presence of the molecule itself. For polymers, it implies that two parts of the chain cannot occupy the same space. It also has the consequence that the ends of the chain are further apart than in the absence of excluded volume (ideal chain).[330]

For electrolyte solutions, the solvent-excluded volume effect depends on the type of ion (i.e., ion hydration).[397] The addition of a strongly hydrated salt to an aqueous solution suppresses the solvent-density fluctuations, causing the polymer to collapse. This conduces to a decrease of the solvent-excluded volume. It is freed into the bulk and turned into an available space for water molecules and ions. This increases the translational entropy for ions, and is the driving force for polymer collapse.[398] This process is depicted in Fig. 2.12. The effect is larger for higher salt concentrations.

Of course, this is different for weakly hydrated salts. A swelling of the polymer chain and, thus, an increase of the solvent accessible surface area occur at low salt concentrations,

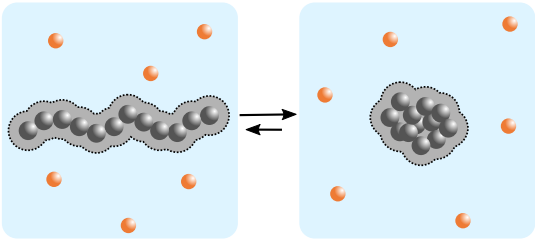

Fig. 2.12 Solvent-excluded volume effect leads to polymer collapse due to an increase of translational entropy for the salts (orange spheres) and water molecules resulting from a smaller excluded volume (gray area around polymer).

owing to the weakly hydrated ions' attractive interactions with the polymer. For this to occur, a cavity for the chain to expand into is needed. A weaker solvent-excluded volume effect (i.e., smaller suppression of the solvent-density fluctuations) than caused by the strongly hydrated ions enables this cavity formation. At larger salt concentration, however, favorable polymer–ion interactions are not enough to overcompensate the solvent-excluded volume effect.

2.5 Experimental techniques

Ion-specific effects in aqueous solutions containing salts with or without polymers (or other macromolecules) can be investigated using thermodynamic techniques, such as phase transition temperature measurements, or spectroscopic techniques, such as VSFS.[2] Specifically, the polymer collapse behavior and ions behavior, as well as their influence on adjacent water molecules close to an air–polymer–water interface are examined.

2.5.1 Phase transition temperature measurements

Phase transition temperature measurements are carried out to determine the LCST of a polymer as a function of salt concentration. The measurements allow for the investigation of noncovalent interactions crucial for the hydrophobic collapse of thermoresponsive polymers in salt solutions. Such temperature measurements can be

[2] The experiments are briefly described here to assist the understanding of the presented research in the following chapters. They were performed in collaboration with the Cremer Research Group at the Department of Chemistry and the Department of Biochemistry and Molecular Biology, Pennsylvania State University, University Park, Pennsylvania 16802, USA.

done using a commercial melting point temperature apparatus. Polymer–salt solutions are loaded in glass capillary tubes, which are sealed on one end and open on the other, and placed in the apparatus. The LCST is determined from a scan of a temperature range around the expected LCST value. This is done by ramping the temperature of the tubes from low to high temperature, with a certain temperature increase per minute. Simultaneously, the light scattering is measured in real-time. More precisely, the turbidity change of the solution is measured using a digital image processing technology. At low temperatures, the polymer–salt solution appears transparent due to soluble and extended chains (Fig. 2.7c). This solution does not scatter light. At temperatures above the LCST, the polymer–salt solution appears cloudy due to collapsed and aggregated polymer chains (Fig. 2.7c). This solution scatters light. By measuring the onset of light scattering intensity relative to the flat and low-intensity baseline observed at cold temperatures, the LCST can be determined.

2.5.2 Vibrational sum frequency spectroscopy

Surfaces and interfaces such as polymer, protein or lipid monolayers at an air–water interface can be analyzed using VSFS.[399] The spectroscopic technique can be utilized to investigate the influence of ions on the hydration shell water molecules of the polymer, and, hence, on polymer–ion interactions upon addition of different salts. Specifically, an air–polymer–water interface containing a Gibbs monolayer of the polymer and salt in the subphase can be probed, as illustrated in Fig. 2.13. The basis for the technique is sum frequency generation (SFG), a second order nonlinear process.[399–403] The incoming electric field consists of two frequencies ω_{VIS} and ω_{IR}, generated simultaneously by two incoming pulsed laser beams, a fixed visible (VIS) and a tunable infrared (IR) beam. An overlap, in time and space, of the two beams on a medium induces emitted light at the sum of the two frequencies $\omega_{\mathrm{SF}} = \omega_{\mathrm{VIS}} + \omega_{\mathrm{IR}}$ (Fig. 2.13, top).[399–403] The emitted light is referred to as the sum frequency (SF) beam. The method is coherent, meaning that the properties of the incoming beams are decisive for the magnitude, direction and phase of the SF beam.[399–401] An IR frequency corresponding to a vibrational mode of the investigated molecules leads to a resonant enhancement of the intensity of the SF light.[399,401] The SFG process arises from surface nonlinear polarization $\boldsymbol{P}^{(2)}(\omega_{\mathrm{VIS}} + \omega_{\mathrm{IR}})$ of the medium. The VSFS (or SFG) intensity I_{VSFS} is given by[399]

$$I_{\mathrm{VSFS}} \propto |\chi^{(2)}|^2 I_{\mathrm{VIS}} I_{\mathrm{IR}}, \tag{2.44}$$

where I_{VIS} and I_{IR} denote the intensities of the respective incoming beams, and $\chi^{(2)}$ denotes the second-order nonlinear susceptibility. The latter can be split into contri-

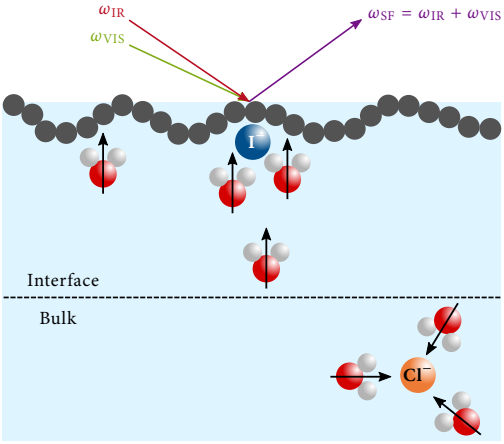

Fig. 2.13 Schematic illustration of a vibrational sum frequency spectroscopy setup where two incoming beams, a fixed visible (VIS) and a tunable infrared (IR) beam, generate a sum frequency (SF) beam. The chain of gray spheres represents the polymer, blue the weakly hydrated iodide ion, orange the strongly hydrated chloride ion, red and white the water molecules, and the black arrows indicate the direction of the water dipoles in the three cases: pure water solution (left), weakly hydrated salt solution (center) and strongly hydrated salt solution (right).

butions

$$\chi^{(2)} = \chi^{(2)}_{NR} + \chi^{(2)}_{R}, \tag{2.45}$$

where $\chi^{(2)}_{NR}$ and $\chi^{(2)}_{R}$ denote the nonresonant and resonant susceptibility terms, respectively. The latter is frequency-dependent, while the former is not. The resonant part of the vibrational modes can be further expressed as [400]

$$\chi^{(2)}_{R} = \sum_{n} \frac{A_n}{\omega_{IR} - \omega_n + i\Gamma_n}, \tag{2.46}$$

where n denotes the n-th resonant mode, A_n the oscillator strength, ω_n the resonant frequency, and Γ_n the peak width.

The molecular response caused by the input beams is reflected in the $\chi^{(2)}$ term.[399] Only SF-active molecular vibrational modes can be detected.[399] It requires an asymmetric environment, which cannot be found in isotropically distributed (centrosymmetric) bulk solutions but at interfaces (not centrosymmetric). Additionally, a net polar orientation of the molecules of interest is required. By scanning the IR laser over a range of frequencies, a vibrational spectrum is obtained.[399] The VSFS signal can be collected in different regions, for example in the CH stretch region from 2800 cm^{-1} to 3000 cm^{-1} and in the

OH stretch region from 3000 cm^{-1} to 3800 cm^{-1}. The generated vibrational spectra provide information about molecules at the interface, such as the polar orientation,[399] molecules' ordering at the interface[399] and the interfacial water structure.[404] VSFS is surface-specific, and a particular advantage is the good molecular selectivity due to the scanned IR frequency generating vibrational transitions.[403]

In particular, VSFS allows for studying interactions between salt ions and polymer surfaces as illustrated in Fig. 2.13. In a pure water solution (Fig. 2.13, left), water molecules are randomly oriented and close to the surface, only few are aligned. With the addition of a weakly hydrated anion, such as I^- binding to the polymer interface, the surface charges up creating an electric field and aligning the water molecules in the hydration shell of the polymer (Fig. 2.13, center). This amplifies the measured OH intensity. In contrast, added strongly hydrated anions, such as Cl^-, remain in the bulk, generate no net polar orientation (Fig. 2.13, right), and, hence, do not influence the OH signal.

Chapter 3

Molecular dynamics simulations

MD simulations are numerical experiments performed using the computer as a virtual laboratory. Hence, they are similar to lab experiments. Macroscopic quantities can be calculated from a microscopic model system through the use of statistical mechanics. In this chapter, the MD simulation process is described, including algorithms, functional forms, and parameters of the intra- and intermolecular interactions. This chapter is based on selected textbooks within the field. [229,310,311]

3.1 Statistical mechanics

Macroscopic thermodynamic properties of a system can be calculated from properties of individual molecules using statistical mechanics. An N-particle system can be described in atomistic detail by specifying the positions $\boldsymbol{r}$ and momenta $\boldsymbol{p}$ of all particles. A point $(\boldsymbol{r}^N, \boldsymbol{p}^N)$ in a $6N$-dimensional space (three coordinates and three components of the momentum per particle) constitutes a microstate. All possible microstates of a system constitute its phase space. From the phase space distribution of microstates, all thermodynamics properties are accessible. The instantaneous value of a property G at time t can be written as $G\left(\boldsymbol{r}^N(t), \boldsymbol{p}^N(t)\right)$. However, solving the theory for many-particle systems is nearly impossible and impractical. Instead, the concept of thermodynamics that the macroscopic state of a system can be described by only a small set of variables is employed. This is possible since the quantities determined from experiments are time averages. Statistical mechanics [405] provides the link between the given microscopic details of a system and the average macroscopic quantities.

For systems with a fixed number of particles N, volume V, and total energy E, all possible microstates are equally likely. This is a fundamental postulate. However, in most experiments, instead of the total energy, the temperature T is fixed. This leads to

different probabilities for different microstates. The probability follows the Boltzmann distribution

$$P\left(\boldsymbol{r}^N, \boldsymbol{p}^N\right) = \frac{\exp\left[-\beta H\left(\boldsymbol{r}^N, \boldsymbol{p}^N\right)\right]}{\iint \exp\left[-\beta H\left(\boldsymbol{r}^N, \boldsymbol{p}^N\right)\right] \mathrm{d}\boldsymbol{r}^N \mathrm{d}\boldsymbol{p}^N}, \tag{3.1}$$

where $\beta = 1/(\mathrm{k_B}\, T)$ and $\mathrm{k_B}$ denotes the Boltzmann constant, and $H\left(\boldsymbol{r}^N, \boldsymbol{p}^N\right)$ the Hamiltonian. The latter allows for deriving the equations of motion of the system. The Hamiltonian is the total energy (sum of kinetic energy K and potential energy V), $H = K + V$. The equilibrium average of a quantity G is then defined as

$$\langle G \rangle = \iint G\left(\boldsymbol{r}^N, \boldsymbol{p}^N\right) P\left(\boldsymbol{r}^N, \boldsymbol{p}^N\right) \mathrm{d}\boldsymbol{r}^N \mathrm{d}\boldsymbol{p}^N, \tag{3.2}$$

where $\langle \cdot \rangle$ indicates the ensemble (statistical) average. The ensemble average of a property in a macroscopic system is the average over all possible states of the system. By combining Eqs. (3.1) and (3.2) the statistical average of G can be defined as

$$\langle G \rangle = \frac{\int G\left(\boldsymbol{r}^N\right) \exp\left[-\beta V\left(\boldsymbol{r}^N\right)\right] \mathrm{d}\boldsymbol{r}^N}{\int \exp\left[-\beta V\left(\boldsymbol{r}^N\right)\right] \mathrm{d}\boldsymbol{r}^N}. \tag{3.3}$$

Here, it is assumed that the averaged quantity G and the potential energy V are both only dependent on the particles' position.

3.2 Ensembles

A statistical ensemble is a collection of all possible microscopic states of the real system having the same thermodynamic or macroscopic properties. It can be seen as the system's state probability distribution. The microcanonical ensemble, also known as NVE ensemble, is common. It allows for studying the time evolution of a system of volume V with N particles at constant energy E. However, in order to relate MD simulation results to most macroscopic physical properties measured in laboratories, where typically temperature and pressure are fixed, other ensembles are desired. The most common ones are the canonical (NVT) ensemble, the isothermal–isobaric (NPT) ensemble and the grand canonical (μVT) ensemble. In each case, the indicated three thermodynamic quantities are the ones kept constant. The NVT ensemble is a closed thermodynamic system with a fixed number of particles in a fixed volume at constant temperature. The NPT ensemble is a closed thermodynamic system with fixed number of particles at constant pressure and temperature. The μVT ensemble is an open thermodynamic system with fixed chemical potential, volume and temperature. Choosing an ensemble other than NVE leads to modifications of the equations of motion. This is done by

using thermostats and barostats (Section 3.5) for NVT and NPT ensembles. For a μVT ensemble, the system is in thermal and chemical equilibrium with a reservoir.

3.3 Concept of molecular dynamics

Calculating the average of a quantity analytically according to Eq. (3.3), is nearly impossible and impractical for many-particle systems. This is due to the large number of degrees of freedom and the coupled particle interactions. Instead, a numerical approach is desired. The average quantity can be computed with computer simulations, either as a time average using MD, or as an ensemble average using Monte Carlo. The basic concepts of MD simulations for an NVE ensemble are be presented below.

MD simulations evaluate the motion of a number of particles in a system by solving Newton's equation of motion for every particle in successive time steps. The equation is given by

$$\boldsymbol{F}_i = m_i \frac{\mathrm{d}^2 \boldsymbol{r}_i(t)}{\mathrm{d}t^2} = -\frac{\partial U\left(\boldsymbol{r}^N\right)}{\partial \boldsymbol{r}_i}, \tag{3.4}$$

where $\boldsymbol{F}_i$ denotes the force acting on particle i in the system, m_i the mass of particle i, $\boldsymbol{r}_i$ the position vector of particle i and t the time. U denotes the potential function and depends on the position of all particles in the system. Equation (3.4) cannot be solved analytically for many-particle systems. Instead a numerical integration scheme is applied. The MD procedure is shown in Fig. 3.1.

First, a system with specified initial particle positions and associated velocities is built. The positions can be generated from a random distribution. Velocities can be selected from a Maxwell–Boltzmann distribution

$$P(v) = 4\pi \left(\frac{m}{2\pi \mathrm{k_B} T}\right)^{\frac{3}{2}} v^2 \exp\left[-\frac{mv^2}{2\mathrm{k_B} T}\right], \tag{3.5}$$

where $P(v)$ denotes the probability distribution of the velocities v, m the particle mass, $\mathrm{k_B}$ the Boltzmann constant and T the temperature of the system. The distribution of the velocities at equilibrium is related to a chosen temperature through the average kinetic energy K by using

$$\left\langle \frac{1}{2} m v^2 \right\rangle = K = \frac{3}{2} N \mathrm{k_B} T, \tag{3.6}$$

where N denotes the number of particles in the system. Equation (3.6) holds for simple particles with three degrees of freedom.

In each iteration step, new particle positions and velocities are predicted based on the current forces $\boldsymbol{F}_i$ acting on each particle i. The forces are determined by the negative

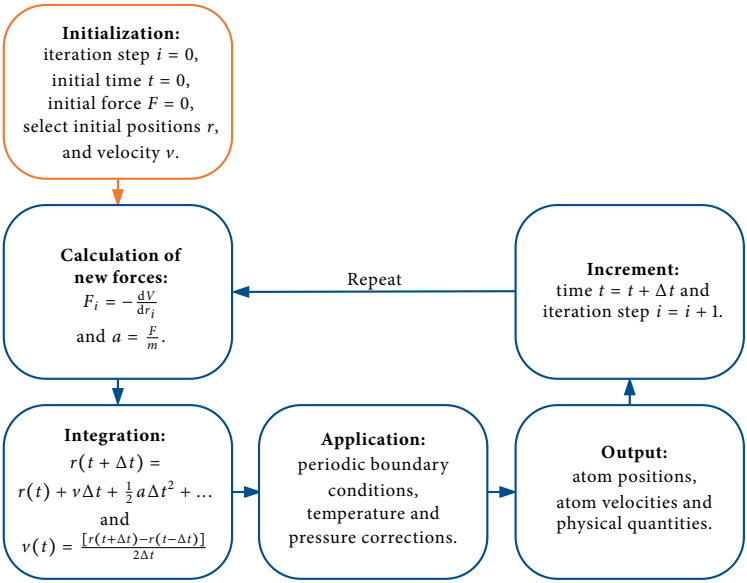

Fig. 3.1 Flow chart of the molecular dynamics simulation process.

derivative of the potential energy V according to Eq. (3.4). The potential is characterized by a set of parameters and is usually referred to as a force field (Section 3.6). The precision of the force field determines the accuracy of MD simulation. Subsequently, forces are recalculated and used to correct the position of the particles. The present particle position and the previous position together with the force acting on the particle are used to predict the next position and not the velocities themselves. In each cycle, boundary conditions (Section 3.4), and temperature and pressure corrections (Section 3.5) are applied to maintain a stable system. An output containing initial and time-dependent atom positions and velocity vectors is written for every particle in the system and at every time step to obtain a trajectory. The time and iteration steps are updated and the numerical integration is repeated n times using an integrator algorithm.

One such algorithm is the Verlet algorithm that uses a Taylor series expansion to numerically obtain the position of particle i at $t + \Delta t$

$$\boldsymbol{r}_i(t + \Delta t) = \boldsymbol{r}_i(t) + \boldsymbol{v}_i(t)\Delta t + \frac{1}{2}\boldsymbol{a}_i(t)\Delta t^2 + \frac{1}{6}\frac{\mathrm{d}^3\boldsymbol{r}_i}{\mathrm{d}t^3}\Delta t^3 + \mathcal{O}\left(\Delta t^4\right), \tag{3.7}$$

and at $t - \Delta t$

$$\boldsymbol{r}_i(t - \Delta t) = \boldsymbol{r}_i(t) - \boldsymbol{v}_i(t)\Delta t + \frac{1}{2}\boldsymbol{a}_i(t)\Delta t^2 - \frac{1}{6}\frac{\mathrm{d}^3\boldsymbol{r}_i}{\mathrm{d}t^3}\Delta t^3 + \mathcal{O}\left(\Delta t^4\right), \tag{3.8}$$

where $\boldsymbol{a}_i = \boldsymbol{F}_i/m_i$ is the acceleration representing the force acting on the particle. By combining Eqs. (3.7) and (3.8), the Verlet algorithm can calculate the position of a particle at $t + \Delta t$ through

$$\boldsymbol{r}_i(t+\Delta t) = 2\boldsymbol{r}_i(t) - \boldsymbol{r}_i(t-\Delta t) + \boldsymbol{a}_i(t)\Delta t^2 + \mathcal{O}\left(\Delta t^4\right) \approx 2\boldsymbol{r}_i(t) - \boldsymbol{r}_i(t-\Delta t) + \boldsymbol{a}_i(t)\Delta t^2. \tag{3.9}$$

The different particle positions at $t + \Delta t$ and $t - \Delta t$ can be used to calculate the velocity using

$$\boldsymbol{v}_i(t) = \frac{\boldsymbol{r}_i(t+\Delta t) - \boldsymbol{r}_i(t-\Delta t)}{2\Delta t}. \tag{3.10}$$

Since the algorithm requires information about the position at t and $t - \Delta t$, it is memory-intensive.

In order to overcome this drawback, various recent algorithms have been developed. The velocity Verlet algorithm and the leap-frog algorithm are among the most common ones. The leap-frog algorithm calculates the velocities at $t + 1/2\Delta t$ by using

$$\boldsymbol{v}_i(t + \frac{1}{2}\Delta t) = \boldsymbol{v}_i(t - \frac{1}{2}\Delta t) + \boldsymbol{a}_i(t)\Delta t. \tag{3.11}$$

Velocities *leap* over the positions calculated at Δt by

$$\boldsymbol{r}_i(t + \Delta t) = \boldsymbol{r}_i(t) + \boldsymbol{v}_i(t + \frac{1}{2}\Delta t)\Delta t. \tag{3.12}$$

Trajectories can be used to calculate averaged macroscopic properties, such as temperature and pressure. They can also be used for post processing to calculate desired properties as a function of time or a time average. Owing to the use of time steps Δt, MD trajectories are discretized and not continuous in time. Hence, the time average of a property is calculated from

$$\langle G \rangle = \frac{1}{M}\sum_{n=1}^{M} G\left(\boldsymbol{r}^N, \boldsymbol{p}^N\right), \tag{3.13}$$

where $\langle \cdot \rangle$ indicates the time average and M denotes the number of integration steps performed. Of course, a sufficient number of integration steps is necessary. According to the ergodic hypothesis, the time average from a single MD simulation given by Eq. (3.13) and the ensemble average given by Eq. (3.2) are equal if if the simulation sampling is long enough. Hence, the intention of MD simulations is to generate as

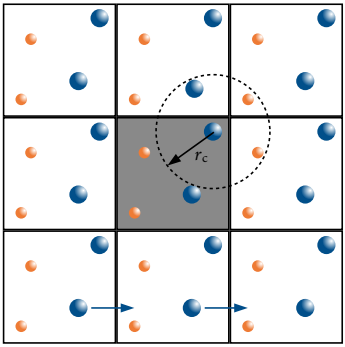

Fig. 3.2 Two dimensional depiction of the periodic boundary condition. The gray box illustrates the model system, while the boxes around are the mirror images. The blue arrows illustrate the reappearance of a particle on the opposite of the box when migrating out. The dashed circle illustrates particle interactions between the particle in center and the closest image of every other particle over the periodic boundary. Interactions with particles outside the nonbonded cutoff r_c are truncated.

many configurations of the system as possible to ensure that the time average practically becomes the ensemble average.

3.4 Periodic boundary conditions

Since the purpose of MD simulations is providing knowledge about macroscopic systems and their properties, an infinitely large simulation box would be desired. This is computationally impractical owing to the consequential vast number of degrees of freedom. Instead, the bulk phase is simulated using an N-particle model system (simulation box) surrounded by an infinite number of identical copies (mirror images) in three dimensions (Fig. 3.2). A particle experiences forces as if it was in a bulk. A particle migrating through one side of the simulation box is replaced by an image particle with the same velocity on the opposite side of the box. The number of particles in the simulation box remains constant. This is done by employing periodic boundary conditions (PBCs). It allows the studying large-scaled molecular systems while only solving Eq. (3.4) for a relatively small number of particles. Only the N-particle model system is used for calculating properties. The PBC also ensures that surface effects are avoided when investigating bulk properties.

In theory, a particle i in the model system interacts with all other particles in the same box and in the copies, including the periodic images. To avoid this infinite sum of interactions, all intermolecular particle interactions beyond a certain distance

are truncated by applying a cutoff r_c. In addition, the minimum-image convention is applied. It assures that only the interactions between a particle i and the closest image of the remaining particles are considered. This is possible since often only short-range interactions are of interest. Additionally, a closest neighbour list[406] is used to avoid distance calculations between all particles. However, it using a truncation of the potential is inappropriate for long-range electrostatic interactions due to their slow decay. Instead, these interactions need to be calculated with other methods, such as Ewald summation.[407]

The choice of the size of the simulation box depends on the type of system and the properties of interest. However, the box size needs to: i) have at least the length of twice the length of the spherical cutoff radius for intermolecular interactions, ii) be larger than the length of any significant correlation and iii) be large enough to avoid that a macromolecule interacts with itself in the neighboring box. This would mean that the "head" of the macromolecule is interacting with the "tail" of the mirror image. Additionally, the total electronic charge of the system in the simulation box needs to be zero when Coulombic interactions are present. Otherwise, the PBCs lead to an infinite charge. If the molecule of interest is charged, counterions (positive or negative) can be added to obtain charge neutrality.

3.5 Temperature and pressure coupling

Thermostats or barostats are used to simulate a system at a specific temperature or pressure, and to guarantee proper ensemble sampling. This is, e.g., needed for simulations of NPT ensembles used for comparisons with experiments that are often performed at constant pressure and temperature. The methods used for temperature and pressure coupling can be divided into two categories: stochastic and extended dynamics. Some thermostats and barostats do not generate a proper canonical ensemble and the perturbation is not sufficient. Even if they do not give correct fluctuations and energies, they do quickly provide correct average values. Therefore, they are recommended to be used for equilibrating the simulated system. Thermostats and barostats generating a proper canonical ensemble are recommended to be used for the production run performed to collect configurations for calculations of desired properties. Additionally, a weak or strong coupling can be used for the thermostats and barostats. This specifies the time constant with which deviations of the temperature and pressure decay during the correction.

Temperature coupling. The temperature can be calculated as a time average of the instantaneous temperature $T(t)$ and can be derived from the kinetic energy K. In a

constant-temperature simulation, the kinetic energy fluctuates. Hence, also the instantaneous temperature fluctuates in a controlled way around the desired temperature. It is defined as

$$T(t) = \sum_{i=1}^{N} \frac{2K_i}{\mathrm{k_B} N_{\mathrm{DOF}}} = \sum_{i=1}^{N} \frac{m_i v_i^2}{\mathrm{k_B} N_{\mathrm{DOF}}}, \tag{3.14}$$

where N denotes the number of particles, N_{DOF} the number of degrees of freedom, m_i the mass and v_i the velocity of particle i.

Examples of thermostats are Berendsen,[408] velocity rescaling[409] and Nosé–Hoover.[410] In the Berendsen method, the system is coupled with an external heat bath with fixed temperature T_0 and the velocities of each atom are scaled. The velocity rescaling method uses a fixed kinetic energy K to match the desired temperature T_0. The algorithm includes a scaling factor for each atomic velocity in order to achieve the desired temperature. The Nosé–Hoover method uses an extra degree of freedom acting as a thermal reservoir. This is done by adding an extra term to the equations of motion. That is, the system is coupled to a heat bath. Both the velocity rescaling and the Nosé–Hoover thermostats maintain the canonical ensemble. The Berendsen thermostat[408] does not because it suppresses fluctuations of the kinetic energy of the system.

Pressure coupling. Using the Clausius virial theorem, the pressure of a system can be expressed by

$$P = \frac{2}{3V}\left(K - \Xi\right), \tag{3.15}$$

where V denotes the box volume and K the kinetic energy (Eq. (3.6)). Ξ denotes the inner virial for pairwise additive interactions. It is defined as

$$\Xi = \frac{1}{2}\sum_{i=1}^{N}\sum_{j>i}^{N} \boldsymbol{r}_{ij}\boldsymbol{F}\left(\boldsymbol{r}_{ij}\right), \tag{3.16}$$

where $\boldsymbol{F}\left(\boldsymbol{r}_{ij}\right)$ is the force between particles i and j at distance r. By using Eqs. (3.6), (3.15) and (3.16), the pressure can be expressed as

$$P = \frac{1}{V}\left[N\mathrm{k_B}T - \frac{1}{3}\sum_{i=1}^{N}\sum_{j>i}^{N} \boldsymbol{r}_{ij}\boldsymbol{F}\left(\boldsymbol{r}_{ij}\right)\right]. \tag{3.17}$$

Note that the hydrostatic pressure $P = \mathrm{tr}\,\boldsymbol{P}/3$ is associated to the trace of the pressure tensor

$$\boldsymbol{P} = \begin{pmatrix} P_{xx} & P_{xy} & P_{xz} \\ P_{yx} & P_{yy} & P_{yz} \\ P_{zx} & P_{zy} & P_{zz} \end{pmatrix}. \tag{3.18}$$

During a constant pressure simulation, the volume is considered a dynamical variable and changes over time. Instead of scaling velocities as for the temperature coupling, the particle positions are scaled during the pressure coupling. That is, the inter-particle distance is scaled, affects the inner virial Ξ, and, thereby, corrects the pressure. This is done by adding an extra term to the equations of motion.

Two examples of barostats are Berendsen[408] and Parrinello–Rahman.[411,412] The former does not generate a canonical ensemble, while the latter does. The Berendsen method uses the least perturbation principle and the system is coupled with an external bath. The Parrinello–Rahman method is a more complex algorithm and allows for changes of the box shape.

In an isotropic system, the pressure is identical in all three directions in space, $P = P_{xx} = P_{yy} = P_{zz} = \mathrm{tr}\,\boldsymbol{P}/3$. A system that is isotropic in x and y, but has a different value in z, is called semi-istropic. A system having six different values, xx, yy, zz, xy/yx, yz/zy and zx/xz, is anisotropic.

Many algorithms for temperature and pressure coupling have been developed over the years. The combination of velocity rescale thermostat and Berendsen barostat is a common choice for equilibrium runs since they are fast and have a smooth first-order approach to equilibrium. The combination of Nosé–Hoover thermostat and Parrinello–Rahman barostat is a common choice for production runs. They are considered the most reliable for systems already in equilibrium and for predicting thermodynamic properties. However, the algorithms are slow and have a second-order approach to equilibrium. Therefore, they are not used during the equilibrium step.

3.6 Force fields

The interaction forces between atoms are described by a force field. The force field is a set of descriptions including parameters and a functional form. It defines the potential energy of the system. Different categories of force fields exist. In an all-atom force field, each atom is explicitly represented by individual parameters. A united atom force field treats the hydrogen atoms together with the adjacent carbon atom. Coarse-grained force fields subsume multiple bonded atoms to a bead. The advantage is a smaller number of interaction sites.

The total (tot) basic functional form of the force field includes both bonded (b) and nonbonded (nb) interactions and can be written as

$$U_{\mathrm{tot}} = U_{\mathrm{b}} + U_{\mathrm{nb}}. \tag{3.19}$$

Bonded interactions. The bonded term in Eq. (3.19) describes the potentials derived from forces acting between atoms that are covalently bonded to each other. The bonded interactions can be divided into three different contributions: the potential of bond stretching, angle bending and bond rotation (torsion). This can be written as

$$U_{\mathrm{b}} = U_{\mathrm{stretch}} + U_{\mathrm{bend}} + U_{\mathrm{rotation}}. \tag{3.20}$$

One model potential is given by

$$\begin{aligned} U_{\mathrm{b}} = & \sum_{\mathrm{bonds}} \frac{k_{ij}^{r}}{2} \left(r_{ij} - r_{ij}^{0}\right)^2 + \sum_{\mathrm{angles}} \frac{k_{ijk}^{\theta}}{2} \left(\theta_{ijk} - \theta_{ijk}^{0}\right)^2 \\ & + \sum_{\mathrm{torsions}} k_{ijkl}^{\phi} [1 + \cos\left(n\phi_{ijkl} - \phi_{ijkl}^{0}\right)]. \end{aligned} \tag{3.21}$$

Here, the first term (bond stretching potential) models the interaction between bonded atoms and is represented by a harmonic potential. k_{ij}^{r} denotes the force constant and $r_{ij} - r_{ij}^{0}$ the displacement of the bond length from the equilibrium distance r_{ij}^{0} between atoms i and j. The second term (bending potential) models the angle deformation energy as a function of the angle change from the lowest energy value and is also represented by a harmonic potential. k_{ij}^{θ} denotes the force constant and θ_{ijk}^{0} the equilibrium angle between three adjunct atoms i, j and k. The third term (bond rotation potential) models the energy barrier associated with the bond rotation between so-called 1-4 pairs (pairs separated by three bonds) and includes a cosine potential. k_{ijkl}^{ϕ} denotes the force constant, ϕ_{ijkl}^{0} the phase shift angle and n the multiplicity for torsions between four joint atoms i, j, k and l. A fourth term describing out-of-plane bending motions (improper torsions) and, thereby, imposing planarity of parts of the molecule can be included, too. More energy is required to distort a bond compared to an angle, which is reflected in the magnitude of the force constants.

Nonbonded interactions. Independent atoms and molecules interact through nonbonded forces. The nonbonded term in Eq. (3.19) describes the sum over all the long-ranged electrostatics (el) and van der Waals (vdW) forces. It can be written as

$$U_{\mathrm{nb}} = U_{\mathrm{el}} + U_{\mathrm{vdW}}. \tag{3.22}$$

The electrostatics are commonly described by Coulomb's law. The van der Waals interactions between uncharged particles are described by the LJ potential shown in Fig. 3.3. Equation (3.22) can therefore be rewritten as

$$U_{\mathrm{nb}} = \frac{1}{4\pi\varepsilon_0} \frac{q_i q_j}{r_{ij}^2} + \sum_{i=j}^{N} \sum_{i>j}^{N} 4\varepsilon_{ij} \left[\left(\frac{\sigma_{ij}}{r_{ij}} \right)^{12} - \left(\frac{\sigma_{ij}}{r_{ij}} \right)^{6} \right]. \tag{3.23}$$

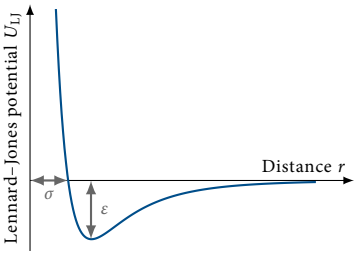

Fig. 3.3 Lennard-Jones potential U_{LJ} as a function of the distance r between two particles. The parameters ε and σ indicate the depth of the potential well and the interaction length, respectively.

Here, the first term (interaction potential between ionic charges) calculates the sum of the interactions between point charges. q_i and q_j denote the ionic charges, r_{ij} denotes the distance between the charges i and j, and ε_0 is the vacuum electric permittivity. The second term (12-6 LJ potential) gives information about the dispersive and exchange-repulsive interactions between atoms and molecules. ε denotes the potential well depth, i.e., dispersion interaction strength, σ the collision diameter, i.e., excluded volume diameter, and r_{ij} the distance between the atoms i and j. That is, σ corresponds to the inter-particle distance where the potential is zero. Nonbonded interactions account for the largest computational cost. Therefore, they are commonly restricted to pairwise interactions.

The number of force field parameters needed to describe the nonbonded interactions are reduced by using mixing rules for all cross terms, i.e., $i \neq j$. The, in MD simulations, commonly applied mixing rules are the geometric mixing rule where

$$\varepsilon_{ij} = \sqrt{\varepsilon_{ii}\varepsilon_{jj}}, \tag{3.24}$$

and

$$\sigma_{ij} = \sqrt{\sigma_{ii}\sigma_{jj}}, \tag{3.25}$$

are used, or the Lorentz–Berthelot mixing rule where Eq. (3.24) is combined with the arithmetic average

$$\sigma_{ij} = \left(\sigma_{ii} + \sigma_{jj}\right)/2. \tag{3.26}$$

For aqueous electrolyte solutions, it is difficult to properly describe ion–ion and ion–water interactions when using the standard mixing rules and values for ε_{ii} and σ_{ii} directly defined from experimental data. A rescaling of the mixing rules, as discussed in Section 1.2, is one solution.

Polarizable force fields. Electrostatic interactions do not only emerge from fixed charge distribution, as described in standard (nonpolarizable) force fields, but also from charge distribution changes of atoms or molecules due to polarization. This can be caused by a neighbouring molecule such as water or other high-dielectric media. For electrolyte solutions, this can lead to inaccuracies in describing short-range ion–ion and ion–water interactions. Polarizable force fields could possibly describe these interactions better by including charge distribution variations with dielectric environment. However, polarizable force fields are computationally costlier than nonpolarizable and also more challenging to parameterize.

Parameterization. The parameterization of a force field is not trivial owing to the large number of parameters involved. It is directed by comparison with chosen data from chemical or physical experiments. Spectroscopy methods can be used to derive a molecule's geometry. The force constants can be derived from vibrational spectra obtained by IR or Raman spectroscopy. For some molecules, experimental data may not exist or be difficult to obtain. For these molecules, quantum mechanics calculations are used. Quantum mechanics calculations are commonly also used for torsions, since experimental information on torsional barriers is usually nonexistent or sparse. The torsions and the nonbonded parameters usually effect the performance of the force field the most. LJ parameters can be derived empirically from, e.g., solvation free energy, lattice energy, solvent density, diffusion coefficient or heat capacity experimental data. Additionally, the type of functional form for the force fields needs to be chosen.

It is of importance to choose the "correct" experimental data to reproduce, i.e., quantities crucial for the simulated system, when empirically tuning the force field. There are no restrictions regarding the choice of these properties or how the optimization process should be performed. However, there are two categories of methods to use to obtain the force field parameters. The parameterization can be carried out by "trial and error", where the parameters are refined gradually. Or the parameterization can be carried out by a least square (or similar) fitting approach to determine a set of parameters giving the optimal fit. For both methods, the goal is to minimize the error between simulated and experimental (or calculated) values of the properties.

Note, specific values for the force field parameters usually only work with the force field they are optimized for. They usually also only work with the specific water model the system is parameterized with. However, values for bonds and angles (so-called hard degrees of freedom) are often transferable from one force field to another. This transferability is crucial. Without it, too many parameters would be required, making the parameterization more demanding.

Chapter 4

Contact ion pairs in the bulk affect anion interactions with poly(*N*-isopropylacrylamide)

This chapter corresponds to and is reproduced with permission from

> Bruce, E. E.; Bui, T. P.; Cremer, P. S.; van der Vegt, N. F A.; Contact ion pairs in the bulk affect anion interactions with poly(*N*-isopropylacrylamide). *J. Phys. Chem. B.*, 125(2): 680–688,2021. Copyright 2021 American Chemical Society.

Abstract. Salt effects on the solubility of uncharged polymers in aqueous solutions are usually dominated by anions, while the role of the cation with which they are paired is often ignored. In this study, we examine the influence of three aqueous metal iodide salt solutions (LiI, NaI, and CsI) on the phase transition temperature of poly(*N*-isopropylacrylamide) (PNIPAM) by measuring the turbidity change of the solutions. Weakly hydrated anions, such as iodide, are known to interact with the polymer and thereby lead to salting-in behavior at low salt concentration followed by salting-out behavior at higher salt concentration. When varying the cation type, an unexpected salting-out trend is observed at higher salt concentrations, $Cs^+ > Na^+ > Li^+$. Using molecular dynamics simulations, it is demonstrated that this originates from contact ion pair formation in the bulk solution, which introduces a competition for iodide ions between the polymer and cations. The weakly hydrated cation, Cs^+, forms contact ion pairs with I^- in the bulk solution, leading to depletion of CsI from the polymer–water interface. Microscopically, this is correlated with the repulsion of iodide ions from the amide moiety.

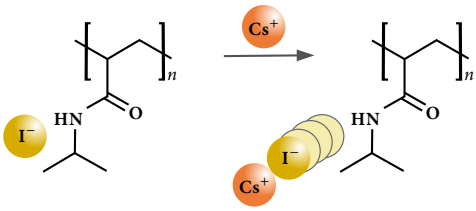

4.1 Introduction

Since the end of the 19th century, it has been known that the addition of salts to water affects the properties of nonelectrolytes dissolved in the solution.[1–3] Anions have, for example, the ability to precipitate macromolecules such as polymers and proteins from an aqueous solution. Their propensity to do so is ranked according to the Hofmeister series. The salting-out order of the anionic Hofmeister series is $CO_3^{2-} > SO_4^{2-} > S_2O_3^{2-} > H_2PO_4^- > F^- > Cl^- > Br^- > NO_3^- > I^- > ClO_4^- > SCN^-$. Anions are usually classified as weakly hydrated (right hand side of the series) or strongly hydrated (left hand side of the series). Weakly hydrated anions partition to nonpolar environments such as air–water[5] and polymer–water interfaces,[4,6] leading to moderately increased polymer solubility (salting-in behavior). Strongly hydrated anions interact repulsively with and are depleted from the polymer surface instead (salting-out behavior).

Hofmeister effects have commonly been investigated with poly(*N*-isopropylacrylamide) (PNIPAM), a thermoresponsive water-soluble polymer broadly used as a model for polymers that exhibit a coil-to-globule transition above their lower critical solution temperature (LCST). Many studies have focused on the effect of the anion in combination with sodium ions,[4,9,11,13,364,379] which act as charge balancing counterions. Indeed, Hofmeister phenomena are stronger for anions than for cations.[21] Despite the focus on anions, a typical consensus cationic Hofmeister series exists in the literature, and the salting-out order for proteins is as follows:[8] $N(CH_3)_4^+ > NH_4^+ > Cs^+ > Rb^+ > K^+ > Na^+ > Li^+ > Ca^{2+} > Mg^{2+}$. This series is not as well understood as the anionic Hofmeister series. Interestingly, the order is opposite to the anionic series. That is, strongly hydrated cations (the right-hand side of the series) lead to salting-in and weakly hydrated cations (the left-hand side of the series) lead to salting-out behavior.

In this study, we report ion-specific effects on the LCST of PNIPAM in salt solutions consisting of the weakly hydrated iodide ion in combination with the alkali metal ions (Li^+, Na^+, and Cs^+). The addition of iodide induces salting-in behavior (swelling of the polymer chain) at low salt concentration due to direct ion binding.[4] This is followed by salting-out behavior (collapse of the polymer chain) at higher concentration where solvation of the metal cations and anions in the bulk solution effectively causes the polymer to precipitate out.[4] We show that the LCST behavior (the rate of change with salt concentration) of PNIPAM in metal iodide salt solutions depends on the specific nature of the cation. By employing all-atom molecular dynamics (MD) simulations, this ion-specific behavior is elucidated at the molecular level.

4.2 Experimental methods

Materials. LiI (99.9 % purity), NaI (99.5 % purity) and CsI (99.9 % purity) were all purchased from Sigma-Aldrich. PNIPAM, with a molecular weight of 186.800 g/mol and a polydispersity of 2.63, was purchased from Polymer Source, Inc. A fixed amount of each salt was dissolved with PNIPAM in nitrogen-purged water (used to avoid iodine formation) to obtain solutions at each desired salt concentration (25 mM–1000 mM).

Phase transition temperature measurements. The change in turbidity was measured in solutions containing 10 mg/ml PNIPAM and various concentrations of LiI, NaI, and CsI to determine the LCST. An automated melting point apparatus (MPA 100 Optimal, Standford research Systems) with digital image processing software was used. A ramp rate of 1 °C/min was used to measure the light scattering intensity as a function of temperature. More specifically, the LCST was determined from the onset of the light scattering increase relative to the flat and low intensity baseline observed at colder temperatures.[7] Details concerning the LCST measurements have been described before.[4]

4.3 Molecular dynamics simulations

System setup and simulation details. All-atom simulations were carried out using the MD package GROMACS 2018.[413] The simulated systems were composed of a PNIPAM 20-mer chain (isotactic-rich with 60% *meso* diad content) in aqueous salt solutions of LiI, NaI, and CsI. The setup featured a stretched polymer chain extending through the periodic z-boundary. By connecting the head and tail, the chain had no end groups and can be considered as virtually infinite. This setup has been reported before.[414,415] By means of the GROMACS pull code, a collapsed structure of the PNIPAM chain was pulled apart generating an elongated chain. The contour length of the 20-mer L_c = 5.32 nm together with the desired elongation of $\lambda = L_z/L_c = 0.88$ defined a box size in the z-direction of L_z = 4.6839 nm. The box dimensions in the x- and y-directions were both initially 6.5 nm. The computational cost was minimized with this size, while interactions between periodic images were still prevented. A modified OPLS-AA force field[416] was used for the PNIPAM chain. LINCS[417] was utilized to constrain all bonds up to a fourth-order expansion. The chain was solvated in water using the SPC/E[418] potential with the SETTLE[419] constraint algorithm keeping the internal geometry of the water molecules rigid. After energy minimization and equilibration, two water molecules at a time were replaced with an anion (I^-) and a cation (Li^+, Na^+ or Cs^+) until a salt concentration of 1 m (6216 water molecules, 112 cations, and 112 anions) was achieved. While molality (m, moles/kg water) was used to describe the concentration in the simulations, molarity (M, moles/liter solution) was used in the experiments. The difference between the two units

is negligible within the concentration range employed in this study. Nonpolarizable force fields were used for LiI, NaI,[244] and CsI[244]. More specifically, the iodide ion model (4) and the cesium ion model (6) were used from the original reference.[244] See below for the details and validation of the LiI force field. Interactions between different atoms within the PNIPAM chain as well as polymer–ion and polymer–water interactions were described with the geometric combination rule. The Lorentz–Berthelot combination rule was used to describe ion–ion and ion–water interactions. Furthermore, an additional scaling factor of 0.9 was used for the dispersion interaction strength ε_{ij} between sodium ions (i) and iodide ions (j) according to the original force field.[244]

The systems were energy-minimized followed by a 2 ns NVT equilibration run using a velocity-rescaling thermostat.[409] Two consecutive NPT equilibration runs were subsequently performed. This started with a 2 ns equilibration using the Berendsen barostat[408] and the velocity-rescaling thermostat.[409] Next, a 3 ns equilibration was performed using the Parrinello–Rahman barostat[411,412] and the Nosé–Hoover thermostat.[410,420] Finally, production runs of 100 ns were performed using the same barostat and thermostat as the last equilibration run. Coupling times of $\tau_\mathrm{P} = 2\,\mathrm{ps}$ and $\tau_\mathrm{T} = 1\,\mathrm{ps}$ were used for the barostats and thermostats, respectively, for all runs. All simulations were performed at 1 bar and 300 K. A semi-isotropic pressure coupling scheme in the x- and y-dimensions was applied with compressibilities of $\kappa_{\mathrm{x,y}} = 4.5 \cdot 10^{-5}\,\mathrm{bar}^{-1}$, and $\kappa_\mathrm{z} = 0\,\mathrm{bar}^{-1}$ was applied in the z-dimension to maintain the stretched PNIPAM chain. Periodic boundary conditions were applied in all three directions. Furthermore, the particle mesh Ewald (PME) method[421] was used with a Fourier spacing of 0.12 nm, PME order of 4, and a real space cutoff of 1.4 nm to treat the long-range electrostatic interactions. A cutoff radius of 1.4 nm was used for van der Waals interactions. No long-range pressure and energy corrections were applied. For the neighbor list, a cutoff distance of 1.4 nm was used and was updated every 0.002 ps. Configurations were saved every 1 ps, and an integration time step of 0.002 ps was used as well.

Based on the general simulation details described above, four sets of simulations (I–Ⅳ) were conducted with the PNIPAM chain and one set without it (V). Setup I corresponds to PNIPAM solvated in different salt solutions with all other parameters according to the description above. Setups Ⅱ and Ⅲ include modifications of the PNIPAM chain solvated in different salt solutions. Setup Ⅱ restrains PNIPAM. That is, a position restraint with a force constant of $1000\,\mathrm{kJ/(molnm^2)}$ was applied to all atoms of the polymer chain in all three dimensions. Setup Ⅲ considers a "nonpolar' PNIPAM, i.e., a PNIPAM 20-mer with all partial atomic charges set equal to zero. Setup Ⅳ includes PNIPAM solvated in modified CsI solutions, i.e., using Lennard-Jones size parameters $\sigma_{ij} = \lambda_\sigma(\sigma_i + \sigma_j)/2$ between cations (i) and anions (j) scaled with factors λ_σ of 1.4 and 1.8, respectively. For setup V, bulk simulations of 1.0 m LiI, NaI, and CsI were performed. A cubic box with dimensions of $4 \times 4 \times 4\,\mathrm{nm}^3$ with 2089 water molecules, 38 anions, and 38 cations was used. Force fields and simulation parameters were the same as for the systems

containing the polymer chain. Production runs were performed for 50 ns. If not stated otherwise, setup I was used.

Validation of the lithium iodide force field. The LiI force field was comprised of a nonpolarizable Li^+ ion[78] combined with the iodide parameters taken from the NaI and CsI models.[244] This force field was validated against the osmotic coefficient, and the procedure has been described before.[422,423] However, a flat-bottom position restraint was used with a harmonic force to confine the ions. A cubic box, $5.4 \times 5.4 \times 5.4\ nm^3$, filled with water, Li^+, and I^- ions was simulated using the GROMACS 2019 package.[413] Three different concentrations were examined: 0.2 (water molecules = 5280, Li^+ = 19, and I^- = 19), 0.6 (water molecules = 5200, Li^+ = 56, and I^- = 56) and 1.0 m (water molecules = 5130, Li^+ = 93, and I^- = 93). Energy minimization was performed followed by a 0.25 ns NVT equilibration and a 1.5 ns NPT equilibration. Next, the simulation box was extended in the z-dimension to a total size of 10.8 nm, and the cubic box was placed in the middle. The new larger box was filled with water molecules leading to total numbers of 10.860, 10.820, and 10.810 water molecules, respectively, for the three concentrations. Another energy minimization was carried out followed by a 0.25 ns NVT equilibration and a 1.5 ns NPT equilibration. Afterward, production runs of 40 ns were performed. This was long enough to generate converged osmotic coefficients. The flat-bottom position restraints acted in the z-dimension. A semi-isotropic pressure coupling scheme was therefore applied, and only the x- and y-dimensions of the box were adjusted. Compressibilities of $\kappa_{x,y} = 4.5 \cdot 10^{-5}\ bar^{-1}$ and $\kappa_z = 0\ bar^{-1}$ were used. All other simulation settings were the same as for the simulations including the PNIPAM chain.

Lithium–iodide Lennard-Jones interactions were scaled to achieve agreement with the experimental osmotic coefficients. This approach has been used before to effectively take polarization effects into account for nonpolarizable force fields and thereby avoid ion clustering.[244,424] A reasonable scaling of ε_{ij} between cations (i) and anions (j) did not affect the osmotic coefficients significantly. Instead, σ_{ij} was scaled according to $\sigma_{ij} = \lambda_\sigma(\sigma_i + \sigma_j)/2$ using a scaling factor of $\lambda_\sigma = 0.93$. This scaling resulted in osmotic coefficients of $\phi = 0.96 \pm 0.12$ (0.966), $\phi = 1.01 \pm 0.11$ (1.022) and $\phi = 1.08 \pm 0.05$ (1.080) for the 0.2, 0.6, and 1.0 m LiI solutions, respectively. The values in parentheses are the corresponding experimentally measured values.[312]

4.4 Results

4.4.1 Phase transition temperatures and ion affinities

Fig. 4.1 shows the phase transition temperature of PNIPAM as a function of metal iodide salt concentration. Nonlinear behavior was seen in each case. The rate of change

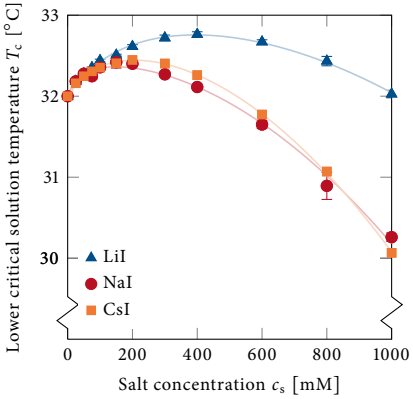

Fig. 4.1 Lower critical solution temperature T_c of PNIPAM (10 mg/ml) in LiI, NaI, and CsI solutions as a function of salt concentration c_s. The symbols are data points representing an average of three measurements. The error bars were calculated as sample standard deviations, and are smaller than the size of the data points when not seen. The lines are guides to the eyes.

of the LCST with salt concentration was cation-specific. The decrease in the LCST at higher salt concentration was largest for CsI (orange squares) and smallest for LiI (blue triangles), while the turnover point took place at the highest salt concentration for LiI and the lowest for NaI (red circles).

To understand the LCST trend, all-atom MD simulations were employed. Fig. 4.2 shows the preferential binding coefficient[211] Γ_{23} for indistinguishable ions (i.e., all cations and anions) for LiI (blue line), NaI (red line), and CsI (orange line) salt solutions (1 m) as a function of the closest distance to the polymer surface. The subscript 2 stands for the polymer, and the subscript 3 for the ions, while the subscript 1 stands for water. Γ_{23} specifies the relation between the number of ions in the vicinity of the polymer and the statistical number in the bulk solution. A negative Γ_{23} value indicates ion depletion, while a positive Γ_{23} value indicates the favorable partitioning of ions to the polymer–water interface. LiI showed the least negative Γ_{23} value indicating the weakest depletion of ions, while CsI showed the most negative Γ_{23} value and thereby the strongest depletion of the three salts considered. The slopes observed in the LCST curves at higher salt concentration (Fig. 4.1) are proportional to the preferential binding coefficients (Fig. 4.2) under the assumption that Γ_{23}, expressed per unit of solvent-accessible surface area, does not depend on the conformation of the chain.[18] Thus, the simulation data for PNIPAM in LiI, NaI, and CsI aqueous salt solutions are in qualitative agreement with the experiments.

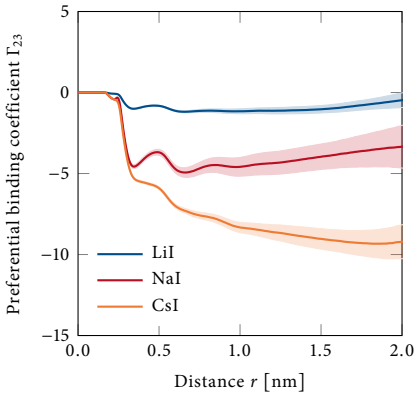

Fig. 4.2 Preferential binding coefficient Γ_{23} to a PNIPAM 20-mer chain for LiI, NaI, and CsI solutions obtained from MD simulations. Γ_{23} is presented as a function of the proximal distance r, i.e., the closest distance between an ion and an atom of the PNIPAM chain. In the calculation of Γ_{23}, cations and anions were treated as indistinguishable. The salt concentration was 1 m. The shaded intervals indicated the standard deviation of the mean $\sigma/\sqrt{N}$ using sample standard deviation σ and $N = 10$ blocks.

4.4.2 Polymer–ion interactions

Interaction energies were calculated in order to elucidate the effect of cations on iodide's preferential interaction with PNIPAM, polymer–ion, polymer–water, and monomer–solution (including all ions and water molecules) interactions. These are presented in Table 4.1. PNIPAM–anion interactions are more favorable than PNIPAM–cation interactions. This is reflected in the radial distribution functions (RDFs) between the polymer backbone and the anions, cations, and all indistinguishable ions. The RDFs are shown in Fig. 4.3 for all cases. The behavior of anions and cations can be seen both in the peak heights of the RDFs and in the cumulative number for the hydration shell of the 20-mer PNIPAM chain (distances up to $r = 0.922$ nm). The numbers of anions in the hydration shell of the 20-mer PNIPAM chain are 5.1, 4.8, and 3.9 for LiI, NaI, and CsI, respectively. The numbers of cations are 4.5, 3.8, and 2.9, respectively. Furthermore, the PNIPAM–anion, PNIPAM–cation, and PNIPAM–water interactions are cation specific. PNIPAM–anion interactions follow the order LiI > NaI > CsI, and the PNIPAM–cation interactions follow the order LiI ≈ NaI > CsI. The PNIPAM–water interactions follow the order CsI > NaI ≈ LiI (Table 4.1). These results agree with the relative ordering between the abovementioned number of ions in the PNIPAM hydration shell for each salt type. That is, more favorable PNIPAM–ion interactions (at the cost of PNIPAM–water interactions) lead to more ions in the polymer hydration shell.

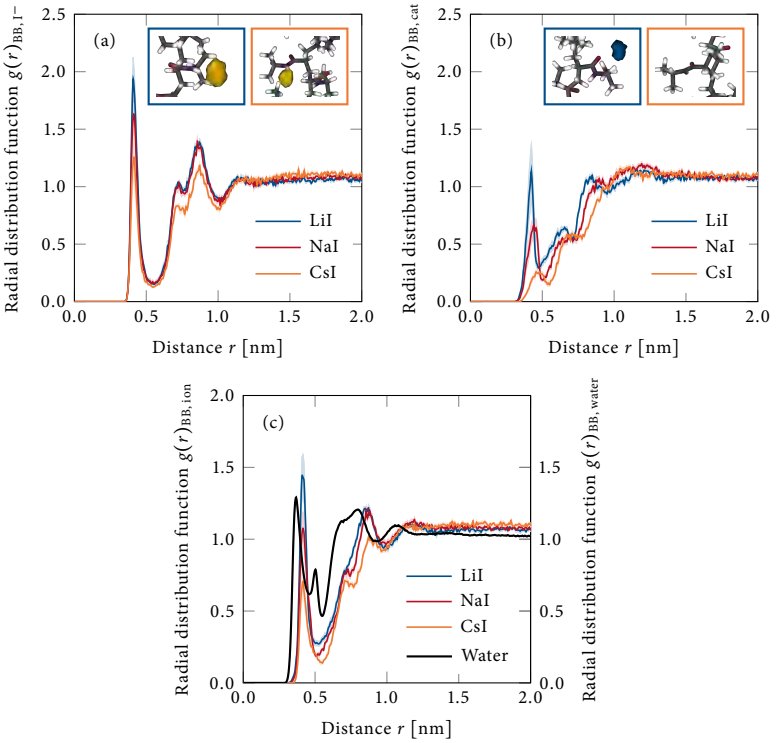

Fig. 4.3 Normalized proximal radial distribution functions $g(r)$ between the polymer backbone (BB) and (a) iodide (I^-), (b) the cations (cat), and (c) indistinguishable ions (ion) and water (right y-axis) as a function of the closest distance r to the polymer backbone for 1 m LiI, NaI, and CsI solutions, respectively. The shaded intervals indicate the standard deviation of the mean $\sigma/\sqrt{N}$, using sample standard deviation σ, and $N = 10$ blocks and are smaller than the line thickness representing the data when not seen. Insets in panel (a) show the spatial probability density maps of iodide ions (dark yellow) around the restrained PNIPAM chain (setup Ⅱ) in LiI (blue box) and CsI (orange box) solutions using Ovito software.[425] The dark yellow area indicates 5 times the bulk anion number density and shows the amide NH group and the terminal methyl groups as the preferential interaction sites. Insets in panel (b) show the spatial probability density maps of lithium ions (blue) and cesium in LiI (blue box) and CsI (orange box) solutions (setup Ⅱ), respectively. The blue area indicates 8 times the bulk cation number density and shows the amide oxygen as the preferential interaction site. Atom colors: red, O; purple, N; gray, C; white, H.

Table 4.1
Total interaction energies (sum of van der Waals and Coulombic interactions) between the 20-mer PNIPAM chain and the iodide, the three different cations and water molecules, respectively, for the three salt solutions (1 m).*

Salt	PNIPAM–anion [kJ/mol]	PNIPAM–cation [kJ/mol]
LiI	−1.45 ± 0.07	−0.8 ± 0.2
NaI	−1.36 ± 0.08	−0.6 ± 0.2
CsI	−1.12 ± 0.08	−0.09 ± 0.07
Salt	**PNIPAM–water [kJ/mol]**	**Monomer–solution [kJ/mol]**
LiI	−0.417 ± 0.003	−142 ± 1
NaI	−0.418 ± 0.004	−141 ± 1
CsI	−0.429 ± 0.006	−140 ± 2

* The energies were obtained by post processing the MD-simulated trajectories using the rerun option in GROMACS, where the electrostatic energies were computed using a reaction field with a dielectric constant of 78. The average interaction energies of PNIPAM with one anion, one cation, and one water molecule are reported. Monomer–solution (including all ions and water molecules) energies represent the total interaction energy between one monomer and the solution (including all water molecules and ions). The given errors are the standard deviation of the mean $\sigma/\sqrt{N}$ using sample standard deviation σ and $N = 10$ blocks.

Spatial probability density maps were created to investigate the spatial position of the ions around the PNIPAM side chain. A distinct preferable position (yellow area) was seen for iodide ions close to the amide NH group and the terminal methyl groups (insets in Fig. 4.3a). The spatial probability density for the iodide ions was, however, affected by the type of cation. The probability at a certain threshold (see details in figure text) is significantly lower for CsI solution (orange box) than for LiI solution (blue box). A distinct preferable position (blue area) was also seen for lithium ions close to the amide oxygen (blue box in the inset of Fig. 4.3b). This was not observed for cesium ions (orange box in the inset of Fig. 4.3b) at the same threshold (see details in figure text), indicating weaker PNIPAM–Cs^+ interactions. Furthermore, the probability of finding iodide ions close to the polymer side chain was higher than for the respective cation. These results are in agreement with the observed weak, but favorable, interactions between the amide oxygen and cations, between the amide NH group and iodide ions, and between the two terminal methyl groups and the iodide ions (not presented in Table 4.1). The interaction sites and the difference between strongly and weakly hydrated cations are in line with earlier studies of other (macro)molecules.[75,81,84,115,118] However, it has been experimentally shown that an NH moiety is not necessary for anion binding.[7]

The abovementioned interactions between part of the PNIPAM chain and ions include an electrostatic contribution. To obtain further insight into the role of these electrostatic interactions, MD simulations of a "nonpolar" PNIPAM molecule without partial atomic charges were performed in LiI, NaI, and CsI solutions (1 m). The absence of favorable ion–polymer electrostatic interactions correlates with vanishing ion-specific binding

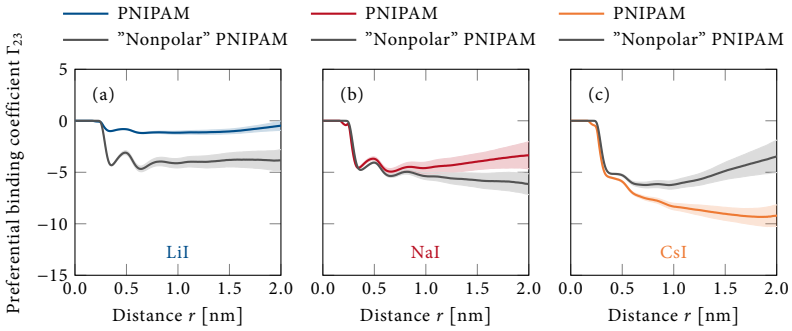

Fig. 4.4 Preferential binding coefficients Γ_{23} to a PNIPAM 20-mer chain and a "nonpolar" PNIPAM 20-mer chain for 1 m (a) LiI, (b) NaI, and (c) CsI solutions (setup III) as a function of the proximal distance r. The shaded intervals indicate the standard deviation of the mean $\sigma/\sqrt{N}$, using sample standard deviation σ, and $N = 10$ blocks. The preferential exclusion of ions from the "nonpolar" PNIPAM 20-mer chain is similar for the three salts, in agreement with the air–water interface.

to the polymer. This can be seen in Fig. 4.4, where all three salts are depleted from the polymer surface to more or less the same extent (compare the gray lines). When the partial charges are reintroduced (blue, red, and orange lines in Fig. 4.4), the ion-specific salting-out series (CsI > NaI > LiI), observed in the experimental data (Fig. 4.1), is recovered. Significantly, the LiI salt is less depleted when partial atomic charges on the polymer are reintroduced. This occurs due to favorable electrostatic interactions of iodide with the amide NH and lithium with the amide oxygen. The difference (PNIPAM chain vs "nonpolar" PNIPAM chain) was larger for LiI than for NaI. This originated from LiI interacting the strongest with the polymer chain, and thereby being affected the most in the absence of partial atomic charges. By contrast, CsI is more depleted when the partial atomic charges on the polymer are reintroduced. This is likely caused by favorable interactions of CsI ion pairs with the "nonpolar" PNIPAM surface. The "nonpolar" PNIPAM chains demonstrate that electrostatic interactions play a role in the ions' preferable affinity for the PNIPAM chain.

4.4.3 Thermodynamic implications of ion pairing

Next, cation–anion pair formation in the bulk solutions was investigated (setup V). Specifically, the fraction of contact ion pairs (CIPs) in 1 m bulk solutions was investigated by integrating the cation–anion RDFs up to the first minimum. The fractions of CIPs were 0.82 for CsI, 0.11 for NaI, and 0.07 for LiI. To investigate the influence of ion pairing in the bulk on polymer–ion interactions, MD simulations of PNIPAM chains

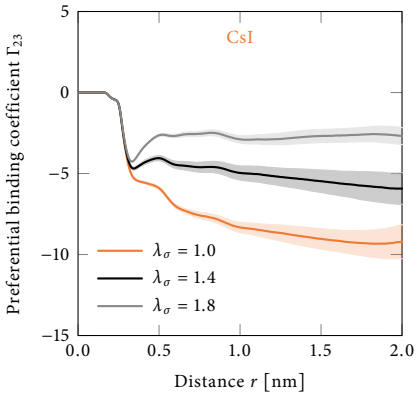

Fig. 4.5 Preferential binding coefficients Γ_{23}, to a PNIPAM 20-mer chain for 1 m CsI with different scaling factors λ_σ for their cation–anion Lennard-Jones size parameters (Setup IV) as a function of the proximal distance r. The shaded intervals indicate the standard deviation of the mean $\sigma/\sqrt{N}$ using sample standard deviation σ and $N = 10$ blocks. Inhibiting CIP formation in bulk solution weakens CsI depletion from the polymer–water interface.

in CsI solutions with modified ion-pairing ability (scaled cation–anion Lennard-Jones size parameter) were performed. A larger scaling factor λ_σ generated less ion pairing. Moreover, it led to less depletion from the PNIPAM chain. This can be seen by comparing the black and gray lines with the orange line in Fig. 4.5.

To quantify the role of ion pairs on a global level, Kirkwood–Buff integrals (KBIs) and nonideality factors were calculated. The dependence of the LCST on the molar salt concentration (c_3) reflects how the chemical potential of the PNIPAM chain (μ_2) depends on c_3. This dependency is provided by the Wyman–Tanford/Kirkwood–Buff relation [211]

$$\left(\frac{\partial \mu_2}{\partial c_3}\right)_{p,T} = \frac{-\mathrm{R}T\,\Gamma_{23}/c_3}{1 + c_3(G_{33} - G_{31})}, \tag{4.1}$$

where G_{33} and G_{31} denote the salt–salt and salt–water KBIs, respectively, R denotes the gas constant, T the temperature and p the pressure. This thermodynamic relation shows that the chemical potential of the polymer increases with salt concentration when $\Gamma_{23} < 0$ (the denominator is alway positive), leading to a negative slope for the LCST (Fig. 4.1) at high salt concentration. The role of ion pairing on a global level should be reflected by the term in the denominator of this equation, $G_{33} - G_{31}$, which accounts for the nonideality of the bulk electrolyte solution. This term is reported in Table 4.2, together with the nonideality factor $[1 + c_3(G_{33} - G_{31})]^{-1}$ and the preferential binding coefficients. Owing to ion pairing in bulk solution, $G_{33} - G_{31}$ is larger for CsI than

Table 4.2
Preferential binding coefficient Γ_{23} corresponding to a PNIPAM 20-mer with three different salts at 1 m (setup I), difference between salt–salt and salt–water Kirkwood–Buff integrals (KBIs), G_{33} and G_{31}, respectively, and the nonideality factor $[1 + c_3(G_{33} - G_{31})]^{-1}$ for the three salt solutions at 1 m (setup V).

Salt	Preferential binding coefficient Γ_{23}	Difference in KBIs $G_{33} - G_{31}$ [nm^3]	Nonideality factor $[1 + c_3(G_{33} - G_{31})]^{-1}$
LiI	−0.8 ± 0.2	−0.130	1.14
NaI	−3.6 ± 0.5	−0.095	1.10
CsI	−9.2 ± 0.4	0.535	0.67

Preferential binding coefficients and KBIs were calculated from converged running interval values between 1.5 nm and 2.0 nm. The KBIs were calculated with an RDF correction and a Krüger volume correction,[426] (see Eq. 8 in reference 427). The given errors are the standard deviation of the mean $\sigma/\sqrt{N}$ using sample standard deviation σ and $N = 5$ blocks and propagation of uncertainty for the preferential binding coefficients. Errors for the difference in KBIs and nonideality factor were calculated as sample standard deviation using propagation of uncertainty and are smaller than the reported accuracy.

for NaI (i.e., the nonideality factor is smaller, and, in particular, less than unity). The nonideality factor therefore attenuates the difference between the values of the chemical potential derivatives $(\partial\mu_2/\partial c_3)_{p,T}$ of CsI and NaI obtained if only the values of Γ_{23} (Fig. 4.2 and Table 4.2) of these two salts were considered and ideal solution behavior (i.e., equal salt–salt and salt–water affinities; $G_{33} = G_{31}$) would be assumed.

4.5 Discussion

Stronger salting-out behavior might be expected when I^- is combined with a high-charge-density cation (e.g., Li^+), and weaker salting-out behavior might be expected when combined with a low-charge-density cation (e.g., Cs^+). This expectation is based on the differences in cation hydration free energies,[324] which indicate how easily a cation sheds its hydration shell when it approaches the polymer surface. Therefore, Li^+ would be expected to be more depleted than the weakly hydrated Cs^+, leading to a stronger salting-out behavior. Anions have been shown to follow this behavior.[9,29,72,428,429] The LCST of PNIPAM in the presence of metal iodide salts shows instead the salting-out order $Cs^+ > Na^+ > Li^+$ (Fig. 4.1). This indicates that ion exclusion is subtle and charge density considerations alone cannot explain the Hofmeister effects for cations. The unexpected behavior of Li^+ in view of its charge density has drawn attention before.[65,117,430]

The nonlinear LCST behavior with salt concentration (Fig. 4.1) is indicative of polymer–ion interactions.[18] Another indication is that the observed difference in the LCST data for the different salts shows a discrepancy with ion partitioning to the air–water interface where Li^+, Na^+, and Cs^+ are all excluded to about the same extent.[25] While electrostatic

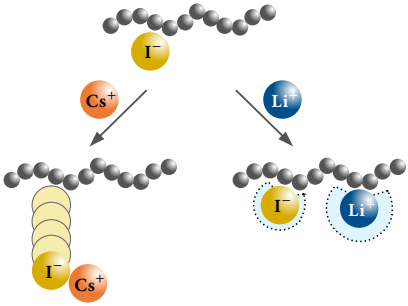

Fig. 4.6 Schematic illustration of the mechanisms of the cation-specific effect on PNIPAM–iodide interactions. The chain of gray spheres represents the polymer. The black dotted circles represent the hydration shells. It should be noted that the relative sizes of the polymer and ions are not drawn to scale.

polymer–ion interactions are crucial for the binding of ions to specific sites on the PNIPAM surface and lead to ion specific features in the preferential binding coefficients (Fig. 4.4), the partitioning of ions to the hydration shell of the "nonpolar" PNIPAM chain instead resembles the behavior of the air–water interface. This is in line with earlier studies showing that polar groups draw cations, which are usually excluded from an air–water interface,[103] into the interfacial region.[431]

PNIPAM–iodide interactions are stronger than PNIPAM–cation interactions, but the cation type has an impact on all polymer–ion interactions and thereby on the dependence of the LCST on salt concentration (Fig. 4.3 and Table 4.1). It should be noted that this is contrary to earlier studies that found stronger cation than anion interactions with PNIPAM. In that case, MD simulations found direct cation interactions and indirect anion interactions.[149,432] The MD simulations provided in the current work, however, are more consistent with both LCST data and previous spectroscopic studies. In fact, iodide ions interact favorably with nonpolar surfaces, while cations need specific binding sites such as an amide oxygen. This should explain the greater iodide affinity for the polymer shown in our study. The underlying mechanisms of cation-specific effects on the PNIPAM–iodide interactions proposed in this study are depicted in Fig. 4.6. Various experiments and MD analyses show that aqueous salt solutions do not form statistical mixtures (equally distributed ions) but rather show ion pairing and ion clustering.[126] The more weakly hydrated the cation is, the larger is the propensity for the weakly hydrated iodide to form CIPs with it. This is in line with the law of matching water affinities.[165] In an aqueous CsI solution, CIPs are formed due to both ions being weakly hydrated. This leads to charge neutrality for some ion pairs and a loss of the possibility for iodide ions to electrostatically interact with the amide NH group on the

polymer (the left side of Fig. 4.6). The ions are thereby repelled from the polymer–water interface, and the LCST is strongly suppressed (salting-out of PNIPAM). The degree to which ion pairing is decisive for the partitioning of ions to the polymer–water interface was demonstrated in this study (Fig. 4.5). When Cs^+ and I^- were prevented from forming electrically neutral CIPs in the simulations, weaker salt depletion occured. In an aqueous LiI solution, hardly any CIPs were formed. Instead, the iodide ions could independently move to the polymer–water interface and interact electrostatically with the amide NH group (the right side of Fig. 4.6). Lithium ions followed to avoid charge separation. Lithium ions also showed weakly favorable interactions with the polymer chain themselves (Table 4.1), namely, with the amide oxygen.

Concurrent interactions of iodide (Fig. 4.3a) and lithium ions (Fig. 4.3b) with PNIPAM lead to a smaller suppression of the LCST in LiI solution than in CsI solution. However, both the relative differences in the preferential binding coefficients (Fig. 4.2) and the large differences in the number of CIPs observed in bulk solution were not reflected in the LCST curves (Fig. 4.1), in particular not for NaI and CsI. This was due to a compensation of two effects. While ion pairing drove iodide away from the polymer and caused a decrease of Γ_{23}, it further caused a decrease in the effective concentration (activity) of the salt as expressed by the larger value of the denominator in Eq. (4.1) for CsI than for NaI (Fig. 4.2 and Table 4.2). Ion pairing in bulk solution should therefore have two thermodynamic implications: i) it leads to a weaker iodide interaction with the polymer, contributing to salting out; ii) the corresponding, weaker salt–water interaction attenuates the role of solvent-excluded volume[433] (an effective force related to the entropy of the solvent that drives polymer compaction and hydrophobic interaction), contributing to salting-in. The observed LCST behavior with increasing concentration of iodide salts (Fig. 4.1) is thus determined by the balance of these two effects.

Salting-in behavior is observed at low salt concentration for all salts due to the free energy favorable partitioning of weakly hydrated iodide ions to the polymer surface. At higher salt concentrations, the probability for ion pairing in the bulk is higher. This leads to a competition between PNIPAM–iodide interactions and iodide–cation interactions in the bulk. The latter dominates for weakly hydrated cations (e.g., Cs^+) since they readily form CIPs and they do not show preferable interaction with the polymer. This explains why the driving force to compact the polymer chain (salting-out behavior) sets in at a lower concentration for CsI than for LiI.

The nonadditive and dependent behavior for how ions affect polymer solubility explained in this study updates earlier ideas[25,26] about simple additive and independent ion-specific interactions. In addition to polymer–ion interactions, ion–counterion interactions are demonstrated to be crucial for Hofmeister effects. This follows up on earlier ideas that ion–ion interactions, and not only individual ion interactions, are of importance for the understanding of ion-specific effects.[17] However, the effect of

ion pairing on the LCST of polymers will probably depend on the type of ion pair and the identity of the cations and anions involved. The effects in this work apply to salts containing a weakly hydrated anion. For salts containing a more strongly hydrated anion, such as chloride, the occurrence of solvent-shared ion pairs together with weak, but favorable, polymer–cation interactions instead causes a mitigation of chloride's salting-out effect when paired with a strongly hydrated cation.[434]

4.6 Conclusions

We have shown that the LCST behavior of PNIPAM in iodide salt solutions is affected by the specific combination of the anion and the cation. Electrostatic interactions of anions and cations with the amide group play a role in ion interactions with PNIPAM, and the type of cation affects the PNIPAM–iodide interaction. A weakly hydrated cation (e.g., Cs^+) results in weaker iodide affinity, while a strongly hydrated cation (e.g., Li^+) results in stronger iodide affinity. This speaks against simple additivity and provides yet another example where observed changes in polymer solubility are due to nonadditive effects. The polymer–iodide interaction is inversely correlated with anion–cation ion pairing in the bulk. As we move from the strongly hydrated cation, Li^+, to the weakly hydrated cation, Cs^+, the affinity for CIP formation with iodide ions in the bulk increases. Such charge neutralization leads to a larger loss in the electrostatic interactions with the polymer chain, explaining the greater decrease in the LCST for iodide salts containing Cs^+ than containing Li^+.

Acknowledgement

E.E.B. and N.F.A.vdV. thank the LOEWE project iNAPO funded by the Ministry of Higher Education, Research and the Arts (HMWK) of the state of Hessen. P.S.C. thanks the National Science Foundation (CHE-2 004 050) for funding. Additionally, the authors thank Luis Vollmers for the help with the validation of the LiI force field.

Chapter 5

Molecular mechanism for the interactions of Hofmeister cations with macromolecules in aqueous solution

This chapter corresponds to and is reproduced with permission from

> Bruce, E. E.; Okur, H. I.; Stegmaier, S.; Drexler, C. I.; Rogers, B. A.; van der Vegt, N. F A.; Roke, S.; Cremer, P. S. Molecular mechanism for the interactions of Hofmeister cations with macromolecules in aqueous solution. *J. Am. Chem. Soc.*, 142(45):19094–19100, 2020. Copyright 2020 American Chemical Society.

Abstract. Ion identity and concentration influence the solubility of macromolecules. To date, substantial effort has been focused on obtaining a molecular level understanding of specific effects for anions. By contrast, the role of cations has received significantly less attention and the underlying mechanisms by which cations interact with macromolecules remain more elusive. To address this issue, the solubility of poly(*N*-isopropylacrylamide), a thermoresponsive polymer with an amide moiety on its side chain, was studied in aqueous solutions with a series of nine different cation chloride salts as a function of salt concentration. Phase transition temperature measurements were correlated with molecular dynamics simulations. The results showed that although all cations were on average depleted from the macromolecule–water interface, more strongly hydrated cations were able to locally accumulate around the amide oxygen. These weakly favorable interactions helped to partially offset the salting-out effect. Moreover, the cations approached the interface

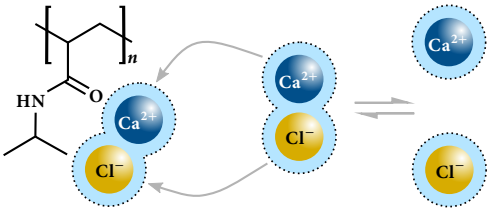

together with chloride counterions in solvent-shared ion pairs. Because ion pairing was concentration-dependent, the mitigation of the dominant salting-out effect became greater as the salt concentration was increased. Weakly hydrated cations showed less propensity for ion pairing and weaker affinity for the amide oxygen. As such, there was substantially less mitigation of the net salting-out effect for these ions, even at high salt concentrations.

5.1 Introduction

It has been known for more than 130 years that salt ions modulate the physical properties of macromolecules in aqueous solutions.[1,3,4,6,9,17,24–26,28,29,34,41,43,53,54,57,69–71,73,74,78,79,82,109,118,125,128,129,131,140,189,435] For proteins, a typical consensus cation series for salting-out behavior is as follows:[8] $Mg^{2+} < Ca^{2+} < Li^{+} < Na^{+} < K^{+} < Rb^{+} < Cs^{+} < NH_4{}^{+} < N(CH_3)_4{}^{+}$. This series is often dominated by cation interactions with negatively charged carboxylate moieties from aspartate and glutamate residues.[75,78,115] Although the above series is widely regarded as a direct cationic Hofmeister series, it is neither generic nor well understood. In the absence of negatively charged functional groups, cation interactions with the polypeptide backbone are generally quite weak. As such, cations have often been treated as passive counterions that balance the charge in aqueous solution. A few studies have, however, explored the interactions of cations with the amide oxygen.[84,116] The results show that strongly hydrated cations (e.g., Mg^{2}, Ca^{2+}, and Li^{+}) interact weakly with the amide oxygen, while weakly hydrated cations (e.g., Na^{+} and K^{+}) are depleted from the amide group.[84,116,118]

Herein, we report the lower critical solution temperature (LCST) for poly(*N*-isopropylacrylamide) (PNIPAM). This thermoresponsive polymer exhibits cation specific salting-out behavior with a series of chloride salts (Mg^{2+}, Ca^{2+}, Sr^{2+}, Li^{+}, $NH_4{}^{+}$, Na^{+}, K^{+}, Rb^{+}, and Cs^{+}). In previous studies, the LCST behavior for the anionic Hofmeister series was found to correlate with changes in surface tension at the air–water interface per mole of added salt $d\gamma_s/dc_s$ when the counterion was Na^{+} (where γ_s denotes the surface tension and c_s stands for the concentration of salt).[4] As will be shown herein, this trend is not followed for cation chloride salts. Instead, a cation specific salting-in contribution was observed for all cations and especially for salt solutions of the most strongly hydrated cations. By employing all-atom molecular dynamics (MD) simulations, we elucidated this partial salting-in contribution to macromolecule solubility at the molecular level.

Fig. 5.1 schematically depicts the molecular level mechanism for the cationic Hofmeister series with PNIPAM. Despite net ion depletion from the macromolecule–water interface, local accumulation of strongly hydrated cations occurs at the amide oxygen. Such weak local ion partitioning originates from weak, but energetically favorable interactions

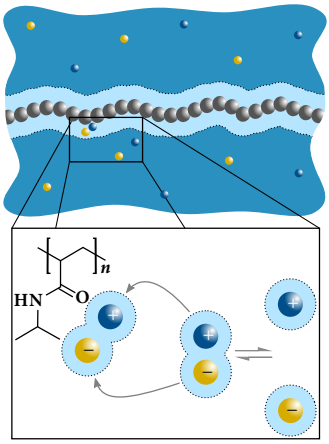

Fig. 5.1 Schematic illustration of the molecular mechanism for the cationic Hofmeister series. (top) The light blue region adjacent to the polymer represents hydration water. (bottom) The partitioning of ions in the form of solvent-shared ion pairs to the vicinity of the amide moiety on a PNIPAM side chain is depicted. The polymer size in the experiments described herein is on the order $n \approx 160$. It should be noted that cations are net depleted from the polymer–water interface. However, when they do come to the interface, they do so together with chloride anions as depicted by the arrows. The relative sizes of the polymer, ions, and hydration shells are not drawn to scale.

between the amide oxygen and the cations. The partitioning of cations to the vicinity of the macromolecule is aided by solvent-shared ion pair formation between cations and chloride counterions at the polymer interface. The preference for ion pairing is greater for strongly hydrated cations (e.g., Ca^{2+} and Li^{+}) than for more weakly hydrated ones (e.g., Na^{+} and Cs^{+}). Because the effect is dependent on the simultaneous presence of both the anion and cation at the polymer surface, it occurs more readily at higher salt concentrations.

5.2 Results

5.2.1 Phase transition measurements

Figures 5.2a and 5.2b plot the phase transition temperature of PNIPAM as a function of chloride salt concentration for monovalent and divalent cations, respectively. In the absence of salt, the phase transition occurred at 32.1 °C. In the presence of salt, the LCST decreased with increasing salt concentration. Moreover, the various salts

influenced the solubility of the macromolecule in a cation-specific manner. The salting-out order at a concentration of 1 M was $Li^+ \approx NH_4^+ < Rb^+ \approx K^+ \approx Cs^+ \approx Na^+$ for the monovalent cations and $Mg^{2+} < Ca^{2+} < Sr^{2+}$ for the divalent cations. As can be seen by comparing the magnitudes on the y-axes of the two plots, the monovalent and divalent salts decreased the LCST to roughly the same extent. This result is surprising because the salts of divalent cations might be expected to be twice as effective at salting-out PNIPAM on a per molar basis. Indeed, the salting-out order for the anionic Hofmeister series correlates strongly with $d\gamma_s/dc_s$ (see Table 5.2)[4,25] and the value of $d\gamma_s/dc_s$ is primarily dependent on the identity of the anion. In fact, the chloride salts of divalent cations show $d\gamma_s/dc_s$ values for the air–water interface that are about twice as large as those for the monovalent cations. Nevertheless, the idea that the salting-out behavior should be twice as large on a per molar basis for salts of divalent metal cations does not hold.

The data in Figs. 5.2a and 5.2b can be fit to an equation of the following form:

$$T_c = T_0 + ac_s + dc_s + fc_s^2, \tag{5.1}$$

whereby the term T_0 represents the value of the LCST in the absence of salt. The next term, ac_s, is a linear salting-out contribution related to the surface tension. By contrast, the third and fourth terms, $dc_s + fc_s^2$, represent a salting-in contribution that corresponds to cation binding with the amide oxygen. See Eqs. (5.3) to (5.5) for more details concerning the empirical model for the LCST. The value of ac_s is known for each salt because it correlates to the value of the surface tension of the air–water interface.[4] As such, the salting-in contribution from cation binding can be isolated and plotted by subtracting off the ac_s term and resetting the initial LCST value to zero (Fig. 5.2c). This residual LCST T_c^{res} has the functional form

$$T_c^{res} = dc_s + fc_s^2, \tag{5.2}$$

where the coefficients d and f are used for the concentration and concentration squared terms, respectively, with units of °C/M and °C/M^2. The functional form of T_c^{res} is completely different from a Langmuir isotherm, which arises from saturable macromolecule–ion interactions. Fig. 5.2c generally shows two distinct groups of salts. The strongly hydrated divalent cations (Mg^{2+}, Ca^{2+}, and Sr^{2+}) have a significant salting-in contribution to polymer solubility. By contrast, most monovalent cations (Cs^+, Rb^+, K^+, and Na^+) display much weaker influence, although Li^+ and NH_4^+ show intermediate behavior.

5.2.2 Preferential binding coefficients

Next, the interactions of the ions in water with a PNIPAM 20-mer chain were explored using all-atom MD simulations. The polymer chain that was employed had no end

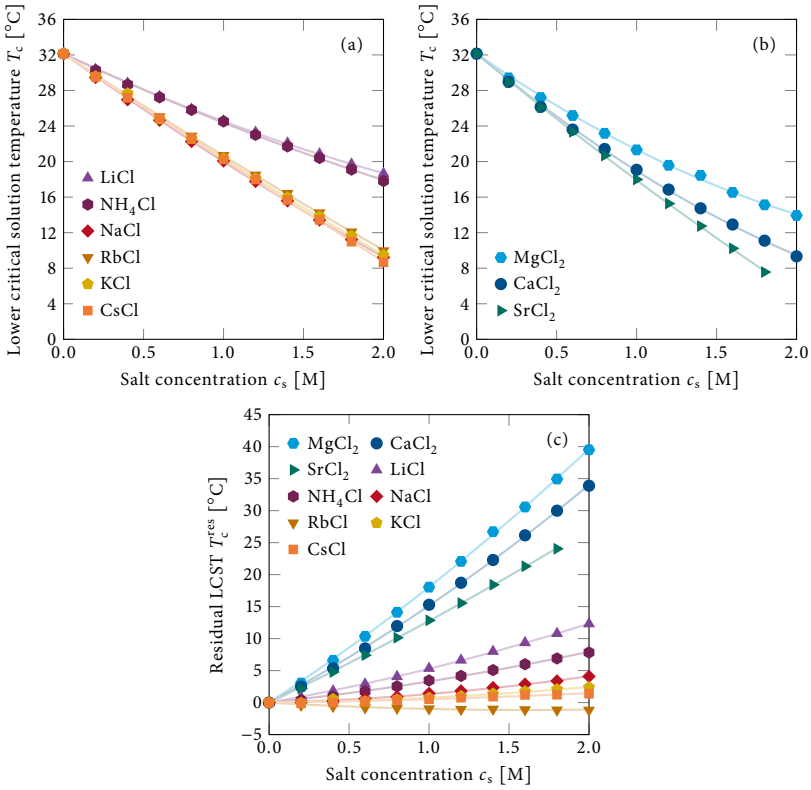

Fig. 5.2 Lower critical solution temperature T_c for 10 mg/ml PNIPAM in chloride salt solutions as a function of salt concentration c_s for (a) monovalent and (b) divalent cations. See Sections 5.4.1 and 5.4.2 for more details regarding these transition temperature measurements. The symbols are data points, and the lines are fits corresponding to an empirical model (see Eqs. (5.2) to (5.5) for details concerning the empirical fitting model for the LCST data). (c) Residual lower critical solution temperature values T_c^{res} for PNIPAM with all nine chloride salts as a function of salt concentration c_s. The symbols represent individual data points, and the lines are fits to the data corresponding to Eq. (5.2) (see Table 5.1 for the fitting parameters for d and f). Each data point represents an average of six measurements. In each case the error bars, which were calculated from sample standard deviations, are smaller than the size of the data points. Note the LCST data for $SrCl_2$ are only reported up to its solubility limit, ≈1.8 M.

groups as it was connected back onto itself by using periodic boundary conditions. The simulations were performed in solutions of $CaCl_2$, LiCl, NaCl, and CsCl at two concentrations (0.3 m and 1.8 m). Fig. 5.3 shows the preferential binding coefficients of these salts (cations and anions were treated as indistinguishable in the calculations). Following standard thermodynamic convention, the water is labeled 1, the polymer chain is labeled 2, and the ions are labeled 3. The preferential binding coefficient quantifies the excess number of ions in the vicinity of the polymer relative to the statistical number in the bulk solution. When ions partition favorably to the polymer interface, then $\Gamma_{23} > 0$. On the other hand, when the ions are depleted, then $\Gamma_{23} < 0$.

As can be seen in Fig. 5.3, net depletion from the PNIPAM chain was observed in all cases. The order of Γ_{23} between the salts follows the observed LCST order (Figs. 5.2a and 5.2b). A sixfold increase in salt concentration from 0.3 to 1.8 m led to an approximately sixfold increase in the absolute value of the preferential binding coefficient for Na^+ and Cs^+. As such, the difference between the polymer–ion and polymer–water affinity remained constant with concentration,[18] and a linear LCST trend should be expected. Indeed, the chloride salts of these ions led to a nearly linear concentration dependence (Fig. 5.2a). For the strongly hydrated cations (Ca^{2+} and Li^+), however, the sixfold concentration increase yielded a much smaller corresponding change in the preferential binding coefficient. As such, the difference between the polymer–ion and polymer–water affinities was concentration-dependent. Specifically, the salts were less depleted than expected, which should contribute to a smaller drop in the LCST. This should be the origin of the nonlinear trends observed in Figs. 5.2a and 5.2b.

5.2.3 Partitioning of ions to the macromolecule surface

The electrolyte structure around the PNIPAM chain was probed in 1.8 m salt solutions by MD simulations. The normalized proximal radial distribution functions (RDFs) between the polymer backbone and the cations are provided in Fig. 5.4a. In close vicinity to the polymer chain, the RDF values between the polymer backbone and the cations fell below unity. This is consistent with a net depletion of all ions from the polymer surface. However, the results revealed local accumulation of strongly hydrated cations close to the polymer surface. This accumulation, which can be seen at a distance of 0.75 nm–1.25 nm from the backbone, came from accumulation around the amide oxygen and terminal methyl groups (Fig. 5.8a). At this distance, the strongly hydrated cations have an intact first hydration shell (Fig. 5.9). Furthermore, weak, but favorable interaction energies were observed between side chain atoms and salt ions (Table 5.5), in agreement with previous studies.[7,75,84,115,118] Namely, net favorable interaction energies were found between the amide oxygen and the cations as well as between the amide nitrogen and chloride and between the two terminal methyl groups and the chloride.

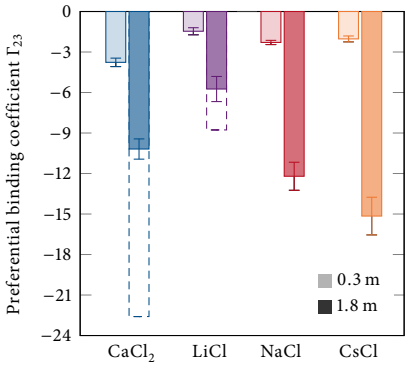

Fig. 5.3 Preferential binding coefficient Γ_{23} corresponding to a PNIPAM 20-mer chain at two salt concentrations with four different salts. The error bars represent the standard deviation of the mean $\sigma/\sqrt{N}$ by using sample standard deviations σ and $N = 20$ (0.3 m) or $N = 5$ (1.8 m) blocks, respectively. The dashed bars depict the preferential binding coefficients that would have been expected if the difference between the polymer–ion and polymer–water affinities had been independent of the salt concentration. Details concerning the MD simulations are provided in Section 5.4.4 and in Tables 5.3 and 5.4. Section 5.4.5 contains more details on the link between the preferential binding coefficients shown in this figure and the LCST values shown in Fig. 5.2. Additionally, distance-dependent preferential binding coefficients are provided in Fig. 5.6.

Next, Fig. 5.4b shows the proximal RDF values between the polymer backbone and the chloride ions. In this case, greater interfacial partitioning for Cl^- is observed beyond 0.75 nm when the countercation was strongly hydrated. Here, too, the peaks in the RDF could be divided into contributions from local accumulation around the amide nitrogen and the terminal methyl groups (Fig. 5.8b). The presence of both anions and cations in the vicinity of the polymer suggests ion pairing close to the side chains, which is explored in the next section.

5.2.4 Cation–anion ion pairing at the macromolecular surface

Figure 5.5 shows the number density $\rho(r)$ of solvent-shared cation–anion pairs (SIPs) normalized to the bulk value $\rho(r \to \infty)$ as a function of the closest distance r between the ion pair and the polymer. Distinct peaks can be seen for the strongly hydrated cations but not for the weakly hydrated ones. Additionally, the number of SIPs was slightly larger in the vicinity of the amide oxygen and the terminal methyl groups compared with the bulk solution (Fig. 5.5 vs Fig. 5.8). Compared with SIPs, the partitioning of contact ion pairs (CIPs) and solvent-separated ion pairs (2SIPs) to the polymer interface was of less importance (Fig. 5.11).

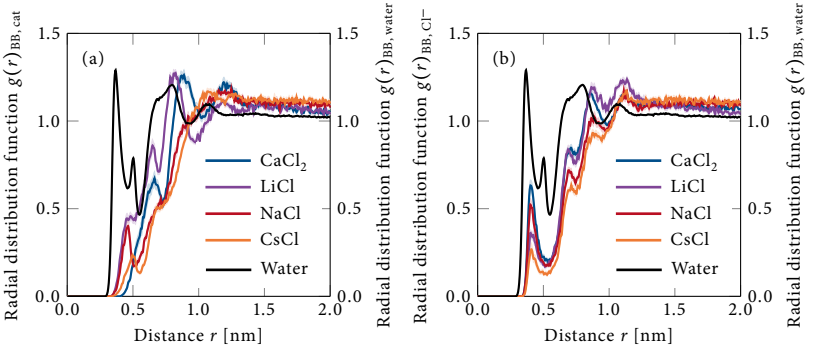

Fig. 5.4 Normalized proximal radial distribution functions $g(r)$ (a) between the polymer backbone (BB) and the cations (cat) and (b) between the polymer backbone (BB) and the chloride anions as a function of the closest distance r to the polymer backbone for four salt solutions. The $g(r)$ for the backbone (BB) to water is shown for reference in both figures as black curves (right y-axis). The shaded intervals indicate the standard deviation of the mean $\sigma/\sqrt{N}$ by using sample standard deviations σ and $N = 10$ blocks. The error bars are smaller than the thickness of the line when not visible. See Fig. 5.7 for details concerning the cylindrical volume element used for the normalization. Note, the RDF values did not completely converge to 1.0 at longer distances due to the finite volume of the box used in these simulations (i.e., depletion gave rise to an increase in the number of ions in the bulk). Moreover, the stretched chain was approximated by a cylinder for the normalization factor, leading to a deviation from 1.0 for the RDF values at longer distances.

Cations do not typically approach hydrophobic interfaces alone. Ion pairs, however, are neutral species (or reduced in charge when one of the ions is divalent) and can more facilely approach the surface. In fact, the probability for Ca^{2+} to partition to the macromolecule surface as an ion pair was very similar to the total partitioning of Ca^{2+} to the surface. This can be seen from the almost identical spatial probability density maps for Ca^{2+} alone and for Ca^{2+} ions in solvent-shared pairs with at least one Cl^- (Fig. 5.12).

5.3 Discussion and conclusions

The air–water interface has often been employed as a simple macroscopic proxy for biological interfaces, including the surfaces of proteins.[103,107] As such, it is instructive to compare the results from the neutral macromolecule–water interface with the air–water interface. In particular, the introduction of ions increases the surface tension of the air–water interface via their depletion from the topmost water layers.[41,306] If a change in the surface tension was the only contribution to an ion's influence on PNIPAM, then

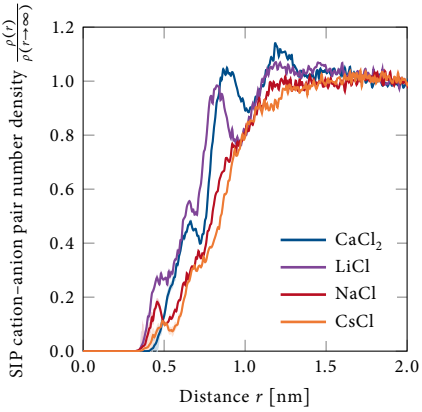

Fig. 5.5 Normalized solvent-shared cation–anion pair (SIP) number density $\rho(r)/\rho(r \to \infty)$ as a function of the closest distance r to the polymer backbone for four chloride salts. See Section 5.4.10 for details concerning the calculation and Fig. 5.10 for the definition of ion pair types. The shaded intervals indicate the standard deviation of the mean $\sigma/\sqrt{N}$ by using sample standard deviations σ and $N = 10$ blocks, and by using propagation of the uncertainty. The error bars are smaller than the thickness of the line when not visible.

the LCST trends as a function of salt concentration would be directly correlated to how the surface tension changed with increasing concentration for each ion.[4] As noted above, the anionic Hofmeister series for sodium salts has been shown to be correlated to these values.[4] By contrast, a similar trend was not seen for the chloride salts examined herein (Fig. 5.2 vs Fig. 5.13). Instead, a substantial residual LCST value remained after subtracting off the surface tension contributions (Fig. 5.2c). Below, the origin of this residual LCST value will be explored.

Ions are typically thought to be repelled from hydrophobic–aqueous interfaces due to the image charge effect.[306] In fact, strongly hydrated cations (e.g., Ca^{2+}) partition away from the air–water interface, remaining in the bulk solution due to the large favorable interaction energy between the ions and water molecules. This contribution dominates over the unfavorable entropic one caused by the restriction of water molecules in the hydration shells of the ions. This picture, however, is more complicated at the macromolecule–water interface where both hydrophilic and hydrophobic moieties are present. Site-specific interactions can occur at hydrophilic sites (i.e., the amide moieties) for both ions and water. Additionally, even the hydrophobic portions of the macromolecule can have dispersion interactions with the solvent. When ions partition toward the macromolecule, weakly favorable interactions between the polymer and

the ions (Figs. 5.4 and 5.5 as well as Table 5.5) partially compensate for the loss of the favorable interaction energy between the ions and water.

As shown herein, the partitioning of cations to the macromolecular interface is more favorable for strongly hydrated cations (e.g., Ca^2 and Li^+) compared to more weakly hydrated ones (e.g., Na^+ and Cs^+) (Fig. 5.4). The number of cations in the vicinity of the macromolecular surface follows the order $Li^+ > Ca^{2+} > Na^+ > Cs^+$. The stronger water–ion interactions for Ca^{2+} make it energetically less favorable for it to come to the surface compared to Li^+. However, Ca^{2+} also binds more tightly to the amide oxygen (Table 5.5). As such, even though there are fewer Ca^{2+} ions at the interface, they nevertheless have a larger effect on the system compared to Li^+, leading to a larger residual LCST value.

Another key consideration for macromolecule solubility is the partitioning of cations paired with chloride counterions as SIPs to the vicinity of the macromolecule (Fig. 5.5). Indeed, it is well-known that ions are often not uniformly distributed in aqueous salt solutions. Instead, cation–anion pairing can be quite abundant at elevated salt concentrations.[126,137] The results found herein are reminiscent of a recent study showing the surprising presence of two strongly hydrated ions (Mg^{2+} and SO_4^{2-}) at an air–water interface due to a SIP formation mechanism.[436] Moreover, the presence of ion pairs near amides also has analogies to ion pair interactions with supramolecular structures.[437] Indeed, ion pairs are neutral (or reduced in charge for a divalent ion paired with a single monovalent counterion) and, thus, can approach the macromolecule surface without causing charge separation in the solution. Aided by SIP formation, cations locally accumulate near the amide. This interaction is the basis for the residual LCST values observed in Fig. 5.2c. This contribution is almost large enough in the case of strongly hydrated cations to offset the surface tension contribution. Moreover, the linear term (dc_s) in Eq. (5.2) can putatively be assigned to cation interactions with the amide oxygen, whereas the quadratic term (fc_s^2) likely corresponds to ion pair formation in the vicinity of the macromolecule. As can be seen, weakly hydrated cations (e.g., Na^+ and Cs^+) show a very small (or nearly zero) linear term dependence (Table 5.1) since they have the weakest interactions with the amide oxygen (Table 5.5). By contrast, the divalent cations as well as Li^+ have stronger interactions with the amide oxygen and give rise to a steeper slope (Fig. 5.2c). The same strongly hydrated cations (e.g., Ca^{2+} and Li^+) also have a larger nonlinear term due to their enhanced ability to form SIPs with Cl^- in the vicinity of the macromolecules (Fig. 5.5). NH_4^+ is an exception due to its directional H-bonding capability. Specifically, its residual salting-in contribution (Fig. 5.2c) is greater than would be expected based on its influence on the air–water surface tension (Table 5.2). As such, the salting-in contributions described above apply specifically to metal ion chloride salts (Fig. 5.1). As a second example, this mechanism also does not hold for a tetramethylammonium cation (Fig. 5.14). Indeed, this much greasier cation would not be expected to interact specifically with the amide oxygen but rather more generally with the hydrophobic portions of the polymer.

The overall cationic series achieved from macromolecular solubility measurements is $Li^+ < NH_4{}^+ < Mg^{2+} < Rb^+ < K^+ < Cs^+ < Na^+ < Ca^{2+} < Sr^2$, which is significantly different from a direct cationic Hofmeister series. In fact, a direct cationic Hofmeister series can only be observed after subtracting off the surface tension contribution (Fig. 5.2c). The underlying reason for this should be twofold. First, the surface tension contribution leads to a salting-out effect that is mostly dependent on the number of chloride counterions in solution, which differs by a factor of 2 between the monovalent and divalent salts. Second, the ion pairing of cations with chloride helps to give rise to a weak salting-in effect that reinforces the weak direct interactions of the cations with the amide. The ion pairing contribution may follow hard–soft acid–base pairing rules,[438] the law of matching water affinity,[165] a partially reversed Hofmeister series,[20,78,122,125,126,165] or other pairing rules rather than a direct Hofmeister series. Together, this work shows that strongly hydrated cations, like $CaCl_2$, give rise to LCST phase diagrams wherein the linear salting-out term is nearly offset by both a linear salting-in contribution from very weak binding (i.e., the binding is still on the linear portion of a Langmuir isotherm) and a squared salting-in term for ion pairing. The latter term highlights the fact that the effect of salt ions should not be assumed to be additive.

Acknowledgement

P.S.C. thanks the National Science Foundation (CHE-1 709 735 and CHE-2 004 050) for support. S.R. acknowledges the Julia Jacobi Foundation and the European Research Council (grant numbers 240 556 and 616 305). N.F.A.v.d.V. thanks the LOEWE project iNAPO funded by the Ministry of Higher Education, Research and the ARTS (HMWK) of the state of Hessen. Furthermore, the simulations for this research were conducted on the Lichtenberg high performance computer at TU Darmstadt. The authors also wish to thank Prof. David E. Bergbreiter for providing the PNIPAM.

5.4 Supporting information

5.4.1 Materials

The inorganic salts $MgCl_2$, $CaCl_2$, $SrCl_2$, LiCl, NH_4Cl, NaCl, KCl, RbCl, and CsCl were all purchased from Acros, Alfa Aesar and Sigma-Aldrich (with minimum 99.9 % salt purity) and used as received. Deionized water, with a minimum resistivity of 18.1 MΩcm, obtained from a NANOpure Ultrapure water system (Barnstead), was used for lower critical solution temperature (LCST) measurements. Poly(*N*-isopropylacrylamide)

(PNIPAM) with a molecular weight of 17 800 g/mol was synthesized according to procedures that have been published previously.[4]

5.4.2 Transition temperature measurements

The details of the LCST measurements have been described previously.[4] Briefly, aqueous polymer solutions were lyophilized to form dry aliquots, which were then redissolved in the desired salt solution. The final polymer concentration was 10 mg/ml for each sample. An automated melting point apparatus (Optimelt MPA 100, Stanford Research Systems) was employed to measure the LCST. In a typical measurement, three capillary tubes filled with the desired PNIPAM solution were placed in the heating chamber of the melting point apparatus and the scattering intensity was recorded as the temperature was ramped at 1 °C/min. The instrument's built-in camera captured real-time images of the samples and then used digital image processing technology to determine the phase transition temperature from the turbidity of the solution. Specifically, the onset of the light scattering intensity increase compared to the scattering intensity baseline was taken to be the transition temperature.[7] All LCST values reported in this study were highly repeatable and the data shown herein represented an average of at least six measurements.

5.4.3 Empirical model for the lower critical solution temperature of macromolecules

Specific ion effects on the phase transition temperature of polymers are commonly modeled with empirical equations that include specific ion binding and surface tension changes in aqueous salt solutions.[4,6] Such equations often appear in the form of a linear term plus a Langmuir binding isotherm along with additional expressions to include other ion specific effects, such as electrostatic interactions between ions and charged groups on a macromolecule, if necessary.[115] Herein, we employed the following empirical equation for the LCST of PNIPAM in aqueous chloride salt solutions:

$$T_c = T_0 + ac_s + \frac{B_{max}c_s}{K_D + c_s} + \left(dc_s + fc_s^2\right), \tag{5.3}$$

where T_0 is the LCST in pure water and c_s is the salt concentration. The coefficient a has units of °C/M. The third term is a Langmuir binding isotherm. K_D represents the dissociation constant of the ions for ion–macromolecule binding interactions in units of molar salt concentration, while B_{max} represents the maximum increase in the LCST at saturation and has units of temperature. For the cationic Hofmeister series, the binding isotherm is negligible because binding is extremely weak. As such, the binding term was

Table 5.1
Fitting parameters d and f for the residual LCST $T_c^{res} = dc_s + fc_s^2$ of PNIPAM.

Salt	d [°C/M]	f [°C/M^2]
$MgCl_2$	16.30	1.76
$SrCl_2$	13.31	1.85
$CaCl_2$	11.95	0.82
LiCl	4.56	0.89
NH_4Cl	2.65	0.66
NaCl	0.62	0.72
KCl	0.30	0.46
RbCl	−1.44	0.45
CsCl	0.32	0.21

set to zero, i.e., $B_{max}c_s/(K_D + c_s) = 0$, for all salts and is not included in Eq. (5.1). The final terms in the parenthesis in Eq. (5.3) represent the residual LCST $T_c^{res} = dc_s + fc_s^2$. The coefficients d and f have units of °C/M and °C/M^2, respectively, and are provided in Table 5.1 for each salt. Figure 5.2c plots T_c^{res} for each salt. Moreover, $T_c^{res} = dc_s + fc_s^2$ serves as Eq. (5.1). It should be noted that this equation was determined empirically and that the LCST data could not be fit without using both terms, at least up to 2 molar salt concentration.

A strong correlation between the salting-out efficacy of ions and the air–water interface surface tension of the pure salt solutions has been found for the anionic Hofmeister series with Na^+ as the counterion.[4,6] Specifically, the coefficient a in Eq. (5.3) has been shown to be directly correlated with changes in surface tension γ_s at the air–water interface per mole of added salt $d\gamma_s/dc_s$.[4,6] Such a correlation between the surface tension gradient and the LCST decrease is found for all inorganic salts including the Cl^- salts of a cationic series. In order to express the a coefficient as a function of the surface tension gradient, the chloride salts of noninteracting monoatomic cations (Na^+, K^+, Rb^+, and Cs^+) can be used as references. CsCl was chosen as the reference salt and used to determine the salt specific surface tension contribution a to the LCST. This choice was made because Cs^+ ions are the most weakly hydrated cations and, thus, the least interacting with the PNIPAM chain. This choice is used to set the following relationship:

$$a = \frac{d\gamma_s}{dc_s} \frac{\Delta T_c\,(\mathrm{CsCl})}{\frac{d\gamma_{CsCl}}{dc_{CsCl}}}, \tag{5.4}$$

where $d\gamma_s/dc_s$ is the salt-specific air–water surface tension gradient (mNm^{-1}mol^{-1}dm^3) and ΔT_c(CsCl) (°C/M) is the change in the LCST per mole for a CsCl solution calculated from the three first data points in Fig. 5.2a. In this low concentration regime, changes in the LCST are almost perfectly linear[4,6] and the surface tension effect dominates changes in the LCST as the ion binding contribution is negligible in this con-

centration range. Table 5.2 provides values of $d\gamma_s/dc_s$ and a for various salts. The ratio $\Delta T_c\,(\mathrm{CsCl}) \,/\, (d\gamma_{\mathrm{CsCl}}/dc_{\mathrm{CsCl}})$ is equal to $-7.66\,^{\circ}\mathrm{C/mNm^{-1}}$. Inserting the definition of a from Eq. (5.4) into Eq. (5.3), yields:

$$T_c = T_0 + \frac{d\gamma_s}{dc_s}\frac{\Delta T_c\,(\mathrm{CsCl})}{\frac{d\gamma_{\mathrm{CsCl}}}{dc_{\mathrm{CsCl}}}}c_s + \left(dc_s + fc_s^2\right). \tag{5.5}$$

This equation was used to model the LCST curves for PNIPAM as a function of chloride salt concentration in Figs. 5.2a and 5.2b. As noted above, the binding term was not needed to fit the LCST. Note, swapping the CsCl reference salt in Eq. (5.4) for NaCl, KCl or RbCl would only slightly change the absolute values of a and, thus, $T_c^{\mathrm{res}} = dc_s + fc_s^2$ in Eq. (5.5). Moreover, the trend seen in Fig. 5.2c and the conclusions drawn would remain exactly the same. Indeed, the chloride salts of Na^+, K^+, Rb^+, and Cs^+ have almost identical $d\gamma_s/dc_s$ values. Moreover, they yield almost identical reductions in the LCST with salt concentration up to 0.4 M (Fig. 5.2a). Table 5.2 also provides polarizability constants for the cations of the respective salt. As can be seen, there is no direct correlation between the a coefficient values (or the $d\gamma_s/dc_s$ values) and the polarizability of the alkali and alkaline earth metal cations. In contrast to polarizability (given for some anions in Table 5.2), the size of the anions plays a key role in macromolecule–anion interactions. In fact, large anions are more weakly hydrated than smaller ones and are more readily pushed to macromolecular surfaces. This may be aided by stronger macromolecule–anion dispersion forces.[82] Also, it should be noted that small variations in the surface tension gradient $d\gamma_s/dc_s$ exist in the literature depending on the type of measurement that is made. The choice of surface tension gradient values used for the fitting in Eq. (5.4) can slightly affect the calculated a values. Therefore, average values from the literature were used. However, even if averages were not employed, the trends and the conclusions drawn would essentially be identical. It should specifically be noted that the surface tension gradient value for RbCl reported in Table 5.2 is only based on one literature value. Due to its low value compared to other salts, it resulted in a negative value for d and thereby a slightly negative residual LCST (Fig. 5.2c). Since the LCST fit is only based on this one measurement and due to the estimated error bars in the reported surface tension gradient data, the residual LCST should probably be assumed to be close to 0.

5.4.4 Molecular dynamics simulations

System details. The simulated PNIPAM systems used a 20-mer. The PNIPAM chain was extended through the periodic z-boundary and coupled back onto itself through periodic boundary conditions. By means of this periodic setup, the end groups on the 20-mer were eliminated. This description of an extended polymer chain has been

Table 5.2
Literature values of surface tension gradients $d\gamma_s/dc_s$, calculated a values for the LCST data of PNIPAM, and literature values of polarizability constants of both metal cations and selected anions.

Salt	$d\gamma_s/dc_s$ [25,52,309,439–441]** [$mNm^{-1}mol^{-1}dm^3$]	a [°C/M]	Polarizability [324]*** [cm^3/mol]
$MgCl_2$	3.77	−28.86	−0.7
$CaCl_2$	3.70	−28.35	1.59
$SrCl_2$	3.53	−27.01	2.65
LiCl	1.68	−12.90	0.08
NH_4Cl	1.45	−11.08	4.7
NaCl	1.76	−13.50	0.65
KCl	1.64	−12.54	2.71
RbCl	1.37	−10.50	4.1
CsCl*	1.62	−12.43	6.89
NaSCN	0.5	–	17
NaCl	1.6	–	8.63
Na_2SO_4	2.7	–	13.79

* CsCl was used as reference salt to calculate a from Eq. (5.4) for the other salts.
** Converted values ($mNm^{-1}mol^{-1}dm^3$) [442] from references 25,52,309,439–441 are used. Averages are calculated if more than one value is reported in the references. The error bars were estimated to be of the order $\pm 0.1\,mNm^{-1}mol^{-1}dm^3$.
*** Polarizability data for the cations for the metal chloride salts and for the anions for sodium salts.

Table 5.3
Number of PNIPAM chains, water molecules, cations, and anions in the respectively simulated systems for the two salt concentrations (0.3 m and 1.8 m) as well as for pure water.

	Salt concentration											
	c = 0 m				c = 0.3 m				c = 1.8 m			
System	N_{PNIPAM}	N_w	N_{cat}	N_{an}	N_{PNIPAM}	N_W	N_{cat}	N_{an}	N_{PNIPAM}	N_w	N_{cat}	N_{an}
$CaCl_2$	–	–	–	–	1	6338	34	68	1	5870	190	380
LiCl	–	–	–	–	1	6370	35	35	1	6048	196	196
NaCl	–	–	–	–	1	6370	35	35	1	6048	196	196
CsCl	–	–	–	–	1	6370	35	35	1	6048	196	196
Water	1	6440	0	0	–	–	–	–	–	–	–	–

reported before.[414,415] The length and elongation of the PNIPAM 20-mer defined a box size in the z-direction of L_z = 4.6839 nm. To minimize interactions between periodic images while still minimizing the computational cost, the lateral box dimensions L_x and L_y were initial set to 6.5 nm. The polymer was solvated in water and, after energy minimization and equilibration, individual water molecules were replaced with cations and anions until the target concentrations were achieved. Four different chloride salts, namely $CaCl_2$, LiCl, NaCl and CsCl at two salt concentrations, 0.3 m and 1.8 m, were simulated. The system compositions can be seen in Table 5.3.

Bulk simulations of 1.8 m $CaCl_2$, LiCl, NaCl, and CsCl, respectively, were performed as

well. A cubic box with a size of $4 \times 4 \times 4\,\mathrm{nm}^3$ was used. The concentration corresponded to 1988 water molecules, 64 cations and 128 anions for the $CaCl_2$ solution, and to 2048 water molecules, 66 cations and 66 anions for the monovalent salts.

Simulation details. All-atom molecular dynamics (MD) simulations were performed using the GROMACS 4.6.7 package.[443] The PNIPAM chain was simulated using the OPLS-AA force field[228] and all bonds were constrained using LINCS[417] up to a fourth order expansion. The SPC/E potential[418] for water was used and the internal geometry was kept rigid using the SETTLE algorithm.[419] The salt solutions were described by nonpolarizable force fields for $CaCl_2$,[245] LiCl,[78] NaCl[244] and CsCl.[244] The chloride anion was described by a modified version of the force field from Dang.[444] See Table 5.4 for the ionic force field parameters.

Note, the original force field for $CaCl_2$ was parameterized with a cutoff of 1.4 nm by employing long range energy and pressure corrections. Due to the PNIPAM force field not utilizing this, the simulations herein were performed without these corrections and it was shown from radial distribution function analyses of bulk electrolytes that no significant effect was observed when switching off the corrections. The geometric combination rule was used for interactions between different atom types in PNIPAM, as well as for the polymer–ion and polymer–water interactions. The Lorentz–Berthelot combination rule was used for ion–ion interactions as well as for ion–water interactions, except for LiCl where the geometric combination rule together with a scaling factor of 0.4 for ε was used for Li^+–water interactions, due to their original parameterization.

The systems were energy minimized followed by an NVT equilibration of 2 ns using a velocity-rescaling thermostat[409] and then by two NPT equilibrations. First, an equilibration was performed for 2 ns using the velocity-rescaling thermostat[409] and the Berendsen barostat.[408] Second, an equilibration using the Nosé–Hoover thermostat[410,420] and the Parrinello–Rahman barostat[411,412] was performed for 3 ns. Production runs were performed with the same thermostat and barostat as for the last equilibration step and for 100 ns for water and the 1.8 m salt systems, and for 400 ns for the 0.3 m salt systems. The coupling times for the thermostat and barostat were $\tau_T = 1\,\mathrm{ps}$ and $\tau_P = 1\,\mathrm{ps}$, respectively, for all equilibration and production runs. The temperature was 300 K and the pressure was 1 bar. To maintain the PNIPAM chain in a stretched conformation, a semi-isotropic pressure coupling scheme was applied and only the lateral (x and y) box dimensions were adjusted. The compressibilities in the x- and y-dimensions were set to $4.5 \cdot 10^{-5}\,\mathrm{bar}^{-1}$, while the compressibility in z-direction was $0\,\mathrm{bar}^{-1}$. The integration time step in all simulations was 2 fs, and the energies and configurations were saved every 1 ps. Long-range electrostatic interactions were treated by the particle mesh Ewald (PME) method[421] with a Fourier spacing of 0.12 nm, PME order 4, and a real space cutoff of 1.4 nm. A van der Waals

Table 5.4
Ionic force field parameters (Lennard-Jones size parameters σ_{ii} and dispersion interaction strengths ε_{ii}) for $CaCl_2$, LiCl, NaCl, and CsCl.

	Cation		Anion	
Salt	σ_{ii} [nm]	ε_{ii} [kJ/mol]	σ_{ii} [nm]	ε_{ii} [kJ/mol]
$CaCl_2$	0.241	0.9400	0.440	0.4100
LiCl	0.182	0.7000	0.440	0.4700
NaCl	0.258	0.4186	0.440	0.4186
CsCl	0.349	0.3250	0.440	0.4186

cutoff of 1.4 nm was used for truncating short-range interactions, no long-range corrections were applied. A cutoff distance of 1.4 nm was used for the neighbor list and was updated every 0.02 ps. Periodic boundary conditions were applied in all three directions.

In addition, a simulation of systems with a position restrained PNIPAM 20-mer solvated in 1.8 m $CaCl_2$ was performed as well. A force constant of 1000 $kJmol^{-1}nm^{-2}$ was applied on every atom of the polymer chain in the x-, y- and z-dimension. Otherwise, all other simulation parameters were the same and the system was identical to the one including the $CaCl_2$ salt described above.

The simulations details (force fields and simulations parameters) for the bulk aqueous solution were the same as for the systems including the PNIPAM chain described above, except that only 1 ns NPT equilibrations were performed with the Nosé–Hoover thermostat[410,420] and the Parinello–Rahman barostat[411,412] after energy minimization. Production runs of 60 ns with the same thermostat and barostat were performed afterwards.

Generation of elongated chain. The elongated chain was obtained by pulling apart the ends of a collapsed PNIPAM 20-mer structure with the GROMACS pull code. The desired elongation was a configuration which maximized the accessible polymer surface area and which could be approximated by a cylinder, but simultaneously maintained the natural backbone carbon angle value of about 121°. As such, an elongation of $\lambda = 0.88$ was used. The elongation was defined as $\lambda = L_z/L_c$, where $L_z = 4.6839$ nm was the box height and $L_c = 5.32$ nm was the contour length of the 20-mer.[415]

5.4.5 Preferential binding coefficients

The preferential binding of macromolecule–solvent over macromolecule–cosolvent, or vice versa, can be expressed by thermodynamic relations. The preferential binding

coefficient of cosolvent ions to a macromolecule can be traced back to Kirkwood–Buff (KB) theory[191] and can be expressed as

$$\Gamma_{23} = \rho_3 \left(G_{23} - G_{21} \right) = N_{23} - \frac{\rho_3}{\rho_1} N_{21}, \tag{5.6}$$

where the subscript 1 represents water, 2 the solute (macromolecule) and 3 the cosolute (ions). Note, all ions are treated as indistinguishable. Here, ρ_3 is the bulk number density of the cosolvent, G_{ij} are the Kirkwood–Buff integrals (KBIs) and N_{ij} are the excess coordination numbers. The KBIs are defined as

$$G_{ij} = G_{ji} = 4\pi \int_0^\infty [g_{ij}^{\mu VT}(r) - 1] r^2 \mathrm{d}r, \tag{5.7}$$

where $g_{ij}^{\mu VT}(r)$ is the radial distribution function for species i and j. The third part of Eq. (5.6) emphasizes that the preferential binding coefficient is an excess quantity. $\Gamma_{23} < 0$ and $\Gamma_{23} > 0$ indicate an excess of water over cosolute molecules or cosolute over water molecules in the solution shell of the macromolecule relative to the bulk composition, respectively. For simulations being carried out in closed systems, approximations (truncated KBIs at a distance where the radial distribution function, RDF, converges to unity as well as the usage of surface referenced RDFs) are necessary as well as a correction to the bulk solution distribution.[387] Herein, the preferential binding coefficient is calculated by following the approach of Pierce et al.[211]

$$\Gamma_{23} = \left\langle n_3(r) - \frac{N_3 - n_3(r)}{N_1 - n_1(r)} n_1(r) \right\rangle, \tag{5.8}$$

where N_1 and N_3 are the total number of water molecules and salt ions, respectively, in the system, $n_1(r)$ and $n_3(r)$ and are the local number of water molecules and salt ions, respectively, within a specific distance, r, to the PNIPAM 20-mer chain. The angle brackets $\langle \cdot \rangle$ denote time averaging. The preferential binding coefficient as a function of distance to the polymer chain for respective salt solutions can be seen in Figs. 5.6a and 5.6b for 0.3 m and 1.8 m salt solutions, respectively.

Equation (5.6) gives the relationship between the preferential binding coefficient and the concentration of cosolvent. Γ_{23} is linearly dependent on the salt concentration, expressed here as ρ_3, if $(G_{23} - G_{21})$ is a constant,[18] i.e., the difference between the solute–cosolute (2 – 3) and the solute–solvent (2 – 1) affinity is independent of the salt concentration. This is expected to be the case when the LCST trend is linear. If $(G_{23} - G_{21})$ is not a constant, a nonlinear LCST trend is expected. Depending on having stronger or weaker affinity for cosolute molecules compared to solvent molecules, an enrichment or depletion of the cosolute is observed.

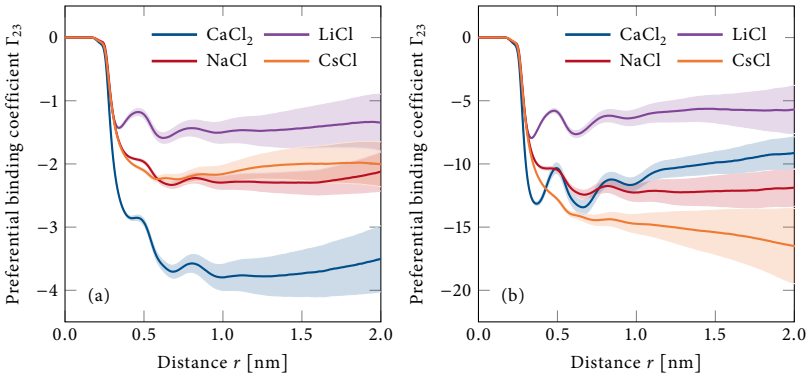

Fig. 5.6 Preferential binding coefficient for salts Γ_{23} as a function of the distance r to the closest part of the PNIPAM 20-mer chain at (a) 0.3 m and (b) 1.8 m, for four different salts. The shaded intervals indicate the standard deviation of the mean $\sigma/\sqrt{N}$ by using sample standard deviations σ and $N = 20$ (0.3 m) or $N = 5$ (1.8 m) blocks, respectively.

The preferential binding coefficients were evaluated in this work by calculating the average values at distances 1.15 nm to 1.5 nm from the polymer surface (Fig. 5.6) for the respective salts at two concentrations (Fig. 5.3). The preferential binding coefficient converges when r approaches infinity. For the finite boxes used in these simulations, a distance range with a converged value was used for calculating the average. A close to constant $(G_{23} - G_{21})$ term was observed for weakly hydrated salts (NaCl and CsCl) and a concentration-dependent $(G_{23} - G_{21})$ term was observed for the strongly hydrated salts ($CaCl_2$ and LiCl).

Additionally, the preferential binding coefficients as a function of the closest distance to the PNIPAM chain (Fig. 5.6) show undulations. This is more pronounced for Ca^{2+} and Li^+ compared to Na^+ and Cs^+ and correlates with how tightly the ions bind water molecules.

5.4.6 Cylindrical volume element for normalization

The proximal RDFs and the number of pairs at each distance r from the polymer backbone (see cation–anion ion pairing structure section below), were both normalized by a cylindrical volume element $\mathrm{d}V(r)$ around the polymer chain, where $V = L_z \pi r^2$. Figure 5.7 depicts a schematic representation of the cylindric volume element.

Fig. 5.7 Schematic representation of the volume element around the polymer chain used for volume normalization.

5.4.7 Contributions of heavy side chain atoms to the radial distribution function

Figure 5.8a,b show the total normalized proximal RDF between the backbone and Ca^{2+} (Fig. 5.4a) and between the backbone and Cl^- (Fig. 5.4b), respectively, as well as the constituents, which are broken up into different heavy side chain atoms. The contributions from the side chain atoms were calculated according to the closest side chain atom for each ion at a certain proximal distance to the backbone. The largest contributions for the cations come from the oxygen ($0.4 \leq r \leq 0.75$) and the terminal methyl groups ($r \geq 0.75$). The largest contributions for the chloride ions come from the nitrogen ($0.3 \leq r \leq 0.6$) and the terminal methyl groups ($r \geq 0.6$).

5.4.8 Hydration numbers

Figure 5.9 shows the number of hydration waters in the first hydration shell (i.e., first hydration number) for the various cations (Ca^{2+}, Li^+, Na^+, and Cs^+), respectively, as a function of the closest distance r to the polymer backbone. The strongly hydrated cations (Ca^{2+} and Li^+) have an intact hydration shell when approaching the polymer chain, while the weakly hydrated cations (Na^+ and Cs^+) lose some hydration waters.

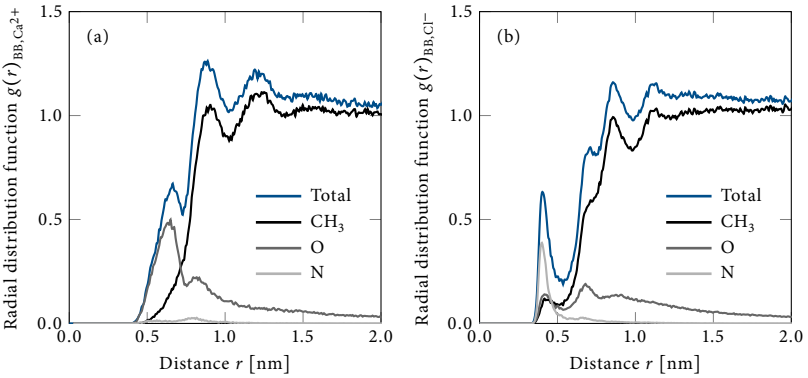

Fig. 5.8 Total normalized proximal radial distribution functions $g(r)$ between (a) the polymer backbone (BB) and Ca^{2+} ions and (b) the polymer backbone (BB) and Cl^- ions as a function of the closest distance r to the polymer backbone (total) and their respectively constituents (CH_3, O and N) represented by different heavy side chain atoms for 1.8 m $CaCl_2$.

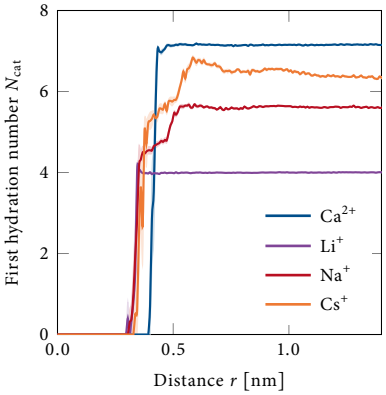

Fig. 5.9 First hydration number as a function of the closest distance r to the polymer backbone for the four cations in 1.8 m salt solutions. The shaded intervals indicate the standard deviation of the mean $\sigma/\sqrt{N}$ by using sample standard deviations σ and $N = 10$ blocks. The error bars are smaller than the line thickness when not visible.

Table 5.5
Total interaction energies (sum of van der Waals and Coulombic interactions) between the amide oxygen (including the associated carbon atom) and the four different cations, respectively, and between both the amide nitrogen (including the amide hydrogen and the neighboring CH group) and the two terminal methyl groups and the chloride ions in four different salt solutions (1.8 m), respectively. The average interaction energies with one cation or anion are reported. The error bars are standard deviation of the mean $\sigma/\sqrt{N}$ by using sample standard deviations σ and $N = 10$ blocks.

	Cation			
	$CaCl_2$	LiCl	NaCl	CsCl
Amide oxygen–cation [J/mol]	−107.6 ± 6.7	−48.8 ± 2.9	−39.9 ± 4.5	−31.0 ± 3.8
	Anion			
	$CaCl_2$	LiCl	NaCl	CsCl
Amide nitrogen–chloride [J/mol]	−25.6 ± 0.7	−26.6 ± 1.2	−33.0 ± 0.9	−24.5 ± 1.1
Two terminal methyl groups–chloride [J/mol]	−8.3 ± 0.1	−8.1 ± 0.2	−8.1 ± 0.2	−6.6 ± 0.2

5.4.9 Interaction energies between PNIPAM side chains and ions

An energetic analysis of the interactions between different parts of the polymer chain and the various cations (Ca^{2+}, Li^+, Na^+ and Cs^+) and Cl^-, respectively, was employed to obtain additional information about the nature of polymer–ion interactions. The energies between the ions and the polymer side chain parts were calculated from simulated trajectories. The sum of the van der Waals and electrostatic (Coulombic) interactions were obtained from the same trajectories using the rerun option in GROMACS, where the electrostatic energies were computed using a reaction field with a dielectric constant of 78. The results for the 1.8 m salt solutions are provided in Table 5.5. Weak, but favorable interactions between the amide oxygen (including the associated carbon atom) and the cations were observed. This agrees with previous experiments and computer simulation results.[7,75,84,115] The order of the interaction energies is: $Ca^{2+} > Li^+ > Na^+ > Cs^+$ (i.e., a direct Hofmeister series), and agrees with trends that have previously been proposed.[84,115,118] Very weak, but favorable interactions between the amide nitrogen (including hydrogen and neighboring CH group) and the chloride and between the two terminal methyl groups and the chloride, respectively, were observed. This is in line with previous experimental results.[7,118]

5.4.10 Cation–anion ion pairing structures

The number density $\rho(r)$ of cation–anion pairs have been calculated for contact ion pairs (CIPs), solvent-shared ion pairs (SIPs) and solvent separated ion pairs (2SIPs) as a function of the closest distance r between the cation in the ion pair and the polymer backbone. A cylindrical volume element $dV(r)$ around the polymer chain (Fig. 5.7)

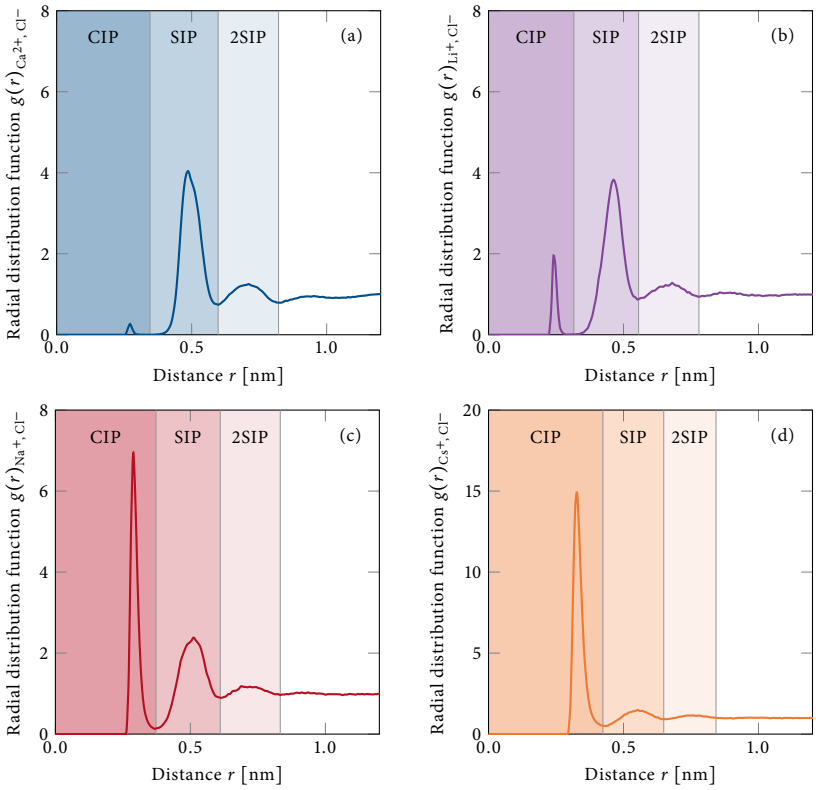

Fig. 5.10 Radial distribution function $g(r)$ between (a) Ca^{2+} and Cl^-, (b) Li^+ and Cl^-, (c) Na^+ and Cl^- and (d) Cs^+ and Cl^- as a function of the distance r for four salt solutions. The shaded, colored areas indicate the different ion pairs: contact ion pair (CIP), solvent-shared ion pair (SIP) and solvent separated ion pair (2SIP).

was used to calculate the number density at each distance. The cation–anion RDFs for 1.8 m bulk solutions of the four salts $CaCl_2$, LiCl, NaCl and CsCl shown in Fig. 5.10 were used for the definition of ion pairs. The different types of cation–anion ion pairs are defined from the local minima in the RDF and are indicated in each graph by the shading.

The number densities for the ion pairs were normalized by the bulk value $\rho\,(r \to \infty)$ and the normalized cation–anion number densities $\rho\,(r)\,/\rho\,(r \to \infty)$ are reported.

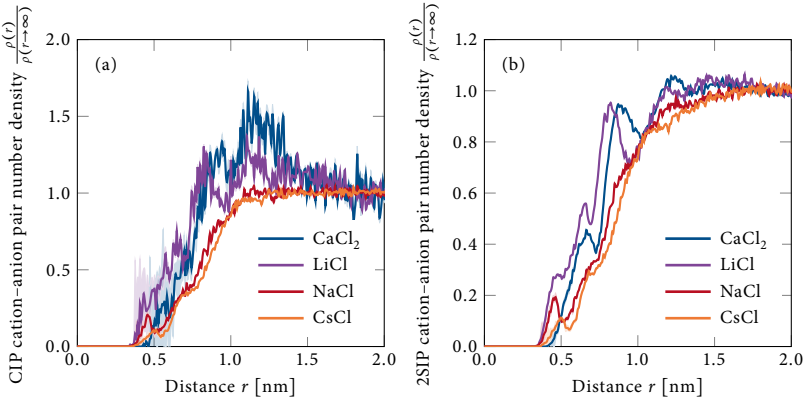

Fig. 5.11 Normalized (a) contact cation–anion pair (CIP) and (b) solvent separated cation–anion pair (2SIP) number densities $\rho(r)/\rho(r\to\infty)$ as a function of the closest cation distance r to the polymer for four different salt solutions (1.8 m). The shaded intervals indicate the standard deviation of the mean $\sigma/\sqrt{N}$ by using sample standard deviations σ and $N = 10$ blocks, and by using propagation of uncertainty. The error bars are smaller than the line thickness when not visible.

The normalized number of cation–anion CIPs (Fig. 5.11a) and 2SIPs (Fig. 5.11b) as a function of the distance to the polymer backbone for each cation, including error bars, is shown. As with SIPs (Fig. 5.5), distinct peaks can be seen for 2SIPs with strongly hydrated cations but not for the weakly hydrated ones. Accumulation at the side chain is, however, less pronounced than for SIPs. No conclusions can be drawn from the CIPs for the salt solutions containing strongly hydrated cations due to the large error bars. The relatively poor statistics were the result of having very few CIPs observed in the simulations due to strong ion–water interactions in combination with their depletion from the macromolecule surface.

5.4.11 Probability spatial density maps

Spatial probability density maps were generated from the simulation of a PNIPAM chain in 1.8 m $CaCl_2$ solution with an applied position restraint on the polymer chain. Heavy atoms from one of the monomers were used to map all the conformations in space before the spatial probability densities were calculated and the probability density maps were generated. Figures 5.12a and 5.12b show the spatial probability density for Ca^{2+} (blue area) and for Ca^{2+} in solvent-shared pairs with at least one Cl^- ion (yellow area), respectively, around the infinite PNIPAM chain averaged over 100.000 frames (100 ns).

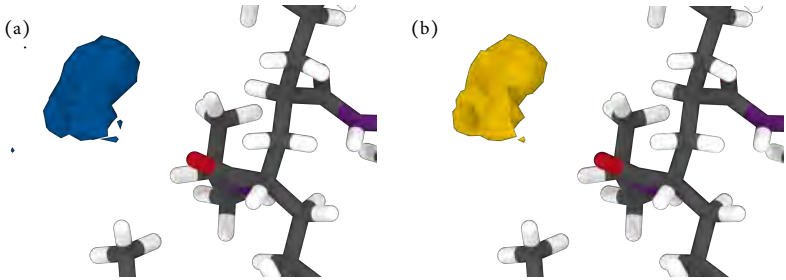

Fig. 5.12 Spatial probability density map of (a) Ca^{2+} around the PNIPAM chain and of (b) Ca^{2+} in a solvent-shared pair configuration around the PNIPAM with at least one Cl^- ion using Ovito software.[425] Both blue and yellow indicate four times the bulk Ca^{2+} number density. Red represents oxygen atoms, purple is used for nitrogen atoms, gray is used for carbon atoms and white is used for hydrogen atoms.

Local accumulation of single ions as well as ion pairs were seen in the vicinity of the amide oxygen. The behavior of the spatial probability density maps is quite similar in the two cases (Ca^{2+} ions only and Ca^{2+} ions in solvent-shared pairs with at least one Cl^- ion). In fact, when changing the threshold, only a slightly lower probability for Ca^{2+} in a SIP with Cl^- versus Ca^{2+} alone is observed. As such, the probability for partitioning Ca^{2+} to the macromolecule surface in the form of ion pairs with Cl^- is similar to the probability of finding Ca^{2+} ions at the same location.

5.4.12 Surface tension and lower critical solution temperatures

Measured surface tension values are known to show salt concentration dependency.[445] The surface tension increment $\Delta\gamma_s$ is the difference between the surface tension of pure water (w) and water with a specific concentration of salt (s):

$$\Delta\gamma_s = \gamma(c_s) - \gamma_w, \tag{5.9}$$

where c_s is the salt concentration. Figure 5.13a shows the $\Delta\gamma_s$ values for $CaCl_2$, LiCl, NaCl and CsCl, respectively, at various salt concentrations.[441] The larger increase for $CaCl_2$ comes from the fact that the concentration of chloride ions is twice as high per mole salt. By contrast, the smaller increase for CsCl originated from the weakly hydrated cesium ions affecting the surrounding water molecules less. If the surface tension were the only contribution to the macromolecule's solubility, then the phase transition temperature of PNIPAM would behave like the hypothetical LCST dependence shown in Fig. 5.13b.

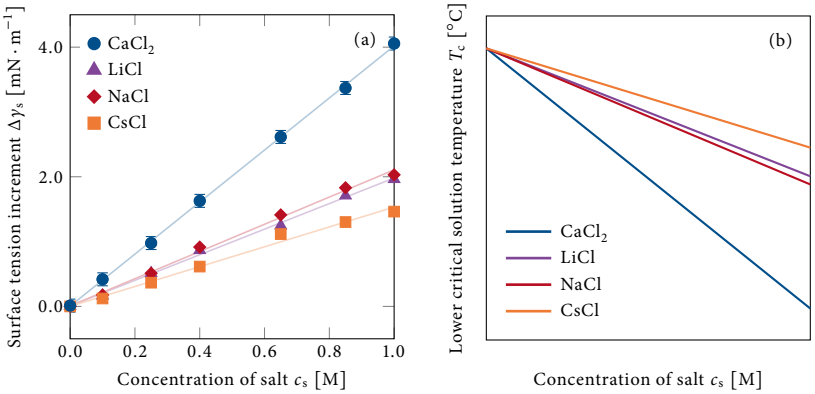

Fig. 5.13 (a) Change in the air–water surface tension $\Delta\gamma_s$ relative to water for four chloride salts as a function of salt concentration c_s adapted from reference 441. The error bars are approximately $\pm 0.1\,\mathrm{mNm^{-1}}$, and are on the order of the size of the data points. The lines represent linear fits to the data. (b) The hypothetical lower critical solution temperature T_c based on a pure surface tension contribution for the four chloride salts. This hypothetical trend is not observed in Fig. 5.2.

5.4.13 Lower critical solution temperatures for other chloride salt solutions

The LCST behavior for NaCl as a function of the salt concentration is compared with the LCST for $N(CH_3)_4Cl$ in Fig. 5.14 to demonstrate the difference in Hofmeister effects with nonmetal cations.

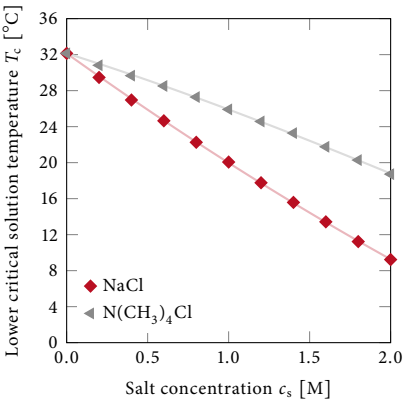

Fig. 5.14 Lower critical solution temperature T_c for 10 mg/ml PNIPAM in sodium chloride and tetramethylammonium chloride salt solutions, respectively, as a function of salt concentration c_s. The symbols are data points and the lines are fits corresponding to empirical models (Eq. (5.5) for NaCl, and Eq. (5.3) excluding last two terms in the parenthesis for $N(CH_3)_4Cl$). Each data point represents an average of six measurements . In each case the error bars, which were calculated from sample standard deviations, are smaller than the size of the data points.

Chapter 6

Nonadditive ion effects drive both collapse and swelling of thermoresponsive polymers in water

This chapter corresponds to and is reproduced with permission from

> Bruce, E. E.; Bui, P. T.; Rogers, B. A.; Cremer, P. S.; van der Vegt, N. F A. Nonadditive ion effects drive both collapse and swelling of thermoresponsive polymers in water. *J. Am. Chem. Soc.*, 141(16):6609–6616, 2019. Copyright 2019 American Chemical Society.

Abstract. When a mixture of two salts in an aqueous solution contains a weakly and a strongly hydrated anion, their combined effect is nonadditive. Herein, we report such nonadditive effects on the lower critical solution temperature (LCST) of poly(*N*-isopropylacrylamide) (PNIPAM) for a fixed concentration of Na_2SO_4 and an increasing concentration of NaI. Using molecular dynamics simulations and vibrational sum frequency spectroscopy, we demonstrate that at low concentrations of the weakly hydrated anion (I^-), the cations (Na^+) preferentially partition to the counterion cloud around the strongly hydrated anion (SO_4^{2-}), leaving I^- more hydrated. However, upon further increase in the NaI concentration, this weakly hydrated anion is forced out of solution to the polymer–water interface by sulfate. Thus, the LCST behavior of PNIPAM involves competing roles for ion hydration and polymer–iodide interactions. This concept can be generally applied to mixtures containing both a strongly and a weakly hydrated anion from the Hofmeister series.

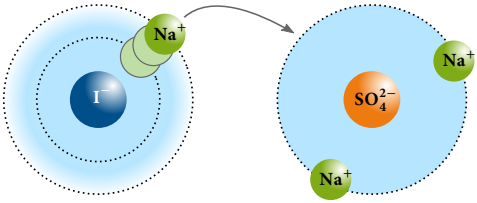

6.1 Introduction

Traditionally, the relative effects of anions on physical behavior in aqueous solutions have been ranked according to the Hofmeister series: $CO_3^{2-} > SO_4^{2-} > S_2O_3^{2-} > H_2PO_4^- > F^- > Cl^- > Br^- > NO_3^- > I^- > ClO_4^- > SCN^-$.[2,3] While weakly hydrated anions (right side of the series) partition to nonpolar environments such as air–water interfaces[5] or polymer surfaces[4,6,7], strongly hydrated anions (left side of the series) prefer the bulk water environment. Herein, however, we demonstrate that the extent of hydration of a weakly hydrated anion can be modulated in the presence of a second strongly hydrated anion . As such, the current Hofmeister series needs to be updated to account for weakly hydrated anions' bifurcated behavior in mixed salt solutions.

The balance between an anion's affinity for water and for nonpolar environments can be exploited to regulate the phase behavior of polymers in aqueous solutions. The total effect of salts on polymer solubility is related to the behavior of both the anions and the cations, whose specific interactions are considered to be independent and additive. This idea goes back to the pioneering work of Guggenheim[22,23] and others,[24,446,447] and is commonly used today to rationalize the actions of Hofmeister ions in chemistry and biology. Additionally, the assumption of additivity is consistent with the behavior of many single salts in the Hofmeister series.[25,26] Very recently, however, it has been argued that not only ion–macromolecule but also ion–counterion interactions in the bulk solution and at the interface can affect polymer phase transitions.[17,182] For example, deviations from the additivity assumption have been observed in systems containing guanidinium cations. These cations have varying abilities to form ion pairs at the macromolecule surface (cooperative binding) depending upon the counteranions with which they are paired.[19,121] This can lead to either polymer swelling or collapse.

Compared to single salts, fewer studies have focused on salt mixtures. Nonadditive effects on aqueous polymer solubility in mixed salt solutions have been reported for poly(propylene oxide) (thermodynamic measurements).[184] Additionally, it has been shown that strongly hydrated anions can drive weakly hydrated anions to the air–water interface in mixed electrolyte solutions (spectroscopic measurements and molecular dynamics (MD) simulations).[190] Although interesting effects from mixed salt solutions were observed in both of these works, the full range of the Hofmeister series has not yet been explored, and the molecular mechanisms remain elusive.

Herein, we report ion-specific effects on the lower critical solution temperature (LCST) of poly(*N*-isopropylacrylamide) (PNIPAM) in three mixed salt solutions, namely NaI and Na_2SO_4, NaI and NaCl, as well as NaCl and Na_2SO_4. The most pronounced non-additive features were observed for the combination of a weakly hydrated salt (i.e., NaI) and a strongly hydrated salt (i.e.,Na_2SO_4). Significantly, it was found that ion hydration and polymer–anion interactions could be regulated in the presence of the weakly and

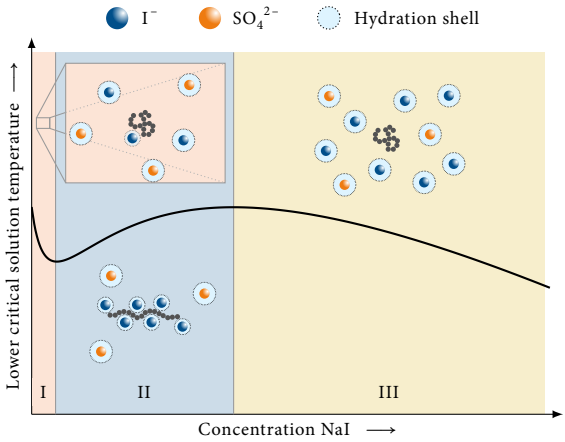

Fig. 6.1 Schematic illustration of nonadditive ion effects on the lower critical solution temperature (LCST) of thermoresponsive polymers in aqueous solution containing a fixed concentration of a strongly hydrated salt (Na_2SO_4) and an increasing concentration of a weakly hydrated salt (NaI). In region I, enhanced iodide hydration drives polymer collapse. In region II, SO_4^{2-} salts out I^-, which in turn becomes enriched at the polymer–water interface, driving polymer swelling. In region III, enhanced ion hydration again drives polymer collapse.

strongly hydrated mixed salts, leading to both collapse and swelling transitions of the polymer. The underlying mechanisms are addressed using atomic-level insight obtained from MD simulations and vibrational sum frequency spectroscopy (VSFS).

Figure 6.1 schematically depicts the collapse and swelling behavior of PNIPAM in the presence of a fixed concentration of Na_2SO_4 and an increasing concentration of NaI. The nonadditive effects were observed at low concentration (region I) and intermediate concentration (region II) of NaI. At low NaI concentration (region I), the presence of Na_2SO_4 does not significantly affect the interaction between iodide and the polymer. Counterintuitively, the polymer collapses more readily. The VSFS measurements and MD simulations suggest that sodium cations preferentially partition to the counterion cloud around sulfate, resulting in a lower excess counterion density around iodide. As such, iodide becomes more hydrated and drives polymer collapse.[136] This effect is saturable and upon further addition of NaI, a re-entrant behavior of the polymer is observed in region II. Under these conditions, the strongly hydrated salt (Na_2SO_4) affects the solubility of the weakly hydrated salt (NaI), in accordance with the mechanism proposed in an earlier work.[190] Specifically, more iodide adsorbs to the polymer, leading to swelling. When the NaI concentration is increased even further (region III), the polymer again collapses, driven by the depletion of hydrated ions. The nonadditive ion

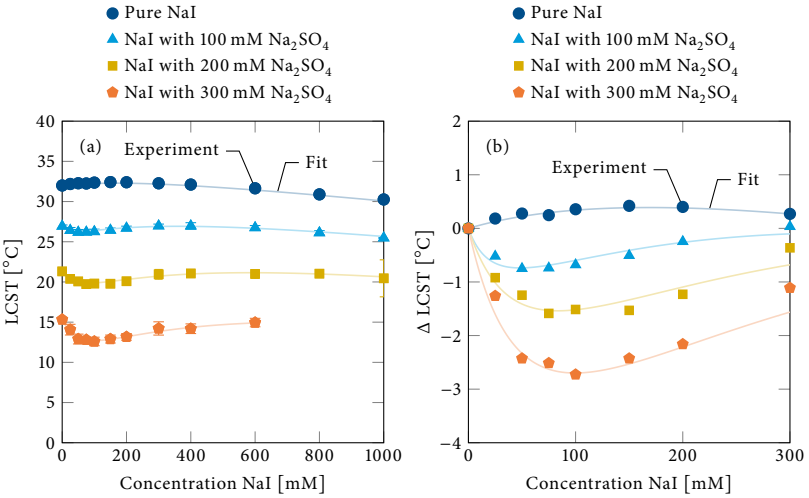

Fig. 6.2 (a) Lower critical solution temperature (LCST) and (b) the change in LCST (ΔLCST) of PNiPAM upon the addition of NaI with 0 mM, 100 mM, 200 mM, and 300 mM Na_2SO_4 as the background salt. Note that ΔLCST is only shown for data points within the 0 mM–300 mM NaI concentration range in order to highlight the dip in the LCST. The error bars are calculated from sample standard deviations from three sets of measurements. See Fig. 6.7 for the error bars corresponding to the ΔLCST values. The fits correspond to the empirical model given in Eq. (6.1). The fitting parameters are reported in Table 6.1.

effects observed herein shed new light on Hofmeister ion chemistry and should help provide new insights into a broad range of complex mixed electrolyte solutions such as ocean waters, dense cellular environments and multicomponent ion solutions found in a typical chemistry laboratory.[57,448,449]

6.2 Results and discussion

6.2.1 Lower critical solution temperature of PNIPAM in aqueous salt solutions

PNIPAM displays an inverse phase transition above its LCST. Herein, we systematically investigated the change in the LCST of PNIPAM in the presence of fixed concentrations of Na_2SO_4 and increasing concentration of NaI. The LCST was determined from

Table 6.1
Fitting parameters (T_0, a, $B_{max,1}$, $K_{D,1}$, $B_{max,2}$ and $K_{D,2}$) for the empirical lower critical solution temperature model of PNIPAM in NaI and mixtures of NaI with Na_2SO_4 given by Eq. (6.1).*

	Na_2SO_4 concentration [mM]			
	0	100	200	300
T_0 [°C]	31.9	27.0	21.4	15.4
$B_{max,1}$ [°C]	3.1	6.9	14.9	23.8
$B_{max,2}$ [°C]	–	−2.5	−8.6	−15.9
$K_{D,2}$ [mM]	–	33.8	81.0	96.0
a [°C/mM]	-4.2×10^{-3}			
$K_{D,1}$ [mM]	308.1			

* The parameters a and $K_{D,1}$ are independent of the Na_2SO_4 concentration (see Section 6.4.5).

the turbidity changes of polymer solutions as a function of temperature. More details on the LCST measurements can be found in Section 6.4.1. As shown in Fig. 6.2a, in the absence of Na_2SO_4, the LCST of PNIPAM initially increases, reaches a maximum, and then decreases upon adding NaI (dark blue curve), consistent with earlier observations.[4] Interestingly, in mixed salt solutions, the solubility of PNIPAM depends on the concentration of NaI, the type of added salt (the background salt) as well as its concentration. In the presence of the highest Na_2SO_4 background concentration (orange curve), the LCST behavior can be divided into three NaI concentration regions: region I (0 mM–100 mM), region II (100 mM–600 mM), and region III (>600 mM). At lower Na_2SO_4 concentrations, the boundary between regions II and III shifts to lower NaI concentration. In the presence of Na_2SO_4, the LCST decreases in region I, in marked contrast to the increase observed in the pure NaI system. Upon further addition of NaI, the LCST increases (region II) and then eventually decreases (region III) in the presence of 100 mM and 200 mM Na_2SO_4 (light blue and yellow curves, respectively). With 300 mM Na_2SO_4, this decrease is not observed (orange curve) but would presumably occur at a higher NaI concentration, if the solubility limit of the salts was not reached. The magnitude of the initial decrease, which is manifested as a dip, is dependent on the background salt concentration. For comparison, ΔLCST, defined as the change in the LCST upon adding NaI, is shown in Fig. 6.2b. The dip becomes more pronounced as the concentration of the background salt increases.

The LCST of PNIPAM as a function of NaI concentration can be empirically modeled by

$$T = T_0 + ac_{salt} + \frac{B_{max,1}c_{salt}}{K_{D,1} + c_{salt}} + \frac{B_{max,2}c_{salt}}{K_{D,2} + c_{salt}}, \tag{6.1}$$

where T_0 is the LCST in the absence of NaI, and ac_{salt} (with c_{salt} being the NaI concentration) is a linear term related to the surface tension at the polymer–water interface.

The third term is a Langmuir binding isotherm, which quantifies the magnitude of the increase in the LCST from the initial LCST (T_0) due to iodide adsorption to the PNIPAM chain. The dissociation constant ($K_{D,1}$) quantifies the strength of the iodide adsorption process, which at saturation produces a maximum increase in the LCST ($B_{max,1}$). The LCST of PNIPAM in single electrolyte solutions can be fully explained by the first three terms and has been utilized previously.[4] The fourth term, which is needed to describe mixed salt solutions, is reminiscent of a Langmuir binding isotherm but originates from ion pairing and ion hydration. This term quantifies the decrease in the LCST due to enhanced iodide hydration and has a negative $B_{max,2}$ value. The fitting parameters are summarized in Table 6.1. More details on the fitting procedure are provided in Section 6.4.5.

6.2.2 Polymer–ion interactions

To elucidate the mechanisms of nonadditivity in the LCST measurements, we analyzed the number of iodide ions in proximity to a PNIPAM 5-mer (oligomer) using MD simulations. Details concerning the simulations and the force fields can be found in Section 6.4.2 and in Table 6.2, respectively. Note that while molarity is used to describe concentration in the experiments, molality is used in the simulations where 0.1 m is equivalent to 100 mM. The difference between the two units is negligible within the range considered in these studies. Figure 6.3 shows the number of iodide ions in proximity to the oligomer surface as defined by the first peak of the proximal radial distribution function.

In region I (0.1 m NaI), the number of iodide ions is not affected by the presence of Na_2SO_4, yet the polymer collapses more readily. By contrast, in regions II and III, Na_2SO_4 pushes iodide toward the PNIPAM–water interface. This agrees with the observed increase in $B_{max,1}$ as Na_2SO_4 concentration increases (Table 6.1). In a mixed electrolyte solution, the strongly hydrated salt may salt out the weakly hydrated salt, as has previously been demonstrated by monitoring ions at the air–water interface with a combination of photoelectron spectroscopy and MD simulations.[190] Our simulations confirm that the surface enhancement of the large polarizable anion (I^-) is driven by the strongly hydrated ion (SO_4^{2-}). As such, the observed increase in the LCST in region II results from a forced iodide adsorption effect.

The iodide–polymer interactions were further explored using VSFS measurements. To do this, a Gibbs monolayer of PNIPAM was formed at the air–water interface in the presence of salts in the subphase, as schematically shown in Fig. 6.4a. More details on the VSFS measurements are described in Section 6.4.1. Figure 6.4b shows the OH stretch region (3000 cm^{-1}–3800 cm^{-1}) of the air–PNIPAM–water interface in pure Na_2SO_4 and mixtures of Na_2SO_4 and NaI. For complete spectra (2800 cm^{-1}–3800 cm^{-1}) as a

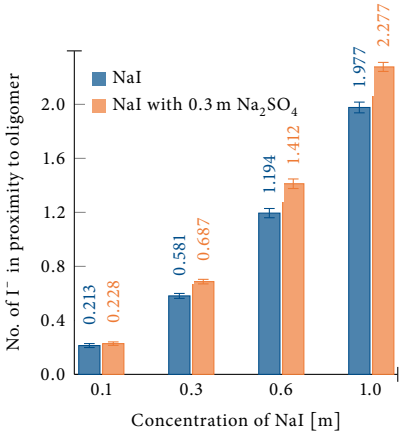

Fig. 6.3 Number of iodide ions in proximity to the PNIPAM oligomer at different concentrations of NaI in the absence (blue bars) and presence (orange bars) of 0.3 m Na_2SO_4. The proximity is defined by the first peak in the proximal radial distribution function between the oligomer surface and iodide and is equal to 0.52 nm. The error bars are error estimates calculated from 20 blocks and sample standard deviations.

function of NaI concentration in the absence and presence of Na_2SO_4, see Fig. 6.8. The peak assignments and the fitting parameters are summarized in Table 6.3 and Table 6.4. The spectra are dominated by two broad features at 3200 and 3400 cm^{-1}, consistent with previous studies of this interface.[12] The 3200 cm^{-1} peak reports on more ordered water molecules, while the peak around 3400 cm^{-1} arises from water molecules with less ordered hydrogen bonds.[450–452] It has been previously shown that this lower coordination water population (3400 cm^{-1}) is closer to the interface because that is where registry between interfacial water molecules and hydrogen bond donors/acceptors from adjacent organic or inorganic layers is most easily disrupted (red water molecules, Fig. 6.4a).[404] Further away from the interface, it is possible to achieve more tetrahedral water structure, giving rise to the peak around 3200 cm^{-1} (orange water molecules).[404] As such, the 3200 cm^{-1} feature should represent water molecules that are further away from the polymer surface and are aligned by the interfacial potential, while the 3400 cm^{-1} feature should arise mostly from the water structure in the inner hydration shell of the polymer, adjacent to the polymer–water interface.

Upon introducing NaI to the subphase, the oscillator strength of the 3400 cm^{-1} peak increases monotonically (red curve in Fig. 6.4c). This increase is consistent with the direct adsorption of I^- to the PNIPAM surface, which aligns water molecules in the first hydration layer (red water molecules, Fig. 6.4a). At higher NaI concentration, the

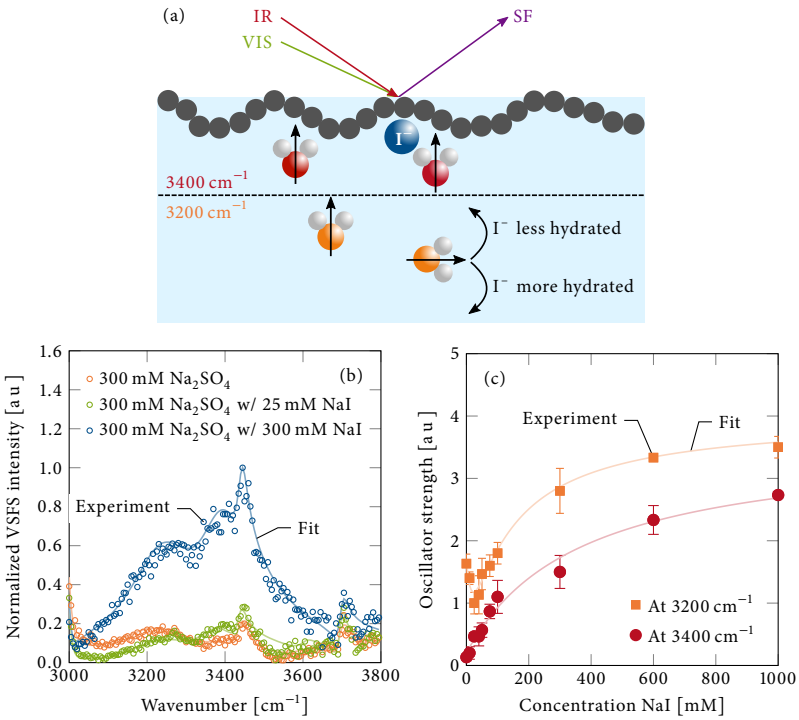

Fig. 6.4 (a) Schematic illustration of the orientation of the water molecules at the air–PNIPAM–water interface in the absence and presence of salts. Two major water populations are colored in red (3400 cm^{-1}) and orange (3200 cm^{-1}), with the black arrows indicating the direction of the water dipoles. The curved arrows indicate possible disruptions of the alignment. (b) Vibrational sum frequency spectroscopy (VSFS) spectra of the water region (3000 cm^{-1}–3800 cm^{-1}) of a PNIPAM monolayer at the air–water interface in the presence of 300 mM Na_2SO_4 background and 0 mM (orange), 25 mM (green), and 300 mM (blue) NaI in the subphase. The data were fitted using Eq. (6.4). See Table 6.4 for peak assignments and fitting parameters. (c) The oscillator strengths at 3200 cm^{-1} (orange) and 3400 cm^{-1} (red) as a function of the NaI concentration in the presence of 300 mM Na_2SO_4. The error bars are calculated from standard deviations from three sets of measurements. Equation (6.5) was used to fit the data, and Table 6.5 provides the fitting parameters.

surface becomes saturated with iodide, and the oscillator strength of the 3400 cm^{-1} peak approaches a maximum value, $B_{max,1}$ (Table 6.5). The value of $B_{max,1}$ in the presence of Na_2SO_4 is larger than that in the pure NaI case (Table 6.5), supporting the notion of enhanced iodide loading found in the MD simulations (Fig. 6.3).

By contrast with the 3400 cm^{-1} peak, the oscillator strength of the 3200 cm^{-1} resonance decreases and then increases as NaI is added to the solution (orange curve in Fig. 6.4c). The dip in the oscillator strength is reminiscent of the dip in the LCST measurements. Presumably, the minimum occurs at a lower NaI concentration in the VSFS experiments because of differences in the binding sites exposed to water for polymers in the bulk solution (LCST measurements) versus at the Gibbs monolayer (VSFS measurements). In pure NaI solutions, a monotonic increase in the oscillator strength of the 3200 cm^{-1} peak is observed and is related to the change in the interfacial potential as iodide binds to the surface (light blue curve in Fig. 6.8c). By contrast, in pure Na_2SO_4 solutions, the oscillator strength of the 3200 cm^{-1} peak continuously decreases (Fig. 6.9). This decreasing trend is caused by disruption in the alignment of water molecules further from the polymer surface as more well-hydrated ions are introduced. As such, the initial decrease in the oscillator strength of the 3200 cm^{-1} peak in the mixtures of NaI with Na_2SO_4 implies that iodide behaves like a strongly hydrated ion in region I of mixed salt solutions.

6.2.3 Ion pairing and ion hydration

The nonmonotonic response of the 3200 cm^{-1} peak in the salt mixture suggests that the behavior of iodide beyond the first hydration shell of PNIPAM is distinct from that in the pure NaI solution. MD simulations were performed on bulk solutions, i.e., without PNIPAM, to explore the nature of ion pairing and ion hydration in single and mixed salt solutions. The ion-pairing affinity between an anion and a cation (ΔN), also referred to as the excess ion pairing, is defined as

$$\Delta N = \frac{N_{\mathrm{cat}}}{V} \int_0^{r_2} [g_{\mathrm{an,cat}}(r) - 1] 4\pi r^2 \mathrm{d}r, \tag{6.2}$$

where $g_{\mathrm{an,cat}}(r)$ is the anion–cation radial distribution function, and N_{cat}/V is the number density of cations, here sodium ions. ΔN is determined by the balance of ion–ion, ion–water and water–water (hydrogen bonding) interactions and can be interpreted as the change in the number of cations in a spherical observation volume of radius r_2 before and after placing an anion at the center of that region. r_2 is picked to include both contact ion pairs (CIPs) and solvent-shared ion pairs (SIPs).[126] As can be seen in Fig. 6.5a, excess ion pairing between iodide and sodium decreases in the presence of Na_2SO_4 (orange data points) compared to in pure NaI solutions (blue data points). In contrast, Fig. 6.5b shows that the excess ion pairing between sulfate and sodium increases as NaI is added to Na_2SO_4. Significantly, some sodium ions from the introduction of the NaI partition from iodide to the counterion cloud around sulfate in the mixed salt case.

This partitioning of sodium cations has a profound effect on iodide hydration. The anion–water affinity (ΔN) was quantified using an equation similar to Eq. (6.2) (see Eq. (6.7) for definition) where the anion–cation terms are replaced by anion–water equivalents and r_2 is the radius of the second hydration shell. The water affinity of iodide increases (orange data points in Fig. 6.5c) in mixed salt systems compared to the pure NaI systems (blue data points). Iodide ions therefore become more hydrated in the presence of Na_2SO_4. Detailed analysis of the MD simulations including the CIPs and SIPs as well as the first and second hydration shells for the anions in various mixtures are summarized in Figs. 6.10 to 6.15. Similar trends for ion pairing and ion hydration were observed in the simulations at various temperatures (Fig. 6.16), suggesting that this mechanism is operative across the temperature range spanned by the LCST measurements.

6.2.4 Mechanisms of nonadditivity in mixed salt solutions

The LCST of PNIPAM displays pronounced signatures of nonadditivity upon the addition of NaI to solutions containing a fixed concentration of Na_2SO_4 (Fig. 6.2). The combination of VSFS measurements and MD simulations reveals that SO_4^{2-} enhances the iodide–water affinity in the bulk solution, while simultaneously driving I^- to the polymer–water interface. These two effects provide a molecular-level mechanism for the observed nonadditivity in salt mixtures containing weakly and strongly hydrated anions with a common cation. A schematic illustration of this mechanism is provided in Fig. 6.6. The concentration dependence of these two effects is distinct and gives rise to the three regions in the LCST phase diagram. At low concentrations of NaI (region I), Na^+ is recruited into the counterion cloud of SO_4^{2-} (black curved arrow in Na_2SO_4), leaving I^- more hydrated than in a pure salt solution. The enhanced iodide–water affinity in the presence of SO_4^{2-} increases the NaI activity[78,126] and drives the salting-out effect observed in region I. At intermediate NaI concentrations (region II), I^- is forced out of solution to the polymer–water interface by SO_4^{2-}. The enhanced binding of I^- to the polymer dominates over the enhanced hydration effect and gives rise to reentrant swelling of the PNIPAM chain. At the highest concentrations of NaI (region III), the addition of more salt decreases the LCST in a manner similar to the single salt case. This effect is related to the increased surface tension at the polymer–water interface.

6.2.5 Other mixed salt cases

Using NaCl in place of Na_2SO_4 as the background salt, we demonstrate that the valency of the background anion, rather than its identity, is crucial for the nonadditive behavior of mixed salt solutions.[453,454] In the presence of NaCl, adding NaI produced a smaller

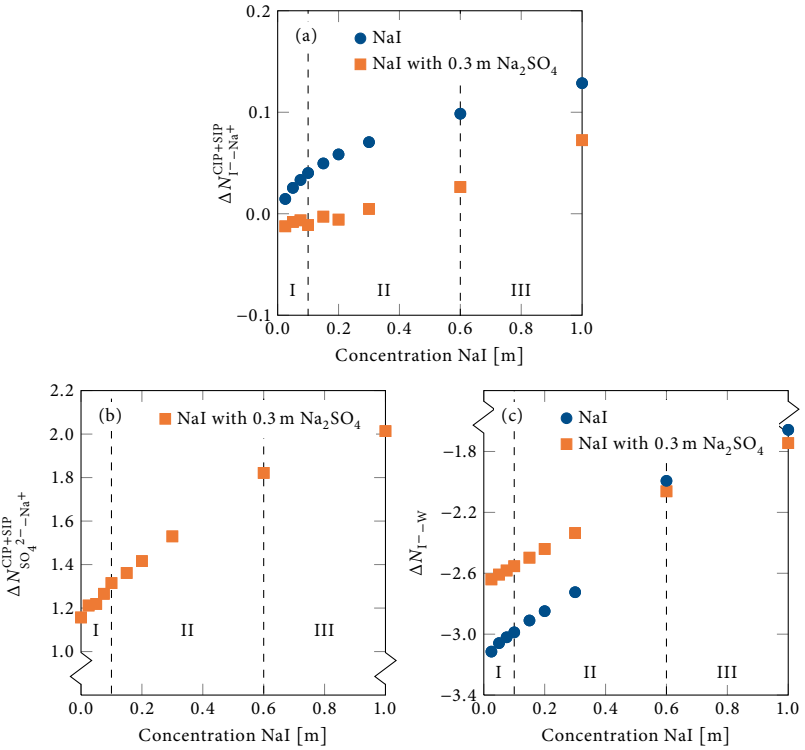

Fig. 6.5 (a) Excess ion pairing between iodide and sodium for both contact and solvent-shared ion pairs (CIP+SIP) as a function of NaI concentration in the absence (blue) and presence (orange) of 0.3 m Na_2SO_4. (b) Excess ion pairing between sulfate and sodium for both contact and solvent shared ion pairs (CIP+SIP) as a function of NaI concentration in the presence of 0.3 m Na_2SO_4. (c) Iodide–water affinity as a function of NaI concentration in the absence (blue) and presence (orange) of 0.3 m Na_2SO_4. The dashed lines show the boundaries between regions I, II, and III. The error bars are error estimates calculated from 20 blocks and sample standard deviations and are smaller than the symbols.

dip in the LCST (Fig. 6.17 and Table 6.6). This is expected, as the countercation cloud around a divalent ion (i.e., SO_4^{2-}) is denser than the one around a monovalent ion (i.e., Cl^-). This idea concurs with the known pairing affinity between Na^+ and anions in pure salt solutions, which follows the series $SO_4^{2-} > Cl^- > I^-$ with dissociation constants of 150 mM,[455] 250 mM,[456] and 1.4 M,[457] respectively. That is, the partitioning of Na^+ from the countercation cloud around I^- to the one around Cl^- is less effective than to the one around SO_4^{2-}, leaving iodide less hydrated in the former case. As such,

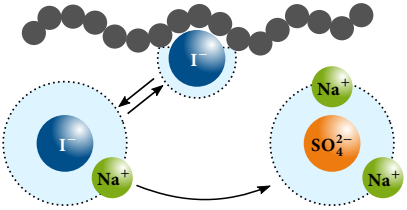

Fig. 6.6 Schematic illustration of the mechanisms of nonadditivity in mixed salt solutions. The chain of gray spheres represents the polymer, while the anion hydration shells are drawn as black dashed circles. The partitioning of Na^+ from I^- to SO_4^{2-}, depicted by the curved arrow, causes I^- to be more hydrated and thereby drives polymer collapse. The adsorption of I^- to the polymer–water interface, influenced by Na_2SO_4, affecting the solubility of iodide drives polymer swelling instead. The flexible hydration shell of iodide causing the bifurcated behavior is indicated by the double arrows.

the nonadditive effect in mixtures containing a divalent and a monovalent anion is substantially more pronounced than when both anions are monovalent. Moreover, further increase in the NaI concentration only causes a subtle increase in the LCST of PNIPAM in region Ⅱ, followed by a decrease in region Ⅲ (Fig. 6.17). As a background anion, Cl^- is simply not as strongly hydrated as SO_4^{2-}. Therefore, it cannot salt iodide out of solution very effectively. This results in a smaller driving force for iodide to adsorb to the polymer–water interface, as reflected in the number of iodide ions in proximity with a PNIPAM 5-mer in MD simulations (Fig. 6.18) and a smaller $B_{max,1}$ value for chloride than for sulfate (Table 6.6). Finally, region Ⅲ looks mostly the same when NaCl replaces Na_2SO_4.

Next, in order to test whether the flexibility of an anion's hydration shell is essential for displaying nonadditive behavior, we also ran experiments where NaI was switched for NaCl in the presence of Na_2SO_4 as the background salt. Interestingly, no evidence was found for nonadditivity in regions I and Ⅱ (Fig. 6.19 and Table 6.7). The excess ion pairing between chloride and sodium increases in the presence of Na_2SO_4 (Fig. 6.11), in contrast to the decreasing excess ion pairing between iodide and sodium. Similar to NaI, the presence of NaCl causes an increase in the pairing affinity between sulfate and sodium ions (Fig. 6.12). However, the pairing affinity is less pronounced than in the presence of NaI, originating from sodium pairing more strongly with chloride than with iodide. Thus, a negligible preferential partitioning of sodium ions from the counterion cloud around chloride to that around sulfate is observed. Consequentially, the hydration shell around chloride is less affected than the one around iodide in the presence of Na_2SO_4 (Figs. 6.13 and 6.14). In fact, this observation is consistent with previous studies, which showed that the increase in ion-pairing affinity between SO_4^{2-} and Na^+ is smaller in the presence of NaCl [458] than in the presence of $NaClO_4$ [459], another weakly hydrated anion. Compared to the mixture containing NaI

and Na_2SO_4, the less flexible hydration shell for chloride leads to a shallower decrease in the LCST in region I in the presence of Na_2SO_4. Additionally, both chloride and sulfate remain well-hydrated and thus salt out the polymer at all concentrations of NaCl (Fig. 6.19).

6.2.6 Using different polymers

Other thermoresponsive polymers were investigated with mixed salts in addition to PNIPAM. A dip feature in the LCST could also be observed with poly(*N*,*N*-dimethylacrylamide) (PDMA) in mixtures of NaI and Na_2SO_4 (Fig. 6.20a) as well as with polyethylene glycol (PEG) in mixtures of NaSCN with Na_3PO_4 (Fig. 6.20b). The fitting parameters are provided in Table 6.8. As such, the LCST behavior observed herein for PNIPAM with NaI and Na_2SO_4 is quite generic. Interestingly, the magnitudes and positions of the dip clearly depend on polymer chemistry as well as on the ion identities. Such differences are expected since the driving forces for nonadditivity of mixed salt solutions come from a competition between ion hydration in the bulk solution (universal behavior) and polymer–anion interactions, whereby the latter should be polymer specific.

6.3 Conclusions

We have shown that the phase behavior of PNIPAM in aqueous mixed salt solutions is determined by the subtle balance of ion hydration and direct interactions of weakly hydrated anions with the polymer. Significantly, in the presence of the strongly hydrated anion (i.e., SO_4^{2-}), the weakly hydrated anion (i.e., I^-) exhibits bifurcated behavior, driving consecutive polymer collapse and swelling transitions. In mixed salt solutions, sodium cations preferentially partition to the counterion cloud around sulfate, leaving iodide more hydrated in the bulk solution, driving polymer collapse. Concurrently, the strongly hydrated anion salts out the weakly hydrated anion to the polymer surface, causing polymer swelling.

The work reported herein illustrates that nonadditive ion effects in mixed salt solutions are caused by changes in the water affinity of weakly hydrated anions. The flexible hydration shell behavior, demonstrated with I^- in this work, is expected to apply to other weakly hydrated anions, such as SCN^- and ClO_4^-. We expect that these new insights into Hofmeister ion chemistry will have consequences beyond the newly discovered effects on the aqueous polymer solubility reported herein. This is quite significant, as the origins of the Hofmeister series in single salt solutions are just now beginning to be understood. Significantly more work will need to be done to understand the behavior of complex environments, like the solutions inside living cells,

the brine solutions of ocean waters, as well as the numerous solutions employed in electrochemical setups, where a large number of different ions can be present simultaneously.

Acknowledgement

The simulations for this research were conducted on the Lichtenberg high performance computer at the TU Darmstadt. Furthermore, the Darmstadt authors thank the LOEWE project from iNAPO which is funded by the Ministry for Higher Education, Research and the Arts (HMWK) of the state of Hessen. The Penn State authors thank the National Science Foundation (CHE-1709735) for support. Additionally, the authors thank William Hunn, Kelvin Rembert, and Halil Okur for the initial observation of the nonadditive ion effects on lower critical solution temperature (LCST) measurements and Dr. Tinglu Yang for maintenance of the vibrational sum frequency spectroscopy system.

6.4 Supporting information

6.4.1 Experimental techniques

Materials. All salts (NaI, Na_2SO_4, NaCl, NaSCN, and Na_3PO_4) were purchased from Sigma Aldrich (>99 % purity). Poly(*N*-isopropyl-acrylamide) (PNIPAM) was purchased from Polymer Source, Inc., with a molecular weight of 186 800 g/mol and a polydispersity of 2.63. Poly(*N*,*N*-dimethylacrylamide) (PDMA) was purchased from Polymer Source, Inc., with a molecular weight of 396 000 g/mol and a polydispersity of 1.7. Polyethylene glycol (PEG) was purchased from Sigma Aldrich with a molecular weight of 900 000 g/mol. Salts and polymers were dissolved in nitrogen-purged water (to avoid iodine formation) until the desired concentrations were reached.

Lower critical solution temperature measurements. An automated melting point apparatus (MPA 100 Optimelt, Stanford Research Systems) with digital image processing software was used to determined the lower critical solution temperature (LCST) of PNIPAM, PDMA and PEG (all at 10 mg/ml) through a turbidity change. The light scattering intensity was measured as a function of temperature using a ramping rate of 1 °C/min. The LCST values were determined from the onset of the light scattering increase relative to the baseline.

Vibrational sum frequency spectroscopy. The vibrational sum frequency spectroscopy (VSFS) experimental setup (EKSPLA, Lithuania) consisted of a 1064 nm Nd:YAG laser (pulse duration: 30 ps; pulse energy: 40 mJ; maximum repetition rate: 50 Hz) directed to a harmonic unit (H500). The second harmonic (532 nm) and the fundamental beams from the harmonic unit were used to pump an optical parametric generator/difference frequency generator (PG501/DFG) unit. The infrared frequency could be tuned between 900 and 4000 cm^{-1}, and the spectral resolution was <6 cm^{-1}. A Gibbs monolayer of PNIPAM was formed at the air–water interface by spreading droplets of 1 mg/ml PNIPAM in chloroform (10 μl) on salt solutions on a PTFE Langmuir trough (NIMA technology, England). The incident angles of the IR and visible beams were 55° and 60°, respectively, with respect to the surface normal at the air–water interface. The VSFS signal was collected at an angle of 59° and at 3 cm^{-1} intervals in the CH stretch region (2800 cm^{-1}–3000 cm^{-1}) and 5 cm^{-1} intervals in the water region (3000 cm^{-1}–3800 cm^{-1}). All experiments were conducted at room temperature (~21 °C). The spectra reported in this study were all collected over a period of 30 minutes. Longer time periods showed no additional spectral changes, indicating that the system had reached a steady state. All data were taken with the ssp polarization combination (s-polarized sum frequency, s-polarized visible and p-polarized infrared), and were reproduced multiple times on different days. Additionally, each data point in the spectrum was an average of 300 laser shots.

6.4.2 Molecular dynamics simulations

Simulation details. Molecular dynamics (MD) simulations were performed using the GROMACS 4.6.7[443] package. A nonpolarizable force field was used for NaI[244] and NaCl[244], while an updated version of the nonpolarizable force field was used for Na_2SO_4.[230] See below for details about the modifications. The SPC/E potential[418] for water was used and the internal geometry was kept rigid using the SETTLE algorithm.[419] Cubic boxes were used and periodic boundary conditions were applied in all three dimensions. The electrolyte concentrations used in the MD simulations are reported in moles/kg of water (m) while experiments (LCST and VSFS measurements) are reported in moles/liter of solution (M). Conversion between the two units reveals that 100 mM is about 0.1 m, 1000 mM is about 1.0 m etc. The system energy was minimized using the steepest descent algorithm. Equilibration runs of 1 ns were carried out in the canonical (NVT) ensemble followed by 5 ns runs under isothermal-isobaric (NPT) conditions at 300 K and 1 atm using the velocity rescaling thermostat[409] and Berendsen barostat[408] with τ_T = 1 ps and τ_P = 1 ps. Production runs were conducted for 200 ns in the isothermal-isobaric (NPT) ensemble at same pressure and temperature using the Nosé–Hoover thermostat[410,420] and the

Parrinello–Rahman barostat[411,412] with the same coupling constants as during equilibration. The integration time step in all simulations was 2 fs and configurations were saved every 1 ps. All bonds were constrained using LINCS.[417] Long-range electrostatic interactions were treated by the particle mesh Ewald (PME) method[460] with a Fourier spacing of 0.12 nm, PME order 4, and a real space cutoff of 1.4 nm. A van der Waals cutoff of 1.4 nm was used for truncation of short-range interactions. A cutoff of 1.4 nm was used for the neighbor list as well, which was updated every 0.02 ps. The geometric combination rule was used for all nonbonded interactions except cation–anion and ion–water interactions, where the Lorentz–Berthelot combination rule was used instead. No long-range correction was used for the dispersion interactions.

poly(*N*-isopropylacrylamide) 5-mer simulations. The systems were comprised of a PNIPAM 5-mer, using the OPLS-AA force field,[228] in NaI solutions in the absence and presence of 0.3 m Na_2SO_4. Concentrations of NaI in the range between 0.1 m and 1.0 m of were simulated as well as a solution containing only 0.3 m Na_2SO_4. Additionally, the PNIPAM 5-mer in NaI solutions in the absence and presence of 0.3 m NaCl were simulated. The NaI concentrations were in the range between 0.1 m and 1.0 m. The side length of the box was about 4 nm.

Bulk electrolyte solution simulations. Concentrations between 0.025 m and 1.0 m of NaI in the absence and presence of 0.3 m Na_2SO_4, as well as a system with only 0.3 m Na_2SO_4, were simulated. Additionally, concentrations of NaCl in the range between 0.1 m and 1.0 m were simulated in the absence and presence of 0.3 m Na_2SO_4. The side length of the boxes was about 10 nm.

6.4.3 Validation of the sodium sulfate force field

Various force fields for Na_2SO_4, nonpolarizable and polarizable, have earlier been investigated.[230] We used the nonpolarizable Na_2SO_4 force field reported in the work of Wernersson and Jungwirth.[230] However, usage of this force field, called run 7 (sodium model 2 and sulfate model 2) in original reference, caused large ion clustering when tested. Wernersson and Jungwirth already observed a tendency for clustering during their 30 ns simulations and an even longer simulation led to clear clustering. The force field was used as a starting point, but needed further modifications. It should be noted that another nonpolarizable force field for Na_2SO_4 is available.[255] However, it cannot be used since this force field uses the electronic continuum correction approach and cannot be combined with the force fields used for NaCl and NaI within this work.

Table 6.2
Force field parameters for the updated Na_2SO_4 force field.

Nonbonded parameters				
Atomtype	Charge	σ [nm]	ε [kJ/mol]	Reference
Na	1	0.2583	0.4186	Fyta–Netz [244]
S	2	0.3550	1.0460	Cannon–Pettitt–McCammon [462]
O	−1	0.3150	0.8368	Cannon–Pettitt–McCammon [462]

Bonds				
i	j	r_{ij}^0 [nm]	k_r^{ij} [kJ/(mol nm^2)]	Reference
S	O	0.148 98	396 980	Bond length [462], Force constant [463]

Angles					
i	j	k	θ_{ijk}^0 [deg]	k_θ^{ijk} [kJ/mol]	Reference
O	S	O	109.5	1589.00	Angle [462], Force constant [463]

Scaling factors				
i	j	λ_σ	λ_ε	Reference
Na	S	1.7	1.0	This work
Na	O	1.7	1.0	This work

The force field for Na_2SO_4 was re-optimized by scaling the cation–anion interactions. Scaling cation–anion interactions has been used earlier as an approach to effectively take polarization effects into account for nonpolarizable force fields and thereby to avoid ion clustering.[244,245,461] For these force fields, the cation–anion interactions were usually scaled through the ε_{ij} parameter ($\varepsilon_{ij} = \lambda_\varepsilon \sqrt{\varepsilon_i \varepsilon_j}$), but also the σ_{ij} parameter was scaled in some cases according to $\sigma_{ij} = \lambda_\sigma(\sigma_i + \sigma_j)/2$. Herein, we scale σ_{ij} for the Na-O (of SO_4^{2-}) and Na-S (of SO_4^{2-}) cation–anion interactions.

Force field parameters for the updated Na_2SO_4 force field are reported in Table 6.2. The SPC/E[418] water model used here uses the LJ parameters $\sigma_{OO} = 0.3169$ nm and $\varepsilon_{OO} = 0.6500$ kJ/mol, and the charges $q_O = -0.8476$ and $q_H = 0.4283$, respectively. As opposed to the original rigid SO_4^{2-} model,[230] we used a flexible version. Therefore, the geometry and corresponding force constants were taken from the literature. Note, the Lorentz–Berthelot mixing rule was used for σ_{ij} and ε_{ij} involving ion–ion and ion–water interactions. Additionally, various scaling factors (λ_ε and λ_σ) were examined to avoid the observed clustering in the original force field and the final one is reported in Table 6.2.

The updated force field was validated against the osmotic coefficient following the approach described in earlier work[423] and adapted from Luo and Roux.[422] MD simulations at 298 K resulted in an osmotic coefficient of 0.624 ± 0.036 for 0.3 m Na_2SO_4, which is close to the experimental value of 0.725.[312] This is a large improvement compared to the osmotic coefficient without the scaling factor ($\lambda_\sigma = 1.0$), which is 0.465 ± 0.052.

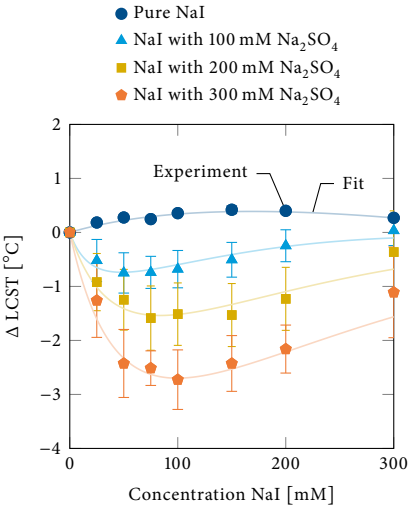

Fig. 6.7 Change in LCST (ΔLCST) of PNIPAM upon the addition of NaI, calculated for data reported in Fig. 6.2a with 0 mM 100 mM, 200 mM, and 300 mM Na_2SO_4 as the background salt. Note that ΔLCST is only shown for data points within the 0 mM–300 mM NaI range in order to highlight the dip feature in the LCST. The error bars are calculated from sample standard deviations from three sets of measurements and propagation of uncertainty. The fits correspond to the empirical model given in Eq. (6.1). The fitting parameters are reported in Table 6.1.

Additionally, the system (λ_σ = 1.0) was not stable and the clustering of ions increases with time resulting in an even smaller osmotic coefficient when simulated longer.

6.4.4 ΔLCST of PNIPAM

The change in LCST (ΔLCST) of PNIPAM upon the addition of NaI in the absence and presence of Na_2SO_4 including error bars is shown in Fig. 6.7. The LCST of PNIPAM as a function of NaI concentration can be empirically modeled by Eq. (6.1). See Table 6.1 for the fitting parameters.

6.4.5 Lower critical solution temperature fitting

The LCST of PNIPAM as a function of NaI concentration can be modeled by the empirical expression in Eq. (6.1). The values of a and $K_{D,1}$ were extracted from the

LCST of PNIPAM as a function of NaI concentration in the absence of background salt. It is shown in this work that the PNIPAM–iodide interactions are independent of the presence of background salt in region I. This leads to a constant $K_{D,1}$ value at the different background salt concentrations. Additionally, a was kept constant over the different background salt concentrations because of all LCST curves having the same slope in region III. See Table 6.1 for the fitting parameters for LCST measurement of PNIPAM in NaI and mixtures of NaI and Na_2SO_4.

6.4.6 Vibrational Sum Frequency Spectroscopy Measurements

The intensity of the vibrational sum frequency spectroscopy (VSFS) signal follows[399]

$$I_{VSFS} \propto |\chi^{(2)}_{eff}|^2 I_{VIS} I_{IR}, \tag{6.3}$$

where I_{VIS} and I_{IR} are the intensities of the incoming visible (VIS) and infrared (IR) beams, respectively. $\chi^{(2)}_{eff}$ represents the second order nonlinear susceptibility, and can be further expressed as

$$\chi^{(2)}_{eff} = \chi^{(2)}_{NR} + \chi^{(2)}_{R} = \chi^{(2)}_{NR} + \sum_n \frac{A_n}{\omega_{IR} - \omega_n + i\Gamma_n}, \tag{6.4}$$

where $\chi^{(2)}_{NR}$ and $\chi^{(2)}_{R}$ are the frequency-independent nonresonant susceptibility term and the frequency-dependent resonant susceptibility term, respectively. $\chi^{(2)}_{R}$ of the n^{th} resonant mode is a function of the oscillator strength (A_n), resonant frequency (ω_n), peak width (Γ_n), and the frequency of the input IR beam (ω_{IR}). The spectra are each normalized to the intensities of the incoming visible and IR beams. The peak assignments can be found in Table 6.3 for NaI and Table 6.4 for NaI with 300 mM Na_2SO_4. The spectra can be seen in Fig. 6.8a for NaI and Fig. 6.8b for NaI with 300 m Na_2SO_4. All VSFS spectra are normalized with respect to the highest intensity of the highest concentration. Figure 6.8c shows the oscillator strengths for the two water peaks, 3200 and 3400 cm^{-1} as a function of NaI concentration for pure NaI solutions.

The oscillator strengths (A) of the peaks positioned around 3200 cm^{-1} and 3400 cm^{-1} (OH stretch region) as a function of NaI concentration are fitted according to

$$A = A_0 + \frac{B_{max,1} c_{salt}}{K_{D,1} + c_{salt}} + \frac{B_{max,2} c_{salt}}{K_{D,2} + c_{salt}}, \tag{6.5}$$

where A_0 refers to the oscillator strength in the absence of NaI, and c_{salt} is the concentration of added NaI. The second term describes the increase of the oscillator strength as iodide ions partition to the polymer surface and has the form of a Langmuir binding

Table 6.3
Fitted oscillator strengths (A_n) and peak widths (Γ_n [cm^{-1}]) in the 2800 cm^{-1}–3800 cm^{-1} region of the air–PNIPAM–water interface as a function of NaI concentration from vibrational sum frequency spectroscopy intensity using Eq. (6.4).

Wavenumber	NaI concentration [mM]									
[cm^{-1}]	0	10	25	40	50	75	100	300	600	1000
2850	−0.1 ± 0 (A_n)	−0.1 ± 0	−0.1 ± 0	−0.1 ± 0	−0.1 ± 0	−0.1 ± 0	−0.1 ± 0	−0.1 ± 0	−0.1 ± 0	−0.1 ± 0
(CH_2 sym.)	9.3 ± 0.2 (Γ_n)	9.4 ± 0.2	8.2 ± 1.5	8.1 ± 0.7	8.2 ± 0.8	7.9 ± 1.1	7.9 ± 1.0	7.7 ± 1.2	7.7 ± 1.2	7.8 ± 1.0
2876	−0.8 ± 0.1	−0.8 ± 0	−0.8 ± 0.1	−0.8 ± 0.1	−0.8 ± 0	−0.7 ± 0.1	−0.7 ± 0.1	−0.8 ± 0.1	−0.8 ± 0.1	−0.8 ± 0
(CH_3 sym.)	9.5 ± 0.3	9.7 ± 0.2	9.1 ± 0.3	9.3 ± 0.2	9.6 ± 0.3	9.2 ± 0.1	9.1 ± 0.2	9.5 ± 0.2	9.4 ± 0.3	9.2 ± 0.3
2910	−0.6 ± 0.1	−0.5 ± 0.1	−0.6 ± 0.1	−0.5 ± 0.1	−0.5 ± 0	−0.5(1)	−0.5 ± 0.1	−0.5 ± 0	−0.5 ± 0.1	−0.5 ± 0.1
(CH)	12.5 ± 0.9	12.0 ± 0.3	12.4 ± 1.2	12.2 ± 0.4	12.2 ± 0.5	12.2 ± 0.6	12.2 ± 0.3	11.5 ± 0.5	11.5 ± 0.6	11.3 ± 0.2
2936	0.4 ± 0	0.8 ± 0.2	0.6 ± 0.2	0.7 ± 0.3	0.6 ± 0.2	0.8 ± 0.1	0.8 ± 0.1	0.6 ± 0.1	0.7 ± 0.1	0.5 ± 0.2
(CH_2 asym.)	4.1 ± 0.2	6.3 ± 1.6	5.5 ± 0.7	6.2 ± 0.8	5.1 ± 0.8	5.7 ± 0.3	5.8 ± 0.5	5.2 ± 0.3	5.1 ± 0.5	4.4 ± 0.8
2947	−0.8 ± 0.1	−1.0 ± 0.2	−1.0 ± 0.2	−1.1 ± 0.2	−1.1 ± 0.2	−1.2 ± 0.1	−1.2 ± 0.1	−1.1 ± 0.1	−1.2 ± 0.1	−1.0 ± 0.2
(CH_3 Fermi)	8.0 ± 0	7.9 ± 0.2	8.0 ± 0	8.0 ± 0	8.0 ± 0	8.0 ± 0	8.0 ± 0	8.0 ± 0.1	8.0 ± 0	7.8 ± 0.3
2984	0.6 ± 0.1	0.6 ± 0.1	0.6 ± 0.1	0.6 ± 0	0.6 ± 0	0.6 ± 0.1	0.6 ± 0.1	10.3 ± 0.4	0.7 ± 0.1	0.6 ± 0.1
(CH_3 asym.)	11.5 ± 0.6	11.3 ± 0.3	11.3 ± 0.4	10.8 ± 0.7	11.5 ± 0.5	11.3 ± 0.4	10.7 ± 0.9	3.5 ± 0.4	10.8 ± 0.5	11.1 ± 0.2
3240	1.4 ± 0.2	1.5 ± 0	1.9 ± 0.2	2.0 ± 0.1	2.0 ± 0.2	2.6 ± 0.4	2.7 ± 0.2	3.5 ± 0.4	3.7 ± 0.1	4.2 ± 0.4
(OH peak 1)	81.0 ± 5.5	92.0 ± 4.5	100.7 ± 5.0	99.1 ± 4.3	102.4 ± 6.2	105.8 ± 11.8	110.7 ± 2.1	119.6 ± 4.9	114.5 ± 3.5	116.2 ± 3.9
3390	0.5 ± 0.2	0.7 ± 0.1	0.9 ± 0.1	1.0 ± 0.2	1.3 ± 0.2	1.4 ± 0.2	1.4 ± 0.1	1.8 ± 0.2	2.1 ± 0.2	2.1 ± 0.2
(OH peak 2)	51.4 ± 14.1	50.9 ± 4.5	58.4 ± 1.6	61.0 ± 8.1	71.5 ± 6.3	70.9 ± 7.3	70.9 ± 4.5	80.2 ± 5.8	83.0 ± 3.9	77.0 ± 5.1
3605	0.1 ± 0	0.1 ± 0	–	–	–	–	–	–	–	–
(OH peak 3)	25.3 ± 0.5	31.0 ± 4.1	–	–	–	–	–	–	–	–
3695	0.1 ± 0.1	0.2 ± 0.1	0.1 ± 0	0.1 ± 0	0.1 ± 0	0.1 ± 0	0.1 ± 0	0.1 ± 0	0.1 ± 0	0.1 ± 0
(OH peak 4)	11.1 ± 1.4	14.8 ± 6.8	12.0 ± 3.4	7.0 ± 0.6	11.9 ± 3.4	7.6 ± 0.1	7.6 ± 0.2	7.1 ± 1.2	5.3 ± 1.7	8.1 ± 2.3
3440	0.2 ± 0.1	0.1 ± 0	0.1 ± 0	0.1 ± 0	0.1 ± 0	0.1 ± 0	0.1 ± 0	0.1 ± 0	0.1 ± 0.1	0.2 ± 0.1
(Free NH)	15.9 ± 3.7	8.6 ± 1.2	11.2 ± 1.8	13.0 ± 3.4	12.7 ± 1.2	12.1 ± 3.0	11.2 ± 1.9	12.5 ± 3.2	16.4 ± 1.6	18.0 ± 2.0

Table 6.4
Fitted oscillator strengths (A_n) and peak widths (Γ_n [cm^{-1}]) in the 2800 cm^{-1}–3800 cm^{-1} region of the air–PNIPAM–water interface as a function of NaI concentration in the presence of 300 mM Na_2SO_4 from vibrational sum frequency spectroscopy intensity using Eq. (6.4).

Wavenumber	NaI concentration [mM]									
[cm^{-1}]	0	10	25	40	50	75	100	300	600	1000
2850	−0.1 ± 0 (A_n)	−0.1 ± 0	−0.1 ± 0	−0.1 ± 0	−0.1 ± 0	−0.1 ± 0	−0.1 ± 0	−0.1 ± 0	−0.1 ± 0	−0.1 ± 0
(CH_2 sym.)	9.8 ± 0.2 (Γ_n)	9.9 ± 0.1	9.7 ± 0.4	9.6 ± 0.3	8.5 ± 1.3	9.2 ± 0.7	8.6 ± 1.4	6.6 ± 0.4	6.6 ± 0.2	6.6 ± 0.2
2876	−0.8 ± 0	−0.8 ± 0.1	−0.8 ± 0	−0.8 ± 0.1	−0.8 ± 0	−0.8 ± 0	−0.7 ± 0.1	−0.8 ± 0.1	−0.8 ± 0	−0.8 ± 0
(CH_3 sym.)	9.6 ± 0.3	9.2 ± 0.5	9.1 ± 0.3	9.2 ± 0.3	9.4 ± 0.2	9.6 ± 0.2	9.1 ± 0.4	9.4 ± 0.4	9.5 ± 0.4	9.7 ± 0.1
2910	−0.6 ± 0.1	−0.6 ± 0.1	−0.6 ± 0	−0.6 ± 0	−0.6 ± 0.1	−0.6 ± 0.1	−0.5 ± 0.1	−0.5 ± 0.1	−0.5 ± 0.1	−0.4 ± 0.1
(CH)	12.7 ± 0.5	13.2 ± 0.5	12.9 ± 0.2	13.4 ± 0.4	12.6 ± 0.6	13.0 ± 0.8	12.8 ± 0.8	11.3 ± 0.2	11.8 ± 0.4	10.5 ± 1.3
2936	0.5 ± 0.2	0.5 ± 0.1	0.5 ± 0.1	0.6 ± 0.1	0.6 ± 0.2	0.5 ± 0.1	0.6 ± 0.2	0.7 ± 0.2	0.7 ± 0.1	0.6 ± 0.1
(CH_2 asym.)	5.4 ± 1.9	5.5 ± 1.4	5.0 ± 0.6	5.8 ± 0.7	6.1 ± 1.1	4.9 ± 0.5	5.4 ± 0.9	5.6 ± 0.4	5.2 ± 0.2	5.4 ± 0.1
2947	−0.8 ± 0.1	−0.8 ± 0	−0.8 ± 0.1	−0.9 ± 0.1	−1.0 ± 0.1	−0.9 ± 0.1	−1.0 ± 0.1	−1.1 ± 0.1	−1.2 ± 0.1	−1.1 ± 0.1
(CH_3 Fermi)	8.0 ± 0.1	7.9 ± 0.2	7.9 ± 0.1	8.0 ± 0	8.0 ± 0	7.9 ± 0.1	8.0 ± 0	8.0 ± 0	7.9 ± 0.2	8.0 ± 0
2984	0.6 ± 0	0.6 ± 0.1	0.6 ± 0	0.6 ± 0	0.6 ± 0.1	0.6 ± 0	0.6 ± 0	0.6 ± 0.1	0.6 ± 0.1	0.6 ± 0
(CH_3 asym.)	12.5 ± 0.7	12.1 ± 0.3	12.1 ± 0.2	11.4 ± 0.2	11.5 ± 0.9	11.7 ± 0.6	11.5 ± 0.9	11.5 ± 0.3	11.3 ± 0.4	10.8 ± 0
3240	1.6 ± 0.2	1.4 ± 0.1	1.0 ± 0.2	1.1 ± 0.3	1.5 ± 0.3	1.6 ± 0.2	1.8 ± 0.2	2.8 ± 0.4	3.3 ± 0.1	3.5 ± 0.2
(OH peak 1)	104.8 ± 3.7	98.3 ± 5.2	96.7 ± 22.9	95.2 ± 15.9	109.0 ± 6.4	107.9 ± 10.0	110.8 ± 5.8	111.2 ± 3.5	115.6 ± 6.6	114.6 ± 4.9
3390	0.1 ± 0.1	0.2 ± 0.1	0.5 ± 0.1	0.5 ± 0.2	0.6 ± 0.1	0.9 ± 0.1	1.1 ± 0.3	1.5 ± 0.3	2.3 ± 0.2	2.7 ± 0.1
(OH peak 2)	75.3 ± 4.8	65.5 ± 8.6	68.9 ± 5.9	73.1 ± 19.7	58.1 ± 8.7	68.5 ± 11.1	75.1 ± 16.3	77.0 ± 8.7	91.4 ± 5.5	97.6 ± 2.8
3605	0.1 ± 0	0.2 ± 0.1	0.2 ± 0.1	0.2 ± 0.1	–	–	–	–	–	–
(OH peak 3)	22.0 ± 6.1	26.7 ± 7.3	32.2 ± 5.8	35.7 ± 5.5	–	–	–	–	–	–
3695	0.1 ± 0.1	0.2 ± 0.1	0.2 ± 0.1	0.1 ± 0.1	0.2 ± 0.1	0.2 ± 0.1	0.2 ± 0	0.1 ± 0	0.1 ± 0	0.1 ± 0
(OH peak 4)	12.9 ± 6.8	16.6 ± 5.8	12.0 ± 2.4	12.6 ± 1.4	19.0 ± 4.9	21.6 ± 5.5	23.7 ± 3.5	10.8 ± 2.2	10.3 ± 2.3	10.9 ± 4.5
3440	0.2 ± 0.1	0.1 ± 0	0.1 ± 0.1	0.1 ± 0	0.1 ± 0	0.1 ± 0	0.1 ± 0	0.1 ± 0	0.1 ± 0	0.1 ± 0.1
(Free NH)	16.1 ± 1.1	14.7 ± 2.2	14.8 ± 1.6	15.0 ± 2.3	10.0 ± 2.8	12.3 ± 3.4	11.0 ± 3.9	14.1 ± 1.3	14.4 ± 0.6	16.3 ± 2.5

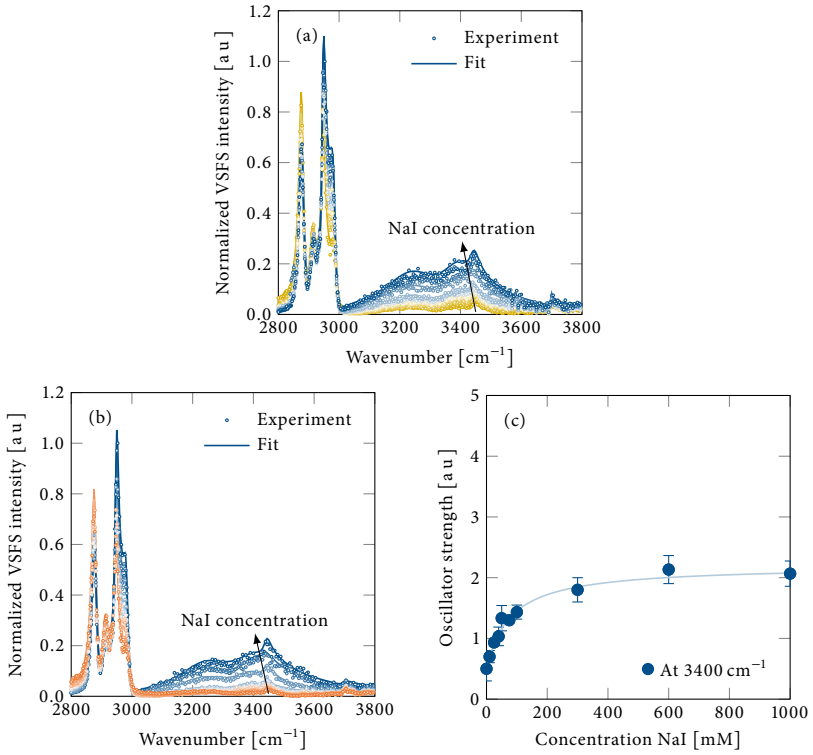

Fig. 6.8 Vibrational sum frequency spectra (VSFS) of PNIPAM at the air–water interface as a function of NaI concentration (0 mM–1000 mM) in (a) the absence of Na_2SO_4 and in (b) the presence of 300 mM Na_2SO_4. (c) The oscillator strengths of the 3200 cm^{-1} peak (light blue) and 3400 cm^{-1} peak (dark blue) as a function of NaI concentration in the absence of Na_2SO_4. The error bars are calculated from sample standard deviations from three sets of measurements. The fits correspond to Eq. (6.5). The fitting parameters are reported in Table 6.5.

isotherm. $B_{max,1}$ and $K_{D,1}$ are the saturation point and dissociation constant, respectively. The third term originates from the ion hydration. It behaves, with a negative $B_{max,2}$, opposite to the second term in Eq. (6.5). That is, it quantifies the decrease of the oscillator strength due to the disruption of the alignment of the interfacial water structure caused by iodide behaving like a strongly hydrated ion in the bulk. In the absence of 300 mM Na_2SO_4, both peaks around 3200 cm^{-1} and 3400 cm^{-1} are modeled with the first two terms in Eq. (6.5). In contrast, in the presence of Na_2SO_4, only the

Table 6.5
Fitting parameters (A_0, , $B_{max,1}$, $K_{D,1}$, $B_{max,2}$, and $K_{D,2}$) for the oscillator strengths of the 3200 and 3400 cm^{-1} OH vibrational peaks using Eq. (6.5) for NaI solutions and NaI solutions with 300 mM Na_2SO_4.

	NaI		NaI with 300 mM Na_2SO_4	
Wavenumber [cm^{-1}]	3200	3400	3200	3400
A_0 [a u]	1.3	0.5	1.7	0.2
$B_{max,1}$ [a u]	3.1	1.7	7.3	3.4
$K_{D,1}$ [mM]	139.1	78.7	86.1	367.2
$B_{max,2}$ [a u]	–	–	−5.0	–
$K_{D,2}$ [mM]	–	–	32.8	–

3400 cm^{-1} peak is modeled with the first two terms. The third term is required for the 3200 cm^{-1} peak. See Table 6.5 for the fitting parameters. VSFS spectra of various Na_2SO_4 solutions can be seen in Fig. 6.9.

6.4.7 Ion pairing and ion hydration

The excess ion pairing is defined as

$$\Delta N = \frac{N_{cat}}{V} \int_{r_{in}}^{r_{out}} [g_{an,cat}(r) - 1] 4\pi r^2 dr, \tag{6.6}$$

where $g_{an,cat}(r)$ is the anion–cation radial distribution function, and N_{cat}/V is the number density of cations. ΔN is determined by the balance of ion–water, ion–ion and water–water (hydrogen bonding) interactions and can be interpreted as the change in the number of cations in an observation volume of the shape of a sphere or a spherical shell defined by the radii (r_{in} and r_{out}) before and after placing an anion at the center of the region. The choice of ion-pairing radii r_{in} and r_{out} determines whether only the contact ion pairs (CIPs), the solvent-shared ion pairs (SIPs) or both are investigated. In this work we use the wording increased or decreased excess ion pairing in the context of this definition. Specifically, increased or decreased ion pairing indicates a change in ΔN in the presence of the background salt with respect to the absence of it.

The affinity for iodide to pair with sodium decreases (see Fig. 6.5a and Fig. 6.10), while the affinity for sulfate to pair with sodium increases (see Fig. 6.5b and Fig. 6.12) in mixed salt solutions compared to pure salt solutions. The affinity for chloride to pair with sodium increases (see Fig. 6.11) in mixed salt solutions compared to pure salt solutions. The affinity for sulfate to pair with sodium increases more in mixed salt solutions with NaI compared to mixed salt solutions with NaCl (see Fig. 6.12 for the comparison between the two mixtures).

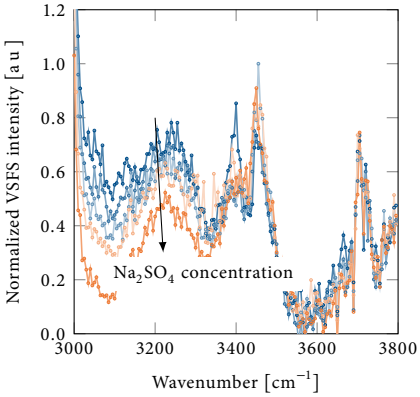

Fig. 6.9 Vibrational sum frequency spectra (VSFS) of the water region (3000 cm^{-1}–3800 cm^{-1}) of PNIPAM at the air–water interface as a function of Na_2SO_4 for 0 mM, 100 mM, 300 mM, 600 mM, and 800 mM Na_2SO_4 solutions.

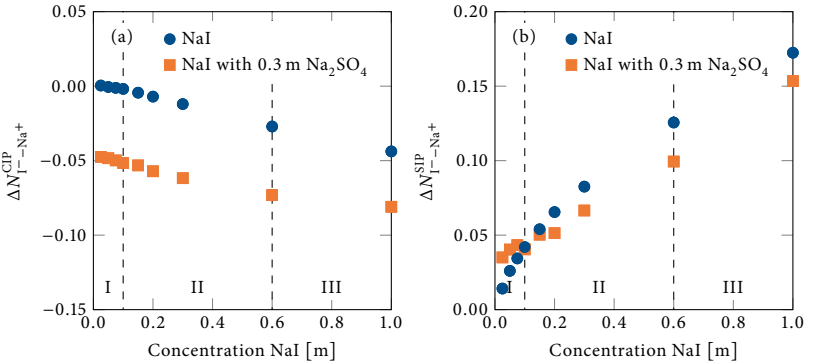

Fig. 6.10 Excess ion pairing between iodide and sodium for (a) contact ion-pairs (CIP) and (b) solvent-shared ion-pairs (SIP) as a function of NaI concentration in the absence (blue) and presence (orange) of 0.3 m Na_2SO_4. The dashed lines show the boundaries between region I, II, and III. The error bars are error estimates calculated from 20 blocks and sample standard deviations and are smaller than the symbols.

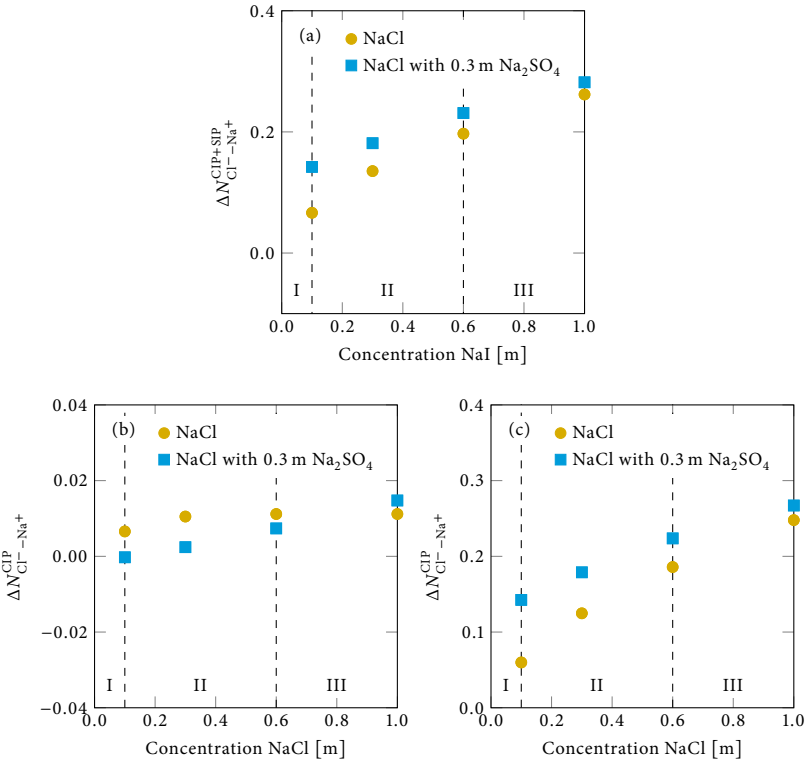

Fig. 6.11 Excess ion pairing between chloride and sodium for (a) contact and solvent-shared ion-pairs (CIP+SIP), (b) contact ion-pairs (CIP) and (c) solvent-shared ion-pairs (SIP) as a function of NaCl concentration in the absence (yellow) and presence (light blue) of 0.3 m Na_2SO_4. The dashed lines show the boundaries between region I, II, and III. The error bars are error estimates calculated from 20 blocks and sample standard deviations and are smaller than the symbols.

Concomitant with the excess ion pairing, the anion–water affinity has been investigated. The ion–water affinity (ΔN) for the first and second hydration shell is defined as

$$\Delta N = \frac{N_w}{V} \int_{r_{in}}^{r_{out}} [g_{an,w}(r) - 1] 4\pi r^2 dr, \tag{6.7}$$

where $g_{an,w}(r)$ is the anion–water radial distribution function, and N_w/V is the number density of water molecules. ΔN can be interpreted as the change in the number of water

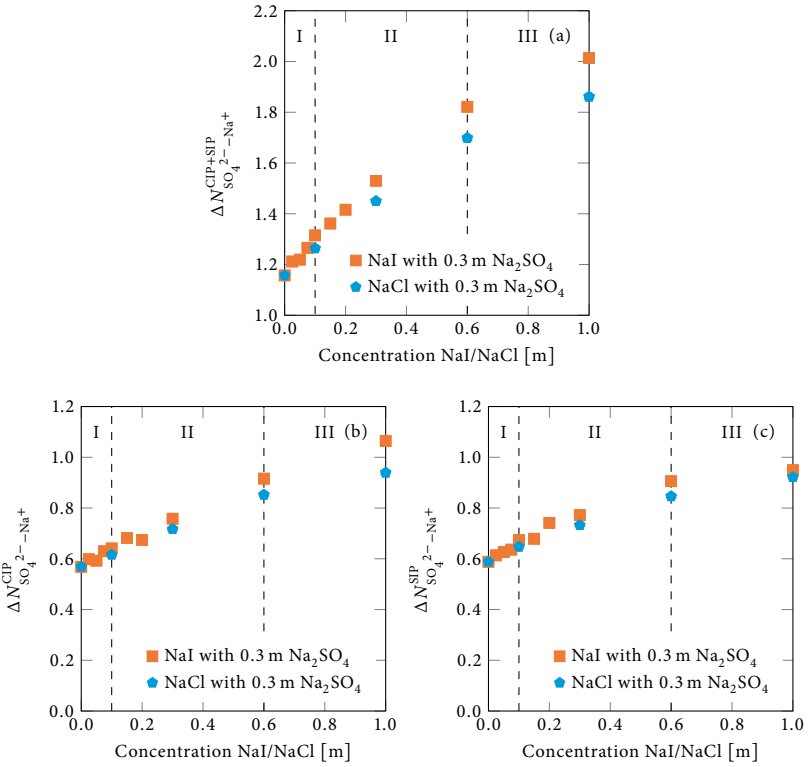

Fig. 6.12 Excess ion pairing between sulfate and sodium for (a) contact and solvent-shared ion-pairs (CIP+SIP), (b) contact ion-pairs (CIP) and (c) solvent-shared ion-pairs (SIP) as a function of NaI or NaCl concentration in the mixtures of NaI with Na_2SO_4 (orange) and NaCl with Na_2SO_4 (light blue), respectively. The dashed lines show the boundaries between region I, II, and III. The error bars are error estimates calculated from 20 blocks and sample standard deviations and are smaller than the symbols.

molecules in a spherical observation volume of radius r_2 before and after placing an anion at the center of that region. The choice of radii r_{in} and r_{out} determines whether only the first hydration shell, only the second hydration shell or both hydration shells are investigated. The integration limits for iodide–water affinity are 0.42 nm and 0.66 nm (0.64 nm for 0.6 m and 1.0 m) for first and second hydration shell, respectively, in NaI and 0.42 nm and 0.64 nm, respectively, in NaI with Na_2SO_4. The integration limits for chloride–water affinity are 0.40 nm and 0.62 nm for first and second hydration shell, respectively, in both NaCl and in NaCl with Na_2SO_4. The integration limits for sulfate–

water affinity are 0.44 nm and 0.68 nm for first and second hydration shell, respectively, in all solutions (Na_2SO_4, NaI with Na_2SO_4 and NaCl with Na_2SO_4). These values are based on the first and second minima in the ion–water radial distribution functions with Δr binning of 0.02 nm. There is a slight dependence of the ΔN on the choice of Δr bin size which however does not qualitatively change the data. For the NaCl systems (Fig. 6.14) this means that NaCl (blue) and NaCl with Na_2SO_4 (yellow) data points are the same within this accuracy. In this work we use the wording more or less hydrated in the context of this definition. Specifically, more or less hydrated indicates a change in ΔN in the presence of the background salt with respect to the absence of it.

The iodide–water affinity in the first hydration shell and in the second hydration shell can be seen in Figs. 6.13a and 6.13b, respectively. The increasing iodide water affinity (Fig. 6.5c), dominated by the change in the second hydration shell, in the presence of Na_2SO_4 agrees with the decreasing affinity for iodide to pair with sodium (Fig. 6.5a and Fig. 6.10). The sulfate–water affinity in the first hydration shell and in the second hydration shell can be seen in Figs. 6.15b and 6.15c, respectively. The sulfate–water affinity increases in the presence of a second salt. That is, the increasing affinity for sulfate to pair with sodium occurs without replacing water. The increased sulfate–water affinity arises from higher bulk salt concentration. The chloride–water affinity for both the first and second hydration shell can be seen in Fig. 6.14a and the separate hydration shells can be seen in Figs. 6.14b and 6.14c, respectively. The chloride–water affinity is not affected in the presence of Na_2SO_4 (Fig. 6.14). This agrees with the less affected affinity for sulfate to pair with sodium in the presence of NaCl compared to in the presence of NaI (Fig. 6.12) and the increased ion-pairing affinity between chloride and sodium (Fig. 6.11). The sulfate–water affinity increases more in mixed salt solutions with NaI compared to mixed salt solutions with NaCl (see Fig. 6.15 for the comparison between the two mixtures).

Additionally, Fig. 6.15a, Fig. 6.14a, and Fig. 6.5c show that the anion–water affinities are ranked $SO_4^{2-} > Cl^- > I^-$. That is, ΔN predicts what is expected from the Hofmeister series.

6.4.8 Temperature dependency regarding anion–water and ion-pairing affinities

The following systems have been simulated at the two additional temperatures 285 K and 305 K: 0.1 m NaI, 0.1 m NaI with 0.3 m Na_2SO_4, 0.1 m NaCl, 0.1 m NaCl with 0.3 m Na_2SO_4, and 0.3 m Na_2SO_4. See the Molecular dynamics simulations section for simulation details. The excess ion pairing between respective anion and sodium ($\Delta N_{\text{anion}-\text{Na}^+}$) and the water affinity for respective anion ($\Delta N_{\text{anion}-\text{W}}$) have been calculated, see Fig. 6.16. See Eqs. (6.6) and (6.7) for the definition of ion-pairing affinity and anion–water affinity,

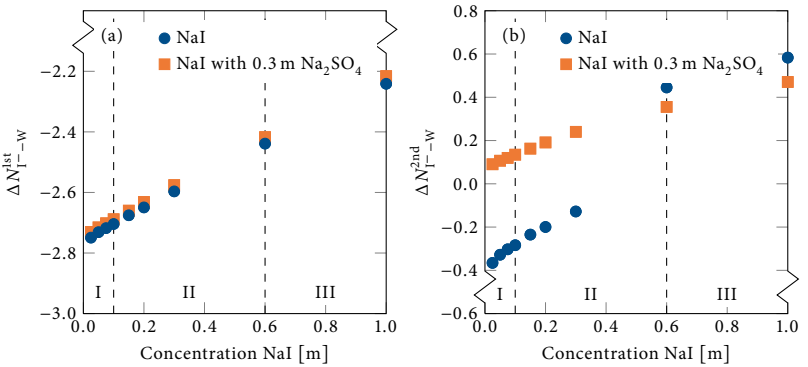

Fig. 6.13 Iodide–water affinity in (a) the first hydration shell and (b) the second hydration shell as a function of NaI in the absence (blue) and presence (orange) of 0.3 m Na_2SO_4. The dashed lines show the boundaries between region I, II, and III. The error bars are error estimates calculated from 20 blocks and sample standard deviations and are smaller than the symbols.

respectively. The trends between NaI, NaCl and Na_2SO_4 and the influence of Na_2SO_4 on NaI and NaCl, respectively, can be observed. The two additional temperatures indicate that the explained behavior and mechanism in region I are independent of the temperature. That is, for all temperatures the anion–cation pairing decreases for NaI in the presence of Na_2SO_4, while it increases for NaCl in the presence of Na_2SO_4. The sulfate–sodium pairing increases in the presence of NaI and NaCl, respectively, and the effect is larger for when NaI is added compared to when NaCl is. These observations apply for all three temperatures. Additionally, the trend among the water affinity for anions are $SO_4^{2-} > Cl^- > I^-$ for all three temperatures. In the presence of Na_2SO_4 the iodide–water affinity increases (except for 285 K where it is unchanged), while the chloride–water affinity decreases. The sulfate–water affinity increases in the presence of NaI and NaCl, respectively, and the effect is larger for when NaI is present compared to when NaCl is. These observations apply for all three temperatures. All data for the three different temperatures thereby imply that the observed phenomena and proposed mechanism are robust.

6.4.9 NaCl as the background salt

LCST experiments and MD simulations are carried out for mixed salt solutions with NaCl as the background salt instead of Na_2SO_4. See the Experimental techniques and Molecular dynamics simulations sections for details about the experiments and

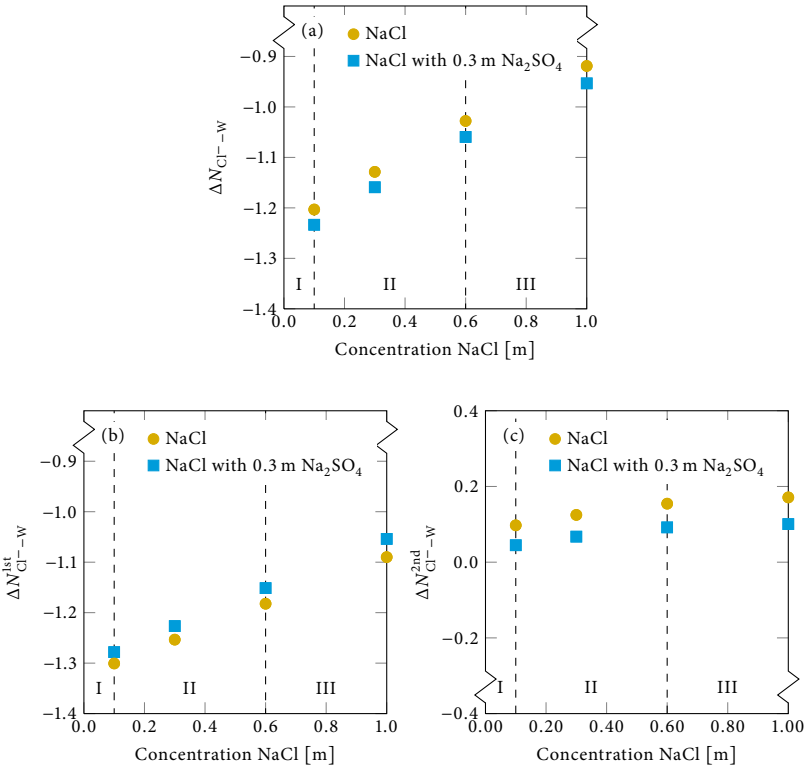

Fig. 6.14 Chloride–water affinity in (a) both the first and second hydration shells, (b) the first hydration shell and (c) the second hydration shell as a function of NaCl concentration in the absence (yellow) and presence (light blue) of 0.3 m Na_2SO_4. The dashed lines show the boundaries between region I, II, and III. The error bars are error estimates calculated from 20 blocks and sample standard deviations and are smaller than the symbols.

simulations. The LCST graph can be seen in Fig. 6.17a for various NaCl concentrations, while Fig. 6.17b shows ΔLCST. The LCST of PNIPAM as a function of NaI concentration can be empirically modeled by Eq. (6.1). See Table 6.6 for the fitting parameters. It is shown in this work that the PNIPAM–iodide interactions are independent of the presence of background salt in region I. This leads to a constant $K_{D,1}$ value at the different background salt concentrations. Additionally, a was kept constant over the different background salt concentrations because of all LCST curves having the same slope in region III.

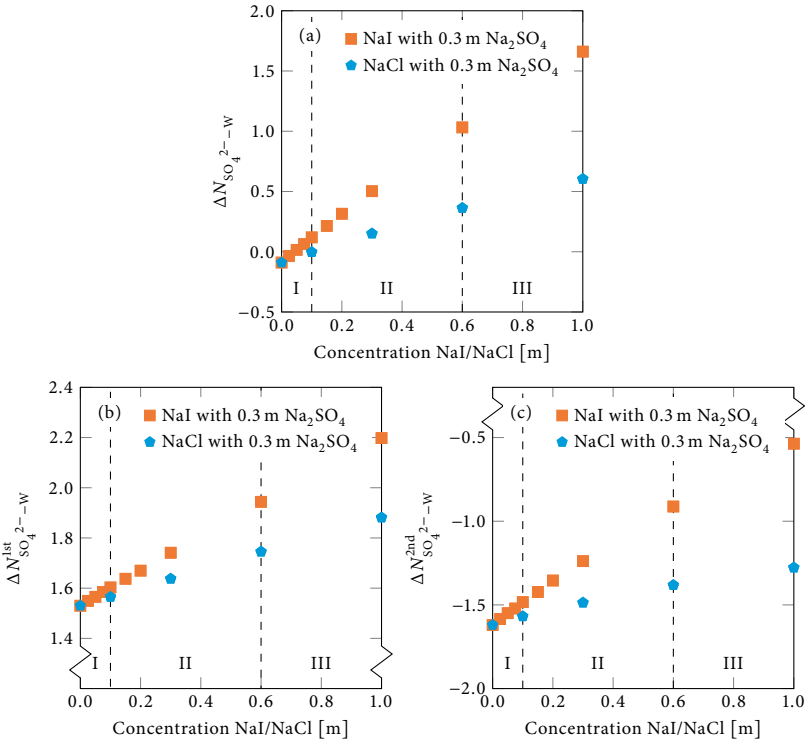

Fig. 6.15 Sulfate–water affinity in (a) both the first and second hydration shells, (b) the first hydration shell and (c) the second hydration shell as a function of NaI or NaCl concentration in the mixtures of NaI with Na_2SO_4 (orange) and NaCl with Na_2SO_4 (light blue), respectively. The dashed lines show the boundaries between region I, II, and III. The error bars are error estimates calculated from 20 blocks and sample standard deviations and are smaller than the symbols.

The number of iodide ions in the proximity (defined from the proximal radial distribution function between oligomer surface and iodide) calculated from MD simulations can be seen in Fig. 6.18.

6.4.10 Mixtures of NaCl and Na_2SO_4

The LCST of PNIPAM upon the addition of NaCl in the presence of Na_2SO_4 as the background salt was measured. See the Experimental techniques section for details.

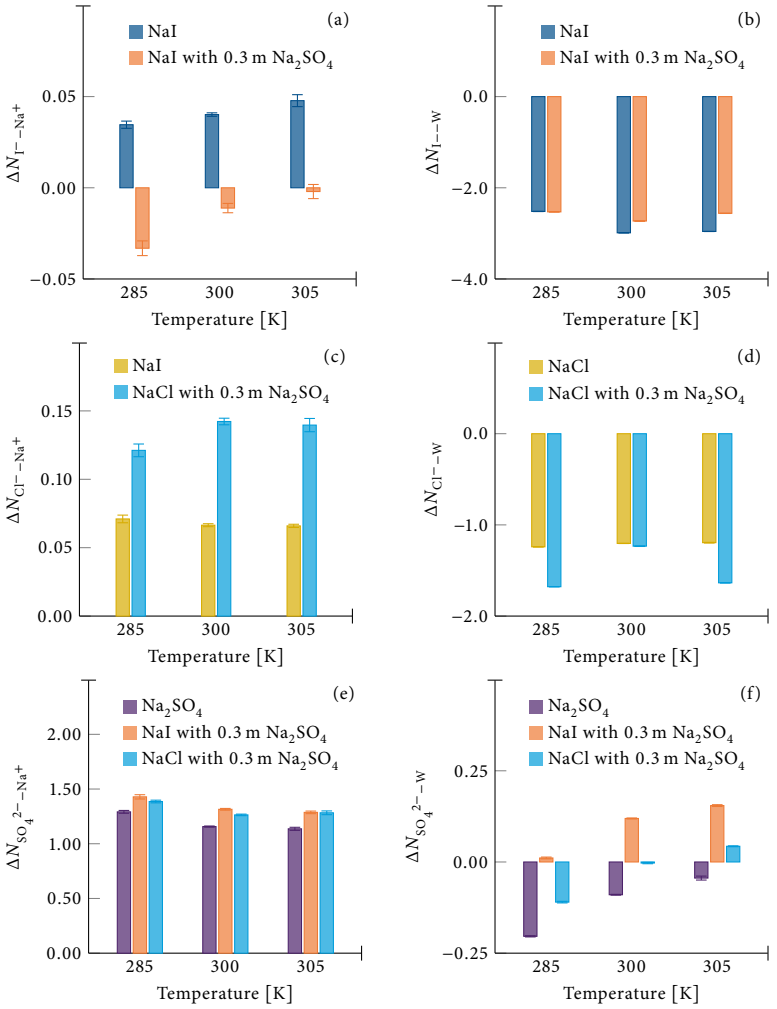

Fig. 6.16 Temperature dependency of ion pairing (for both contact and solvent-shared ion-pairs) and anion–water affinities (for first and second hydration shell). (a) Excess iodide-sodium pairing and (b) iodide–water affinity for 0.1 m NaI in the absence (dark blue) and presence (orange) of Na_2SO_4. (c) Excess chloride-sodium pairing and (d) chloride–water affinity for 0.1 m NaCl in the absence (yellow) and presence (light blue) of Na_2SO_4. (e) Excess sulfate-sodium pairing and (f) sulfate–water affinity for 0.3 m Na_2SO_4 in the absence (purple) and presence of 0.1 m NaI (orange) and 0.1 m NaCl (light blue), respectively.

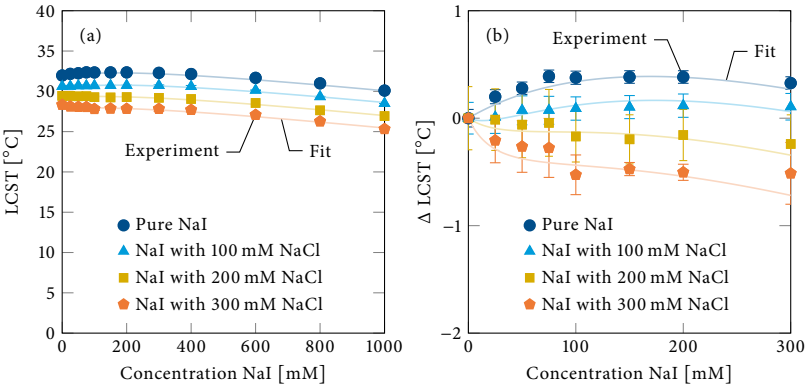

Fig. 6.17 (a) Lower critical solution temperature (LCST) and (b) the change in LCST (ΔLCST) of PNIPAM upon the addition of NaI with 0 mM, 100 mM, 200 mM, and 300 mM NaCl. Note that the ΔLCST is only shown for data points within the 0 mM–300 mM NaI range in order to highlight the dip feature in the LCST. The error bars are calculated from sample standard deviations from three sets of measurements and with propagation of uncertainty for ΔLCST. The fits correspond to the empirical model given in Eq. (6.1).

Table 6.6
Fitting parameters (T_0, a, $B_{max,1}$, $K_{D,1}$, $B_{max,2}$ and $K_{D,2}$) for the empirical lower critical solution model of PNIPAM in NaI and mixtures of NaI with NaCl given by Eq. (6.1).*

	NaCl concentration [mM]			
	0	100	200	300
T_0 [°C]	31.9	30.6	29.5	28.4
$B_{max,1}$ [°C]	3.1	3.4	3.2	2.9
$B_{max,2}$ [°C]	–	−0.4	−0.8	−1.0
$K_{D,2}$ [mM]	–	36.4	61.9	37.4
a [°C/mM]	-4.2×10^{-3}			
$K_{D,1}$ [mM]	308.1			

* The parameters a and $K_{D,1}$ are independent of the NaCl concentration.

The LCST as a function of NaCl is reported in Fig. 6.19 for pure NaCl and with various concentrations of Na_2SO_4. A linear decrease of the LCST with increasing NaCl concentration is observed. The LCST data has been fitted with

$$T = T_0 + a c_{salt}, \tag{6.8}$$

where T_0 is the LCST in water and $a c_{salt}$ (with c_{salt} being the NaCl concentration) is a linear term corresponding to the surface tension contribution. See Table 6.7 for the fitting parameters.

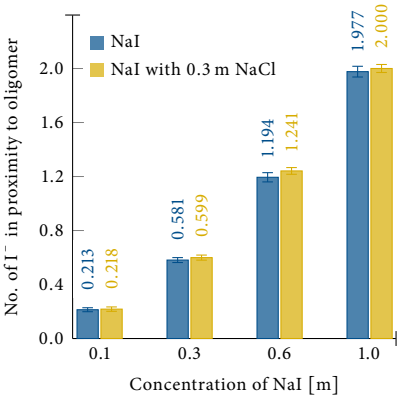

Fig. 6.18 Number of iodide ions in proximity to the PNIPAM oligomer with different concentrations of NaI and with NaCl as the background salt. The proximity is defined from the first peak in the proximal radial distribution function between the oligomer surface and iodide and is equal to 0.52 nm. Error bars are estimates calculated from 20 blocks and sample standard deviations.

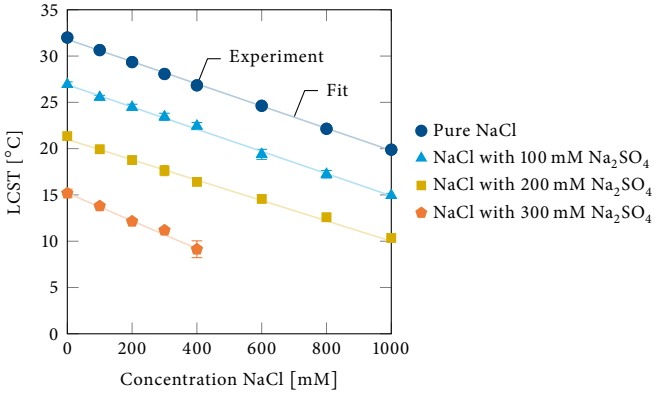

Fig. 6.19 Lower critical solution temperature (LCST) of PNIPAM as a function of NaCl concentration with 0 mM, 100 mM, 200 mM, and 300 mM Na_2SO_4 as the background salt. Error bars are calculated from sample standard deviations from three sets of measurements. The fits correspond to Eq. (6.8).

6.4.11 Lower critical solution temperature of other polymers

The LCST of poly (*N*,*N*-dimethylacrylamide) (PDMA) in mixtures of NaI with Na_2SO_4 and polyethylene glycol (PEG) in mixtures of NaSCN with Na_3PO_4 (Figs. 6.20a and

Table 6.7
Fitting parameters (T_0 and a) for the empirical lower critical solution temperature model of PNIPAM in NaCl and mixtures of NaCl with Na_2SO_4, respectively, given by Eq. (6.8).

	Na_2SO_4 concentration [mM]			
	0	100	200	300
T_0 [°C]	31.8	26.9	21.0	15.2
a [°C/mM]	−1.2	−1.2	−1.1	−1.5

Table 6.8
Fitting parameters (T_0, a, $B_{max,1}$, $K_{D,1}$, $B_{max,2}$ and $K_{D,2}$) for the empirical lower critical solution temperature model of PDMA and PEG in mixtures of NaI with Na_2SO_4 and mixtures of NaSCN with Na_3PO_4, respectively, given by Eq. (6.1). The structures of PDMA and PEG are shown in the insets in Fig. 6.20a and b, respectively.

	PDMA in NaI with Na_2SO_4	PEG in NaSCN with Na_3PO_4
T_0 [°C]	63.1	29.4
a [°C/mM]*	–	–
$B_{max,1}$ [°C]	278.8	140.5
$K_{D,1}$ [mM]	477.4	395.9
$B_{max,2}$ [°C]	−200.0	−135.7
$K_{D,2}$ [mM]	237.5	191.8

* Note that since the data does not show an observed decrease in the LCST (region Ⅲ) in the concentration range examined here, the second term in Eq. (6.1) is absent in the fitting process.

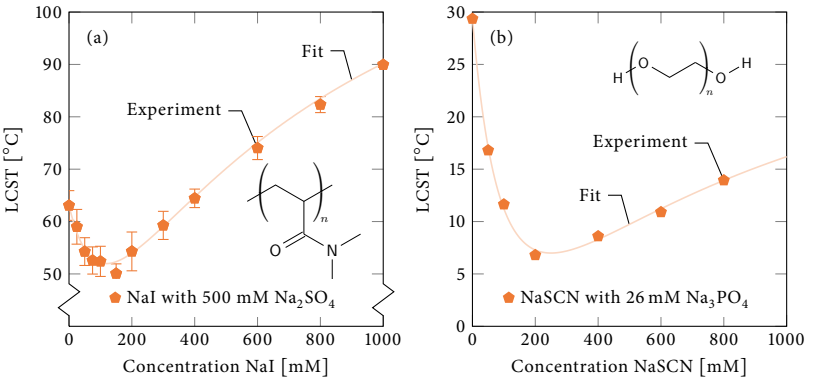

Fig. 6.20 (a) Lower critical solution temperature (LCST) of a) PDMA upon addition of NaI with 500 mM Na_2SO_4 as the background salt and (b) PEG upon addition of NaSCN with 262 mM Na_3PO_4 as the background salt. The error bars for PDMA are calculated from sample standard deviations from three sets of measurements. Both fits correspond to the empirical model given in Eq. (6.1). The fitting parameters are reported in Table 6.8.

6.20b, respectively) were measured. See the Experimental techniques section for details and Table 6.8 for fitting parameters.

6.5 Addition

This section corresponds to the following addition to the above original publication:

> Bruce, E. E.; Bui, P. T.; Rogers, B. A.; Cremer, P. S.; van der Vegt, N. F A. Addition to "Nonadditive ion effects drive both collapse and swelling of thermoresponsive polymers in water". *J. Am. Chem. Soc.*, 143(5):2456, 2021. Copyright 2021 American Chemical Society.

In our recent publication, we used an iodide model from Fyta and NetzFyta and Netz [244] for molecular dynamics simulations. Since two different iodide models were reported in their paper, we here explicitly state the ionic force field parameters used in our study. Our simulations were performed using the iodide force field model corresponding to the iodide ion model I(4) in the Fyta and Netz.Fyta and Netz [244] The ion–ion and ion–water parameters are reported in Table 6.9 for iodide, together with the parameters used for chloride and sodium. The parameters for Na_2SO_4 are reported in Table 6.2 in the Supporting Information (Section 6.4) of our original publication.

The Lorentz–Berthelot combination rule was used for cation–anion and ion–water interactions. The cation–anion interactions were scaled by λ_ε, i.e., $\varepsilon_{ij} = \lambda_\varepsilon \sqrt{\varepsilon_i \varepsilon_j}$, according to the reference 244. The scaling factors (λ_ε) for NaI and NaCl were 0.9 and 1.0, respectively.

Table 6.9
Ionic force field parameters (Lennard-Jones size parameters σ_{ii} and dispersion interaction strengths ε_{ii}) and ion–water force field parameters (σ_{iO} and ε_{iO}).

Ion	σ_{ii} [nm]	ε_{ii} [kJ/mol]	σ_{iO} [nm]	ε_{iO} [kJ/mol]
Na^+	0.2583	0.4186	0.2876	0.5216
I^-	0.5331	0.157	0.425	0.32
Cl^-	0.440	0.4186	0.3785	0.5216

Chapter 7

Molecular scale solvation in complex solutions

This chapter corresponds to and is reproduced with permission from

Bruce, E. E.; van der Vegt, N. F A. Molecular scale solvation in complex solutions. *J. Am. Chem. Soc.* **2019**, 141, 12948–12956.

Abstract. Complex solution environments are ubiquitous in nature. Most life science systems contain hydrated macromolecules whose solubility, function and stability are modulated by several small organic molecules or salts (cosolutes) present simultaneously. This Perspective discusses solvation of mixed cosolutes in water. Recent computer simulations and experiments have shown that nonadditive cosolute effects on the water solubility of thermoresponsive polymers and on protein stability have a common physical origin, rooted in solvent-excluded volume effects determined by mutually enhanced cosolute hydration in bulk. We discuss mixtures of weakly and strongly hydrated salts in the anionic Hofmeister series and mixtures of urea and trimethylamine *N*-oxide. Nonadditive phenomena in these mixtures lead to intriguing effects including consecutive polymer collapse and swelling transitions and counteraction of denaturant-induced protein unfolding. The combination of today's advanced simulation methods and spectroscopy techniques should be used to improve further the understanding of these complex aqueous solubility problems.

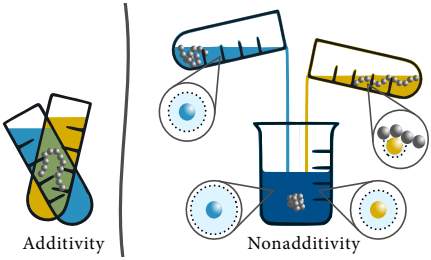

7.1 Introduction

The study of the properties of water as a solvent has a long history. Most chemical processes on earth, whether they occur in the earth's atmosphere, its ocean waters, or in living cells, rely on the versatility with which water solvates molecules of varying sizes and polarities. The water-mediated interactions between these molecules are directly linked to molecular scale hydration mechanisms, which we are just beginning to understand and which remain largely unexplored in aqueous environments containing multiple chemical compounds. Herein, we discuss the water solubility of polymers, as well as aspects of protein stability, in environments containing codissolved solutes (cosolutes) such as salts or protein (de)stabilizing molecules (osmolytes). Our focus will be on newly discovered, nonadditive, solvation phenomena which occur in systems containing multiple cosolute components simultaneously. These complex solvent environments are not rare exceptions. They are found in the aqueous environments of the living cell, in the application of soft functional materials like hydrogels, and in the brine solutions of ocean waters, to name just a few examples.

In systems with single-component salts as cosolutes, the current state of affairs in our understanding of their solvent-mediated interactions with macromolecules can be illustrated with the Hofmeister series of salt ions.[1,3] A common ordering for the anions in this series is $CO_3^{2-} > SO_4^{2-} > S_2O_3^{2-} > H_2PO_4^- > F^- > Cl^- > Br^- > NO_3^- > I^- > ClO_4^- > SCN^-$. Strongly hydrated anions, placed on the left side of the series, prefer the bulk water environment. Weakly hydrated anions, placed on the right side of the series, are driven to nonpolar environments such as air–water[103] and polymer–water interfaces.[9] Hence, strongly hydrated ions repulsively interact with polymers, are depleted from the polymer–water interface, and decrease their aqueous solubility (salting-out). Weakly hydrated ions instead tend to increase moderately aqueous polymer solubility (salting-in).[4] The latter effect cannot be understood exclusively in terms of interactions between the ion and chemical moieities along the polymer chain, but also depends on ion hydration in the bulk solution. Due to their attractive interaction with weakly hydrated ions, polymer chains swell and increase their solvent accessible surface area. A prerequisite for this to occur is that local solvent density fluctuations in the bulk solvent create empty space for the swelling polymer to expand into. This so-called solvent-excluded volume effect[136] plays an important role in the phenomena which we will discuss in this Perspective and is schematically illustrated in Fig. 7.1. In systems with a salt as cosolute, solvent-excluded volume effects depend on ion hydration.[397] Ion–water electrostatic interactions attenuate local solvent-density fluctuations more significantly in systems with strongly hydrated ions than in systems with weakly hydrated ions. For strongly hydrated ions (left-hand-side of the Hofmeister series), solvent-excluded volume drives salting-out. For weakly hydrated ions (right-hand-side of the Hofmeister series), solvent-excluded volume and ion–polymer interactions counterbalance in a salt

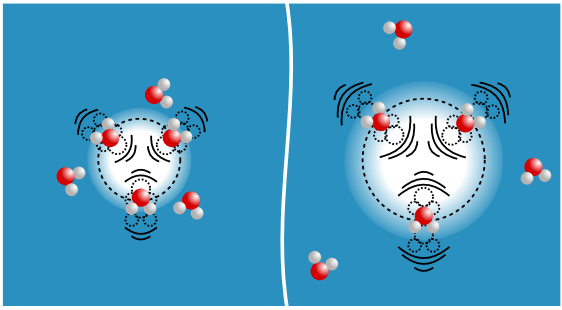

Fig. 7.1 Schematic representation of solvent-excluded volume in molecular liquids.

concentration-dependent fashion leading to weak salting-in at low salt concentrations followed by a salting-out at high salt concentrations.

Historically, ion interactions and cosolute effects have been considered independent and additive, both for salts[22–26,446,447] and osmolytes.[464–467] Herein, we discuss recent computer simulations and experiments which show that nonadditive cosolute effects lead to intriguing new phenomena. We will discuss mechanisms for consecutive polymer collapse and swelling transitions as well as mixed-osmolyte effects on protein stability and highlight the role of solvent-excluded volume as a key driving force in these systems. Future perpectives on experiments and computer simulations of cosolute hydration in mixed salts and osmolytes will also be provided.

7.2 Solvent-excluded volume affects polymer solubility

We herein discuss cosolute effects on polymer solubility and protein stability in terms of a transition temperature T_{EC} at which an extended chain collapses/folds into a disordered globule/native protein. The extended and collapsed chains are here referred to as E and C, respectively. If the cosolute shifts T_{EC} up or down away from the experimental temperature T, polymer solubility/protein stability increases or decreases. In protein folding, cosolute effects are typically studied starting from a two-state description C⇌E. For water-soluble polymers like poly(*N*-isopropylacrylamide) (PNIPAM), a two-state description can be used as well.[391,392] PNIPAM is soluble in cold water and collapses at

temperatures above $T_{EC} = 32°C$. This temperature is referred to as the lower critical solution temperature (LCST). Salting-in and salting-out of PNIPAM therefore occurs when T_{EC} increases and decreases, respectively, as a function of the cosolute concentration.

The transition temperature T_{EC} is related to the collapse enthalpy $\Delta H^{E\to C}$ and collapse entropy $\Delta S^{E\to C}$ according to

$$T_{EC} = \frac{\Delta H^{E\to C}}{\Delta S^{E\to C}}. \tag{7.1}$$

The systems considered here have a lower transition temperature. The conditions $\Delta H^{E\to C} > 0$ and $\Delta S^{E\to C} > 0$ therefore apply. Equation (7.1) shows that cosolvent effects on the water solubility of polymers, or on the stability of proteins, are generally determined by a compensation of enthalpy and entropy effects.[136] Strongly hydrated salt ions on the left-hand-side of the Hofmeister series do not interact with PNIPAM and, therefore, do not significantly shift $\Delta H^{E\to C}$ in comparison to pure water. These ions, however, decrease the solubility of the polymer (decrease T_{EC}) due to their effect on $\Delta S^{E\to C}$, which increases with the concentration of the salt. When the polymer chain collapses, a part of its solvent-excluded volume is "released" into the bulk and becomes available not only for the water molecules, but also for the salt ions. The gain in translational entropy of the ions can therefore be viewed as driving force for polymer collapse.[398] The corresponding mechanism is schematically shown in Fig. 7.2a. This well-known effect gives rise to the linear behavior schematically shown in Fig. 7.2b.

In contrast to the linear behavior, nonlinear trends in T_{EC}, illustrated in Fig. 7.2b, are indicative of cosolute interactions with the macromolecule. At the thermodynamic level, these excluded-volume and ion binding interactions can be discussed in terms of preferential cosolute binding (preferential adsorption or preferential interaction are equivalent terms).[18,211] The preferential binding coefficient, denoted as Γ in Fig. 7.2c, refers to the excess number of cosolute molecules in the solvation shell of the macromolecule. Systems in which positive preferential binding ($\Gamma > 0$) has been observed include acrylamide polymers such as PNIPAM in water containing salts with specific anion–cation combinations,[4,19] or urea.[396,469,470] In these systems, electrostatic and hydrogen bonding interactions between the cosolute and the polymer have been observed which are strong enough such that cosolute bridging may lead to consecutive coil-to-globule and globule-to-coil transitions with increasing cosolute concentration.[19,160] Such transitions also occur for PNIPAM, and other thermoresponsive polymers, in solvent-cosolvent (e.g., water–alcohol) mixtures, a phenomenon which is referred to as cononsolvency. In these systems, positive preferential alcohol binding is observed; however, the interactions that drive the consecutive coil-to-globule and globule-to-coil transitions are not well understood.[381,468,471–474] Viewed from the perspective of polymer physics, ideas have been proposed that allude to the universality of the cononsolvency effect which is independent of the nature of the local interactions but can be

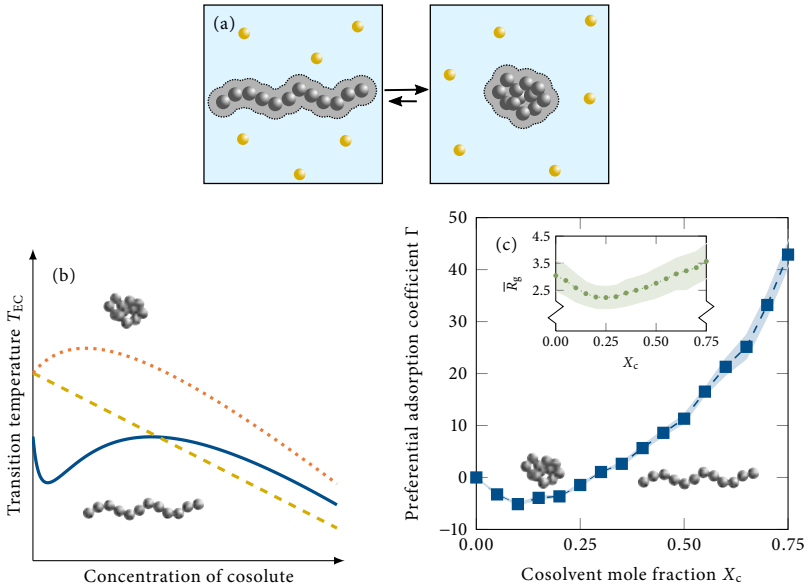

Fig. 7.2 (a) Solvent-excluded volume effect leads to polymer collapse due to an increase of the translational entropy for the cosolutes (yellow spheres) and water molecules resulting from a smaller excluded volume (gray area around polymer). (b) Addition of cosolute can change the transition temperature T_{EC} in a salting-out manner (example PNIPAM in NaCl or Na_2SO_4 aqueous solutions [4]) like the yellow dashed line, salting-in manner (example PNIPAM in NaI aqueous solutions [4]) like the orange dotted line or in a complex manner (example PNIPAM in mixed NaI and Na_2SO_4 aqueous solutions [424]) like the blue solid line. Extended polymer conformations are present below the transition temperature, while collapsed conformations are present above. (c) Preferential adsorption coefficient Γ and normalized polymer radius of gyration ($\overline{R}_g = R_g$/monomer size) as a function of cosolvent mole fraction X_c for a generic polymer–solvent–cosolvent model. [468] Representative conformations for the collapsed and extended polymer chain are shown.

explained by an effective attraction between monomers and cosolvent molecules. [471] Recent work has shown that this universality does not exist. [468] To illustrate this, computer simulations with a generic polymer model have recently been reported which demonstrate that the coil-to-globule transition in solvent-cosolvent mixtures can be observed not only under conditions of positive preferential cosolvent binding ($\Gamma > 0$), but also under conditions of negative preferential cosolvent binding ($\Gamma < 0$) as illustrated in Fig. 7.2c. [468] Experimentally, this observation has been made with PNIPAM in water–dimethyl sulfoxide mixtures. [475,476] The negative preferential cosolvent binding that leads to a coil-to-globule collapse shown in Fig. 7.2c corresponds to a system with

strongly attractive cosolvent–solvent interactions in the bulk and weakly attractive cosolvent–polymer interactions.[468] With these interactions, solvent-excluded volume (Fig. 7.1) dominates over weakly attractive cosolvent–polymer interactions, leading to polymer collapse.

Our understanding of solvent-excluded volume driving forces in aqueous solutions, beyond observations obtained with the above model system,[468] is very limited. Theoretical models that assign effective hard sphere diameters to water and cosolute molecules may be used, but require experimental density data and rely on the specific choices made for the effective hard-sphere diameters of the solution components.[477] Computer simulations, on the other hand, provide an atomistically resolved description, and allow to relate solvent-excluded volume to aspects of local solution structure, solvation effects and the interactions between the specific cosolute and water molecules in solution. Applied to different cosolutes in water, computer simulations have shown that cosolute hydration effects may strengthen (or weaken) interactions in the bulk solution and attenuate (or amplify) local solvent-density fluctuations causing a corresponding increase (or decrease) in solvent-excluded volume.[136,478] Cosolutes which attenuate solvent-density fluctuations enforce a solvent-excluded volume penalty which opposes small molecule solvation, drives polymer collapse and stabilizes native protein folds. In pioneering work performed in the mid-1990s, Dijkstra, Frenkel and Hansen showed that increasing the solvent volume fraction causes a purely entropy-driven polymer collapse in a model system with only hard-core repulsive interactions.[479] Today, atomistic simulations provide the means to quantify and understand the magnitude of these effects in complex fluid mixtures and to relate the corresponding entropy changes to the molecular interactions involved.[136]

7.3 Nonadditive solvation phenomena

7.3.1 Mixed salt solutions

Solvent-excluded volume effects in aqueous solutions correlate with Kirkwood–Buff integrals (KBIs) which describe the affinities between solution components.[211] This is illustrated for SO_4^{2-}, Cl^- and I^-, whose KBIs with water (their water affinities) follow the order $SO_4^{2-} > Cl^- > I^-$.[424] The same series applies to the efficacy with which these ions modulate hydrophobic interactions and salt out polymers such as PNIPAM from water. KBIs therefore provide a useful metric for categorizing ions within the Hofmeister series. As they are experimentally accessible,[205] and can also be calculated from computer simulations,[211,241,387,426,427,480] we shall use them here to rationalize solvent-excluded volume effects in mixed salt solutions.

Cosolute–water, cosolute–cosolute and water–water KBIs hold information on the excess (or deficiency) of molecules of a given type around a central molecule of another (or the same) type. The notation $\Delta N_{\mathrm{ion-W}} = \rho_{\mathrm{W}} G_{\mathrm{ion-W}}$ will be used here to denote the *e*xcess coordination number[211] of water around the ion. Here, ρ_{W} is the molar water concentration of the solution and $G_{\mathrm{ion-W}}$ the ion–water KBI. $\Delta N_{\mathrm{ion-W}}$ usually increases as a function of the bulk salt concentration, indicating that most water molecules are eventually bound to ions. Under these conditions, local solvent-density fluctuations are suppressed, $\Delta S^{\mathrm{E}\to\mathrm{C}}$ increases, and T_{EC} decreases (see Eq. (7.1)), as a function of salt concentration.

In mixed salt solutions, complex behavior has recently been reported in which the combined effect of a weakly (I^-) and a strongly (SO_4^{2-}) hydrated anion is nonadditive.[424] In mixtures with a fixed concentration of Na_2SO_4 and a variable concentration of NaI, $|\Delta N_{\mathrm{I^-W}}|$ is smaller than in pure NaI salt solutions (see data in Fig. 7.3a). This occurs despite the fact that ρ_{W} is larger in the mixed salt systems, i.e., the smaller blue bars on the negative scale of Fig. 7.3a illustrate that iodide increases its water affinity in the presence of Na_2SO_4. Significantly, this effect is not observed if NaI is being replaced by NaCl.[424] Therefore, iodide is more hydrated in the mixture with Na_2SO_4 due to a mechanism which is ion specific and can not be ascribed to a simple bulk salt concentration effect. At a structural level, the differences between the orange and blue bars in Fig. 7.3a origate from very subtle differences. Comparison of the iodide–water pair correlation functions of the two systems (not shown) reveals small differences in the extrema corresponding to the first two hydration shells and the location of the second minimum (extension of the second hydration shell). These observations raise several questions, which we will consecutively address: What is the mechanism that causes iodide to be more hydrated in the mixture? How does it impact bulk thermodynamic properties of mixed electrolytes? Does it lead to nonadditive effects in the water solubility of macromolecules?

The mechanism involves the sodium ions.[424] In the mixed salt, some of the sodium ions introduced with NaI partition to the counterion cloud around SO_4^{2-}. This leaves a lower excess density of sodium ions around the I^- ions. The iodide ions therefore become more hydrated in the mixture with Na_2SO_4. Notwithstanding the fact that SO_4^{2-} ions recruit the sodiums of the added NaI, SO_4^{2-} is also more hydrated in the mixed salt solution (see data in Fig. 7.3b). This occurs because sodium ions attracted in the counterion cloud of sulfate do not replace water.

Nonadditive effects in bulk thermodynamic properties of mixed electrolytes can be related to the quantities discussed above by means of the Kirkwood–Buff theory, which we apply here by considering the pure and mixed salt solutions as effective binary systems composed of salt (indistinguishable ions) and water. We consider changes of the mean molar ionic activity coefficient (y_{ion}) with total salt concentration. Positive changes of this quantity correspond with negative changes in the water activity coefficient and

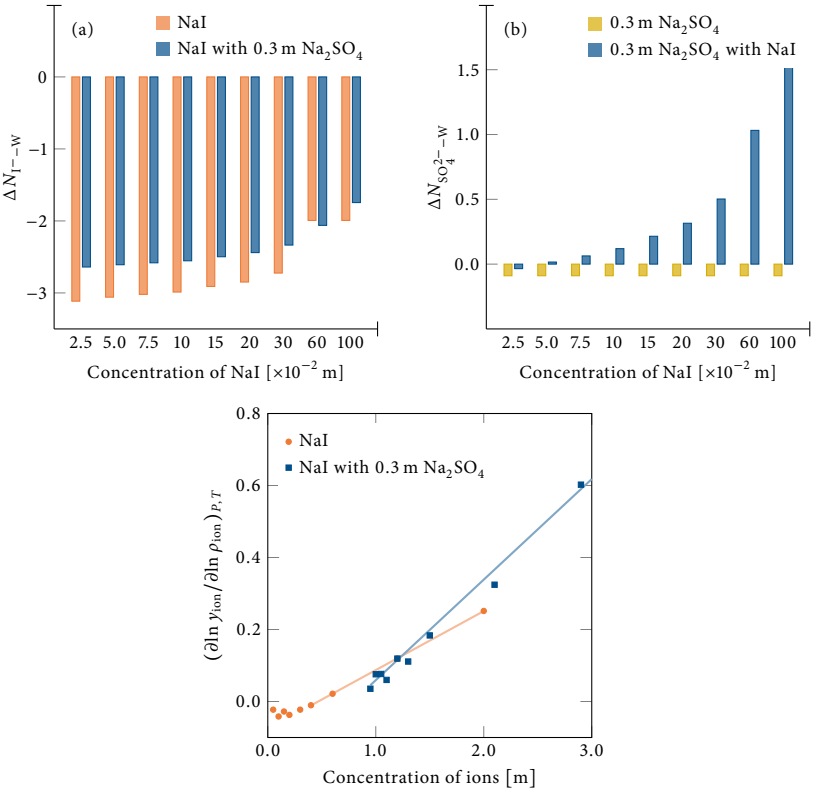

Fig. 7.3 (a) Iodide–water excess coordination number ΔN_{I^--W} as a function of NaI concentration in the absence (orange bars) and presence (blue bars) of Na_2SO_4. (b) Sulfate–water excess coordination number $\Delta N_{SO_4^{2-}-W}$ as a function of NaI concentration in the absence (yellow bars) and presence (blue bars) of NaI. Note, the yellow bars are for comparison shown at all concentrations of NaI. All error bars are error estimates calculated from 20 blocks and sample standard deviations. (c) The partial derivative $(\partial \ln y_{ion}/\partial \ln \rho_{ion})_{P,T}$ as a function of ion concentration (all ions treated indistinguishable), where y_{ion} is the molar ionic activity coefficient and ρ_{ion} is the total ion number density for NaI (orange circles) and NaI with 0.3 m Na_2SO_4 solutions (blue squares), respectively. The data for the solutions with NaI and Na_2SO_4 is for comparison shifted upward with ~0.59 in y-direction to match the 1.2 m ion solution of NaI. The linear part after the minimum in NaI solutions as well as the whole concentration range of solutions with NaI and Na_2SO_4 are fitted with a linear fit.

reflect larger effective ion–ion repulsion and larger ion–water affinity, respectively, as further salt is added. The change of the mean ionic activity coefficient with total salt concentration is related to the quantities discussed above:[423]

$$\left(\frac{\partial \ln y_{\text{ion}}}{\partial \ln \rho_{\text{ion}}}\right)_{P,T} = \frac{-\left(\Delta N_{\text{ion-ion}} - \Delta N_{\text{W-ion}}\right)}{1 + \left(\Delta N_{\text{ion-ion}} - \Delta N_{\text{W-ion}}\right)}, \tag{7.2}$$

with ρ_{ion} the total ion number density. This quantity, shown in Fig. 7.3c, is negative at low electrolyte concentrations and turns positive at higher electrolyte concentrations where electrostatic interactions are screened and ion hydration dominates. The data in Fig. 7.3c show that, in the mixed salt solution with a fixed concentration of Na_2SO_4 (blue squares), y_{ion} increases faster with increasing NaI concentration than in the solution containing NaI only (orange circles). This nonadditive thermodynamic effect corresponds with a faster decrease of the water activity coefficient (water is more strongly bound) in the mixed salt solution and a stronger solvent-excluded volume effect in macromolecular solvation.

The observed nonadditive effects in ionic hydration strongly impact the water solubility of PNIPAM due to suppression of solvent-density fluctuations, which affect $\Delta S^{\text{E}\to\text{C}}$ in Eq. (7.1). In the system with a fixed concentration of Na_2SO_4 and a variable concentration of NaI, the LCST of PNIPAM shows a remarkable decrease up to 100 mM NaI (see blue squares in the gray area in Fig. 7.4a). This stands in stark contrast to changes in PNIPAM solubility observed in the corresponding system without Na_2SO_4 (orange circles). In that system, the PNIPAM solubility instead moderately increases when the same concentration of NaI is introduced. We here only discuss the initial decrease (gray area) and refer to reference[424] for a complete description of the whole LCST curve in mixed salts. It should be noted that the observed nonadditive effects in polymer solubility occur only in those salt mixtures in which the two salts have been selected from the opposite ends of the Hofmeister series. The same behavior is expected for SCN^-, ClO_4^- and other weakly hydrated anions combined with SO_4^{2-}, but certainly more work is needed to study Hofmeister ion chemistry in these systems further. The observed minimum of the LCST (Fig. 7.4a) does not appear in mixed salt solutions with NaCl and Na_2SO_4 where a linear LCST behavior indicative of additive behavior is observed.[424]

7.3.2 Vibrational sum frequency spectroscopy

The new insights on ion hydration and water solubility of PNIPAM were obtained by combining information from computer simulations (ion–water affinities) and experiments (LCST data). While ion–water affinities can in principle be obtained experimentally using thermodynamic measurements, spectroscopic methods provide an interesting

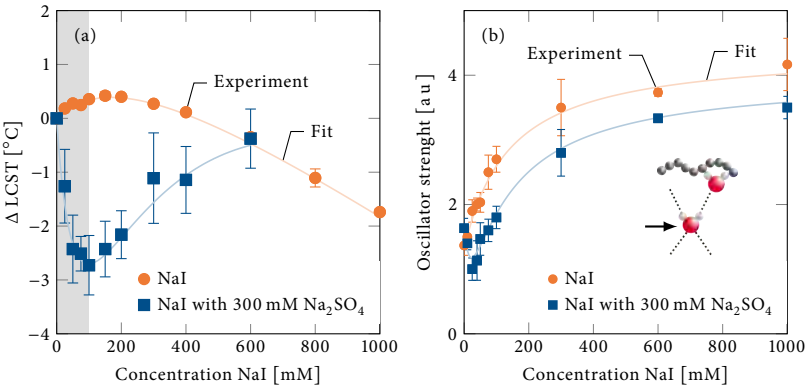

Fig. 7.4 (a) The change in the lower critical solution temperature (ΔLCST) of PNIPAM upon the addition of NaI in the absence (orange circles) and presence (blue squares) of Na_2SO_4. The error bars are calculated from sample standard deviations from three sets of measurements. The fits correspond to empirical models.[424] (b) The oscillator strength at 3200 cm^{-1} as a function of NaI concentration in the absence (orange circles) and presence (blue squares) of Na_2SO_4. The error bars are calculated from sample standard deviations from three sets of measurements. The fits correspond to empirical models.[424] The 3200 cm^{-1} oscillator strength is a reporter for water located slightly below the polymer–water interface (indicated by the arrow in the schematic diagram) where hydrogen bonding is more ordered than at the polymer–water interface.

alternative angle on this problem. Fig. 7.4b shows data obtained with vibrational sum frequency spectroscopy measurements.[424] These measurements were performed by adsorbing a Gibbs monolayer of PNIPAM at the air–water interface. The 3200 cm^{-1} oscillator strength (OS) shown in Fig. 7.4b corresponds to the symmetric OH stretch mode of highly coordinated water molecules (making 3–4 hydrogen bonds to other water molecules)[404,451] and is a reporter for aligned water molecules located below the polymer surface (see inset in Fig. 7.4b). Variations in the 3200 cm^{-1} OS are caused by changes in the interfacial potential. In the system with pure NaI (orange circles in Fig. 7.4b), the OS monotonically increases as a function of the bulk NaI concentration, reflecting the binding of iodide. In systems with pure Na_2SO_4 (not shown), the OS instead monotonically decreases as a function of the bulk Na_2SO_4 concentration, indicating that strongly hydrated SO_4^{2-} ions below the interface disrupt water alignment. When, however, a fixed Na_2SO_4 concentration is present in the aqueous subphase (blue squares in Fig. 7.4b), the introduction of NaI leads to a minimum in the 3200 cm^{-1} OS. This indicates that iodide ions located below the interface disrupt water alignment, i.e., in the mixed salt solution, iodide behaves as the strongly hydrated SO_4^{2-} ion. This observation provides further evidence that iodide ions become more hydrated in systems with codissolved Na_2SO_4.

The experiments performed so far indicate that the phenomenon in Fig. 7.4a is quite robust and that nonadditive ion effects occur in other systems as well. Specifically, the LCST of polydimethylacrylamide in the same mixed salt solution with 500 mM Na_2SO_4 decreases with 13 °C. For polyethylene glycol in mixtures of NaSCN and Na_3PO_4, a ΔLCST of −23 °C has been measured.[424]

7.3.3 Mixed osmolyte solutions

Osmolytes are small organic molecules that can modulate the function and stability of proteins in the living cell. The naturally occurring protective osmolyte trimethylamine *N*-oxide (TMAO) counteracts the denaturing effects of another osmolyte, urea, in marine animals such as sharks, skates and rays.[481] The molecular mechanism of urea-induced protein denaturation is well established. Urea interacts favorably with the protein backbone and with its amino acid side chains and, therefore, shifts the folding–unfolding equilibrium in favor of the unfolded state.[482] Concurrent interactions of TMAO and urea with proteins have been studied with computer simulations in recent years; however, the mechanism through which TMAO counteracts urea-induced protein denaturation remains incompletely understood.

Recently reported molecular dynamics simulations have provided evidence that urea and TMAO are mutually excluded from amino acids in mixed solvent environments[483] and, therefore, inhibit protein–urea preferential interactions.[484] The molecular origin of this nonadditive effect is not yet completely uncovered. Without attempting to provide a comprehensive overview of the literature on this problem, we will here draw an analogy to the nonadditive mechanism in mixed salts described in the previous section. A recent dielectric spectroscopy study has provided interesting information that points in this direction.[485] This study concludes that the hydration of TMAO involves three tight hydrogen bonds with the hydrophilic amine oxide group of TMAO which remain unaffected by the presence of urea in the ternary mixture. Moreover, no long-lived TMAO–urea interactions could be detected.[485] These observations are consistent with trends in urea–water and TMAO–water KBIs in mixed solvent environments with different amino acids obtained with molecular dynamics simulations.[483] Fig. 7.5 summarizes these KBIs.[483] In analogy with mixed salt solutions, both urea and TMAO increase their water affinity in the mixed solutions compared to pure urea and pure TMAO solutions. We note that this observation does not exclude the occurrence of direct TMAO–urea interactions.[486] Since TMAO and urea are mutually more hydrated in the mixture, their preferential interaction with proteins decreases. The observed urea exclusion from the protein surface is, however, moderate.[484] Without the action of further driving forces, the loss of protein–urea interactions does therefore not hint at a strong stabilizing mechanism per se. The additional, in a sense hidden, driving

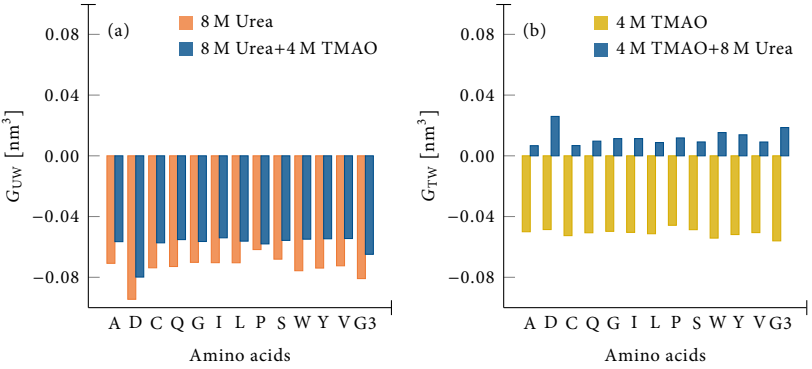

Fig. 7.5 Kirkwood–Buff integrals in solutions with various amino acids and peptide backbone (G3). (a) Urea–water Kirkwood–Buff integrals G_{UW} for 8 M urea (orange bars) and mixed 8 M urea and 4 M TMAO (blue bars) solutions. (b) TMAO–water Kirkwood–Buff integrals G_{TW} for 4 M TMAO (yellow bars) and mixed 4 M TMAO and 8 M urea (blue bars) solutions.

force is the solvent-excluded volume. It originates from the enhanced TMAO–water and urea–water affinities in the mixed-osmolyte solution (Fig. 7.5), which, along with a cooperatively enhanced hydrogen-bond structure of this ternary solution,[485] indicate that bulk solvent interactions are stronger than in binary urea–water solutions and local solvent-density fluctuations are reduced.

7.3.4 Nonadditive effects in mixed solvent environments

The mixed salt and mixed osmolyte solutions discussed above share a common feature. A nonadditive behavior is observed when a strongly hydrated (Na_2SO_4, TMAO) and a weakly hydrated (NaI, urea) cosolute are codissolved in water. This observation raises several questions: Is the strong-plus-weak cosolute combination a general requirement for nonadditive effects to be observed? What is the molecular origin that leads to mutually increased cosolute–water affinities in the ternary mixtures? How do these changes in molecular scale solvation couple to changes in protein folding–unfolding equilibria, or to complex polymer solubility behavior, macroscopically observed?

Mutually increased water affinities can be interpreted in terms of water-mediated interactions between the polar cosolute molecules involved: hydrogen bonds between the (extended) hydration shells of the two cosolutes may stabilize the individual cosolute hydration shells. In ternary urea–TMAO–water mixtures, a water-mediated hydrogen bonding interaction between TMAO and urea has been postulated that involves a

collective effect on length scales longer than those of individual hydrogen bonds.[485] Significantly, this interaction involves a strongly hydrated TMAO molecule, which has three hydrogen bonding acceptor sites at the hydrophilic amine oxide group, and a weaker hydrated urea molecule, which has four hydrogen bonding donor sites.

Water-mediated interactions between hydrated ions have been reported as well.[78,126,487] In aqueous Na_2SO_4 solutions, water-mediated interactions between Na^+ and SO_4^{2-} cause a slowing down in water reorientation dynamics probed by femtosecond infrared spectroscopy.[487] When NaI is introduced in the solution, this slowing-down effect may be enhanced due to partitioning of Na^+ ions from the added NaI to the counterion cloud of sulfate. Although we are not aware of such experiments on mixed salts, these would certainly provide important new information needed to understand nonadditive Hofmeister effects better. For example, the slowing down of water reorientational dynamics caused by water-mediated ion pairing between Na^+ and SO_4^{2-} should be less pronounced with NaCl than with NaI as a second salt. We expect this because NaCl has a stronger propensity to form ion pairs than NaI,[303] i.e., a sodium ion in the counterion cloud of chloride does not as easily partition to sulfate than a sodium ion in the counterion cloud of iodide. This mechanism for increased mutual water affinity hence requires the combination of a weakly and strongly hydrated cosolute.

The protein stability and polymer solubility problem requires considering entropy effects, which are emphasized here, and have been discussed in greater detail elsewhere.[136] Solvent-excluded volume effects play an important role, but a comprehensive view on this problem requires additional insight in solute–solvent and solute–cosolvent interactions together with the enthalpy–entropy compensation effects involved.[136] The decrease in PNIPAM solubility (gray area in Fig. 7.4a) in the mixed salt system with NaI and Na_2SO_4 is quite surprising in view of the fact that Na_2SO_4 has no effect on the favorable interactions of the PNIPAM chain with iodide which, in the pure NaI salt solution, instead cause a moderate increase in PNIPAM solubility.[424] In the mixed salt solution, these favorable enthalpic interactions with the polymer are however compensated by unfavorable entropic interactions, which are caused by increasing mutual water affinity of the ions in the mixture and drive the observed decrease in polymer solubility. Polymer solubility in mixed solvents, such as the cononsolvency problem addressed above, also depends on enthalpic and entropic interactions, which may balance differently depending on the cosolvent. PNIPAM coil–globule collapse in methanol/water mixtures is driven by an enthalpic mechanism.[416,473] This mechanism involves preferential methanol binding and a concurrent dehydration of the polymer that leads to a decrease of $\Delta H^{E\to C}$ as a function of methanol concentration in the water-rich region of the phase diagram.

Protein folding–unfolding equilibria in binary urea–water mixtures are shifted to the unfolded state due to favorable protein–urea interactions. In the ternary mixture

with TMAO, protein–urea interactions are reduced. This enthalpic contribution shifts the folding–unfolding equilibrium back to the folded state, reinforced by an (solvent-excluded volume) entropy contribution originating from increased mutual water affinity of TMAO and urea. On a similar note, counteraction of denaturant induced protein unfolding has recently been discussed by Cozzolino et al. [477]

7.4 Conclusions and future directions

In this Perspective, nonadditive cosolute effects in mixed salt and mixed osmolyte aqueous solutions have been discussed. These effects include intriguing new phenomena, like consecutive collapse and swelling transitions of thermoresponsive polymers, and the well-known counteraction of urea-induced protein denaturation by codissolved protective osmolytes.

Nonadditive effects occur when the properties of one cosolute depend on the presence of another. Herein, we have shown that cosolutes in mixed solutions may mutually increase each others water affinity, and we have discussed the molecular mechanisms responsible for their action in polymer and protein solutions. The examples discussed show that cosolute–water affinities are affected strongest when different cosolutes, which in their pure form are commonly classified as "weakly hydrate" and "strongly hydrated", are mixed. This was illustrated for mixed salt solutions with iodide (weakly hydrated) and sulfate (strongly hydrated) ions: Replacing the weakly hydrated iodide ion with a more strongly hydrated chloride ion in a mixture with Na_2SO_4 removes nonadditive effects observed in the aqueous solubility of PNIPAM. This intriguing observation could be related to changes in the partitioning of sodium ions between the counterion clouds of the two anions and the resulting changes in the anion–water affinities. In analogy to mixed salts, it could be inferred that enhanced cosolute–water affinities in mixed TMAO–urea solutions provide a solvent-excluded volume driving force that shifts the protein folding–unfolding equilibrium toward the folded state. Hence, stabilization of folded proteins and collapsed states of a water-soluble polymers in mixed cosolute environments have a common physical origin rooted in solvent-excluded volume effects determined by mutually enhanced cosolute hydration.

The Hofmeister ion chemistry of mixed salt solutions, however, remains largely unexplored. Little is known about ion pairing and ion hydration in mixtures of different Hofmeister salts. The examples of our recent work presented here illustrate that these "bulk solution" phenomena couple to polymer conformational behavior and protein stability, and we expect that further effects exist in biomolecular and soft matter systems which are driven by similar types of interactions in the bulk. Nonadditive effects may furthermore impact the properties of atmospheric aerosols [488] originating from the

brine solutions of ocean waters containing mixed electrolytes. One aspect of this problem is ion pairing, which has received little attention in mixed salts, but has previously been demonstrated to affect the propensity of strongly hydrated ions for the air–water interface.[436]

In addition to the important role of computer simulations, molecular spectroscopy provides powerful tools to study the role of water and, particularly, the hydration shells of cosolutes.[485,487,489–491] We expect significant contributions coming from this field in the near future. Computer simulations rely on force fields that are accurate enough to represent known properties of multicomponent systems available in the experimental literature. To this end, developments made in recent years to compute Kirkwood–Buff integrals in finite systems will prove to be important.[211,241,387,426,427,480] Although the Pitzer model[492] for mixed electrolyte solutions provides experimental information for several systems, additional thermodynamic data on mixed electrolytes is required to facilitate the development of improved force field models.

Undoubtedly, more work needs to be conducted to achieve a better understanding of complex solution phenomena in environments that contain multiple cosolutes simultaneously. The mixed cosolute solutions discussed in this Perspective are just a start, and we presume that there are many more nonadditive effects that will be discovered. The discussed phenomena are not only important for polymer solubility and protein stabilization as mentioned herein, but also for micelle formation, self-assembly and other hydrophobic effects. The mixed cosolute solutions should have great significance for all kinds of physical properties of aqueous solutions containing these complex mixtures.

Acknowledgement

Part of the research described in this Perspective was supported by the LOEWE project iNAPO funded by the Ministry of Higher Education, Research and the Arts (HMWK) of the state of Hessen. The authors thank Swaminath Bharadwaj, Pho Bui, Paul Cremer, Pritam Ganguly, Bradley Rogers and Joan-Emma Shea for insightful discussions. Calculations for this research were conducted on the Lichtenberg high performance computer on the TU Darmstadt.

Chapter 8

Does an electronic continuum correction improve effective short-range ion–ion interactions in aqueous solution?

This chapter corresponds to and is reproduced from

> Bruce, E. E.; van der Vegt, N. F. A. Does an electronic continuum correction improve effective short-range ion–ion interactions in aqueous solution? *J. Chem. Phys.*, 148(22):222816, 2018, with the permission of AIP Publishing.

Abstract. Nonpolarizable force fields for hydrated ions not always accurately describe short range ion–ion interactions, frequently leading to artificial ion clustering in bulk aqueous solutions. This can be avoided by adjusting the nonbonded anion–cation or cation–water Lennard-Jones parameters. This approach has been successfully applied to different systems, but the parameterization is demanding owing to the necessity of separate investigations of each ion pair. Alternatively, polarization effects may effectively be accounted for using the electronic continuum correction (ECC) of Leontyev et al.[246] which involves scaling the ionic charges with the inverse square-root of the water high-frequency dielectric permittivity. ECC has proven to perform well for monovalent salts as well as for divalent salts in water. Its performance, however, for multivalent salts with higher valency remains unexplored. The present work illustrates the applicability of the ECC model to trivalent K_3PO_4 and divalent K_2HPO_4 in water. We demonstrate that the ECC

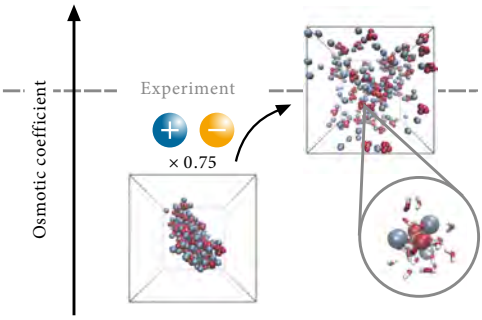

models, without additional tuning of force field parameters, provide an accurate description of water-mediated interactions between salt ions. This results in predictions of the osmotic coefficients of aqueous K_3PO_4 and K_2HPO_4 solutions in good agreement with experimental data. Analysis of ion pairing thermodynamics in terms of contact ion pair (CIP), solvent-separated ion pair, and double solvent-separated ion pair contributions shows that potassium–phosphate CIP formation is stronger with trivalent than with divalent phosphate ions.

8.1 Introduction

Molecular simulations have contributed significantly to the understanding of ion pairing mechanisms in water and to Hofmeister ion effects.[2,3,9,17,118] Because short-range interactions of ions with other ions, or with the hydration shells of aqueous polymers and proteins, are important in most of these effects, accurate force field models are needed.

Over the years, many nonpolarizable force fields have been developed for aqueous electrolyte solutions. However, electronic polarization effects play a role in these systems, leading to inaccuracies in describing short-range ion–water and ion–ion interactions with nonpolarizable force fields, sometimes resulting in artificially strong ion clustering.[253,256,257,259] Although polarizable models may potentially describe the interactions in these systems better, nonpolarizable models are widely used because they are computationally cheaper and easier to parameterize.

Various methods have been studied to effectively incorporate polarization effects into nonpolarizable force fields. For instance, a number of approaches investigated if an adjustment of Lennard-Jones (LJ) parameters is sufficient to resolve the ion clustering issue. Weerasinghe and Smith[241] and Gee et al.[242] scaled the cation–water oxygen LJ interaction for various alkali halides. These force fields reproduce the salt activity coefficient derivatives for each salt as well as the experimental Kirkwood–Buff integrals. The same approach was followed in the work of Hess and van der Vegt[78] for alkali acetate salts. Fyta and Netz[244] instead scaled the cation–anion interactions for various alkali halide systems. The force fields were parameterized using Kirkwood–Buff theory and by comparison to experimentally determined activity coefficient derivatives for each salt. All the developed force fields demonstrate that a modification of LJ parameters is sufficient to avoid ion clustering and to reproduce bulk experimental properties for monovalent salts in water. Such approaches, however, require individual parameter identification for each ion pair and involves extensive simulations to carefully parameterize the force fields.

Alternatively, and arguably also consistent with the fact that the role of electronic polarization is effectively included in nonpolarizable water models and biomolecular force fields through parameterization of partial atomic charges, ionic charges may instead be modified to improve short range ion–ion and ion–water interactions. This can be justified because the Coulomb interaction between two ions in close proximity is in reality screened by virtue of the high-frequency (electronic) contribution to the water dielectric permittivity which is not accounted for in simulations with nonpolarizable water models and ions that carry their full integer charges. The simplest way to account for this type of screening in nonpolarizable models is to scale all ion charges with the inverse square-root of the water high-frequency dielectric permittivity (i.e., with $1/\sqrt{\varepsilon_{\mathrm{el}}} \approx 0.75$). This electronic continuum correction (ECC), originally proposed by Leontyev et al.,[246–252] has been followed up and promoted by Jungwirth and others and has proven successful.[253–257,259,261,493] Although charge rescaling has been demonstrated to perform well if properties determined by short-range ion–ion correlations are investigated, it, however, is not entirely clear whether the corresponding weaker long-range electrostatic interactions between ions are also in good agreement with experimental reality.

Herein, we apply ECC to trivalent and divalent potassium phosphate salts in water (K_3PO_4 and K_2HPO_4). This choice is motivated by the question whether in multivalent salt solutions, in which polarization effects are expected to be strong, ECC can provide an accurate description of effective (solvent-mediated) ion–ion interactions. Previous studies applying ECC have examined monovalent and divalent salts only.[253–257,259,261,493] Some of these studies validated the ECC models by comparing the ion–ion correlations obtained from simulations with experimental information obtained by neutron scattering.[253,256,257,259,261,493] While information on ion–ion correlations in aqueous electrolytes is relatively scarce in the experimental literature, information on integral quantities can be readily found. For example, the osmotic coefficient ϕ can therefore be used for validation of the ECC model instead. The salt osmotic coefficient ϕ relates to effective ion–ion interactions and can be written in terms of a virial expression[494]

$$\phi = 1 - \frac{\beta}{6\rho} \sum_{ij} \rho_i \rho_j \int_0^\infty r \frac{\mathrm{d}V_{ij}^{\mathrm{eff}}(r)}{\mathrm{d}r} g_{ij}(r) 4\pi r^2 \mathrm{d}r, \tag{8.1}$$

with ρ denoting the total particle number density, ρ_i denoting the component number density, $g_{ij}(r)$ denoting the pair correlation function, $-\mathrm{d}V_{ij}^{\mathrm{eff}}/\mathrm{d}r$ denoting the effective pair force, and $\beta = (k_B T)^{-1}$. In Eq. (8.1), it is assumed that the effective pair potential V_{ij}^{eff} is density independent. The osmotic coefficient has been investigated for atomistic force field models[78,235,243,244,422,495–497] and is determined by the structural distribution $g_{ij}(r)$ of the ions as well as by the effective forces $-\mathrm{d}V_{ij}^{\mathrm{eff}}/\mathrm{d}r$ between them, as illustrated by Eq. (8.1). If $g_{ij}(r)$ is poorly represented, ϕ is poorly represented, too. Therefore, ϕ

serves as a sensitive probe for the quality of an aqueous electrolyte model and provides a stringent test for assessing the quality of ECC models. Because changes in ϕ are related to changes in ion pairing propensities,[78,126,498] molecular simulations of ion pairing mechanisms should be based on force fields models that reproduce ϕ. The aim of the present work is to assess whether ECC models for multivalent salts provide sufficient accuracy to achieve this. We do not aim to provide new force field models for K_3PO_4 and K_2HPO_4 as that would require the validation of addition properties. It will be shown that the ECC correction leads to accurate predictions of solution osmotic properties. Therefore, the ECC models are used herein to study microscopic aspects of ion hydration and potassium–phosphate ion pairing.

8.2 Simulation details

All atomistic simulations are carried out using the MD package GROMACS[499] version 4.5.1.[443] in the isothermal-isobaric (NPT) ensemble with constant particle numbers (N), pressure (P) of 1 bar, and temperature (T) of 298 K. Pressure and temperature are controlled using a Parrinello–Rahman barostat[411,412] with a coupling time τ_P of 1.0 ps and a Nosé–Hoover thermostat[410,420] with a coupling time τ_T of 0.4 ps. Periodic boundary conditions are applied in all three dimensions to the cubic simulation box. 9–59 K_3PO_4 molecules with 5115–4702 water molecules or 10–83 K_2HPO_4 molecules and 5111–4622 water molecules depending on the specific salt concentration are used. The examined concentrations are 0.1 m, 0.3 m, 0.4 m, 0.5 m, and 0.7 m for K_3PO_4 and 0.1 m, 0.3 m, 0.5 m, 0.7 m, and 1.0 m for K_2HPO_4. The hydrolysis of K_3PO_4 is taken into account and mixtures of PO_4^{3-}, HPO_4^{2-}, and OH^- are simulated as well. The extended simple point-charge (SPC/E) water model[418] is used and the internal geometry is kept rigid using the SETTLE algorithm.[419] LINCS[417] is used to constrain all bonds. Long-range electrostatic interactions are treated by the particle mesh Ewald (PME) method[460] using a Fourier spacing of 0.12 nm, PME order 4, and a real space cutoff of 1.4 nm. Short-range Lennard-Jones interactions are truncated at 1.4 nm. The neighbor list is updated every 0.02 ps and also features a cutoff at 1.4 nm. No long-range correction is used for the dispersion interactions.

The MD simulations are equilibrated in a 5 ns simulation. Consecutive independent simulations are performed for each concentration of K_3PO_4 and K_2HPO_4. Osmotic coefficients are calculated from 50 ns simulations after additional 0.5 ns simulations for equilibration (see below for further details about these simulations). All other properties are calculated from simulations of 100 ns duration. The integration time step in all types of simulations is 2 fs and configurations are saved every 5 ps. Errors bars, both for the osmotic coefficients and for the ion-pairing properties are calculated from 10 ns blocks and using sample standard deviation.

The force field parameters, except for atomic partial charges, are based on an Assisted Model Building with Energy Refinement (AMBER) force field[225] for phosphate and on a KB force field[242] for potassium. For the two phosphate ions, the restrained electrostatic potential (RESP) method[500] with HF/6-31G(d,p) is used to derive the partial atomic charges of the ions in vacuum. ECC force field charges are obtained from rescaling the full charges with a factor of 0.75. This value is obtained from $1/\sqrt{\varepsilon}_{\mathrm{el}}$ using $\varepsilon_{\mathrm{el}} = 1.78$ for water. All force field parameters are summarized in Appendix A (Section 8.5.1). While nonbonded parameters are presented in Table 8.2 for K_3PO_4 and in Table 8.3 for K_2HPO_4, bonded force fields parameters for the two phosphate ions are summarized in Table 8.4. The SPC/E water model is used to construct the hydroxide ion.[501–503]

To confirm if ECC applied on an AMBER force field together with RESP derived charges can improve the ion interactions for multivalent ions (PO_4^{3-} and HPO_4^{2-}), two nonpolarizable force fields are compared. The first force field uses the approach of Gee et al.[242] and will be called the "full charge force field" in the following. In this approach, the LJ repulsion between cations and the water oxygen is reduced, leading to a stronger electrostatic interaction between cations and water molecules. The second force field effectively accounts for polarization by applying the ECC correction. The force field using this model will subsequently be called "ECC force field".

The osmotic coefficient relates the osmotic pressure for a nonideal solution (Π) to an ideal solution (Π_{id}) according to $\phi = \Pi/\Pi_{\mathrm{id}}$, where $\Pi_{\mathrm{id}} = \nu c \mathrm{R} T$. The constant ν is the number of components originating from dissolution of the solute (e.g., 2 for NaCl). c is the solute molarity of the solution, R is the gas constant and T is the temperature. In this study, the osmotic pressure (Π) is calculated directly from all-atom MD simulations in a procedure adapted from Luo and Roux.[422] The simulation box is extended to twice its size in the z-direction. The region with the salt solution is separated from the two new regions of pure water with "virtual" walls representing a semipermeable membrane, see Fig. 8.1. While water molecules can freely cross the "virtual" walls and equilibrate the water chemical potential throughout the entire simulation cell, the ions are enclosed in the confinement between the two walls. The osmotic pressure (Π) is determined from the average force exerted by the ions on the walls according to the relation $\Pi = \langle F_{\mathrm{wall}} \rangle / A$, with A being the area of the wall and $F_{\mathrm{wall}} = 2\kappa \sum_i{}' |z_i - z_{\mathrm{wall}}|$ being the force exerted by the confined ions on the wall. The prime on the summation symbol means summation of only those ions whose positions z_i are outside the confining wall located at position z_{wall}, where z_{wall} is the z coordinate of the respective walls ions have passed (see Fig. 8.1). Π is finally obtained by averaging $\langle F_{\mathrm{wall}} \rangle / A$ for the two walls. The "virtual" walls are implemented by PLUMED 1.3.[504] A force constant of κ =4180 kJ/(mol nm^2) is used.[422] Furthermore, the osmotic coefficients are calculated from two independent simulations to provide better statistics.

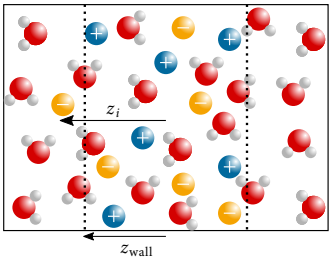

Fig. 8.1 Schematic sketch of simulation box with "virtual" walls (dotted lines) for the calculation of osmotic pressure. The walls confine the ions while water molecules freely pass through them.

8.3 Results and discussion

8.3.1 Osmotic coefficients

Figure 8.2 shows calculated osmotic coefficients and the corresponding experimental values[505] for both K_3PO_4 (a) and K_2HPO_4 (b). For K_3PO_4, a good agreement between the values obtained from simulations with the ECC force field and the experimental osmotic coefficients can be observed in the concentration range between 0.1 m and 0.7 m. However, the computed osmotic coefficient tends to slightly lower values than measured experimentally at high concentrations. That is, the ion-pair interactions are slightly overestimated at high concentrations using the ECC force field for K_3PO_4. For K_2HPO_4, the effective interactions between the ions are slightly too weak, which can be seen in the somewhat higher osmotic coefficients compared to the experimental data. That is, the ECC force field overestimates the hydration of the salt for K_2HPO_4. Yet, the ECC force field reproduces the trend of the experimental osmotic coefficients as opposed to the full charge force field. The deviation of the osmotic coefficients for the full charge force field for K_2HPO_4 is due to that the salt is forming clusters and is not soluble anymore at higher concentrations when simulated with that force field. The ion–ion interactions are overestimated and the osmotic coefficient is low. The same holds for all concentration of K_3PO_4 simulated with the full charge force field. The larger error bars at low molality are due to the lower statistics as a result from the few ions.

It should be noted that hydrolysis of K_3PO_4 introduces some uncertainty in the comparison of experimental and simulation data for K_3PO_4. We here take the hydrolysis of PO_4^{3-} into consideration by replacing the appropriate number of PO_4^{3-} ions with HPO_4^{2-} and OH^- ions based on the HPO_4^{2-} pKa value. Hydrolysis of HPO_4^{2-} and $H_2PO_4^-$ plays a negligible role and is therefore neglected. The molality of each species,

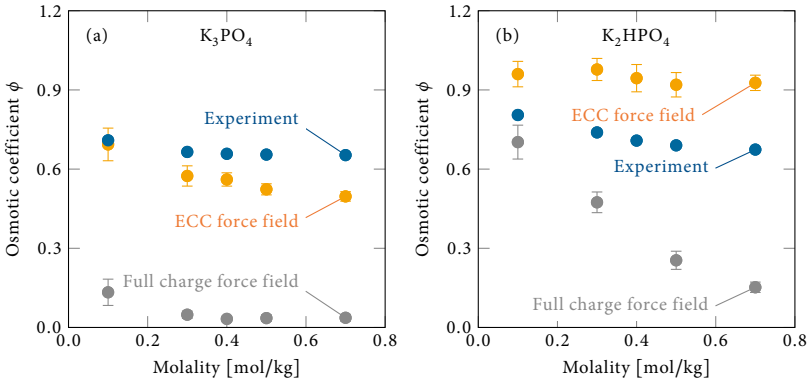

Fig. 8.2 Osmotic coefficients ϕ of (a) aqueous K_3PO_4 solutions and (b) aqueous K_2HPO_4 solutions, as a function of salt concentration calculated as an average of two consecutive simulations. Error bars are calculated from five blocks and sample standard deviation for each simulation.

Table 8.1
Concentrations (mol/kg) of PO_4^{3-}, HPO_4^{2-}, and OH^- in aqueous K_3PO_4 solutions.

K_3PO_4	PO_4^{3-}	HPO_4^{2-}	OH^-
0.1	0.07	0.03	0.03
0.3	0.23	0.07	0.07
0.4	0.32	0.08	0.08
0.5	0.40	0.10	0.10
0.7	0.59	0.11	0.11

PO_4^{3-}, HPO_4^{2-}, and OH^-, in aqueous K_3PO_4 solutions with K_3PO_4 concentrations ranging from 0.1 m to 0.7 m, is shown in Table 8.1. The ratio of the two phosphate anions is calculated from the pKa value of 12.32 for HPO_4^{2-}.[506] Fig. 8.3 shows the corresponding osmotic coefficients obtained from the simulations. Excellent agreement is observed by comparison of the simulation and experimental data. Moreover, the concentration dependent trend is reproduced as well.

To summarize this section, we find that the ECC force field provides a significant improvement over the full charge force field for K_3PO_4 and K_2HPO_4. For K_3PO_4 (Fig. 8.3), the osmotic coefficient is reproduced quantitatively. The ECC model also reproduces the experimental observation that osmotic coefficients for K_2HPO_4 are higher than for K_3PO_4, but overestimates the ion–water interactions for K_2HPO_4.

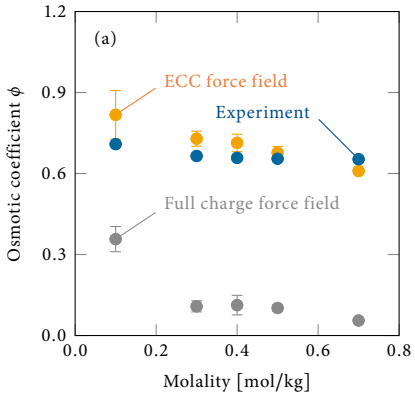

Fig. 8.3 Osmotic coefficients ϕ of aqueous K_3PO_4 solutions as a function of K_3PO_4 concentration calculated as an average of two consecutive simulations. To account for K_3PO_4 hydrolysis, PO_4^{3-}, HPO_4^{2-}, and OH^- ions are included (see Table 8.1). Error bars are calculated from five blocks and sample standard deviation for each simulation.

8.3.2 Linking electrolyte structure and thermodynamics

The KB theory[191] relates solution structure to thermodynamics. Applied to the osmotic coefficient, the KB theory provides the exact relation (see Appendix B (Section 8.5.2))

$$\left(\frac{\partial[\rho_s(\phi-1)]}{\partial\rho_s}\right)_{P,T} = \frac{-(\Delta N_{ss}-\Delta N_{ws})}{1+(\Delta N_{ss}-\Delta N_{ws})}, \tag{8.2}$$

where ρ_s is the molar total ion concentration and $\Delta N_{ss} = \rho_s G_{ss}$ and $\Delta N_{ws} = \rho_s G_{ws}$ are the salt–salt and salt–water excess coordination numbers, respectively, with G_{ss} and G_{ws} the salt–salt and salt–water Kirkwood–Buff integrals, defined as

$$G_{\alpha\beta} = 4\pi\int_0^\infty [g_{\alpha\beta}(r)-1]r^2\,\mathrm{d}r, \tag{8.3}$$

where $g_{\alpha\beta}(r)$ is the radial distribution function (RDF) for the $\alpha\beta$ pair. Cations and anions are treated as indistinguishable species. Figure 8.4 shows the running integral values of $\Delta N_{ss} - \Delta N_{ws}$ which in the limit $r \to \infty$ correspond to the excess coordinations numbers in Eq. (8.2). This quantity is positive for the three salt concentrations shown in Fig. 8.4 indicating that effective ion–ion attractions overcompensate ionic hydration. The limiting values of $\Delta N_{ss} - \Delta N_{ws}$ are significantly smaller for K_2HPO_4 than for K_3PO_4, in agreement with the fact that the slope of the ECC data for K_2HPO_4 in Fig. 8.2b is

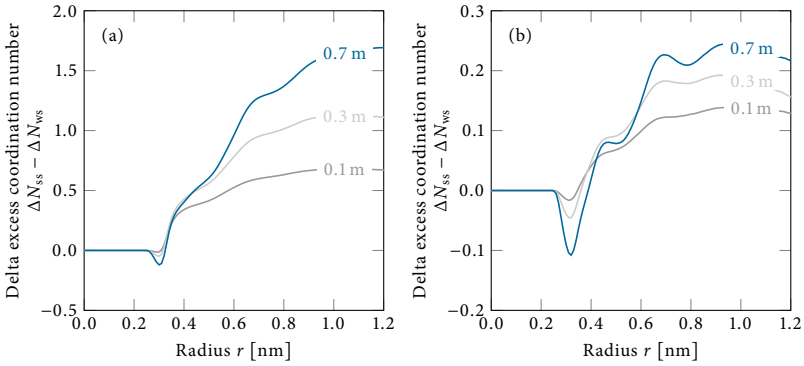

Fig. 8.4 Difference in excess coordination numbers for "salt–salt" and "salt–water" in (a) K_3PO_4 and (b) K_2HPO_4 for 0.1 m, 0.3 m, and 0.7 m from ECC force field simulations.

smaller than the slope of the ECC data for K_3PO_4 in Fig. 8.2a. As a consistency check, we evaluated the derivative $\partial[\rho_s(\phi-1)]/\partial\rho_s$ on the left-hand side of Eq. (8.2) using the ECC osmotic coefficient values in Fig. 8.2 and compared that with the right-hand side of Eq. (8.2) calculated with the data in Fig. 8.4. At 0.3 m K_3PO_4, the derivative is $\partial[\rho_s(\phi-1)]/\partial\rho_s \approx -0.56$ (Fig. 8.2a). For 0.3 m K_3PO_4, $\Delta N_{ss} - \Delta N_{ws} \approx 1.12$ (Fig. 8.4a), and therefore, the right-hand side of Eq. (8.2) is about −0.53, in agreement with the data in Fig. 8.2a.

Changes in solution osmotic properties with salt concentration can be related to excess ion pairing configurations, including contact ion pairs (CIPs), solvent-separated ion pairs (SIPs), and double solvent-separated ion pairs (2SIPs) (see Fig. 8.5).[78,507] To this end, we assume that ΔN_{ss} is dominated by pairing between oppositely charged ions, i.e., $\Delta N_{ss} \approx \Delta N^{+-}$ with $\Delta N^{+-} = \Delta N_{CIP} + \Delta N_{SIP} + \Delta N_{2SIP} + C$. The excess numbers of CIPs, SIPs, and 2SIPs are obtained by integrating the cation–anion RDFs in the corresponding regions shown in Figs. 8.5b and 8.5c. The additive constant C accounts for the contribution to ΔN^{+-} from distances larger than the 2SIP distance. Figure 8.6 shows the excess numbers of CIPs, SIPs, and 2SIPs for K_3PO_4 and for K_2HPO_4. With increasing salt concentration, the excess number of ion pairs increases. Significantly, CIPs contribute most to ΔN^{+-} for K_3PO_4. For K_2HPO_4, ΔN^{+-} is instead dominated by SIPs. Contact ion pair formation in aqueous K_3PO_4 solution therefore explains the decrease of the osmotic coefficient with salt concentration in Fig. 8.2. A dominant contribution of SIPs in ion pairing thermodynamics, observed here for K_2HPO_4, has also been observed in a previous study of monovalent $K(CH_3)_2PO_4$ and KCH_3COO salts in water.[507] Currently no explanation for the different trends of 2SIP for the two

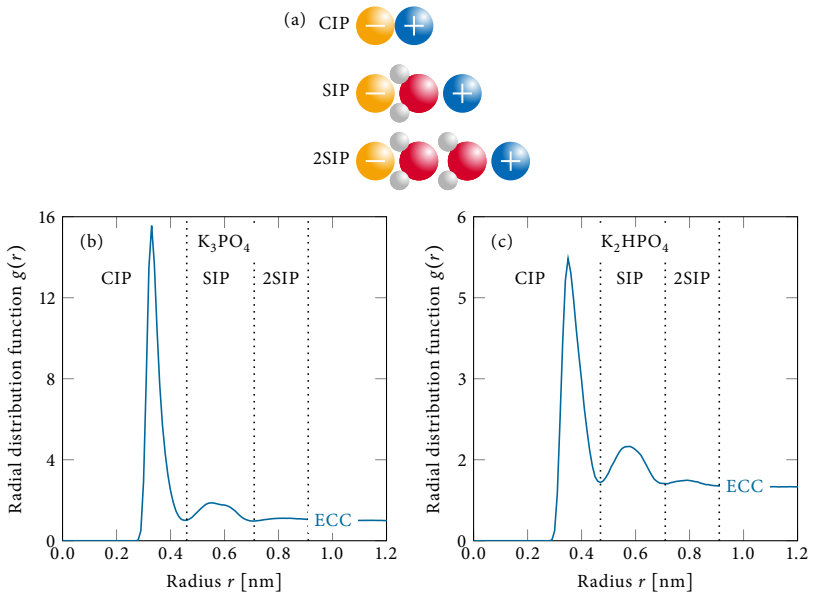

Fig. 8.5 (a) Illustrations of the different types of ion pairs: contact ion pair (CIP), solvent-separated ion pair (SIP), and double solvent-separated ion pair (2SIP). The radial distribution function $g(r)$ between phosphorus in phosphate and potassium for (b) 0.7 m K_3PO_4 and (c) 0.7 m K_2HPO_4. The vertical dotted lines in (b) and (c) separate the different ion pair types.

systems can be given. However, the discussion of the behavior of 2SIP is beyond the scope of this work.

8.3.3 Electrolyte structure: Comparison of the ECC and full charge force fields

The difference between the full charge force field and the ECC force field regarding ion clustering can be seen in the representative simulation snapshots in Fig. 8.7. Due to overestimated ion-pair formation, ion clusters are formed with the full charge force field. The ions precipitate even far below the solubility limit of K_3PO_4 (2.4 M)[508] and K_2HPO_4 (8.6 M),[508] respectively. This is observed for both K_3PO_4 and K_2HPO_4 in the top panel in Fig. 8.7. However, using the ECC force field results in a homogeneous solution below the solubility limit (see the bottom panel in Fig. 8.7). This significant reduction in ion clustering clearly demonstrates that the ECC approach improves the

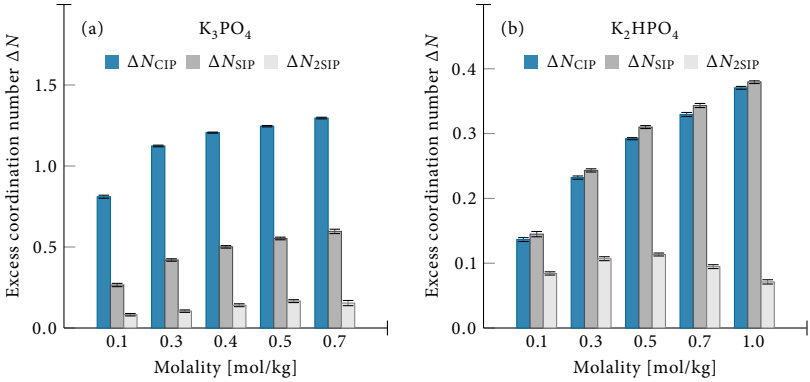

Fig. 8.6 Excess coordination numbers of the different ion pairs (CIP, SIP, and 2SIP) for (a) K_3PO_4 and (b) K_2HPO_4 from ECC force field simulations. Error bars are calculated from ten blocks and sample standard deviation.

multivalent phosphate force field. Previous studies demonstrated the same effects for other salts with monovalent ions such as KNO_3,[253,254] $LiNO_3$,[254] and $NaNO_3$[254] and for divalent ions such as K_2CO_3,[253] Na_2SO_4,[255] Gdm_2CO_3,[256] Li_2SO_4,[257] and $CaCl_2$.[259]

The potassium–phosphate RDFs obtained with the full charge force field and the ECC force field are shown in Fig. 8.8. The different RDFs for 0.7 m and 0.1 m solutions show the same trends but differ in the absolute peak heights. The reduction of ion pairing due to scaling the ionic charges corresponds to a significant decrease of the cation–anion RDF in the entire distance range. Similar obervations are made in the anion–anion and cation–cation RDFs (not shown). Figure 8.9 shows the phosphate–water RDFs. For K_3PO_4, the P–OW distance of 0.36 nm obtained with the ECC force field is in good agreement with 0.37 nm from a neutron diffraction study.[509] Likewise, the O–HW distance of 0.16 nm predicted by the ECC force field (not shown) is in good agreement with 0.18 nm from neutron scattering.[509] The local minimum between the first and second hydration shell is lower for K_3PO_4 than for K_2HPO_4 (see Fig. 8.9a and b). This corresponds to a larger desolvation barrier for K_3PO_4. K_3PO_4 therefore interacts stronger with water than K_2HPO_4, which ensues from the higher ion charge density.

The ECC force field provides a hydration number of the first hydration shell of about 12 to 13 for PO_4^{3-}, which is consistent with the experimental value of 12,[510] 15 ± 3,[509,511] and 16[512] for K_3PO_4. The hydration number of about 11 for K_2HPO_4 is slightly lower than

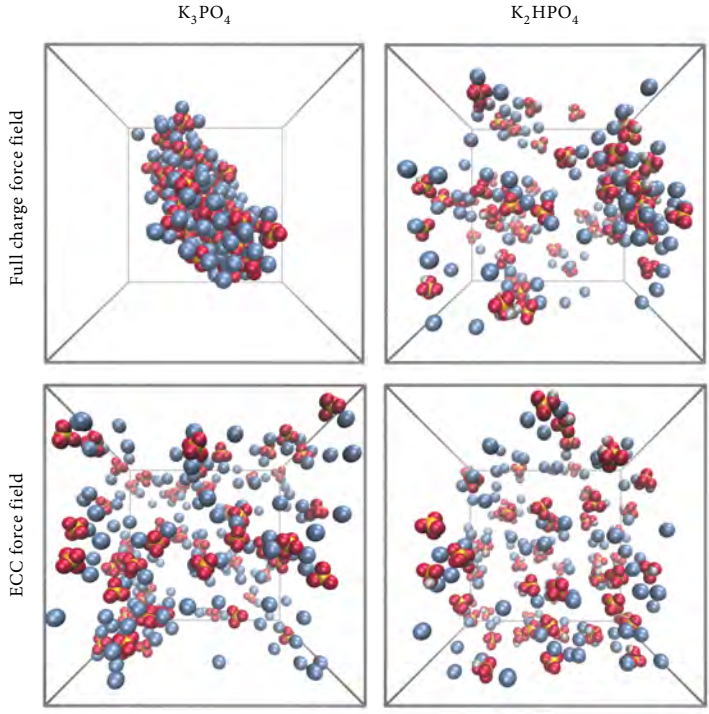

Fig. 8.7 Representative snapshot of 0.7 m K_3PO_4 (left) and 0.7 m K_2HPO_4 (right) with full charge force field (top) and ECC force field (bottom). Potassium–blue, oxygen–red, phosphor–orange, and hydrogen–gray.

for K_3PO_4. This opposes previous MD simulations[512] and experiments,[509] showing a larger hydration number for K_2HPO_4. The first hydration number for K^+ is about 7 which is comparable to the experimentally obtained hydration number of K^+ in the range 4.8–6.1 for various potassium salts.[96,97]

8.3.4 Ion pairing

K^+ is a weakly hydrated cation,[162,165] while PO_4^{3-} is a strongly hydrated multivalent anion. All multivalent ions are strongly hydrated.[513] According to the "law of matching

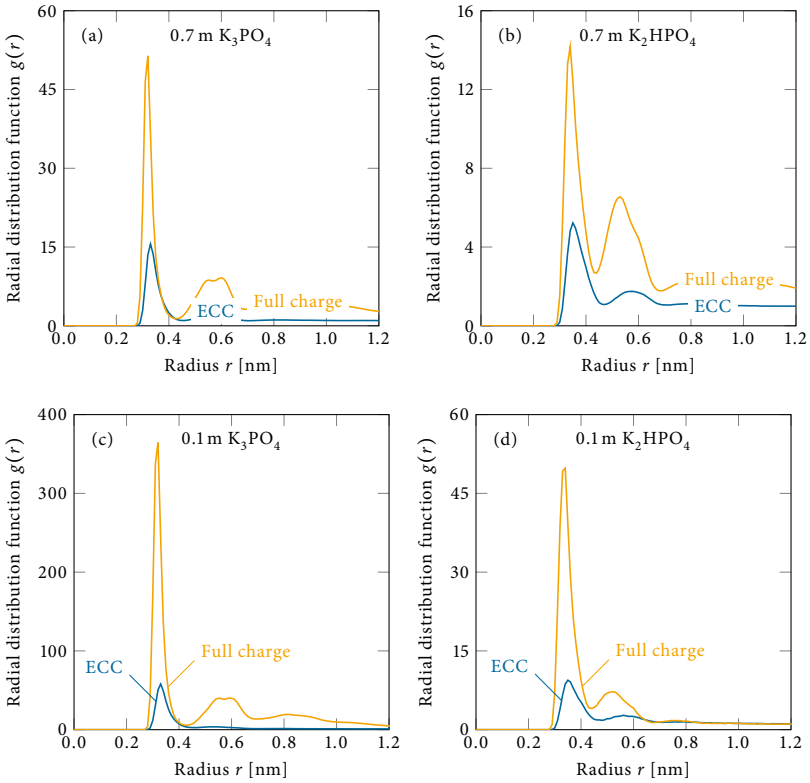

Fig. 8.8 The radial distribution function $g(r)$ between phosphorus in phosphate and potassium for (a) 0.7 m K_3PO_4, (b) 0.7 m K_2HPO_4, (c) 0.1 m K_3PO_4, and (d) 0.1 m K_2HPO_4.

water affinity" (LMWA),[165] cation–anion pairing occurs between ions with equal hydration free energies. For simple spherical ions, this implies that small pairs with small, or large pairs with large, while small–large ion combinations remain solvent separated. This qualitative rule has been confirmed by Fennel et al.[167] based on extensive MD simulations of alkali halide ion pairing in water. The LMWA tells us that K^+ does not form CIPs with PO_4^{3-} and HPO_4^{2-}. Clearly, the LMWA provides a qualitative picture and it is therefore interesting to ask if this law also provides a qualitatively correct picture of ion pairing in systems with multivalent molecular anions such as PO_4^{3-} and HPO_4^{2-}.

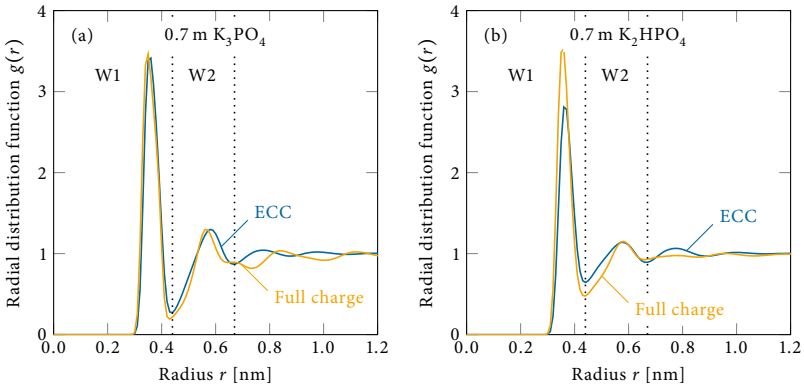

Fig. 8.9 The radial distribution function $g(r)$ between phosphorus in phosphate and oxygen water for (a) 0.7 m K_3PO_4 and (b) 0.7 m K_2HPO_4. The vertical dotted lines separate the different hydration shells for the ECC radial distributions functions.

Figure 8.10 shows the cation–anion coordination numbers obtained using the ECC force field. For K_2HPO_4, $N_{CIP} < N_{SIP} < N_{2SIP}$, as expected based on the fact that more ions can surround a central ion in a spherical shell with larger radius. For K_3PO_4, this trend is not observed. By contrast, the number of CIPs is relatively large compared to SIPs and 2SIPs, indicating that contact ion pairs are ubiquitous in aqueous K_3PO_4 solutions.

The data in Fig. 8.10 are obtained by integrating over RDF peaks and are therefore based on counting pairs without unique assignment of a cation to only one anion and not to another, i.e., for a given cation at CIP distance to one anion and simultaneously at SIP distance to another anion, both the CIP and SIP configurations will be counted. The relative proportions of the different types of ion pairs can alternatively be obtained by first assigning counterions to the *closest* phosphate ion and subsequently analyzing the fractions of CIPs, SIPs, and 2SIPs from the assigned ion pairs. The corresponding number fractions are shown in Fig. 8.11. These data clearly shows that CIP formation is the dominant mode of ion pairing in K_3PO_4 solution. For K_2HPO_4, on the other hand, the formation of SIPs dominates. However, considering the overestimation of ion–water interactions for K_2HPO_4 (see Fig. 8.2b), the exact fraction of CIP and SIP can be different. Additionally, both examined salts follow the same salt concentration dependency. With increasing salt concentration, the CIP and SIP fractions increase, while the 2SIP fraction decreases. This is a concentration effect due to that only the closest counterion is taken into account. The average distance between ions is decreasing when the concentration is increasing. The probability of finding 2SIP ion pairs is therefore lower at higher concentrations.

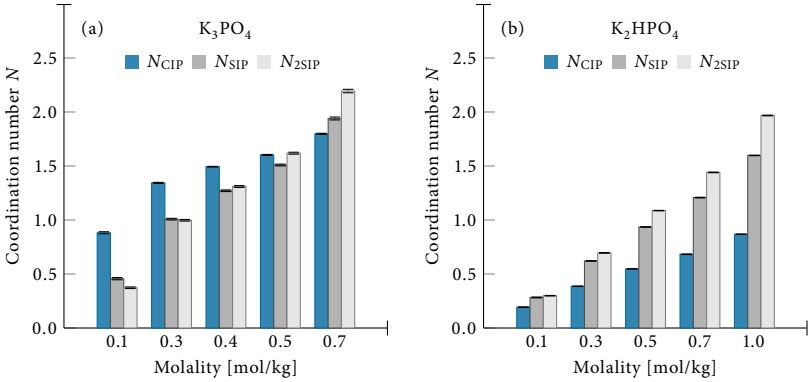

Fig. 8.10 Coordination numbers of the different ion pairs (CIP, SIP, and 2SIP) for (a) K_3PO_4 and (b) K_2HPO_4 from ECC force field simulations. Error bars are calculated from ten blocks and sample standard deviation.

The above observations clearly deviate from the prediction based on Collins' law of matching water affinities.[165] For molecular ions, the application of this law is not straightforward and the surface charge density distributions of the ions need to be considered.[514] PO_4^{3-} has a larger surface charge density than of HPO_4^{2-},[514] and therefore, the mismatch in the hydration free energies of these ions compared with K^+ is larger for PO_4^{3-} than for HPO_4^{2-}. Despite this, K^+ forms CIPs with PO_4^{3-} even at 0.1 m salt concentration, in disagreement with the LMWA prediction. This is, to the authors' knowledge, the first time it has been shown for multivalent anions. However, it has already been demonstrated for divalent cations.[115]

8.3.5 Ion pair structure and water density distribution around PO_4^{3-} and HPO_4^{2-}

Fig. 8.12 shows the spatial density distribution of potassium around phosphate. It is generated using Ovito.[425] The left panel depicts K_3PO_4 and the right panel shows K_2HPO_4. One concentration, 0.7 m, for each salt is shown. All other concentrations follow the same trend. For the CIP of K_3PO_4 (top panel), the density along the four axes through the P–O bonds is smaller than the density in the regimes not on the axes. This indicates that potassium interacts with three oxygen atoms simultaneously. Therefore, potassium can be classified as of tridentate coordination type when paired with PO_4^{3-}. This is in agreement with an earlier study showing that potassium coordinates symmetrically between three phosphate oxygen atoms.[512] Remarkably, for

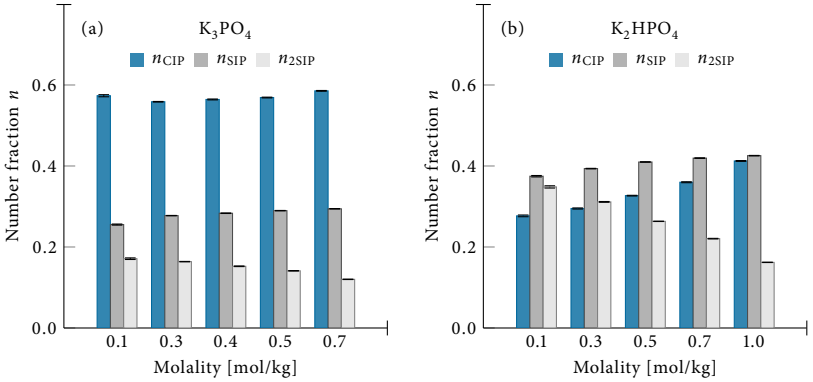

Fig. 8.11 Number fraction of different ion pairs (CIP, SIP, and 2SIP) for (a) K_3PO_4 and (b) K_2HPO_4 from ECC force field simulations when only the closest counterion to K^+ is taken into account. Error bars are calculated from ten blocks and sample standard deviation.

K_2HPO_4, the density distribution of K^+ is different than for K_3PO_4. The K^+ density is low at the phosphate oxygens, similar to K_3PO_4. However, the density of K^+ is rather high at the oxygen bonded to the hydrogen and low at the opposite side. A decreased potassium density around the phosphate in a certain region in the CIP is followed by an increased density in the SIP (middle panel). Likewise, an increased density in a specific region in CIP is followed by a decreased density in the same region in SIP. The density distribution of potassium around PO_4^{3-} and HPO_4^{2-} becomes more uniform with increasing distance from the phosphate ion. At a distance where 2SIPs (bottom panel) are formed, potassium forms a uniform spherical shell around the anion. The effect of the anion–cation interactions vanishes with increasing distance from the phosphate molecule. The phosphate ion perturbation on the cation vanishes after 2SIP (bottom panel).

Figure 8.13 shows the density distribution of water around PO_4^{3-} and HPO_4^{2-}. These densities are based on water oxygen atom locations. The water density along the four axes through the P–O bonds is lower in the first hydration shell compared to the bulk (top panel). Instead, the water density is higher in the vicinity of the axes. The water molecules fit between the tetrahedral coordination sites in the nonspherical phosphate molecules. However, in the second hydration shell, the density is the highest along the four axes through the P–O bonds. Each phosphate oxygen coordinates to in average three water molecules.[509,515] Pribil et al.[515] distinguish between strongly coordinated water molecules in a linear arrangement from water molecules located interstitially in the first hydration shell. In the present work, it is shown that the probability of

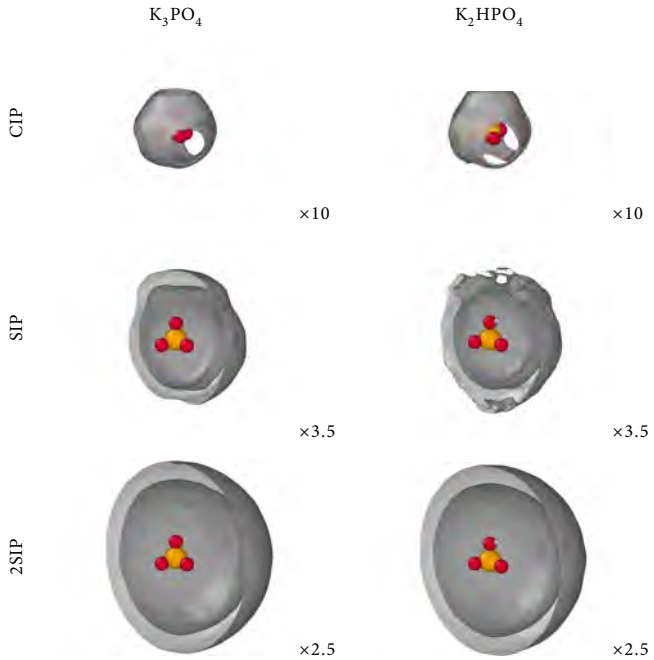

Fig. 8.12 Illustrations of three dimensional density distributions of K^+ for 0.7 m K_3PO_4 (left) and 0.7 m K_2HPO_4 (right) from ECC force field simulations. Three regions are displayed: CIP (top), sliced through SIP (middle), and slice through 2SIP (bottom). Numbers indicate density of K^+ in factors of bulk density.

the interstitially water molecules is higher in the first hydration shell. In the second hydration shell, the probability is higher for a water molecule to be linearly arranged. The results agree with earlier simulations,[512] where it was found that an angle of about 90° has the highest probability at small phosphorus water hydrogen distances and a near-linear angle occurs typically for larger distances. Additionally, the water density around the phosphate oxygen binding to the hydrogen in the K_2HPO_4 molecule is lower compared to the three other phosphate oxygens in the first hydration shell. Similar to the distribution of cations around phosphate, the distribution of water molecules becomes more uniform with increasing distance from the anion. The effect of the anion–water interactions is only felt in the immediate neighborhood of the anion, as shown by the water density in the second hydration shell already being close to the bulk density in Fig. 8.13.

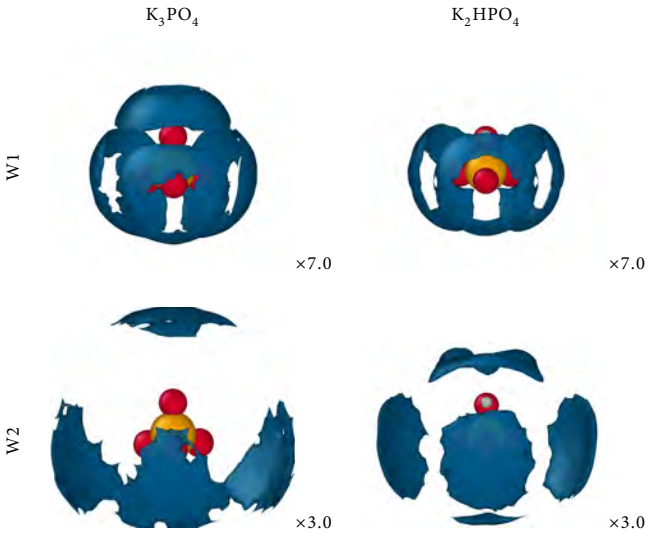

Fig. 8.13 Illustrations of three dimensional density distributions of water molecules (water oxygen) for 0.7 m K_3PO_4 (left) and 0.7 m K_2HPO_4 (right) from ECC force field simulations. Two regions are displayed: first hydration shell W1 (top) and second hydration shell W2 (bottom). Numbers indicate density of water oxygen in factors of bulk density.

8.4 Conclusions

In this study, the application of the ECC model in molecular simulations of multivalent aqueous electrolytes, K_3PO_4 and K_2HPO_4, is reported. ECC effectively accounts for polarization effects through rescaling of the ionic charges with the inverse square-root of the water high-frequency dielectric permittivity. Previously reported work has shown that ECC models reduce artificial ion pairing and aggregation observed in nonpolarizable force field simulations of monovalent and divalent salts and, furthermore, provide structural agreement with neutron scattering data. Herein, we have addressed the question whether ECC models for multivalent salts provide an accurate description of effective (solvent-mediated) ion–ion interactions, which determine the salt activity and osmotic coefficients. We find that osmotic coefficients obtained with ECC models are in very good agreement with experiments. That is, ECC renders applicable not only to mono- and divalent ions but also to trivalent ions for which electronic polarizability effects are significantly more prominent. Importantly, these results have been obtained without performing parameterization of ion model parameters, thus indicating that

Table 8.2
Force field parameters for both the full charge force field and the ECC force field (rescaled charges) for K_3PO_4. The subscript "W" stands for water and "OH" for hydroxide ion. See Fig. 8.14 for labeling of the phosphate atoms.

	Full charge	Rescaled charge	σ [nm]	ε [kJ/mol]
K	1.00	0.75	0.3340	0.1300
P_1	1.52	1.14	0.374 177	0.8368
O_1	−1.13	−0.8475	0.295 992	0.878 64
H_W	0.4238	0.4238	0.0	0.0
O_W	−0.8476	−0.8476	0.316 557	0.650 629
H_{OH}	0.4238	0.317 85	0.0	0.0
O_{OH}	−1.4238	−1.067 85	0.316 557	0.650 629

ECC-based scaling of ionic charges effectively captures the effects of polarization in thermodynamic solution properties. This furthermore implies that time-consuming procedures to parameterize ion force fields against thermodynamic data may be avoided. Further work, is however, needed to test the generality of the ECC approach for other systems.

The ECC models studied in this work have been used to examine ion pairing in K_3PO_4 and K_2HPO_4 aqueous solutions. It is found that K^+ forms CIPs with PO_4^{3-} as well as with HPO_4^{2-} in disagreement with Collins' "law of matching water affinities" which predicts that weakly hydrated K^+ ions and strongly hydrated di- and trivalent phosphate ions remain solvent separated. K^+ forms CIPs with PO_4^{3-} and HPO_4^{2-} in a tridentate coordination type.

Acknowledgement. The authors thank Constanze Kalcher for her help with the Ovito scripting interface. We thank Francisco Rodríguez-Ropero for his help with the calculation of RESP charges for the ions and Timir Hajari for his support regarding the procedure of osmotic coefficient calculations. Furthermore, the calculations for this research were conducted on the Lichtenberg high performance computer of the TU Darmstadt. Finally, the authors thank the LOEWE project iNAPO funded by the Ministry of Higher Education, Research and the Arts (HMWK) of the state of Hessen.

8.5 Appendices

8.5.1 Appendix A: Potassium phosphate force field

In the following, not only modified but all parameters for the force fields based on AMBER[225] (phosphate) and Kirkwood–Buff[242] (potassium) are given for the sake of

Table 8.3
Force field parameters for both the full charge force field and the ECC force field (rescaled charges) for K_2HPO_4. The subscript "W" stands for water and "OH" for hydroxide ion. See Fig. 8.14 for labeling of the phosphate atoms.

	Full charge	Rescaled charge	σ [nm]	ε [kJ/mol]
K	1.00	0.75	0.3340	0.1300
P_2	1.44	1.08	0.374 177	0.8368
O_2	−0.99	−0.7425	0.295 992	0.878 64
O_H	−0.84	−0.63	0.306 647	0.880 314
H	0.37	0.2775	0.0	0.0
H_W	0.4238	0.4238	0.0	0.0
O_W	−0.8476	−0.8476	0.316 557	0.650 629
H_{OH}	0.4238	0.317 85	0.0	0.0
O_{OH}	−1.4238	−1.067 85	0.316 557	0.650 629

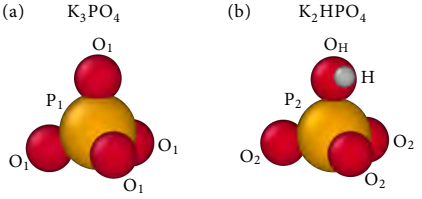

Fig. 8.14 Chemical structure of (a) K_3PO_4 and (b) K_2HPO_4 including labeling of atoms.

completeness. Please note the different labelling of the atoms compared to original papers. The short-range excluded volume interactions between ions are modeled with a 12–6 LJ potential of the form

$$V(r) = 4\varepsilon_{ij}\left[\left(\frac{\sigma_{ij}}{r}\right)^{12} - \left(\frac{\sigma_{ij}}{r}\right)^{6}\right], \tag{8.4}$$

where σ_{ij} is the interaction length and ε_{ij} the depth of the potential well for atom type i and j. The nonbonded parameters for K_3PO_4 and K_2HPO_4 used in this study are summarized in Table 8.2 for K_3PO_4 and in Table 8.3 for K_2HPO_4. Please refer to Fig. 8.14 for the labeling of the atoms. Table 8.2 and Table 8.3 also include the parameters for the SPC/E[418] potential of water and parameters for the hydroxide ion. The hydroxide ion is generated from the SPC/E water model. One hydrogen is removed and the excess negative charge is added to the oxygen atom.[501–503] The LJ parameters are the same as in the SPC/E water model.

The Lorentz–Berthelot mixing rule, $\sigma_{ij} = (\sigma_i + \sigma_j)/2$ and $\varepsilon_{ij} = \sqrt{\varepsilon_i \varepsilon_j}$, is used for all ion–ion and ion–water interactions. The geometric mixing rule, $\sigma_{ij} = \sqrt{\sigma_i \sigma_j}$ and $\varepsilon_{ij} = \sqrt{\varepsilon_i \varepsilon_j}$, is used and, for K^+–O_W interactions, ε is further scaled with a factor of 0.8,

Table 8.4
Bonded force field parameters for K_3PO_4 and K_2HPO_4. See Fig. 8.14 for labeling of the atoms.

Bonds			
i	j	k_r^{ij} [kJ/mol nm^2]	r_{ij}^0 [nm]
O_1	P_1	439 320.0	0.148
O_2	P_2	439 320.0	0.148
O_H	P_2	192 464.0	0.161
O_H	H	46 250.4	0.096

Angles				
i	j	k	k_θ^{ijk} [kJ/mol]	θ_{ijk}^0 [deg]
O_1	P_1	O_1	1171.52	119.9
O_2	P_2	O_2	1171.52	119.9
O_2	P_2	O_H	376.56	108.23
P_2	O_H	H	376.56	108.5

Dihedrals						
i	j	k	l	k_ϕ^{ijkl} [kJ/mol]	ϕ_0^{ijkl}	n
P_1	O_1	O_1	O_1	1.046	0	3
P_2	O_2	O_2	O_2	1.046	0	3
H	O_H	P_2	O_2	1.046	0	3

following the method of the work by Gee et al.[242] This results in $\sigma_{K^+,O_W} = 0.3252$ nm and $\varepsilon_{K^+,O_W} = 0.2327$ kJ/mol for the interaction between K^+ and oxygen water O_W in the full charge force field. This scaling causes an effectively weaker K^+–O_W LJ repulsion leading to a stronger K^+–O_W electrostatic interaction. In the ECC model, ε_{K^+,O_W} is not scaled with the above factor of 0.8.

Bonded force field parameters for the phosphate ions are summarized in Table 8.4. Atoms are labelled according to Fig. 8.14. The model potential used is defined by

$$U_{\text{bonded}} = \sum_{\text{bonds}} \frac{k_r^{ij}}{2}(r_{ij} - r_{ij}^0)^2 + \sum_{\text{angles}} \frac{k_\theta^{ijk}}{2}(\theta_{ijk} - \theta_{ijk}^0)^2 + \sum_{\text{dihedrals}} k_\phi^{ijkl}[1 + \cos(n\phi^{ijkl} - \phi_0^{ijkl})]. \tag{8.5}$$

The first part of Eq. (8.5) describes the bond stretching between atom i and j. k_r^{ij} is a force constant. The equilibrium distance is described by r_{ij}^0. The angular bending between three adjunct atoms i, j, and k is represented by a harmonic potential with force constant k_θ and equilibrium angle θ_{ijk}^0. The third part describes the cosine potential used for dihedrals between four joint atoms i, j, k, and l. k_ϕ^{ijkl}, ϕ_{ijkl}^0, and n represent the force constant, phase angle, and multiplicity, respectively.

8.5.2 Appendix B: Kirkwood–Buff relation for the total solute concentration dependence of ϕ

We consider a two-component system (solute–water) with total molar solute concentration ρ_s and molar water concentration ρ_w. The osmotic coefficient ϕ is a measure of the water activity a_w of the solution according to

$$\phi = -\frac{\rho_w}{\rho_s} \ln a_w \tag{8.6}$$

We use the Gibbs–Duhem relation

$$\rho_s \mathrm{d} \ln a_s + \rho_w \mathrm{d} \ln a_w = 0, \tag{8.7}$$

to relate ϕ to the solute activity a_s,

$$\mathrm{d} \ln a_s = \mathrm{d}\phi. \tag{8.8}$$

To examine the solute concentration dependence of ϕ, we write Eq. (8.8) as

$$\left(\frac{\partial \ln a_s}{\partial \ln \rho_s} \right)_{P,T} = \left(\frac{\partial \phi}{\partial \ln \rho_s} \right)_{P,T}. \tag{8.9}$$

Equation (8.9) can be related to KB integrals and excess coordination numbers of solution components using[192]

$$\left(\frac{\partial \ln a_s}{\partial \ln \rho_s} \right)_{P,T} = \frac{1}{1 + \rho_s (G_{ss} - G_{sw})} = \frac{1}{1 + \Delta N_{ss} - \Delta N_{ws}}. \tag{8.10}$$

The osmotic coefficient ϕ and osmotic pressure Π of the solution are related according to

$$\phi = \frac{\Pi}{\Pi_{id}} = 1 + \frac{\Delta \Pi}{\rho_s \mathrm{R} T}, \tag{8.11}$$

where $\Pi_{id} \equiv \rho_s RT$ is the solute translational entropy contribution to Π and $\Delta\Pi$ the contribution of solute–solute interactions. With

$$\Delta \Pi = (\phi - 1) \rho_s \mathrm{R} T, \tag{8.12}$$

we see that the derivative $(\partial[\rho_s(\phi - 1)]/\partial \rho_s)_{P,T}$ (cf. left-hand side of Eq. (8.2)) describes the contribution of solute–solute interactions in the solute concentration dependence of the osmotic pressure (water activity). Using Eqs. (8.9) and (8.10), this derivative can be written as

$$\left(\frac{\partial [\rho_s (\phi - 1)]}{\partial \rho_s} \right)_{P,T} = \frac{-(\Delta N_{ss} - \Delta N_{ws})}{1 + (\Delta N_{ss} - \Delta N_{ws})}. \tag{8.13}$$

Chapter 9

Conclusions and perspectives

This work contributes to the understanding of ion-specific effects, Hofmeister effects and the Hofmeister series. In particular, analyses of simulations and experiments have explored the role of cations and mixed electrolyte solutions. The work challenges the established simplified concept of separate anionic and cationic series. It employs PNIPAM as an example, a commonly used polymer for investigations of Hofmeister effects because of its coil-to-globule transition at its LCST. As in other studies of the last two decades, ion-specific effects were investigated through ion interactions with the polymer and its hydration shell. However, this work has widened the view by following recent ideas of mutual effects of all ions in the solution. It has identified the ion–counterion interactions to play key roles, both in the hydration shell of the polymer and in bulk solutions. The findings of this work go beyond pure electrolyte solutions and polymer solubilities. They are important for phenomena such as self-assembly, protein stability, micelle formation and other hydrophobic effects. This work may provide inspiration for the effects of osmolytes on polymer solubility,[380,395,396,516,517] solvation of amino acids,[483] on protein stability,[484] on hydrophobic association,[518] and the effect of alcohol,[472,473] and other cosolvents[468] on polymer solubility.

9.1 Summary

Contributions to the electrolyte solution and polymer solvation communities are shown in orange in Fig. 1.5 on Page 24. Together with a summary of the published studies (Chapters 4 to 8), these findings are summarized below.

Cationic effects on the phase transition temperature. Cationic effects have been investigated in combination with both a weakly hydrated anion (Chapter 4) and a strongly hydrated anion (Chapter 5), aiming to understand the effect of cations on the phase transition temperature of uncharged thermoresponsive polymers such as PNIPAM and, thereby, extending the scope of the Hofmeister series. More specifically, the role of cation–anion combinations was addressed.

Weakly hydrated anions (e.g., I^-) are known to give rise to a nonlinear phase transition temperature of PNIPAM with respect to salt concentration caused by a balance between polymer–ion interactions and an entropic solvent-excluded volume effect. That is, a slight salting-in (increase of LCST) behavior at low salt concentrations is followed by salting-out (decrease of LCST) at higher concentrations. This will be referred to as concave curvature in the following[3] and is depicted in Fig. 9.1 (orange data). Also, different weakly hydrated anions are known to give rise to different concave curvatures owing to their different degree of polymer affinity. This work shows that a weakly hydrated anion paired with different monovalent metal cations also yields different concave curvatures (Chapter 4). In contrast to anions where the solubility of PNIPAM in different salt solutions follows the expected behavior from a charge density and hydration free energy perspective of ions, an unexpected salting-out trend, $Cs^+ > Na^+ > Li^+$, is observed at higher salt concentrations. MD simulations with variations of system setups allowed for investigating the role of the cation through, for instance, preferential binding calculations. Using a "nonpolar" PNIPAM chain, i.e., a chain without atomic charges, it became evident that ion affinities at the polymer surface originate from electrostatic interactions between the polymer and ions. By modifying the amount of cation–anion pairs (one of many advantages of using computer simulations), an inverse correlation between ion pairing in the bulk and the polymer–ion affinities was found. This explains the different concave curvatures of the LCST as a function of salt concentration. That is, Cs^+ as a weakly hydrated cation interacts stronger with I^- ions forming more CIPs in the bulk solution compared to the strongly hydrated Li^+, leading to a stronger depletion from the polymer surface. A stronger depletion originates from the ion-pairing-induced neutralization of some pairs and, thereby, a loss in iodide's possibility to electrostatically interact with the amide NH group on the polymer. Instead, a mutual effect is observed for LiI since not only I^- ions, but also Li^+ ions show an affinity for the polymer surface due to absence of ion-pairs in the bulk solutions.

Strongly hydrated anions (e.g., Cl^-) are known to give rise to a linear salting-out behavior (decrease of the LCST of e.g., PNIPAM) with increasing salt concentration caused by an entropic solvent-excluded volume effect. This work shows that cations induce a slight concentration-dependent salting-in contribution of PNIPAM (Chapter 5). That is, as the concentration increases, the initially linear salting-out behavior is masked by an increasing salting-in contribution, which yields a nonlinear LCST. This will be referred to as a convex curvature in the following[4] and is depicted in Fig. 9.1 (blue data). The deviation from a linear salting-out trend is large for strongly hydrated cations (e.g., Ca^{2+} and Li^+) and small (almost negligible) for weakly hydrated cations

[3] A function is called concave (concave downwards or synonymously convex upwards) if the line segment between any two points on the graph of the function lies below or on the graph.

[4] A function is called convex (convex downwards or synonymously concave upwards) if the line segment between any two points on the graph of the function lies above or on the graph.

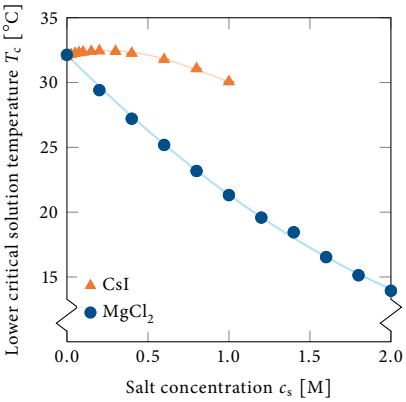

Fig. 9.1 Lower critical solution temperature T_c of PNIPAM in CsI (Chapter 4) and $MgCl_2$ (Chapter 5) solutions as a function of salt concentration c_s. The two systems demonstrate the concave (orange data) and convex (blue data) behavior.

(e.g., Na^+ and Cs^+). A linear air–water surface tension contribution with increasing salt concentration, which is typically correlated with the linear salting-out behavior for NaCl salt solutions, cannot solely explain the polymer collapse in salts containing strongly hydrated cations. This demonstrates that a polymer–water interface deviates from an air–water interface, which is frequently used as macroscopic proxy. For instance, it was investigated how ions and ion pairs spatially relate to the polymer compared to water molecules by means of MD simulations. In contrast to an air–water interface, where strongly hydrated cations are depleted due to large ion–water favorable interaction energy, strongly hydrated cations partition to the polymer surface. This is possible because these ions i) show enthalpically slightly favorable interactions with the amide oxygen, and ii) form SIPs with the otherwise depleted chloride ions. More precisely, the formation of SIPs leads to neutral or charge reduced assemblies and enables the local accumulation of cations near the amide oxygen without charge separation. Ion pairing is concentration-dependent and an increasing salt concentration increases the mitigation of the dominant salting-out effect, causing the convex LCST behavior of PNIPAM. At higher salt concentrations, the polymer–ion affinity and SIP formation (i.e., salting-in contribution) almost outweigh the surface tension contribution (i.e., salting-out contribution). In contrast to strongly hydrated cations, the mitigation of the the salting-out effect is considerably smaller for weakly hydrated cations due to smaller amide oxygen–cation affinity and less cation–anion SIP formation propensity.

The two studies and the corresponding identified molecular mechanisms answer ques-

tion 1 in Chapter 1 regarding the role of cations on the phase transition temperature for uncharged polymers. Interestingly, they demonstrate that cation effects for iodide salts give rise to different net concave curvatures for the phase transition behavior as a function of salt concentration, while for chloride salts they give rise to different net convex curvatures (Fig. 9.1). This mainly originates from the different ion affinities for the polymer–water interface. Iodide ion binding to polymers is orders of magnitude larger than chloride ion binding.[73,150] However, the surface tension contribution of the two ions remains similar.[442] For iodide salts, polymer–iodide interactions (described by a Langmuir binding isotherm) dominate at low salt concentration causing the salting-in behavior. First at higher salt concentrations, the solvent-excluded volume effect overcompensates and generates the concave curvature. For chloride salts, the solvent-excluded volume effect dominates owing to a lack of polymer–chloride interactions and an overall salting-out behavior is observed. At higher salt concentrations, ion pairing at the polymer surface together with the very weak cation binding (i.e., the binding is still on the linear portion of a Langmuir isotherm) generate the offset of the salting-out behavior and, hence, the convex curvature. However, the capability of a cation to turn a salting-out into a salting-in behavior or vice versa has not been observed, yet. Additionally, ion pairing contributes to either salting-out (depletion of ions from polymer surfaces) or salting-in (accumulation of ions at polymer surfaces) depending on the chemical context (i.e., anion and cation type). It should also be noted that the types of ion pairs are different (CIPs versus SIPs) depending on if the anion is weakly or strongly hydrated. Iodide ions are weakly hydrated and a free energy favorable partitioning to hydrophobic polymers occurs, even at low salt concentration. With increasing salt concentration, the likelihood for ion pairing increases. This leads to a competition between polymer–iodide interactions and iodide–cation interactions in the bulk. Ion pairing in the bulk dominates for cations that i) do not interact favorably with the polymer surface, and ii) easily form CIPs with the anion in the bulk solution. This occurs despite the fact that charge neutralization would otherwise support accumulation of ions at the polymer surface. Chloride ions are strongly hydrated and unfavorably partition to hydrophobic polymers. Charge neutralization (or reduction for divalent cations) via SIP formation between strongly hydrated cations and chloride ions aids to mitigate chloride ions' unfavorable partitioning. In addition, divalent cations interact weakly, but favorably with the polymer. This comparison between the two individual studies (metal iodide and metal chloride salt solutions) answers question 3 in Chapter 1, of whether the type of the anion has implications on the cationic effects and vice versa. Additionally, the type of the cation has a larger impact on the chloride salts than on the iodide salts. This can be seen in the larger difference in the LCSTs of PNIPAM in the presence of the chloride salts. However, the anion plays an even larger role since the LCST differences in dependence of the anion type are even more pronounced. This answers question 2 in Chapter 1 on how dominant the cation effects are.

Ion-specific effects in mixed electrolytes solutions. Mixed salt effects have been investigated concerning polymer collapse (Chapters 6 and 7), aiming to understand the effect of a second salt in an aqueous salt mixture on the phase transition temperature of uncharged thermoresponsive polymers such as PNIPAM and, thereby, extending the scope of the Hofmeister series to include mixed salts.

The presence of a fixed concentration of a strongly hydrated salt (i.e., Na_2SO_4) affects the aforementioned well-known phase transition temperature behavior of PNIPAM in weakly hydrated salt (i.e., NaI) solutions with salt concentration in a nonlinear manner (Chapter 6). Three regions can be identified for this salt mixture: a salting-out behavior at low concentrations (region I) followed by a salting-in behavior at intermediate concentrations (region II), and a salting-out behavior at high concentrations (region III). The underlying mechanism for this complex behavior caused by the presence of a second salt was explored by investigating ions' affinities for polymer surfaces, as well as their affinities for each other, and for water molecules in the bulk solutions. This was done on an atomistic level by means of MD simulations and it was found that a balance between the polymer–iodide affinity and ion hydration causes the nonlinear behavior. In region I, the presence of Na_2SO_4 does not affect the favorable polymer–iodide interactions. Instead, the remarkable collapse of the polymer originates from ion pairing and ion hydration in the bulk solution, and especially from iodide's flexible hydration shell. That is, some of the NaI introduced sodium ions preferentially partition to the counterion cloud around SO_4^{2-}. This leads to a lower excess counterion density around I^- and, hence, to a more hydrated I^- driving the polymer collapse. In region II, SO_4^{2-} as the strongly hydrated anion becomes saturated at further increased NaI concentration and, instead, affects the solubility of NaI. That is, SO_4^{2-} forces I^- out of the solution to the polymer–water interface (i.e., one salt salts out the other) leading to an iodide adsorption and, thereby, polymer swelling. In region III, further NaI concentration increase leads to ion depletion from the polymer chain and, hence, polymer collapse originating from the ion hydration contribution (i.e. solvent-excluded volume effect) that usually determines salting out behavior.

The above described nonlinear LCST behavior is unique for the combination of a fixed concentration of a strongly hydrated salt with an increasing concentration of a weakly hydrated salt. Exchanging Na_2SO_4 with NaCl yields a similar, yet weaker, nonlinear behavior. I^- becomes less hydrated originating from a weaker partitioning of added Na^+ ions to Cl^- caused by i) a less dense countercation cloud around the monovalent anion Cl^- and ii) a smaller chloride–sodium pairing affinity. Hence, a weaker salting-out behavior in region I is observed. Further, Cl^- is less strongly hydrated than SO_4^{2-} and cannot salt out iodide from the solution as efficiently in region II. Exchanging NaI with NaCl instead, yields a linear salting-out behavior with increasing salt concentration. This originates from a less flexible hydration shell of Cl^- compared to I^-. A smaller, almost negligible, partitioning of Na^+ ions from Cl^- to SO_4^{2-} due to sodium–chloride

interactions that are stronger than sodium-iodide interactions is observed. In addition, experiments measured phase transition temperatures of poly(*N*,*N*-dimethylacrylamide) and polyethylene glycol in mixed electrolyte solutions and demonstrated a similar, yet different in magnitude, nonlinear behavior as shown for PNIPAM. These studies indicate that mixed electrolyte solutions affect different types of uncharged hydrophobic polymers in similar ways. This answers question 9 in Chapter 1 on the generality of mixed salt effects.

Additive or nonadditive cosolute effects in aqueous solutions. This present study (Chapters 4 to 7) challenged the concept of additivity of specific cation and anion interactions. More specifically, it aimed at clarifying whether cation–anion combinations are additive or nonadditive, and whether ion-effects in mixed salt solutions are additive or nonadditive. Multiple examples, where additivity is not observed, i.e., where the behavior of an anion changes depending on the countercation (Chapters 4 and 5), or where the total effect of two salts is not the same as the sum of the two separate salts (Chapters 6 and 7), have been discussed.

The change in the weakly hydrated anions' affinity for PNIPAM from higher to lower when the countercation is changed from lithium to cesium is one example (Chapter 4). This nonadditivity influences the polymer solubility and goes against a single ion model. Ion-specific effects of chloride ions also depend on the cation it is paired with (Chapter 5). Typically chloride behaves strongly hydrated, i.e., it is typically depleted from polymer–water interfaces, when paired with Na^+, for instance. When paired with strongly hydrated cations (e.g., Ca^{2+} or Li^+), it locally accumulates at the amide moiety of the polymer, which affects polymer solubility in a nonadditive way. These two examples suggest that the assumption of additive ion effects must be questioned, above all regarding their influence on polymer solubility. The examples using iodide and chloride paired with different cations answer question 4 in Chapter 1 whether cation–anion combinations are additive or nonadditive.

Ion effects observed in pure mixed salt solutions of NaI with a fixed concentration of Na_2SO_4 are nonadditive due to iodide's bifurcated behavior (Chapters 6 and 7). The other two examined mixed salt solutions (NaI with a fixed concentration of NaCl, and NaCl with a fixed concentration of Na_2SO_4) demonstrate that the specific salt combination is decisive for additive or nonadditive effects. I^- has a weaker bifurcated behavior when combined with NaCl than with Na_2SO_4, while Cl^- does not show any bifurcated behavior when combined with Na_2SO_4. This answers question 5 in Chapter 1 whether ion effects in aqueous mixed electrolyte solutions are additive or nonadditive. Further, the nonadditive ion effects in mixed electrolyte solutions containing NaI and Na_2SO_4 influences the phase transition temperature of PNIPAM in salt concentration regions I and II in a nonadditive way (see above for a molecular description of the mechanism). NaI mixed with a fixed concentration of NaCl also influences the phase

transition of PNIPAM nonadditively, yet weaker. NaCl with a fixed concentration of Na_2SO_4, instead, results in additive effects. This answers question 7 in Chapter 1 whether ion effects in mixed electrolyte solutions lead to additivity or nonadditivity of polymer solubility.

Given "bulk solution" phenomena (i.e., ion pairing and ion hydration in bulk solutions caused by flexible hydration shells of ions) drive the complex nonadditive LCST behavior of PNIPAM in mixed salt solutions, a crucial question arises whether other mixtures (e.g., mixed osmolyte solutions) show similar effects. To investigate this, affinities between solution components were correlated to solvent-excluded volume effects through their KBIs (Chapter 7). A mixture of a strongly hydrated (i.e., TMAO) and a weakly hydrated (i.e., urea) cosolute leads to nonadditive solvation phenomena, i.e., to a counteraction of denaturant-induced protein unfolding. The nonadditive cosolute effects on protein stability in mixed cosolute environments have the same physical origin as thermoresponsive polymers' water solubility. That is, solvent-excluded volume effects driven by mutually increased water affinities in bulk for both cosolutes drive the shift of the equilibrium. The hydration of the cosolutes is affected most when one cosolute classified as strongly hydrated (i.e., Na_2SO_4 or TMAO) is combined with one classified as weakly hydrated (i.e., NaI or urea). This suggests that mixed electrolyte solutions and mixed osmolyte solutions share a common feature regarding polymer solubility and protein stability, which was asked in question 8 in Chapter 1.

Force fields for electrolyte solutions. The present work re-optimized nonpolarizable ionic force fields applying ionic charge rescaling through ECC (Chapter 8) and by adjusting the nonbonded cation–anion interactions (Chapters 4 and 6), aiming to provide force fields accurately describing short-range ion–ion interactions. The osmotic coefficient, which relates to these interactions through the pair correlation function and effective pair force, was used for validation. The two approaches applied on different salt solutions answer question 13 in Chapter 1 how polarizable effects can be accounted for in nonpolarizable force fields.

ECC was applied to aqueous solutions containing K_3PO_4, K_2HPO_4 or both salts (Chapter 8). The ionic charge reduction with a factor of 0.75 lead to a decrease of ion pairing, decisive for a correct osmotic coefficient. Moreover, this study extended the application of ECC to trivalent ions.

Nonbonded LJ size parameters between cations and anions were scaled for LiI solutions (Chapter 4) as well as for Na_2SO_4 solutions (Chapter 6). A small reduction of the cation–anion interactions was necessary for the specific choice of force fields for lithium and iodide ions owing to slightly too weak nonbonded interactions. Osmotic coefficients agreeing with experimentally observed values were obtained with a scaling factor of 0.93. For Na_2SO_4, a scaling factor of 1.7 was used between Na^+ ions and both the

sulfur and the oxygen atoms of the sulfate ion to achieve an osmotic coefficient in agreement with the experimentally measured one. This comparatively large scaling was necessary to avoid unnatural ion pairing and ion clustering. A scaling of the cation–anion dispersion interaction strength (i.e., the other nonbonded force field parameter) within a reasonable range was first examined for both salt solutions but showed no considerable improvement of the osmotic coefficient.

9.2 Outlook

Although the present work sheds light on certain unexplored effects and phenomena in the Hofmeister series, many more complex interactions remain to be investigated.

Unanswered questions. For a complete understanding of the whole Hofmeister series regarding the phase transition behavior of PNIPAM in metal iodide solutions, alkaline metal ions and not only alkali metal ions, need to be investigated. Because these ions are divalent, they could affect the underlying mechanisms for polymer collapse differently. In addition, the polymer–ion interactions competing with ion pairing in the bulk observed in these metal iodide solutions may be sensitive to the polymer type. More polymers need to be examined, for a general interpretation of the role of cations and in order to answer question 9 in Chapter 1 on the generality of cation effects. Regarding the mechanism for the cationic Hofmeister series explained in Chapter 5, it is expected to apply for other anions similar to chloride. The underlying mechanism is completely different for weakly hydrated anions as explained in Chapter 4. Other anions that are more strongly hydrated than chloride, and, hence, show an even steeper decrease of the LCST with salt concentration, such as sulfate, may also show a slightly different behavior. Ion pairing, decisive for the underlying mechanism, is weaker for sulfate anions than for chloride anions. However, the role of cations on the LCST of polymers in salt solutions containing anions belonging to the very far left end of the anionic Hofmeister series (e.g., SO_4^{2-}) needs to be investigated. Further, the present study of mixed electrolyte solutions on phase transition temperatures of PNIPAM does not include all combinations of mixtures. So far, only three combinations of anions have been investigated. Combinations, such as a fixed concentration of a center anion of the anionic Hofmeister series (Fig. 1.1) with an anion found on the left, a fixed concentration of an anion found on the right with a center or left anion, and combinations of anions of the same category, remain to be explored. Additionally, the bifurcated behavior caused by flexible hydration shells of iodide ions is expected to apply to other weakly hydrated anions, too, but needs to be proven (especially for molecular ions). Moreover, nonadditive effects observed in this work have not considered the role of the cation, which remains to be investigated. First, nonadditive effects in mixed electrolyte solutions

presumably depend on the specific identity of the countercation. Second, the observed Hofmeister chemistry for mixed electrolyte solutions in this study may also be valid for a weakly hydrated and a strongly hydrated mixed cation system.

Perspectives. Exploring the additional systems proposed above (see "Unanswered questions") will contribute to the clarification of some of the remaining questions illustrated in Fig. 1.5 on Page 24 (yellow boxes). Further questions that were raised in Chapter 1 but are outside the scope of this work are also illustrated with yellow boxes in Fig. 1.5. Nonadditive ion effects observed in this work explaining the polymer solubility in mixed electrolyte solutions at low salt concentrations are expected to play an important role for pure mixed electrolyte solutions in general. The reason is that the effects are caused by mutually enhanced cosolute hydration in bulk solutions, and, hence, are independent of the presence of the polymer. To explore whether this assumption holds, bulk solution measurements should be re-investigated with mixed electrolyte solutions in order to explore the impact on thermodynamic properties (e.g., activity coefficients). This could answer question 6 in Chapter 1 concerning nonadditivity of bulk thermodynamic properties. To further explore question 9 in Chapter 1 on the generality of cationic and mixed salt effects other than pure electrolyte solutions and polymer solutions can be investigated. For instance, aggregation of hydrophobic particles can answer whether specific interactions with amide moieties are actually always necessary. Biological systems may contain mixtures of polymers. These systems have not been a part of this study, and, thus, question 10 in Chapter 1 cannot be answered, yet. Turbidity measurements of copolymers and mixtures of polymers in different (mixed) electrolyte solutions, where both the anion and cation are varied, can probe whether effects are additive or nonadditive. Underlying mechanisms can be clarified afterwards using MD simulations and molecular spectroscopic measurements. In this work, ion effects have been addressed by investigations of affinities (ion and water), accumulation or exclusion of ions from polymer surfaces and ion–counterion pairing. Beyond this, dynamic properties remain unexplored. Quantities such as self-diffusion and ionic conductivity can be calculated to explore if dynamic properties of ions follow the Hofmeister ordering. This could answer question 11 in Chapter 1 whether ion-specific trends are observed for dynamic properties. In addition, all present studies examined bulk solutions with and without polymers. No simulations of confinements have been performed in order to address question 12 in Chapter 1, whether effects observed in this work are the same when the solutions are confined. To investigate this, carbon nanotubes or silica nanopores can be used to study ion behavior in confinement. Next, polymer-grafted pores need to be examined to observe the influence of confinement on ion-induced polymer solubility. An understanding of the effect of the confinement on both polymer solubility and on ion transport is necessary for the utilization of grafted polymer chains on pore walls in sensors, one of the applications that serves as motivation for the present work (Chapter 1).

The Hofmeister community has only started to investigate topics like cationic Hofmeister effects, concurrent anion and cation effects, and reverse Hofmeister effects. This work has added insights to these fields (e.g., a molecular level understanding of the cationic Hofmeister series with uncharged polymers or an updated Hofmeister series considering the bifurcated behavior of ions), but many further studies will be vital for further advancements. The combination of computer simulations with experiments and theory will facilitate substantial progress on ion-specific effects in aqueous bulk solutions and at surfaces, where polymer solubility is just one example. For a complete picture of the Hofmeister ion chemistry, a thorough understanding of all interactions between components in solutions (solutes, cosolutes, and solvent molecules) is necessary. This work has focused on ion pairing and ion hydration. However, the priority of Hofmeister studies has been shifted to these properties only recently, and there still is much to learn about them. The role of the water needs to be revisited, and especially the hydration shells of salt ions need to be studied. From an energetic perspective, it is particularly interesting whether it is possible for ions to push away their hydration shell water molecules and instead interact noncovalently with other ions, counterions and macromolecules. The herein observed flexible hydration shells of weakly hydrated anions in specific mixed electrolyte solutions are one example in this direction.

Computer simulations will play a crucial role for investigations on ion paring and ion hydration. The deciding factor is the force field. Concerning mixed electrolyte solutions, experimentally obtained thermodynamic data is scarce, but would facilitate the development of force fields. Also, the use of KBIs for force field developments is expected to have a considerable impact. Another useful development for molecular simulations would be ECC force fields, not only for a wide range of salt ions, but also for macromolecules. This would enable the use of these types of force fields, which indirectly account for polarization effects, in polymer collapse studies. In addition, for studies of ion-induced polymer collapse, and to use more advanced computer simulation methods, coarse grained models are desired. This can be achieved using a coarse grained polymer, implicit water and explicit ions. For validation, the dielectric permittivity could be used, for instance. Such a model must capture ion-specific effects (e.g., additive or nonadditive effects). Computer simulations can also be utilized to investigate properties not accessible by means of experimental measurements. One issue in need of attention is the analogy between air–water and macromolecule–water interfaces when explaining polymer collapse in electrolyte solutions. To explore (and validate) this, the work of cavity formation can be calculated by means of MD simulations. If there is a correlation between solvent-excluded volume effects and the air–water surface tension gradient, the work of cavity formation should scale with the surface tension. This should be examined for both pure electrolyte solutions and mixed electrolyte solutions to provide better understanding of nonadditive effects in mixtures. It can also be done with monomers, dimers, and oligomers in order to investigate size effects. Further, good theoretical

models are desired to enable predictions and not only interpretations of data. Models, such as the thermodynamic model for macromolecule conformational transition by Heyda and Dzubiella,[18] must serve for various cations and mixed electrolyte solutions, and not only different anions.

Powerful experimental tools for the Hofmeister community are molecular spectroscopic techniques, such as VSFS, dielectric spectroscopy, femtosecond IR spectroscopy, terahertz dielectric relaxation spectroscopy (DRS), Raman multivariate curve resolution, and femtosecond second elastic harmonic scattering. Surface-specific techniques, such as VSFS, will continue to play an important role when investigating ion interactions with macromolecules, since these interactions take place at the air–macromolecule–water interface. Improved, and especially more sensitive spectroscopy techniques will make it easier to study weak cation effects and the relative order between cationic Hofmeister effects. Cation effects are still important for macromolecule–salt solution stability, even if the variation between different cations is significantly smaller than for anions. DRS is capable of providing a microscopic picture of ion pairing in electrolyte solutions. Ion pairs (i.e., charged separated cations and anions) can be investigated, since the technique measures the movement of dipoles. Both CIPs and SIPs have been suggested to be detectable with DRS.[455,519] That is, the technique can be used to confirm the cation partitioning between weakly and strongly hydrated anions in salt mixtures. Spectra can be obtained experimentally, but also be generated from computer simulations. Seeking answers about ion-specific effects inspires the development of new techniques and motivates new applications for existing techniques. For instance, the femtosecond elastic second harmonic scattering technique used for probing changes in hydrogen bonding network of pure electrolyte solutions could be used for polymer solutions, as well. This allows for both revisiting the role of water and approaching the questions on Hofmeister effects from an opposite perspective. That is, to investigate the impact of the presence of the polymer on the ion–water structuring instead of the effect of ions on the polymer solubility that is usually investigated with thermodynamic or surface-specific measurements. Further, bulk properties should be revisited to measure, e.g., viscosities and hydration free energies for mixed electrolyte solutions. This would enable a link between these macroscopic properties, and molecular and nanoscopic quantities from, e,g., femtosecond second elastic harmonic scattering measurements in terms of orientational ordering of water.

This work has directly or indirectly raised the following questions, in addition to the unanswered questions from Chapter 1, that may partly be answered with the studies suggested above.

1. How does the type of cation affect ion pairing in mixed electrolyte solutions?

2. Does the presence of macromolecules affect ion–ion, ion–water, and water–water correlations?
3. What is the molecular origin behind flexible hydration shells (i.e, ions pushing away/receiving water molecules from/to their hydration shells)?
4. Which role do cations play for reverse Hofmeister effects?
5. How do ion effects look like at (usually unexplored) higher salt concentrations?
6. Are ion effects in mixed electrolyte solutions additive or nonadditive for charged macromolecules?
7. How do cation effects and mixed salt effects look for superchaotropic ions (e.g., $B_{12}I_{12}^{2-}$) and hydrophobic ions (e.g., BPh_4^-)?
8. Is there a correlation between work of cavity formation and surface tension?
9. Can models such as the conformational transition model by Heyda and Dzubiella[18] capture cation effects and mixed salt effects, too?
10. Is a coarse-grained general model capable of capturing all necessary phenomena for studying Hofmeister effects?

Despite intense research activities regarding ion-specific effects on macromolecules, lately, and a considerable gain of knowledge in the last 130 years, critical information on the simple system of aqueous salt solutions is still missing. Maybe it will even require a new "Hofmeister renaissance" before all issues regarding interactions between the three components of the solution, solvent, solutes and cosolutes, are clarified. The very last question is whether a unified Hofmeister theory can be anticipated. An absolute answer cannot be given, yet, but the complexity and the interplay between different mechanisms observed in this work indicates that it is unlikely. Hence, a general combined cationic and anionic Hofmeister series, and a series for mixed electrolyte solutions should probably not be the goals. Instead, the rich variety in chemistry should be appreciated and utilized in the myriad of different sciences where salt solutions are involved.

References

[1] F. Hofmeister. Zur Lehre von der Wirkung der Salze. *Naunyn-Schmiedeberg's Arch. Pharmacol.*, 24(4-5):247–260, 1888.

[2] F. Hofmeister. Zur Lehre von der Wirkung der Salze. *Naunyn-Schmiedeberg's Arch. Pharmacol.*, 25(1):1–30, 1888.

[3] W. Kunz, J. Henle, and B. W. Ninham. 'Zur Lehre von der Wirkung der Salze' (About the science of the effect of salts): Franz Hofmeister's historical papers. *Curr. Opin. Colloid Interface Sci.*, 9(1-2):19–37, 2004.

[4] Y. Zhang, S. Furyk, D. E. Bergbreiter, and P. S. Cremer. Specific ion effects on the water solubility of macromolecules: PNIPAM and the Hofmeister series. *J. Am. Chem. Soc.*, 127 (41):14505–14510, 2005.

[5] P. Jungwirth and D. J. Tobias. Molecular structure of salt solutions: A new view of the interface with implications for heterogeneous atmospheric chemistry. *J. Phys. Chem. B*, 105 (43):10468–10472, 2001.

[6] Y. Cho, Y. Zhang, T. Christensen, L. B. Sagle, A. Chilkoti, and P. S. Cremer. Effects of Hofmeister anions on the phase transition temperature of elastin-like polypeptides. *J. Phys. Chem. B*, 112(44):13765–13771, 2008.

[7] K. B. Rembert, H. I. Okur, C. Hilty, and P. S. Cremer. An NH moiety is not required for anion binding to amides in aqueous solution. *Langmuir*, 31(11):3459–3464, 2015.

[8] J. Traube. The attraction pressure. *J. Phys. Chem.*, 14(5):452–470, 1910.

[9] Y. Zhang and P. S. Cremer. Interactions between macromolecules and ions: The Hofmeister series. *Curr. Opin. Chem. Biol.*, 10(6):658–663, 2006.

[10] V. Mazzini and V. S. J. Craig. What is the fundamental ion-specific series for anions and cations? Ion specificity in standard partial molar volumes of electrolytes and electrostriction in water and non-aqueous solvents. *Chem. Sci.*, 8(10):7052–7065, 2017.

[11] Y. Zhang, S. Furyk, L. B. Sagle, Y. Cho, D. E. Bergbreiter, and P. S. Cremer. Effects of Hofmeister anions on the LCST of PNIPAM as a function of molecular weight. *J. Phys. Chem. C*, 111(25):8916–8924, 2007.

[12] X. Chen, T. Yang, S. Kataoka, and P. S. Cremer. Specific ion effects on interfacial water structure near macromolecules. *J. Am. Chem. Soc.*, 129(40):12272–12279, 2007.

[13] Y. Zhang and P. S. Cremer. Chemistry of Hofmeister anions and osmolytes. *Annu. Rev. Phys. Chem.*, 61:63–83, 2010.

[14] M. C. Gurau, S.-M. Lim, E. T. Castellana, F. Albertorio, S. Kataoka, and P. S. Cremer. On the mechanism of the Hofmeister effect. *J. Am. Chem. Soc.*, 126(34):10522–10523, 2004.

[15] E. A. Algaer and N. F. A. van der Vegt. Hofmeister ion interactions with model amide compounds. *J. Phys. Chem. B*, 115(46):13781–13787, 2011.

[16] L. Patra, A. Vidyasagar, and R. Toomey. The effect of the Hofmeister series on the deswelling isotherms of poly(N-isopropylacrylamide) and poly(N,N-diethylacrylamide). *Soft Matter*, 7 (13):6061–6067, 2011.

[17] P. Jungwirth and P. S. Cremer. Beyond Hofmeister. *Nat. Chem.*, 6:261–263, 2014.

[18] J. Heyda and J. Dzubiella. Thermodynamic description of Hofmeister effects on the LCST of thermosensitive polymers. *J. Phys. Chem. B*, 118(37):10979–10988, 2014.

[19] J. Heyda, H. I. Okur, J. Hladílková, K. B. Rembert, W. Hunn, T. Yang, J. Dzubiella, P. Jungwirth, and P. S. Cremer. Guanidinium can both cause and prevent the hydrophobic collapse of biomacromolecules. *J. Am. Chem. Soc.*, 139(2):863–870, 2017.

[20] N. E. Ernst and B. C. Gibb. Water runs deep. In Stefan Kubik, editor, *Supramol. Chem. Water*, pages 1–33. Wiley-VCH Verlag GmbH & Co. KGaA, Weinheim, 2019.

[21] B. C. Gibb. Hofmeister's curse. *Nat. Chem.*, 11:963–965, 2019.

[22] E. A. Guggenheim. The specific thermodynamic properties of aqueous solutions of strong electrolytes. *London Edinb. Dubl. Philos. Mag.*, 19(127):588–643, 1935.

[23] E. A. Guggenheim and J. C. Turgeon. Specific interaction of ions. *Trans. Faraday Soc.*, 51: 747–761, 1955.

[24] K. D. Collins and M. W. Washabaugh. The Hofmeister effect and the behaviour of water at interfaces. *Q. Rev. Biophys.*, 18(4):323–422, 1985.

[25] L. M. Pegram and M. T. Record Jr. Hofmeister salt effects on surface tension arise from partitioning of anions and cations between bulk water and the air–water interface. *J. Phys. Chem. B*, 111(19):5411–5417, 2007.

[26] L. M. Pegram and M. T. Record Jr. Thermodynamic origin of Hofmeister ion effects. *J. Phys. Chem. B*, 112(31):9428–9436, 2008.

[27] H. Mao, C. Li, Y. Zhang, S. Furyk, P. S. Cremer, and D. E. Bergbreiter. High-throughput studies of the effects of polymer structure and solution components on the phase separation of thermoresponsive polymers. *Macromolecules*, 37(3):1031–1036, 2004.

[28] P. H. von Hippel and K. Y. Wong. Neutral salts: The generality of their effects on the stability of macromolecular conformations. *Science*, 145(3632):577–580, 1964.

[29] R. L. Baldwin. How Hofmeister ion interactions affect protein stability. *Biophys. J.*, 71(4): 2056–2063, 1996.

[30] C. Ebel, P. Faou, B. Kernel, and G. Zaccai. Relative role of anions and cations in the stabilization of halophilic malate dehydrogenase. *Biochemistry*, 38(28):9039–9047, 1999.

[31] J. M. Broering and A. S. Bommarius. Evaluation of Hofmeister effects on the kinetic stability of proteins. *J. Phys. Chem. B*, 109(43):20612–20619, 2005.

[32] R. Perez-Jimenez, R. Godoy-Ruiz, B. Ibarra-Molero, and J. M. Sanchez-Ruiz. The efficiency of different salts to screen charge interactions in proteins: A Hofmeister effect? *Biophys. J.*, 86(4):2414–2429, 2004.

[33] R. A. Curtis and L. Lue. A molecular approach to bioseparations: Protein–protein and protein–salt interactions. *Chem. Eng. Sci.*, 61(3):907–923, 2006.

[34] M. G. Cacace, E. M. Landau, and J. J. Ramsden. The Hofmeister series: Salt and solvent effects on interfacial phenomena. *Q. Rev. Biophys.*, 30(3):241–277, 1997.

[35] K. D. Collins. Ion hydration: Implications for cellular function, polyelectrolytes, and protein crystallization. *Biophys. Chem.*, 119(3):271–281, 2006.

[36] D. F. Evans, D. J. Mitchell, and B. W. Ninham. Ion binding and dressed micelles. *J. Phys. Chem.*, 88(25):6344–6348, 1984.

[37] M. Boström, D. R. M. Williams, and B. W. Ninham. Ion specificity of micelles explained by ionic dispersion forces. *Langmuir*, 18(16):6010–6014, 2002.

[38] L. Abezgauz, K. Kuperkar, P. A. Hassan, O. Ramon, P. Bahadur, and D. Danino. Effect of Hofmeister anions on micellization and micellar growth of the surfactant cetylpyridinium chloride. *J. Colloid Interface Sci.*, 342(1):83–92, 2010.

[39] I. B. Ivanov, R. I. Slavchov, E. S. Basheva, D. Sidzhakova, and S. I. Karakashev. Hofmeister effect on micellization, thin films and emulsion stability. *Adv. Colloid Interface Sci.*, 168(1-2): 93–104, 2011.

[40] A. P. dos Santos and Y. Levin. Ion specificity and the theory of stability of colloidal suspensions. *Phys. Rev. Lett.*, 106(16):167801, 2011.

[41] N. L. Jarvis and M. A. Scheiman. Surface potentials of aqueous electrolyte solutions. *J. Phys. Chem.*, 72(1):74–78, 1968.

[42] P. B. Petersen and R. J. Saykally. On the nature of ions at the liquid water surface. *Annu. Rev. Phys. Chem.*, 57:333–364, 2006.

[43] N. Schwierz, D. Horinek, and R. R. Netz. Anionic and cationic Hofmeister effects on hydrophobic and hydrophilic surfaces. *Langmuir*, 29(8):2602–2614, 2013.

[44] R. Zangi, M. Hagen, and B. J. Berne. Effect of ions on the Hydrophobic interaction between two plates. *J. Am. Chem. Soc.*, 129(15):4678–4686, 2007.

[45] M. C. Pinna, P. Bauduin, D. Touraud, M. Monduzzi, B. W. Ninham, and W. Kunz. Hofmeister effects in biology: Effect of choline addition on the salt-induced super activity of horseradish peroxidase and its implication for salt resistance of plants. *J. Phys. Chem. B*, 109(34):16511–16514, 2005.

[46] M. C. Pinna, A. Salis, M. Monduzzi, and B. W. Ninham. Hofmeister series: The hydrolytic activity of aspergillus niger lipase depends on specific anion effects. *J. Phys. Chem. B*, 109 (12):5406–5408, 2005.

[47] P. Bauduin, F. Nohmie, D. Touraud, R. Neueder, W. Kunz, and B. W. Ninham. Hofmeister specific-ion effects on enzyme activity and buffer pH: Horseradish peroxidase in citrate buffer. *J. Mol. Liq.*, 123(1):14–19, 2006.

[48] L. Vrbka, P. Jungwirth, P. Bauduin, D. Touraud, and W. Kunz. Specific ion effects at protein surfaces: A molecular dynamics study of bovine pancreatic trypsin inhibitor and horseradish peroxidase in selected salt solutions. *J. Phys. Chem. B*, 110(13):7036–7043, 2006.

[49] A. Salis, D. Bilaničová, B. W. Ninham, and M. Monduzzi. Hofmeister effects in enzymatic activity: Weak and strong electrolyte influences on the activity of candida rugosa lipase. *J. Phys. Chem. B*, 111(5):1149–1156, 2007.

[50] H. I. Petrache, T. Zemb, L. Belloni, and V. A. Parsegian. Salt screening and specific ion adsorption determine neutral-lipid membrane interactions. *Proc. Natl. Acad. Sci. U. S. A.*, 103(21):7982–7987, 2006.

[51] V. S. J. Craig. Bubble coalescence and specific-ion effects. *Curr. Opin. Colloid Interface Sci.*, 9(1-2):178–184, 2004.

[52] C. L. Henry, C. N. Dalton, L. Scruton, and V. S. J. Craig. Ion-specific coalescence of bubbles in mixed electrolyte solutions. *J. Phys. Chem. C*, 111(2):1015–1023, 2007.

[53] C. L. Henry and V. S. J. Craig. The link between ion specific bubble coalescence and Hofmeister effects is the partitioning of ions within the interface. *Langmuir*, 26(9):6478–6483, 2010.

[54] R. M. Leberman and A. M. Soper. Effect of high salt concentrations on water structure. *Nature*, 378:364–366, 1995.

[55] P. Lo Nostro, A. Lo Nostro, B. W. Ninham, G. Pesavento, L. Fratoni, and P. Baglioni. Hofmeister specific ion effects in two biological systems. *Curr. Opin. Colloid Interface Sci.*, 9(1-2): 97–101, 2004.

[56] P. Lo Nostro, B. W. Ninham, A. Lo Nostro, G. Pesavento, L. Fratoni, and P. Baglioni. Specific ion effects on the growth rates of staphylococcus aureus and pseudomonas aeruginosa. *Phys. Biol.*, 2(1):1–7, 2005.

[57] P. Lo Nostro and B. W. Ninham. Hofmeister phenomena: An update on ion specificity in biology. *Chem. Rev.*, 112(4):2286–2322, 2012.

[58] G. Jones and M. Dole. The viscosity of aqueous solutions of strong electrolytes with special reference to barium chloride. *J. Am. Chem. Soc.*, 51(10):2950–2964, 1929.

[59] W. M. Cox and J. H. Wolfenden. The viscosity of strong electrolytes measured by a differential method. *Proc. R. Soc. A Math. Phys. Eng. Sci.*, 145(855):475–488, 1934.

[60] R. W. Gurney. *Ionic processes in solution*. McGraw-Hill, New York, 1953.

[61] H. S. Frank and M. W. Evans. Free volume and entropy in condensed systems III. Entropy in binary liquid mixtures; partial molal entropy in dilute solutions; structure and thermodynamics in aqueous electrolytes. *J. Chem. Phys.*, 13(11):507–532, 1945.

[62] K. Hamaguchi and E. P. Geiduschek. The Effect of Electrolytes on the Stability of the Deoxyribonucleate Helix. *J. Am. Chem. Soc.*, 84(8):1329–1338, 1962.

[63] P. Ball and J. E. Hallsworth. Water structure and chaotropicity: Their uses, abuses and biological implications. *Phys. Chem. Chem. Phys.*, 17(13):8297–8305, 2015.

[64] B. Hribar, N. T. Southall, V. Vlachy, and K. A. Dill. How ions affect the structure of water. *J. Am. Chem. Soc.*, 124(41):12302–12311, 2002.

[65] A. S. Thomas and A. H. Elcock. Molecular dynamics simulations of hydrophobic associations in aqueous salt solutions indicate a connection between water hydrogen bonding and the Hofmeister effect. *J. Am. Chem. Soc.*, 129(48):14887–14898, 2007.

[66] Y. Marcus. Effect of ions on the structure of water: Structure making and breaking. *Chem. Rev.*, 109(3):1346–1370, 2009.

[67] J. Bello and H. R. Bello. Interaction of model peptides with water and lithium bromide. *Nature*, 190:440–441, 1961.

[68] J. Bello and H. R. Bello. Evidence from model peptides relating to the denaturation of proteins by lithium salts. *Nature*, 194:681–682, 1962.

[69] D. R. Robinson and W. P. Jencks. The effect of concentrated salt solutions on the activity coefficient of acetyltetraglycine ethyl ester. *J. Am. Chem. Soc.*, 87(11):2470–2479, 1965.

[70] P. K. Nandi and D. R. Robinson. The effects of salts on the free energy of the peptide group. *J. Am. Chem. Soc.*, 94(4):1299–1308, 1972.

[71] P. K. Nandi and D. R. Robinson. The effects of salts on the free energies of nonpolar groups in model peptides. *J. Am. Chem. Soc.*, 94(4):1308–1315, 1972.

[72] T. Arakawa and S. N. Timasheff. Preferential interactions of proteins with salts in concentrated solutions. *Biochemistry*, 21(25):6545–6552, 1982.

[73] P. H. von Hippel, V. Peticolas, L. Schack, and L. Karlson. Model studies on the effects of neutral salts on the conformational stability of biological macromolecules. I. Ion binding to polyacrylamide and polystyrene columns. *Biochemistry*, 12(7):1256–1264, 1973.

[74] W. Kunz, P. Lo Nostro, and B. W. Ninham. The present state of affairs with Hofmeister effects. *Curr. Opin. Colloid Interface Sci.*, 9(1-2):1–18, 2004.

[75] L. Vrbka, J. Vondrášek, B. Jagoda-Cwiklik, R. Vácha, and P. Jungwirth. Quantification and rationalization of the higher affinity of sodium over potassium to protein surfaces. *Proc. Natl. Acad. Sci. U. S. A.*, 103(42):15440–15444, 2006.

[76] J. S. Uejio, C. P. Schwartz, A. M. Duffin, W. S. Drisdell, R. C. Cohen, and R. J. Saykally. Characterization of selective binding of alkali cations with carboxylate by X-ray absorption spectroscopy of liquid microjets. *Proc. Natl. Acad. Sci. U. S. A.*, 105(19):6809–6812, 2008.

[77] E. F. Aziz, N. Ottosson, S. Eisebitt, W. Eberhardt, B. Jagoda-Cwiklik, R. Vácha, P. Jungwirth, and B. Winter. Cation-specific interactions with carboxylate in amino acid and acetate aqueous solutions: X-ray absorption and ab initia calculations. *J. Phys. Chem. B*, 112(40): 12567–12570, 2008.

[78] B. Hess and N. F. A. van der Vegt. Cation specific binding with protein surface charges. *Proc. Natl. Acad. Sci. U. S. A.*, 106(32):13296–13300, 2009.

[79] J. Heyda, T. Hrobárik, and P. Jungwirth. Ion-specific interactions between halides and basic amino acids in water. *J. Phys. Chem. A*, 113(10):1969–1975, 2009.

[80] I. Kalcher, D. Horinek, R. R. Netz, and J. Dzubiella. Ion specific correlations in bulk and at biointerfaces. *J. Phys. Condens. Matter*, 21(42):424108, 2009.

[81] J. Heyda, J. C. Vincent, D. J. Tobias, J. Dzubiella, and P. Jungwirth. Ion specificity at the peptide bond: Molecular dynamics simulations of N-methylacetamide in aqueous salt solutions. *J. Phys. Chem. B*, 114(2):1213–1220, 2010.

[82] K. B. Rembert, J. Paterová, J. Heyda, C. Hilty, P. Jungwirth, and P. S. Cremer. Molecular mechanisms of ion-specific effects on proteins. *J. Am. Chem. Soc.*, 134(24):10039–10046, 2012.

[83] E. Thormann. On understanding of the Hofmeister effect: How addition of salt alters the stability of temperature responsive polymers in aqueous solutions. *RSC Adv.*, 2(22): 8297–8305, 2012.

[84] H. I. Okur, J. Kherb, and P. S. Cremer. Cations bind only weakly to amides in aqueous solutions. *J. Am. Chem. Soc.*, 135(13):5062–5067, 2013.

[85] E. K. Wilson. A renaissance for Hofmeister. *Chem. Eng. News*, 85(48):47–49, 2007.

[86] A. W. Omta, M. F. Kropman, S. Woutersen, and H. J. Bakker. Negligible effect of ions on the hydrogen-bond structure in liquid water. *Science*, 301(5631):347–349, 2003.

[87] A. W. Omta, M. F. Kropman, S. Woutersen, and H. J. Bakker. Influence of ions on the hydrogen-bond structure in liquid water. *J. Chem. Phys.*, 119(23):12457–12461, 2003.

[88] M. F. Kropman and H. J. Bakker. Vibrational relaxation of liquid water in ionic solvation shells. *Chem. Phys. Lett.*, 370(5-6):741–746, 2003.

[89] M. F. Kropman and H. J. Bakker. Effect of ions on the vibrational relaxation of liquid water. *J. Am. Chem. Soc.*, 126(29):9135–9141, 2004.

[90] J. D. Batchelor, A. Olteanu, A. Tripathy, and G. J. Pielak. Impact of protein denaturants and stabilizers on water structure. *J. Am. Chem. Soc.*, 126(7):1958–1961, 2004.

[91] B. W. Ninham and V. Yaminsky. Ion binding and ion specificity: The Hofmeister effect and Onsager and Lifshitz theories. *Langmuir*, 13(7):2097–2108, 1997.

[92] M. Boström, D. R. M. Williams, and B. W. Ninham. Specific ion effects: Why DLVO theory fails for biology and colloid systems. *Phys. Rev. Lett.*, 87(16):168103, 2001.

[93] M. Boström, D. R. M. Williams, and B. W. Ninham. The influence of ionic dispersion potentials on counterion condensation on polyelectrolytes. *J. Phys. Chem. B*, 106(32):7908–7912, 2002.

[94] M. Boström, D. R. M. Williams, and B. W. Ninham. Specific ion effects: Why the properties of lysozyme in salt solutions follow a Hofmeister series. *Biophys. J.*, 85(2):686–694, 2003.

[95] J. D. Smith, R. J. Saykally, and P. L. Geissler. The effects of dissolved halide anions on hydrogen bonding in liquid water. *J. Am. Chem. Soc.*, 129(45):13847–13856, 2007.

[96] A. K. Soper and K. Weckström. Ion solvation and water structure in potassium halide aqueous solutions. *Biophys. Chem.*, 124(3):180–191, 2006.

[97] R. Mancinelli, A. Botti, F. Bruni, M. A. Ricci, and A. K. Soper. Hydration of sodium, potassium, and chloride ions in solution and the concept of structure maker/breaker. *J. Phys. Chem. B*, 111(48):13570–13577, 2007.

[98] S. Funkner, G. Niehues, D. A. Schmidt, M. Heyden, G. Schwaab, K. M. Callahan, D. J. Tobias, and M. Havenith. Watching the low-frequency motions in aqueous salt solutions: The terahertz vibrational signatures of hydrated ions. *J. Am. Chem. Soc.*, 134(2):1030–1035, 2012.

[99] D. J. Tobias and J. C. Hemminger. Getting specific about specific ion effects. *Science*, 319 (5867):1197–1198, 2008.

[100] P. Jungwirth and D. J. Tobias. Surface effects on aqueous ionic solvation: A molecular dynamics simulation study of NaCl at the air/water interface from infinite dilution to saturation. *J. Phys. Chem. B*, 104(32):7702–7706, 2000.

[101] E. M. Knipping, M. J. Lakin, K. L. Foster, P. Jungwirth, D. J. Tobias, R. B. Gerber, D. Dabdub, and B. J. Finlayson-Pitts. Experiments and simulations of ion-enhanced interfacial chemistry on aqueous NaCl aerosols. *Science*, 288(5464):301–306, 2000.

[102] P. Jungwirth and D. J. Tobias. Ions at the air/water interface. *J. Phys. Chem. B*, 106(25): 6361–6373, 2002.

[103] P. Jungwirth and D. J. Tobias. Specific ion effects at the air/water interface. *Chem. Rev.*, 106 (4):1259–1281, 2006.

[104] S. Ghosal, J. C. Hemminger, H. Bluhm, B. S. Mun, E. L. D. Hebenstreit, G. Ketteler, D. F. Ogletree, F. G. Requejo, and M. Salmeron. Electron spectroscopy of aqueous solution interfaces reveals surface enhancement of halides. *Science*, 307(5709):563–566, 2005.

[105] S. Gopalakrishnan, P. Jungwirth, D. J. Tobias, and H. C. Allen. Air-liquid interfaces of aqueous solutions containing ammonium and sulfate: Spectroscopic and molecular dynamics studies. *J. Phys. Chem. B*, 109(18):8861–8872, 2005.

[106] S. Gopalakrishnan, D. Liu, H. C. Allen, M. Kuo, and M. J. Shultz. Vibrational spectroscopic studies of aqueous interfaces: Salts, acids, bases, and nanodrops. *Chem. Rev.*, 106(4):1155–1175, 2006.

[107] P. Jungwirth and B. Winter. Ions at aqueous interfaces: From water surface to hydrated proteins. *Annu. Rev. Phys. Chem.*, 59:343–366, 2008.

[108] M. Lund, P. Jungwirth, and C. E. Woodward. Ion specific protein assembly and hydrophobic surface forces. *Phys. Rev. Lett.*, 100(25):258105, 2008.

[109] M. Lund, L. Vrbka, and P. Jungwirth. Specific ion binding to nonpolar surface patches of proteins. *J. Am. Chem. Soc.*, 130(35):11582–11583, 2008.

[110] A. Aroti, E. Leontidis, E. Maltseva, and G. Brezesinski. Effects of Hofmeister anions on DPPC Langmuir monolayers at the air–water interface. *J. Phys. Chem. B*, 108(39):15238–15245, 2004.

[111] E. Leontidis, A. Aroti, and L. Belloni. Liquid expanded monolayers of lipids as model systems to understand the anionic Hofmeister series: 1. A tale of models. *J. Phys. Chem. B*, 113(5):1447–1459, 2009.

[112] E. Leontidis and A. Aroti. Liquid expanded monolayers of lipids as model systems to understand the anionic Hofmeister series: 2. Ion partitioning is mostly a matter of size. *J. Phys. Chem. B*, 113(5):1460–1467, 2009.

[113] L. M. Pegram and M. T. Record Jr. Partitioning of atmospherically relevant ions between bulk water and the water/vapor interface. *Proc. Natl. Acad. Sci. U. S. A.*, 103(39):14278–14281, 2006.

[114] S. Z. Moghaddam and E. Thormann. The Hofmeister series: Specific ion effects in aqueous polymer solutions. *J. Colloid Interface Sci.*, 555:615–635, 2019.

[115] J. Kherb, S. C. Flores, and P. S. Cremer. Role of carboxylate side chains in the cation Hofmeister series. *J. Phys. Chem. B*, 116(25):7389–7397, 2012.

[116] E. Pluhařová, M. D. Baer, C. J. Mundy, B. Schmidt, and P. Jungwirth. Aqueous cation–amide binding: Free energies and IR spectral signatures by ab initio molecular dynamics. *J. Phys. Chem. Lett.*, 5(13):2235–2240, 2014.

[117] P. Ganguly, T. Hajari, and N. F. A. van der Vegt. Molecular simulation study on Hofmeister cations and the aqueous solubility of benzene. *J. Phys. Chem. B*, 118(20):5331–5339, 2014.

[118] H. I. Okur, J. Hladílková, K. B. Rembert, Y. Cho, J. Heyda, J. Dzubiella, P. S. Cremer, and P. Jungwirth. Beyond the Hofmeister series: Ion-specific effects on proteins and their biological functions. *J. Phys. Chem. B*, 121(9):1997–2014, 2017.

[119] P. E. Mason, C. E. Dempsey, L. Vrbka, J. Heyda, J. W. Brady, and P. Jungwirth. Specificity of ion-protein interactions: Complementary and competitive effects of tetrapropylammonium, guanidinium, sulfate, and chloride ions. *J. Phys. Chem. B*, 113(10):3227–3234, 2009.

[120] C. E. Dempsey, P. E. Mason, and P. Jungwirth. Complex ion effects on polypeptide conformational stability: Chloride and sulfate salts of guanidinium and tetrapropylammonium. *J. Am. Chem. Soc.*, 133(19):7300–7303, 2011.

[121] V. Balos, M. Bonn, and J. Hunger. Anionic and cationic Hofmeister effects are non-additive for guanidinium salts. *Phys. Chem. Chem. Phys.*, 19(15):9724–9728, 2017.

[122] Y. Zhang and P. S. Cremer. The inverse and direct Hofmeister series for lysozyme. *Proc. Natl. Acad. Sci. U. S. A.*, 106(36):15249–15253, 2009.

[123] N. Schwierz, D. Horinek, and R. R. Netz. Reversed anionic Hofmeister series: The interplay of surface charge and surface polarity. *Langmuir*, 26(10):7370–7379, 2010.

[124] S. C. Flores, J. Kherb, and P. S. Cremer. Direct and reverse Hofmeister effects on interfacial water structure. *J. Phys. Chem. C*, 116(27):14408–14413, 2012.

[125] N. Schwierz, D. Horinek, U. Sivan, and R. R. Netz. Reversed Hofmeister series—The rule rather than the exception. *Curr. Opin. Colloid Interface Sci.*, 23:10–18, 2016.

[126] N. F. A. van der Vegt, K. Haldrup, S. Roke, J. Zheng, M. Lund, and H. J. Bakker. Water-mediated ion pairing: Occurrence and relevance. *Chem. Rev.*, 116(13):7626–7641, 2016.

[127] J. H. Jordan, C. L. D. Gibb, A. Wishard, T. Pham, and B. C. Gibb. Ion–hydrocarbon and/or ion–ion interactions: Direct and reverse Hofmeister effects in a synthetic host. *J. Am. Chem. Soc.*, 140(11):4092–4099, 2018.

[128] V. A. Parsegian. Hopes for Hofmeister. *Nature*, 378:335–336, 1995.

[129] M. T. Record Jr., W. Zhang, and C. F. Anderson. Analysis of effects of salts and uncharged solutes on protein and nucleic acid equilibria and processes: A practical guide to recognizing and interpreting polyelectrolyte effects, Hofmeister effects, and osmotic effects of salts. *Adv. Protein Chem.*, 51:281–353, 1998.

[130] E. K. Wilson. Hofmeister still mystifies. *Chem. Eng. News Arch.*, 90(29):42–43, 2012.

[131] W. J. Xie and Y. Q. Gao. A simple theory for the Hofmeister series. *J. Phys. Chem. Lett.*, 4 (24):4247–4252, 2013.

[132] B. Kang, H. Tang, Z. Zhao, and S. Song. Hofmeister series: Insights of ion specificity from amphiphilic assembly and interface property. *ACS Omega*, 5(12):6229–6239, 2020.

[133] R. S. Carnegie, C. L. D. Gibb, and B. C. Gibb. Anion complexation and the Hofmeister effect. *Angew. Chemie Int. Ed.*, 53(43):11498–11500, 2014.

[134] P. Sokkalingam, J. Shraberg, S. W. Rick, and B. C. Gibb. Binding hydrated anions with hydrophobic pockets. *J. Am. Chem. Soc.*, 138(1):48–51, 2016.

[135] M. B. Hillyer, H. Gan, and B. C. Gibb. Precision switching in a discrete supramolecular assembly: Alkali metal ion-carboxylate selectivities and the cationic Hofmeister effect. *ChemPhysChem*, 19(18):2285–2289, 2018.

[136] N. F. A. van der Vegt and D. Nayar. The hydrophobic effect and the role of cosolvents. *J. Phys. Chem. B*, 121(43):9986–9998, 2017.

[137] S. J. Hawkes. Salts are mostly NOT ionized. *J. Chem. Educ.*, 73(5):421–423, 1996.

[138] J. Paterová, K. B. Rembert, J. Heyda, Y. Kurra, H. I. Okur, W. R. Liu, C. Hilty, P. S. Cremer, and P. Jungwirth. Reversal of the Hofmeister series: Specific ion effects on peptides. *J. Phys. Chem. B*, 117(27):8150–8158, 2013.

[139] B. M. Rankin, M. D. Hands, D. S. Wilcox, K. R. Fega, L. V. Slipchenko, and D. Ben-Amotz. Interactions between halide anions and a molecular hydrophobic interface. *Faraday Discuss.*, 160:255–270, 2013.

[140] J. Hladílková, J. Heyda, K. B. Rembert, H. I. Okur, Y. Kurra, W. R. Liu, C. Hilty, P. S. Cremer, and P. Jungwirth. Effects of end-group termination on salting-out constants for triglycine. *J. Phys. Chem. Lett.*, 4(23):4069–4073, 2013.

[141] X. Chen, S. C. Flores, S.-M. Lim, Y. Zhang, T. Yang, J. Kherb, and P. S. Cremer. Specific anion effects on water structure adjacent to protein monolayers. *Langmuir*, 26(21):16447–16454, 2010.

[142] J. P. Coates. The interpretation of infrared spectra: Published reference sources. *Appl. Spectrosc. Rev.*, 31(1-2):179–192, 1996.

[143] S. Bykov and S. Asher. Raman studies of solution polyglycine conformations. *J. Phys. Chem. B*, 114(19):6636–6641, 2010.

[144] B. Jagoda-Cwiklik, R. Vácha, M. Lund, M. Srebro, and P. Jungwirth. Ion pairing as a possible clue for discriminating between sodium and potassium in biological and other complex environments. *J. Phys. Chem. B*, 111(51):14077–14079, 2007.

[145] T. Hajari, P. Ganguly, and N. F. A. van der Vegt. Enthalpy–entropy of cation association with the acetate anion in water. *J. Chem. Theory Comput.*, 8(10):3804–3809, 2012.

[146] D. M. De Oliveira, S. R. Zukowski, V. Palivec, J. Hénin, H. Martinez-Seara, D. Ben-Amotz, P. Jungwirth, and E. Duboué-Dijon. Binding of divalent cations to acetate: Molecular simulations guided by Raman spectroscopy. *Phys. Chem. Chem. Phys.*, 22(41):24014–24027, 2020.

[147] C. P. Rao, P. Balaram, and C. N. R. Rao. 13C nuclear magnetic resonance studies of the binding of alkali and alkaline earth metal salts to amides. *J. Chem. Soc. Faraday Trans. 1 Phys. Chem. Condens. Phases*, 76:1008–1013, 1980.

[148] F. Ioannou, G. Archontis, and E. Leontidis. Specific interactions of sodium salts with alanine dipeptide and tetrapeptide in water: Insights from molecular dynamics. *J. Phys. Chem. B*, 115(45):13389–13400, 2011.

[149] H. Du, R. Wickramasinghe, and X. Qian. Effects of salt on the lower critical solution temperature of poly(N-isopropylacrylamide). *J. Phys. Chem. B*, 114(49):16594–16604, 2010.

[150] J. D. Song, R. Ryoo, and M. S. Jhon. Anion binding properties of poly(vinylpyrrolidone) in aqueous solution studied by halide NMR spectroscopy. *Macromolecules*, 24(8):1727–1730, 1991.

[151] S. C. Flores, J. Kherb, N. Konelick, X. Chen, and P. S. Cremer. The effects of Hofmeister cations at negatively charged hydrophilic surfaces. *J. Phys. Chem. C*, 116(9):5730–5734, 2012.

[152] M. T. Record Jr., E. Guinn, L. Pegram, and M. Capp. Introductory lecture: Interpreting and predicting Hofmeister salt ion and solute effects on biopolymer and model processes using the solute partitioning model. *Faraday Discuss.*, 160:9–44, 2013.

[153] L. M. Pegram and M. T. Record Jr. Using surface tension data to predict differences in surface and bulk concentrations of nonelectrolytes in water. *J. Phys. Chem. C*, 113(6):2171–2174, 2009.

[154] L. M. Pegram and M. T. Record Jr. Quantifying accumulation or exclusion of H+, HO-, and Hofmeister salt ions near interfaces. *Chem. Phys. Lett.*, 467(1-3):1–8, 2008.

[155] M. W. Capp, L. M. Pegram, R. M. Saecker, M. Kratz, D. Riccardi, T. Wendorff, J. G. Cannon, and M. T. Record Jr. Interactions of the osmolyte glycine betaine with molecular surfaces in water: Thermodynamics, structural interpretation, and prediction of m-values. *Biochemistry*, 48(43):10372–10379, 2009.

[156] L. Ma, L. Pegram, M. T. Record Jr., and Q. Cui. Preferential interactions between small solutes and the protein backbone: A computational analysis. *Biochemistry*, 49(9):1954–1962, 2010.

[157] E. J. Guinn, L. M. Pegram, M. W. Capp, M. N. Pollock, and M. T. Record Jr. Quantifying why urea is a protein denaturant, whereas glycine betaine is a protein stabilizer. *Proc. Natl. Acad. Sci. U. S. A.*, 108(41):16932–16937, 2011.

[158] L. M. Pegram, T. Wendorff, R. Erdmann, I. Shkel, D. Bellissimo, D. J. Felitsky, and M. T. Record Jr. Why Hofmeister effects of many salts favor protein folding but not DNA helix formation. *Proc. Natl. Acad. Sci. U. S. A.*, 107(17):7716–7721, 2010.

[159] J. Heyda and J. Dzubiella. Ion-specific counterion condensation on charged peptides: Poisson–Boltzmann vs. atomistic simulations. *Soft Matter*, 8(36):9338, 2012.

[160] J. Heyda, A. Muzdalo, and J. Dzubiella. Rationalizing polymer swelling and collapse under attractive cosolvent conditions. *Macromolecules*, 46(3):1231–1238, 2013.

[161] J. Heyda, S. Soll, J. Yuan, and J. Dzubiella. Thermodynamic description of the LCST of charged thermoresponsive copolymers. *Macromolecules*, 47(6):2096–2102, 2014.

[162] K. D. Collins. Sticky ions in biological systems. *Proc. Natl. Acad. Sci.*, 92(12):5553–5557, 1995.

[163] K. D. Collins. Ions from the Hofmeister series and osmolytes: Effects on proteins in solution and in the crystallization process. *Methods*, 34(3):300–311, 2004.

[164] K. D. Collins, G. W. Neilson, and J. E. Enderby. Ions in water: Characterizing the forces that control chemical processes and biological structure. *Biophys. Chem.*, 128(2-3):95–104, 2007.

[165] K. D. Collins. Charge density-dependent strength of hydration and biological structure. *Biophys. J.*, 72(1):65–76, 1997.

[166] W. Kunz. Specific ion effects in colloidal and biological systems. *Curr. Opin. Colloid Interface Sci.*, 15(1-2):34–39, 2010.

[167] C. J. Fennell, A. Bizjak, V. Vlachy, and K. A. Dill. Ion pairing in molecular simulations of aqueous alkali halide solutions. *J. Phys. Chem. B*, 113(19):6782–6791, 2009.

[168] S. J. Miklavic and B. W. Ninham. Competition for adsorption sites by hydrated ions. *J. Colloid Interface Sci.*, 134(2):305–311, 1990.

[169] P. Bauduin, A. Renoncourt, D. Touraud, W. Kunz, and B. W. Ninham. Hofmeister effect on enzymatic catalysis and colloidal structures. *Curr. Opin. Colloid Interface Sci.*, 9(1-2):43–47, 2004.

[170] M. Boström, D. R. M. Williams, and B. W. Ninham. Why the properties of proteins in salt solutions follow a Hofmeister series. *Curr. Opin. Colloid Interface Sci.*, 9(1-2):48–52, 2004.

[171] M. Boström and B. W. Ninham. Dispersion self-free energies and interaction free energies of finite-sized ions in salt solutions. *Langmuir*, 20(18):7569–7574, 2004.

[172] M. Boström, D. R. M. Williams, and B. W. Ninham. Specific ion effects: Why colloid science has failed to contribute to biology. In *Trends Colloid Interface Sci. XVI. Progress in Colloid and Polymer Science*, volume 123, pages 110–113. Springer, Berlin, Heidelberg, 2004.

[173] M. Boström, F. W. Tavares, S. Finet, F. Skouri-Panet, A. Tardieu, and B. W. Ninham. Why forces between proteins follow different Hofmeister series for pH above and below pI. *Biophys. Chem.*, 117(3):217–224, 2005.

[174] M. Boström, W. Kunz, and B. W. Ninham. Hofmeister effects in surface tension of aqueous electrolyte solution. *Langmuir*, 21(6):2619–2623, 2005.

[175] P. Lo Nostro, B. W. Ninham, S. Milani, A. Lo Nostro, G. Pesavento, and P. Baglioni. Hofmeister effects in supramolecular and biological systems. *Biophys. Chem.*, 124(3):208–213, 2006.

[176] M. Boström, D. F. Parsons, A. Salis, B. W. Ninham, and M. Monduzzi. Possible origin of the inverse and direct Hofmeister series for lysozyme at low and high salt concentrations. *Langmuir*, 27(15):9504–9511, 2011.

[177] J. M. Borah, S. Mahiuddin, N. Sarma, D. F. Parsons, and B. W. Ninham. Specific ion effects on adsorption at the solid/electrolyte interface: A probe into the concentration limit. *Langmuir*, 27(14):8710–8717, 2011.

[178] A. Salis, F. Cugia, D. F. Parsons, B. W. Ninham, and M. Monduzzi. Hofmeister series reversal for lysozyme by change in pH and salt concentration: Insights from electrophoretic mobility measurements. *Phys. Chem. Chem. Phys.*, 14(13):4343–4346, 2012.

[179] T. T. Duignan, D. F. Parsons, and B. W. Ninham. A continuum model of solvation energies including electrostatic, dispersion, and cavity contributions. *J. Phys. Chem. B*, 117(32): 9421–9429, 2013.

[180] T. T. Duignan, D. F. Parsons, and B. W. Ninham. Ion interactions with the air–water interface using a continuum solvent model. *J. Phys. Chem. B*, 118(29):8700–8710, 2014.

[181] T. T. Duignan, D. F. Parsons, and B. W. Ninham. A continuum solvent model of ion–ion interactions in water. *Phys. Chem. Chem. Phys.*, 16(40):22014–22027, 2014.

[182] C. P. Schneider, D. Shukla, and B. L. Trout. Arginine and the Hofmeister series: The role of ion–ion interactions in protein aggregation suppression. *J. Phys. Chem. B*, 115(22):7447–7458, 2011.

[183] T. López-León, J. L. Ortega-Vinuesa, D. Bastos-González, and A. Elaissari. Thermally sensitive reversible microgels formed by poly(N-isopropylacrylamide) charged chains: A Hofmeister effect study. *J. Colloid Interface Sci.*, 426:300–307, 2014.

[184] S. Z. Moghaddam and E. Thormann. Hofmeister effect of salt mixtures on thermo-responsive poly(propylene oxide). *Phys. Chem. Chem. Phys.*, 17(9):6359–6366, 2015.

[185] E. C. Johnson, T. J. Murdoch, I. J. Gresham, B. A. Humphreys, S. W. Prescott, A. Nelson, G. B. Webber, and E. J. Wanless. Temperature dependent specific ion effects in mixed salt environments on a thermoresponsive poly(oligoethylene glycol methacrylate) brush. *Phys. Chem. Chem. Phys.*, 21(8):4650–4662, 2019.

[186] J. D. Willott, T. J. Murdoch, F. A. M. Leermakers, and Wiebe M. de Vos. Behavior of weak polyelectrolyte brushes in mixed salt solutions. *Macromolecules*, 51(3):1198–1206, 2018.

[187] J. D. Willott, B. A. Humphreys, G. B. Webber, E. J. Wanless, and W. M. de Vos. Combined experimental and theoretical study of weak polyelectrolyte brushes in salt mixtures. *Langmuir*, 35(7):2709–2718, 2019.

[188] J. A. Loughlin and L. S. Romsted. A new method for estimating counter-ion selectivity of a cationic association colloid: Trapping of interfacial chloride and bromide counter-ions by reaction with micellar bound aryldiazonium salts. *Colloids and Surfaces*, 48:123–137, 1990.

[189] T. J. Murdoch, B. A. Humphreys, E. C. Johnson, G. B. Webber, and E. J. Wanless. Specific ion effects on thermoresponsive polymer brushes: Comparison to other architectures. *J. Colloid Interface Sci.*, 526:429–450, 2018.

[190] N. Ottosson, J. Heyda, E. Wernersson, W. Pokapanich, S. Svensson, B. Winter, G. Öhrwall, P. Jungwirth, and O. Björneholm. The influence of concentration on the molecular surface structure of simple and mixed aqueous electrolytes. *Phys. Chem. Chem. Phys.*, 12(36): 10693–10700, 2010.

[191] J. G. Kirkwood and F. P. Buff. The statistical mechanical theory of solutions. I. *J. Chem. Phys.*, 19(6):774–777, 1951.

[192] A. Ben-Naim. *Molecular theory of solutions*. Oxford University Press Inc., New York, 2006.

[193] A. Ben-Naim. Mixture-model approach to the theory of classical fluids. II. Application to liquid water. *J. Chem. Phys.*, 57(9):3605–3612, 1972.

[194] A. Ben-Naim. Standard thermodynamics of transfer. Uses and misuses. *J. Phys. Chem.*, 82 (7):792–803, 1978.

[195] K. Nishikawa. Simple relationship between the Kirkwood–Buff parameters and the fluctuations in the particle number and concentration obtained by small-angle X-ray scattering. *Chem. Phys. Lett.*, 132(1):50–54, 1986.

[196] K. Nishikawa, H. Hayashi, and T. Iijima. Temperature dependence of the concentration fluctuation, the Kirkwood–Buff parameters, and the correlation length of tert-butyl alcohol and water mixtures studied by small-angle X-ray scattering. *J. Phys. Chem.*, 93(17):6559–6565, 1989.

[197] H. Hayashi, K. Nishikawa, and T. Iijima. Small-angle X-ray scattering study of fluctuations in 1-propanol-water and 2-propanol-water systems. *J. Phys. Chem.*, 94(21):8334–8338, 1990.

[198] M. Misawa and K. Yoshida. Concentration fluctuation and salt-induced percolation in 1-propanol aqueous solution. *J. Phys. Soc. Japan*, 69(10):3308–3314, 2000.

[199] L. Almásy, G. Jancsó, and L. Cser. Application of SANS to the determination of Kirkwood–Buff integrals in liquid mixtures. *Appl. Phys. A*, 74:s1376–s1378, 2002.

[200] L. Almásy, L. Cser, and G. Jancsó. Kirkwood–Buff integrals in aqueous solutions of 3-methylpyridine. *J. Mol. Liq.*, 101(1-3):89–98, 2002.

[201] S. Dixit, J. Crain, W. C. K. Poon, J. L. Finney, and A. K. Soper. Molecular segregation observed in a concentrated alcohol–water solution. *Nature*, 416:829–832, 2002.

[202] T. Kato. Kirkwood–Buff parameters and correlation length in aqueous solutions of N-alkoxyethanols. *J. Phys. Chem.*, 88(6):1248–1252, 1984.

[203] A. L. Zaitsev, V. E. Petrenko, and Y. M. Kessler. Solution structure and Kirkwood–Buff theory: Informativity and sensitivity to specific interactions. *J. Solution Chem.*, 18:115–130, 1989.

[204] E. Matteoli and L. Lepori. Solute–solute interactions in water. II. An analysis through the Kirkwood–Buff integrals for 14 organic solutes. *J. Chem. Phys.*, 80(6):2856–2863, 1984.

[205] A. Ben-Naim. Inversion of the Kirkwood–Buff theory of solutions: Application to the water–ethanol system. *J. Chem. Phys.*, 67(11):4884–4890, 1977.

[206] M. C. A. Donkersloot. The structure of binary liquids. The Kirkwood–Buff theory of liquid mixtures, illustrated on the basis of the systems water/methanol, water/ethanol, and cyclohexane/2,3-dimethylbutane, as a link between thermodynamic data and X-ray and neutron scattering. *J. Solution Chem.*, 8:293–307, 1979.

[207] M. C. A. Donkersloot. Concentration dependence of the zero-angle X-ray scattering from liquid mixtures of water and methanol. *Chem. Phys. Lett.*, 60(3):435–438, 1979.

[208] K. J. Patil. Application of Kirkwood–Buff theory of liquid mixtures to water–butanol system. *J. Solution Chem.*, 10:315–320, 1981.

[209] J. Wyman. Linked functions and reciprocal effects in hemoglobin: A second look. In *Adv. Protein Chem.*, volume 19, pages 223–286. 1964.

[210] C. Tanford. Protein denaturation: Part C. Theoretical models for the mechanism of denaturation. In *Adv. Protein Chem.*, volume 24, pages 1–95. 1970.

[211] V. Pierce, M. Kang, M. Aburi, S. Weerasinghe, and P. E. Smith. Recent applications of Kirkwood–Buff theory to biological systems. *Cell Biochem. Biophys.*, 50(1):1–22, 2008.

[212] H. Eisenberg. *Biological macromolecules and polyelectrolytes in solution*. Clarendon Press, Oxford, 1976.

[213] J. A. Schellman. Fifty years of solvent denaturation. *Biophys. Chem.*, 96(2-3):91–101, 2002.

[214] H. L. Friedman and P. S. Ramanathan. Theory of mixed electrolyte solutions and application to a model for aqueous lithium chloride–cesium chloride. *J. Phys. Chem.*, 74(21):3756–3765, 1970.

[215] P. G. Kusalik and G. N. Patey. The thermodynamic properties of electrolyte solutions: Some formal results. *J. Chem. Phys.*, 86(9):5110–5116, 1987.

[216] P. E. Smith. Computer simulation of cosolvent effects on hydrophobic hydration. *J. Phys. Chem. B*, 103(3):525–534, 1999.

[217] P. E. Smith. Cosolvent interactions with biomolecules: Relating computer simulation data to experimental thermodynamic data. *J. Phys. Chem. B*, 108(48):18716–18724, 2004.

[218] R. Chitra and P. E. Smith. Molecular association in solution: A Kirkwood–Buff analysis of sodium chloride, ammonium sulfate, guanidinium chloride, urea, and 2,2,2-trifluoroethanol in water. *J. Phys. Chem. B*, 106(6):1491–1500, 2002.

[219] A. Ben-Naim. Solute and solvent effects on chemical equilibria. *J. Chem. Phys.*, 63(5): 2064–2073, 1975.

[220] A. Ben-Naim. Theory of preferential solvation of nonelectrolytes. *Cell Biophys.*, 12(1): 255–269, 1988.

[221] A. Ben-Naim. *Statistical thermodynamics for chemists and biochemists*. Springer, New York, 1992.

[222] R. Chitra and P. E. Smith. Preferential interactions of cosolvents with hydrophobic solutes. *J. Phys. Chem. B*, 105(46):11513–11522, 2001.

[223] S. Shimizu. Estimating hydration changes upon biomolecular reactions from osmotic stress, high pressure, and preferential hydration experiments. *Proc. Natl. Acad. Sci. U. S. A.*, 101(5): 1195–1199, 2004.

[224] J. M. Schurr, D. P. Rangel, and S. R. Aragon. A contribution to the theory of preferential interaction coefficients. *Biophys. J.*, 89(4):2258–2276, 2005.

[225] S. J. Weiner, P. A. Kollman, D. T. Nguyen, and D. A. Case. An all atom force field for simulations of proteins and nucleic acids. *J. Comput. Chem.*, 7(2):230–252, 1986.

[226] W. F. van Gunsteren, S. R. Billeter, A. A. Eising, P. H. Hunenberger, P. Kruger, A. E. Mark, W. R. P. Scott, and I. G. Tironi. *Biomolecular simulation: The GROMOS96 manual and user guide*. Vdf Hochschulverlag AG an der ETH Zuerich, Zuerich, 1996.

[227] A. D. MacKerell, D. Bashford, M. Bellott, R. L. Dunbrack, J. D. Evanseck, M. J. Field, S. Fischer, J. Gao, H. Guo, S. Ha, D. Joseph-McCarthy, L. Kuchnir, K. Kuczera, F. T. K. Lau, C. Mattos, S. Michnick, T. Ngo, D. T. Nguyen, B. Prodhom, W. E. Reiher, B. Roux, M. Schlenkrich, J. C. Smith, R. Stote, J. Straub, M. Watanabe, J. Wiórkiewicz-Kuczera, D. Yin, and M. Karplus. All-atom empirical potential for molecular modeling and dynamics studies of proteins. *J. Phys. Chem. B*, 102(18):3586–3616, 1998.

[228] W. L. Jorgensen and J. Tirado-Rives. The OPLS potential functions for proteins. Energy minimizations for crystals of cyclic peptides and crambin. *J. Am. Chem. Soc.*, 110(6):1657–1666, 1988.

[229] A. R. Leach. *Molecular modelling: Priniciples and applications*. Pearson Education Limited, Harlow, 2nd edition, 2001.

[230] E. Wernersson and P. Jungwirth. Effect of water polarizability on the properties of solutions of polyvalent ions: Simulations of aqueous sodium sulfate with different force fields. *J. Chem. Theory Comput.*, 6(10):3233–3240, 2010.

[231] B. J. Kirby and P. Jungwirth. Charge scaling manifesto: A way of reconciling the inherently macroscopic and microscopic natures of molecular simulations. *J. Phys. Chem. Lett.*, 10(23): 7531–7536, 2019.

[232] I. M. Zeron, J. L. F. Abascal, and C. Vega. A force field of Li+, Na+, K+, Mg2+, Ca2+, Cl−, and SO42− in aqueous solution based on the TIP4P/2005 water model and scaled charges for the ions. *J. Chem. Phys.*, 151(13):134504, 2019.

[233] D. E. Smith and L. X. Dang. Computer simulations of NaCl association in polarizable water. *J. Chem. Phys.*, 100(5):3757–3766, 1994.

[234] A. P. Lyubartsev and A. Laaksonen. Osmotic and activity coefficients from effective potentials for hydrated ions. *Phys. Rev. E*, 55(5):5689–5696, 1997.

[235] B. Hess, C. Holm, and N. F. A. van der Vegt. Osmotic coefficients of atomistic NaCl(aq) force fields. *J. Chem. Phys.*, 124(16):164509, 2006.

[236] P. S. Ramanathan and H. L. Friedman. Study of a refined model for aqueous 1-1 electrolytes. *J. Chem. Phys.*, 54(3):1086–1099, 1971.

[237] B. M. Pettitt and P. J. Rossky. Alkali halides in water: Ion–solvent correlations and ion–ion potentials of mean force at infinite dilution. *J. Chem. Phys.*, 84(10):5836–5844, 1986.

[238] L. X. Dang, B. M. Pettitt, and P. J. Rossky. On the correlation between like ion pairs in water. *J. Chem. Phys.*, 96(5):4046–4047, 1992.

[239] I. S. Joung and T. E. Cheatham. Determination of alkali and halide monovalent ion parameters for use in explicitly solvated biomolecular simulations. *J. Phys. Chem. B*, 112(30): 9020–9041, 2008.

[240] D. Horinek, S. I. Mamatkulov, and R. R. Netz. Rational design of ion force fields based on thermodynamic solvation properties. *J. Chem. Phys.*, 130(12):124507, 2009.

[241] S. Weerasinghe and P. E. Smith. A Kirkwood–Buff derived force field for mixtures of urea and water. *J. Phys. Chem. B*, 107(16):3891–3898, 2003.

[242] M. B. Gee, N. R Cox, Y. Jiao, N. Bentenitis, S. Weerasinghe, and P. E. Smith. A Kirkwood–Buff derived force field for aqueous alkali halides. *J. Chem. Theory Comput.*, 7(5):1369–1380, 2011.

[243] M. Fyta, I. Kalcher, J. Dzubiella, L. Vrbka, and R. R. Netz. Ionic force field optimization based on single-ion and ion-pair solvation properties. *J. Chem. Phys.*, 132(2):024911, 2010.

[244] M. Fyta and R. R. Netz. Ionic force field optimization based on single-ion and ion-pair solvation properties: Going beyond standard mixing rules. *J. Chem. Phys.*, 136(12):124103, 2012.

[245] S. I. Mamatkulov, M. Fyta, and R. R. Netz. Force fields for divalent cations based on single-ion and ion-pair properties. *J. Chem. Phys.*, 138(2):024505, 2013.

[246] I. V. Leontyev, M. V. Vener, I. V. Rostov, M. V. Basilevsky, and M. D. Newton. Continuum level treatment of electronic polarization in the framework of molecular simulations of solvation effects. *J. Chem. Phys.*, 119(15):8024–8037, 2003.

[247] I. V. Leontyev and A. A. Stuchebrukhov. Electronic continuum model for molecular dynamics simulations. *J. Chem. Phys.*, 130(8):085102, 2009.

[248] I. V. Leontyev and A. A. Stuchebrukhov. Electronic continuum model for molecular dynamics simulations of biological molecules. *J. Chem. Theory Comput.*, 6(5):1498–1508, 2010.

[249] I. V. Leontyev and A. A. Stuchebrukhov. Electronic polarizability and the effective pair potentials of water. *J. Chem. Theory Comput.*, 6(10):3153–3161, 2010.

[250] I. V. Leontyev and A. A. Stuchebrukhov. Accounting for electronic polarization in non-polarizable force fields. *Phys. Chem. Chem. Phys.*, 13(7):2613–2626, 2011.

[251] I. V. Leontyev and A. A. Stuchebrukhov. Polarizable mean-field model of water for biological simulations. *J. Chem. Theory Comput.*, 8(9):3207–3216, 2012.

[252] I. V. Leontyev and A. A. Stuchebrukhov. Polarizable molecular interactions in condensed phase and their equivalent nonpolarizable models electronic. *J. Chem. Phys.*, 141(1):014103, 2014.

[253] P. E. Mason, E. Wernersson, and P. Jungwirth. Accurate description of aqueous carbonate ions: An effective polarization model verified by neutron scattering. *J. Phys. Chem. B*, 116 (28):8145–8153, 2012.

[254] W. J. Xie, Z. Zhang, and Y. Q. Gao. Ion pairing in alkali nitrate electrolyte solutions. *J. Phys. Chem. B*, 120(9):2343–2351, 2016.

[255] L. Pegado, O. Marsalek, P. Jungwirth, and E. Wernersson. Solvation and ion-pairing properties of the aqueous sulfate anion: Explicit versus effective electronic polarization. *Phys. Chem. Chem. Phys.*, 14(29):10248–10257, 2012.

[256] M. Vazdar, P. Jungwirth, and P. E. Mason. Aqueous guanidinium–carbonate interactions by molecular dynamics and neutron scattering: Relevance to ion–protein interactions. *J. Phys. Chem. B*, 117(6):1844–1848, 2013.

[257] E. Pluhařová, P. E. Mason, and P. Jungwirth. Ion pairing in aqueous lithium salt solutions with monovalent and divalent counter-anions. *J. Phys. Chem. A*, 117(46):11766–11773, 2013.

[258] E. Pluhařová, H. E. Fischer, P. E. Mason, and P. Jungwirth. Hydration of the chloride ion in concentrated aqueous solutions using neutron scattering and molecular dynamics. *Mol. Phys.*, 112(9-10):1230–1240, 2014.

[259] M. Kohagen, P. E. Mason, and P. Jungwirth. Accurate description of calcium solvation in concentrated aqueous solutions. *J. Phys. Chem. B*, 118(28):7902–7909, 2014.

[260] M. Kohagen, P. E. Mason, and P. Jungwirth. Accounting for electronic polarization effects in aqueous sodium chloride via molecular dynamics aided by neutron scattering. *J. Phys. Chem. B*, 120(8):1454–1460, 2016.

[261] E. Duboué-Dijon, P. E. Mason, H. E. Fischer, and P. Jungwirth. Hydration and ion pairing in aqueous Mg2+ and Zn2+ solutions: Force-field description aided by neutron scattering experiments and ab initio molecular dynamics simulations. *J. Phys. Chem. B*, 122(13): 3296–3306, 2018.

[262] T. Martinek, E. Duboué-Dijon, Š. Timr, P. E. Mason, K. Baxová, H. E. Fischer, B. Schmidt, E. Pluhařová, and P. Jungwirth. Calcium ions in aqueous solutions: Accurate force field description aided by ab initio molecular dynamics and neutron scattering. *J. Chem. Phys.*, 148(22):222813, 2018.

[263] E. Duboué-Dijon, P. Delcroix, H. Martinez-Seara, J. Hladílková, P. Coufal, T. Křížek, and P. Jungwirth. Binding of divalent cations to insulin: Capillary electrophoresis and molecular simulations. *J. Phys. Chem. B*, 122(21):5640–5648, 2018.

[264] P. E. Mason, P. Jungwirth, and E. Duboué-Dijon. Quantifying the strength of a salt bridge by neutron scattering and molecular dynamics. *J. Phys. Chem. Lett.*, 10(12):3254–3259, 2019.

[265] J. Melcr, H. Martinez-Seara, R. Nencini, J. Kolafa, P. Jungwirth, and O. H. S. Ollila. Accurate binding of sodium and calcium to a POPC bilayer by effective inclusion of electronic polarization. *J. Phys. Chem. B*, 122(16):4546–4557, 2018.

[266] R. Fuentes-Azcatl and M. C. Barbosa. Sodium chloride, NaCl/ε: New force field. *J. Phys. Chem. B*, 120(9):2460–2470, 2016.

[267] J. Li and F. Wang. Pairwise-additive force fields for selected aqueous monovalent ions from adaptive force matching. *J. Chem. Phys.*, 143(19):194505, 2015.

[268] J. Li and F. Wang. Accurate prediction of the hydration free energies of 20 salts through adaptive force matching and the proper comparison with experimental references. *J. Phys. Chem. B*, 121(27):6637–6645, 2017.

[269] P. Atkins and J. De Paula. *Atkins' physical chemistry*. Oxford University Press, New York, 8th edition, 2006.

[270] B. Widom. Some topics in the theory of fluids. *J. Chem. Phys.*, 39(11):2808–2812, 1963.

[271] T. A. Özal and N. F. A. van der Vegt. Confusing cause and effect: Energy-entropy compensation in the preferential solvation of a nonpolar solute in dimethyl sulfoxide/water mixtures. *J. Phys. Chem. B*, 110(24):12104–12112, 2006.

[272] M. E. Lee and N. F. A. van der Vegt. Molecular thermodynamics of methane solvation in tert-butanol-water mixtures. *J. Chem. Theory Comput.*, 3(1):194–200, 2007.

[273] C. Peter and N. F. A. van der Vegt. Solvent reorganization contributions in solute transfer thermodynamics: Inferences from the solvent equation of state. *J. Phys. Chem. B*, 111(27): 7836–7842, 2007.

[274] E. A. Symons. Hydrogen gas solubility in the dimethyl sulfoxide–water system: A further clue to solvent structure in these media. *Can. J. Chem.*, 49(24):3940–3947, 1971.

[275] A. Isihara. The Gibbs–Bogoliubov inequality dagger. *J. Phys. A Gen. Phys.*, 1(5):539–548, 1968.

[276] J. P. Hansen and I. R McDonald. *Theory of simple liquids*. Academic Press, New York, 3rd edition, 2006.

[277] W. A. P. Luck. *Structure of water and aqueous solutions*. Physik-verlag, Weinheim, 1974.

[278] C. Tanford. *The hydrophobic effect: Formation of micelles and biological membranes*. Wiley, New York, 2nd edition, 1980.

[279] A. Ben-Naim. *Hydrophobic interactions*. Springer US, New York.

[280] K. A. Dill. Dominant forces in protein folding. *Biochemistry*, 29(31):7133–7155, 1990.

[281] W. Blokzijl and J. B. F. N. Engberts. Hydrophobic effects. Opinions and facts. *Angew. Chemie Int. Ed.*, 32(11):1545–1579, 1993.

[282] H. A. Scheraga. Theory of hydrophobic interactions. *J. Biomol. Struct. Dyn.*, 16(2):447–460, 1998.

[283] G. Hummer, S. Garde, A. E. García, and L. R. Pratt. New perspectives on hydrophobic effects. *Chem. Phys.*, 258(2-3):349–370, 2000.

[284] N. T. Southall, K. A. Dill, and A. D. J. Haymet. A view of the hydrophobic effect. *J. Phys. Chem. B*, 106(3):521–533, 2002.

[285] L. R. Pratt. Molecular theory of hydrophobic effects: "She is too mean to have her name repeated.". *Annu. Rev. Phys. Chem.*, 53:409–436, 2002.

[286] D. Chandler. Interfaces and the driving force of hydrophobic assembly. *Nature*, 437:640–647, 2005.

[287] P. Ball. Water as an active constituent in cell biology. *Chem. Rev.*, 108(1):74–108, 2008.

[288] K. A. Sharp and J. M. Vanderkooi. Water in the half shell: Structure of water, focusing on angular structure and solvation. *Acc. Chem. Res.*, 43(2):231–239, 2010.

[289] D. Ben-Amotz. Water-mediated hydrophobic interactions. *Annu. Rev. Phys. Chem.*, 67: 617–638, 2016.

[290] R. M. Jackson and M. J. E. Sternberg. Protein surface area defined. *Nature*, 366:638, 1993.

[291] F. H. Stillinger. Structure in aqueous solutions of nonpolar molecules from the standpoint of scaled-particle theory. *J. Solution Chem.*, 2(2-3):141–158, 1973.

[292] K. Lum, D. Chandler, and J. D. Weeks. Hydrophobicity at small and large length scales. *J. Phys. Chem. B*, 103(22):4570–4577, 1999.

[293] D. M. Huang and D. Chandler. Temperature and length scale dependence of hydrophobic effects and their possible implications for protein folding. *Proc. Natl. Acad. Sci. U. S. A.*, 97 (15):8324–8327, 2000.

[294] S. Rajamani, T. M. Truskett, and S. Garde. Hydrophobic hydration from small to large lengthscales: Understanding and manipulating the crossover. *Proc. Natl. Acad. Sci. U. S. A.*, 102(27):9475–9480, 2005.

[295] H. S. Ashbaugh and L. R. Pratt. Colloquium: Scaled particle theory and the length scales of hydrophobicity. *Rev. Mod. Phys.*, 78(1):159–178, 2006.

[296] B. J. Berne, J. D. Weeks, and R. Zhou. Dewetting and hydrophobic interaction in physical and biological systems. *Annu. Rev. Phys. Chem.*, 60:85–103, 2009.

[297] S. Garde and A. J. Patel. Unraveling the hydrophobic effect, one molecule at a time. *Proc. Natl. Acad. Sci.*, 108(40):16491–16492, 2011.

[298] G. Hummer, S. Garde, A. E. García, A. Pohorille, and L. R. Pratt. An information theory model of hydrophobic interactions. *Proc. Natl. Acad. Sci. U. S. A.*, 93(17):8951–8955, 1996.

[299] M. B. Hillyer and B. C. Gibb. Molecular shape and the hydrophobic effect. *Annu. Rev. Phys. Chem.*, 67:307–329, 2016.

[300] K. A. Dill and S. Bromberg. *Molecular driving forces. Statisitcal thermodynamics in biology, chemistry, physics, and nanotechnology*. Garland Science, New York, 2nd edition, 2011.

[301] A. Ben-Naim. Solvent-induced interactions: Hydrophobic and hydrophilic phenomena. *J. Chem. Phys.*, 90(12):7412–7425, 1989.

[302] L. Yang, Y. Fan, and Y. Q. Gao. Differences of cations and anions: Their hydration, surface adsorption, and impact on water dynamics. *J. Phys. Chem. B*, 115(43):12456–12465, 2011.

[303] W. Kunz, editor. *Specific ion effects*. World Scientific, 2010.

[304] J. Barthel, H. Krienke, and W. Kunz. *Physical chemistry of electrolyte solutions – modern aspects*. Steinkopp, Darmstadt, Springer, New York, 1998.

[305] P. Debye and E. Hückel. Zur Theorie der Elektrolyte. I. Gefrierpunktserniedrigung und verwandte Erscheinungen. *Phys. Zeitschrift*, 24:185–206, 1923.

[306] L. Onsager and N. N. T. Samaras. The surface tension of Debye–Hückel electrolytes. *J. Chem. Phys.*, 2(8):528–536, 1934.

[307] K. J. Laidler. Reaction between ions. In *Chem. Kinet.*, pages 191–202. Longman, New York, 1987.

[308] B. Lautrup. *Physics of continuous matter exotic and everyday phenomena in the macroscopic world*. CRC Press, Boca Raton, 2nd edition, 2011.

[309] P. K. Weissenborn and R. J. Pugh. Surface tension and bubble coalescence phenomena of aqueous solutions of electrolytes. *Langmuir*, 11(5):1422–1426, 1995.

[310] D. Frenkel and B. Smit. *Understanding molecular simulations: From algorithms to applications*. Academic Press, San Diego, 2nd edition, 2002.

[311] D. C. Rapaport. *The art of molecular dynamics simulation*. Cambridge University Press, New York, 2nd edition, 2004.

[312] R. A. Robinson and R. H. Stokes. *Electrolyte solutions*. Butterworth & Co. Ltd., London, 2nd edition, 2002.

[313] G. N. Patey and J. P. Valleau. A Monte Carlo method for obtaining the interionic potential of mean force in ionic solution. *J. Chem. Phys.*, 63(6):2334–2339, 1975.

[314] M. Mezei and D. L. Beveridge. Monte Carlo studies of the structure of dilute aqueous sclutions of Li+ , Na+ , K+ , F– , and Cl–. *J. Chem. Phys.*, 74(12):6902–6910, 1981.

[315] G. W. Neilson and J. E. Enderby. The structure of an aqueous solution of nickel chloride. *Proc. R. Soc. London. A. Math. Phys. Sci.*, 390(1799):353–371, 1983.

[316] L. X. Dang. Temperature dependence of interactions of an ion pair in water: A molecular dynamics study. *J. Chem. Phys.*, 97(3):1919–1921, 1992.

[317] S. W. W. Chen and P. J. Rossky. Potential of mean force for a sodium dimethyl phosphate ion pair in aqueous solution: A further test of the extended RISM theory. *J. Phys. Chem.*, 97 (22):6078–6082, 1993.

[318] L. R. Pratt, G. Hummer, and A. E. García. Ion pair potentials-of-mean-force in water. *Biophys. Chem.*, 51(2-3):147–165, 1994.

[319] S. Koneshan and J. C. Rasaiah. Computer simulation studies of aqueous sodium chloride solutions at 298 K and 683 K. *J. Chem. Phys.*, 113(18):8125–8137, 2000.

[320] M. Bergdorf, C. Peter, and P. H. Hünenberger. Influence of cut-off truncation and artificial periodicity of electrostatic interactions in molecular simulations of solvated ions: A continuum electrostatics study. *J. Chem. Phys.*, 119(17):9129–9144, 2003.

[321] B. Hess, C. Holm, and N. F. A. van der Vegt. Modeling multibody effects in ionic solutions with a concentration dependent dielectric permittivity. *Phys. Rev. Lett.*, 96(14):147801, 2006.

[322] M. Y. Kiriukhin and K. D. Collins. Dynamic hydration numbers for biologically important ions. *Biophys. Chem.*, 99(2):155–168, 2002.

[323] H. Ohtaki and T. Radnal. Structure and dynamics of hydrated ions. *Chem. Rev.*, 93(3): 1157–1204, 1993.

[324] Y. Marcus. *Ion properties*. Marcel Dekker, Inc., New York, 1997.

[325] E. R. Nightingale Jr. Phenomenological theory of ion solvation. Effective radii of hydrated ions. *J. Phys. Chem.*, 63(9):1381–1387, 1959.

[326] A. W. Adamson. *A textbook of physical chemistry*. Academic Press, New York, 2nd edition, 1979.

[327] B. Roux, H. A. Yu, and M. Karplus. Molecular basmolecular basis for the Born model of ion solvationis for the Born Model of ion solvation. *J. Phys. Chem.*, 94(11):4683–4688, 1990.

[328] R. M. Levy, M. Belhadj, and D. B. Kitchen. Gaussian fluctuation formula for electrostatic free-energy changes in solution. *J. Chem. Phys.*, 95(5):3627–3633, 1991.

[329] S. L. Chan and C. Lim. Reducing the error due to the uncertainty in the Born radius in continuum dielectric calculations. *J. Phys. Chem.*, 98(2):692–695, 1994.

[330] R. J. Young and P. A. Lovell. *Introduction to polymers*. CRC Press, Taylor & Francis Group, Boca Raton, FL, 3rd edition, 2011.

[331] A. S. Hoffman. "Intelligent" polymers in medicine and biotechnology. *Macromol. Symp.*, 98 (1):645–664, 1995.

[332] I. Galaev and B. Mattiasson. *Smart polymers: Applications in biotechnology and biomedicine*. CRC Press, Taylor & Francis Group, Boca Raton, USA, 2nd edition, 2007.

[333] V. A. Ganesh, A. Baji, and S. Ramakrishna. Smart functional polymers – a new route towards creating a sustainable environment. *RSC Adv.*, 4(95):53352–53364, 2014.

[334] M. Wei, Y. Gao, X. Li, and M. J. Serpe. Stimuli-responsive polymers and their applications. *Polym. Chem.*, 8(1):127–143, 2017.

[335] E. Cabane, X. Zhang, K. Langowska, C. G. Palivan, and W. Meier. Stimuli-responsive polymers and their applications in nanomedicine. *Biointerphases*, 7:9, 2012.

[336] J. Zhuang, M. R. Gordon, J. Ventura, L. Li, and S. Thayumanavan. Multi-stimuli responsive macromolecules and their assemblies. *Chem. Soc. Rev.*, 42(17):7421–7435, 2013.

[337] P. Schattling, F. D. Jochum, and P. Theato. Multi-stimuli responsive polymers-the all-in-one talents. *Polym. Chem.*, 5(1):25–36, 2014.

[338] M. A. Cohen Stuart, W. T. S. Huck, J. Genzer, M. Müller, C. Ober, M. Stamm, G. B. Sukhorukov, I. Szleifer, V. V. Tsukruk, M. Urban, F. M. Winnik, S. Zauscher, I. Luzinov, and S. Minko. Emerging applications of stimuli-responsive polymer materials. *Nat. Mater.*, 9: 101–113, 2010.

[339] C. de las Heras Alarcón, S. Pennadam, and C. Alexander. Stimuli responsive polymers for biomedical applications. *Chem. Soc. Rev.*, 34(3):276–285, 2005.

[340] J. Hu and S. Liu. Responsive polymers for detection and sensing applications: Current status and future developments. *Macromolecules*, 43(20):8315–8330, 2010.

[341] A. K. Bajpai, S. K. Shukla, S. Bhanu, and S. Kankane. Responsive polymers in controlled drug delivery. *Prog. Polym. Sci.*, 33(11):1088–1118, 2008.

[342] A. C. Hunter and S. M. Moghimi. Smart polymers in drug delivery: A biological perspective. *Polym. Chem.*, 8(1):41–51, 2017.

[343] J. Wang, H. Zhang, F. Wang, X. Ai, D. Huang, G. Liu, and P. Mi. Enzyme-responsive polymers for drug delivery and molecular imaging. In *Stimuli Responsive Polym. Nanocarriers Drug Deliv. Appl. Vol. 1*, pages 101–119. Elsevier Ltd., 2018.

[344] M. C. García. Ionic-strength-responsive polymers for drug delivery applications. In *Stimuli Responsive Polym. Nanocarriers Drug Deliv. Appl.*, pages 393–409. Elsevier Ltd., 2019.

[345] D. Parasuraman and M. J. Serpe. Poly(N-isopropylacrylamide) microgels for organic dye removal from water. *ACS Appl. Mater. Interfaces*, 3(7):2732–2737, 2011.

[346] M. Ma, L. Guo, D. G. Anderson, and R. Langer. Bio-inspired polymer composite actuator and generator driven by water gradients. *Science*, 339(6116):186–189, 2013.

[347] Q. Zhao, J. W. C. Dunlop, X. Qiu, F. Huang, Z. Zhang, J. Heyda, J. Dzubiella, M. Antonietti, and J. Yuan. An instant multi-responsive porous polymer actuator driven by solvent molecule sorption. *Nat. Commun.*, 5:4293, 2014.

[348] D. Roy, J. N. Cambre, and B. S. Sumerlin. Future perspectives and recent advances in stimuli-responsive materials. *Prog. Polym. Sci.*, 35(1-2):278–301, 2010.

[349] F. Liu and M. W. Urban. Recent advances and challenges in designing stimuli-responsive polymers. *Prog. Polym. Sci.*, 35(1-2):3–23, 2010.

[350] M. Motornov, Y. Roiter, I. Tokarev, and S. Minko. Stimuli-responsive nanoparticles, nanogels and capsules for integrated multifunctional intelligent systems. *Prog. Polym. Sci.*, 35(1-2): 174–211, 2010.

[351] I. Cobo, M. Li, B. S. Sumerlin, and S. Perrier. Smart hybrid materials by conjugation of responsive polymers to biomacromolecules. *Nat. Mater.*, 14:143–159, 2015.

[352] M. J. Webber, E. A. Appel, E. W. Meijer, and R. Langer. Supramolecular biomaterials. *Nat. Mater.*, 15:13–26, 2016.

[353] A. K. Teotia, H. Sami, and A. Kumar. Thermo-responsive polymers: Structure and design of smart materials. In *Switch. Responsive Surfaces Mater. Biomed. Appl.*, pages 3–43. Elsevier Ltd, 2015.

[354] A. Kumar, A. Srivastava, I. Y. Galaev, and B. Mattiasson. Smart polymers: Physical forms and bioengineering applications. *Prog. Polym. Sci.*, 32(10):1205–1237, 2007.

[355] K. N. Plunkett, X. Zhu, J. S. Moore, and D. E. Leckband. PNIPAM chain collapse depends on the molecular weight and grafting density. *Langmuir*, 22(9):4259–4266, 2006.

[356] R. Hoogenboom, H. M. L. Thijs, M. J. H. C. Jochems, B. M. van Lankvelt, M. W. M. Fijten, and U. S. Schubert. Tuning the LCST of poly(2-oxazoline) by varying composition and molecular weight: Alternatives to poly(N-isopropylacrylamide)? *Chem. Commun.*, 44: 5758–5760, 2008.

[357] S. Z. Moghaddam and E. Thormann. Hofmeister effect on thermo-responsive poly(propylene oxide): Role of polymer molecular weight and concentration. *J. Colloid Interface Sci.*, 465: 67–75, 2016.

[358] B. Ray, Y. Okamoto, M. Kamigaito, M. Sawamoto, K. Seno, Shokyoku Kanaoka, and Sadahito Aoshima. Effect of tacticity of poly(N-isopropylacrylamide) on the phase separation temperature of its aqueous solutions. *Polym. J.*, 37(3):234–237, 2005.

[359] Y. Katsumoto and N. Kubosaki. Tacticity effects on the phase diagram for poly(N-isopropylacrylamide) in water. *Macromolecules*, 41(15):5955–5956, 2008.

[360] E. Chiessi and G. Paradossi. Influence of tacticity on tydrophobicity of poly(N-isopropylacrylamide): A single chain molecular dynamics simulation study. *J. Phys. Chem. B*, 120(15):3765–3776, 2016.

[361] G. Paradossi and E. Chiessi. Tacticity-dependent interchain interactions of poly(N-Isopropylacrylamide) in water: Toward the molecular dynamics simulation of a thermoresponsive microgel. *Gels*, 3(2):13, 2017.

[362] F. Meersman, J. Wang, Y. Wu, and K. Heremans. Pressure effect on the hydration properties of poly(N-isopropylacrylamide) in aqueous solution studied by FTIR spectroscopy. *Macromolecules*, 38(21):8923–8928, 2005.

[363] H. Feil, Y. H. Bae, J. Feijen, and S. W. Kim. Effect of comonomer hydrophilicity and ionization on the lower critical solution temperature of N-isopropylacrylamide copolymers. *Macromolecules*, 26(10):2496–2500, 1993.

[364] S. Furyk, Y. Zhang, D. Ortiz-Acosta, P. S. Cremer, and D. E. Bergbreiter. Effects of end group polarity and molecular weight on the lower critical solution temperature of poly(N-isopropylacrylamide). *J. Polym. Sci. Part A Polym. Chem.*, 44(4):1492–1501, 2006.

[365] P. J. Roth, F. D. Jochum, F. R. Forst, R. Zentel, and P. Theato. Influence of end groups on the stimulus-responsive behavior of poly[oligo(ethylene glycol) methacrylate] in water. *Macromolecules*, 43(10):4638–4645, 2010.

[366] R. Pelton. Poly(N-isopropylacrylamide) (PNIPAM) is never hydrophobic. *J. Colloid Interface Sci.*, 348(2):673–674, 2010.

[367] M. Kobayashi, Y. Matsumoto, M. Uchiyama, and T. Ohwada. A new chemoselective anionic polymerization method for poly(N-isopropylacrylamide) (PNIPAM) in aqueous media: Design and application of bulky zincate possessing little basicity. *Macromolecules*, 37(12): 4339–4341, 2004.

[368] Y.-P. Wang, K. Yuan, Q.-L. Li, L.-P. Wang, S.-J. Gu, and X.-W. Pei. Preparation and characterization of poly(N-isopropylacrylamide) films on a modified glass surface via surface initiated redox polymerization. *Mater. Lett.*, 59(14-15):1736–1740, 2005.

[369] S. Senel, B. Isik-Yuruksoy, H. Cicek, and A. Tuncel. Thermoresponsive isopropylacrylamide-vinylpyrrolidone copolymer by radiation polymerization. *J. Appl. Polym. Sci.*, 64(9):1775–1784, 1997.

[370] F. M. Winnik, H. Ringsdorf, and J. Venzmer. Methanol-water as a co-nonsolvent system for poly(N-isopropylacrylamide). *Macromolecules*, 23(8):2415–2416, 1990.

[371] F. Ganachaud, M. J. Monteiro, R. G. Gilbert, M.-A. Dourges, S. H. Thang, and E. Rizzardo. Molecular weight characterization of poly(N-isopropylacrylamide) prepared by living free-radical polymerization. *Macromolecules*, 33(18):6738–6745, 2000.

[372] X. Yin, A. S. Hoffman, and P. S. Stayton. Poly(N-isopropylacrylamide-co-propylacrylic acid) copolymers that respond sharply to temperature and pH. *Biomacromolecules*, 7(5): 1381–1385, 2006.

[373] M. Heskins and J. E. Guillet. Solution properties of poly(N-isopropylacrylamide). *J. Macromol. Sci. Part A - Chem.*, 2(8):1441–1455, 1968.

[374] H. G. Schild. Poly(N-isopropylacrylamide): Experiment, theory and application. *Prog. Polym. Sci.*, 17(2):163–249, 1992.

[375] M. Najafi, E. Hebels, W. E. Hennink, and T. Vermonden. Poly(N-isopropylacrylamide): Physicochemical properties and biomedical applications. In Vitaliy V. Khutoryanskiy and Theoni K. Georgiou, editors, *Temp. Polym. Chem. Prop. Appl.*, pages 1–34. John Wiley & Sons Ltd., 2018.

[376] Z. Tong, F. Zeng, X. Zheng, and T. Sato. Inverse molecular weight dependence of cloud points for aqueous poly(N-isopropylacrylamide) solutions. *Macromolecules*, 32(13):4488–4490, 1999.

[377] C. Wu and X. Wang. Globule-to-coil transition of a single homopolymer chain in solution. *Phys. Rev. Lett.*, 80(18):4092–4094, 1998.

[378] M. Podewitz, Y. Wang, P. K. Quoika, J. R. Loeffler, M. Schauperl, and K. R. Liedl. Coil-globule transition thermodynamics of poly(N-isopropylacrylamide). *J. Phys. Chem. B*, 123 (41):8838–8847, 2019.

[379] L. Pérez-Fuentes, D. Bastos-González, J. Faraudo, and C. Drummond. Effect of organic and inorganic ions on the lower critical solution transition and aggregation of PNIPAM. *Soft Matter*, 14(38):7818–7828, 2018.

[380] D. Nayar and N. F. A. van der Vegt. Cosolvent effects on polymer hydration drive hydrophobic collapse. *J. Phys. Chem. B*, 122(13):3587–3595, 2018.

[381] I. Bischofberger, D. C. E. Calzolari, P. De Los Rios, I. Jelezarov, and V. Trappe. Hydrophobic hydration of poly-N-isopropyl acrylamide: A matter of the mean energetic state of water. *Sci. Rep.*, 4:4377, 2015.

[382] H. Torii, T. Tatsumi, and M. Tasumi. Effects of hydration on the structure, vibrational wavenumbers, vibrational force field and resonance Raman intensities of N-methylacetamide. *J. Raman Spectrosc.*, 29(6):537–546, 1998.

[383] G. V. R. Rao, M. E. Krug, S. Balamurugan, H. Xu, Q. Xu, and G. P. López. Synthesis and characterization of silica-poly(N-isopropylacrylamide) hybrid membranes: Switchable molecular filters. *Chem. Mater.*, 14(12):5075–5080, 2002.

[384] S. Balamurugan, S. Mendez, S. S. Balamurugan, M. J. O'Brien II, and G. P. López. Thermal response of poly(N-isopropylacrylamide) brushes probed by surface plasmon resonance. *Langmuir*, 19(7):2545–2549, 2003.

[385] D. Magerl, M. Philipp, X.-P. Qiu, F. M. Winnik, and P. Müller-Buschbaum. Swelling and thermoresponsive behavior of linear versus cyclic poly(N-isopropylacrylamide) thin films. *Macromolecules*, 48(9):3104–3111, 2015.

[386] B. M. Baynes and B. L. Trout. Proteins in mixed solvents: A molecular-level perspective. *J. Phys. Chem. B*, 107(50):14058–14067, 2003.

[387] P. Ganguly and N. F. A. van der Vegt. Convergence of sampling Kirkwood–Buff integrals of aqueous solutions with molecular dynamics simulations. *J. Chem. Theory Comput.*, 9(3): 1347–1355, 2013.

[388] C. Y. Hu, H. Kokubo, G. C. Lynch, D. W. Bolen, and B. M. Pettitt. Backbone additivity in the transfer model of protein solvation. *Protein Sci.*, 19(5):1011–1022, 2010.

[389] V. Vagenende and B. L. Trout. Quantitative characterization of local protein solvation to predict solvent effects on protein structure. *Biophys. J.*, 103(6):1354–1362, 2012.

[390] C. Tanford. Extension of the theory of linked functions to incorporate the effects of protein hydration. *J. Mol. Biol.*, 39(3):539–544, 1969.

[391] G. Graziano. On the temperature-induced coil to globule transition of poly-N-isopropylacrylamide in dilute aqueous solutions. *Int. J. Biol. Macromol.*, 27(1):89–97, 2000.

[392] C. Maffi, M. Baiesi, L. Casetti, F. Piazza, and P. De Los Rios. First-order coil-globule transition driven by vibrational entropy. *Nat. Commun.*, 3:1065, 2012.

[393] R. Zangi, R. Zhou, and B. J. Berne. Urea's action on hydrophobic interactions. *J. Am. Chem. Soc.*, 131(4):1535–1541, 2009.

[394] J. Mondal, G. Stirnemann, and B. J. Berne. When does trimethylamine N-oxide fold a polymer chain and urea unfold it? *J. Phys. Chem. B*, 117(29):8723–8732, 2013.

[395] F. Rodríguez-Ropero, P. Rötzscher, and N. F. A. van der Vegt. Comparison of different TMAO force fields and their impact on the folding equilibrium of a hydrophobic polymer. *J. Phys. Chem. BJournal Phys. Chem. B*, 120(34):8757–8767, 2016.

[396] D. Nayar, A. Folberth, and N. F. A. van der Vegt. Molecular origin of urea driven hydrophobic polymer collapse and unfolding depending on side chain chemistry. *Phys. Chem. Chem. Phys.*, 19(28):18156–18161, 2017.

[397] G. Graziano. Salting out of methane by sodium chloride: A scaled particle theory study. *J. Chem. Phys.*, 129(8):084506, 2008.

[398] S. Asakura and F. Oosawa. On interaction between two bodies immersed in a solution of macromolecules. *J. Chem. Phys.*, 22(7):1255–1256, 1954.

[399] A. G. Lambert, P. B. Davies, and D. J. Neivandt. Implementing the theory of sum frequency generation vibrational spectroscopy: A tutorial review. *Appl. Spectrosc. Rev.*, 40(2):103–145, 2005.

[400] X. D. Zhu, H. Suhr, and Y. R. Shen. Surface vibrational spectroscopy by infrared-visible sum frequency generation. *Phys. Rev. B*, 35(6):3047–3050, 1987.

[401] J. H. Hunt, P. Guyot-Sionnest, and Y. R. Shen. Observation of C-H stretch vibrations of monolayers of molecules optical sum-frequency generation. *Chem. Phys. Lett.*, 133(3): 189–192, 1987.

[402] P. Guyot-Sionnest, J. H. Hunt, and Y. R. Shen. Sum-frequency vibrational spectroscopy of a Langmuir film: Study of molecular orientation of a two-dimensional system. *Phys. Rev. Lett.*, 59(14):1597–1600, 1987.

[403] Y. R. Shen. Surface properties probed by second-harmonic and sum-frequency generation. *Nature*, 337:519–525, 1989.

[404] K. C Jena and D. K Hore. Variation of ionic strength reveals the interfacial water structure at a charged mineral surface. *J. Phys. Chem. C*, 113(34):15364–15372, 2009.

[405] D. A. McQuarrie. *Statistical mechanics*. Harper & Row, New York, 1st edition, 1976.

[406] L. Verlet. Computer "experiments" on classical fluids. II. Equilibrium correlation functions. *Phys. Rev.*, 165(1):201–214, 1968.

[407] P. P. Ewald. Die Berechnung optischer und elektrostatischer Gitterpotentiale. *Ann. Phys.*, 369(3):253–287, 1921.

[408] H. J. C. Berendsen, J. P. M. Postma, W. F. van Gunsteren, A. DiNola, and J. R. Haak. Molecular dynamics with coupling to an external bath. *J. Chem. Phys.*, 81(8):3684–3690, 1984.

[409] G. Bussi, D. Donadio, and M. Parrinello. Canonical sampling through velocity rescaling. *J. Chem. Phys.*, 126(1):014101, 2007.

[410] S. Nosé. A molecular dynamics method for simulations in the canonical ensemble. *Mol. Phys.*, 52(2):255–268, 1984.

[411] M. Parrinello and A. Rahman. Polymorphic transitions in single crystals: A new molecular dynamics method. *J. Appl. Phys.*, 52(12):7182–7190, 1981.

[412] S. Nosé and M. L. Klein. Constant pressure molecular dynamics for molecular systems. *Mol. Phys.*, 50(5):1055–1076, 1983.

[413] M. J. Abraham, T. Murtola, R. Schulz, S. Páll, J. C. Smith, B. Hess, and E. Lindahl. GROMACS: High performance molecular simulations through multi-level parallelism from laptops to supercomputers. *SoftwareX*, 1-2:19–25, 2015.

[414] D. Horinek and R. R. Netz. Can simulations quantitatively predict peptide transfer free energies to urea solutions? Thermodynamic concepts and force field limitations. *J. Phys. Chem. A*, 115(23):6125–6136, 2011.

[415] M. Kanduč, R. Chudoba, K. Palczynski, W. K. Kim, R. Roa, and J. Dzubiella. Selective solute adsorption and partitioning around single PNIPAM chains. *Phys. Chem. Chem. Phys.*, 19(8): 5906–5916, 2017.

[416] C. Dalgicdir and N. F. A. van der Vegt. Improved temperature behavior of PNIPAM in water with a modified OPLS model. *J. Phys. Chem. B*, 123(17):3875–3883, 2019.

[417] B. Hess, H. Bekker, H. J. C. Berendsen, and J. G. E. M. Fraaije. LINCS: A linear constraint solver for molecular simulations. *J. Comput. Chem.*, 18(12):1463–1472, 1997.

[418] H. J. C. Berendsen, J. R. Grigera, and T. P. Straatsma. The missing term in effective pair potentials. *J. Phys. Chem.*, 91(24):6269–6271, 1987.

[419] S. Miyamoto and P. A. Kollman. SETTLE: An Analytical Version of the SHAKE and RATTLE Algorithm for Rigid Water Models. *J. Comput. Chem.*, 13(8):952–962, 1992.

[420] W. G. Hoover. Canonical dynamics: Equilibrium phase-space distributions. *Phys. Rev. A*, 31(3):1695–1697, 1985.

[421] T. Darden, D York, and L Pedersen. Particle mesh Ewald: An Nlog(N) method for Ewald sums in large systems. *J. Chem. Phys.*, 98(12):10089–10092, 1993.

[422] Y. Luo and B. Roux. Simulation of osmotic pressure in concentrated aqueous salt solutions. *J. Phys. Chem. Lett.*, 1(1):183–189, 2010.

[423] E. E. Bruce and N. F. A. van der Vegt. Does an electronic continuum correction improve effective short-range ion–ion interactions in aqueous solution? *J. Chem. Phys.*, 148(22): 222816, 2018.

[424] E. E. Bruce, P. T. Bui, B. A. Rogers, P. S. Cremer, and N. F. A. van der Vegt. Nonadditive ion effects drive both collapse and swelling of thermoresponsive polymers in water. *J. Am. Chem. Soc.*, 141(16):6609–6616, 2019.

[425] A. Stukowski. Visualization and analysis of atomistic simulation data with OVITO–the Open visualization tool. *Model. Simul. Mater. Sci. Eng.*, 18(1):015012, 2010.

[426] P. Krüger, S. K. Schnell, D. Bedeaux, S. Kjelstrup, T. J. H. Vlugt, and J.-M. Simon. Kirkwood–Buff integrals for finite volumes. *J. Phys. Chem. Lett.*, 4(2):235–238, 2013.

[427] J. Milzetti, D. Nayar, and N. F. A. van der Vegt. Convergence of Kirkwood–Buff integrals of ideal and nonideal aqueous solutions using molecular dynamics simulations. *J. Phys. Chem. B*, 122(21):5515–5526, 2018.

[428] W. Melander and C. Horváth. Salt effects on hydrophobic interactions in precipitation and chromatography of proteins: An interpretation of the lyotropic series. *Arch. Biochem. Biophys.*, 183(1):200–215, 1977.

[429] T. Arakawa and S. N. Timasheff. Mechanism of protein salting in and salting out by divalent cation salts: Balance between hydration and salt binding. *Biochemistry*, 23(25):5912–5923, 1984.

[430] A. S. Thomas and A. H. Elcock. Molecular dynamics simulations predict a favorable and unique mode of interaction between lithium (Li+) ions and hydrophobic molecules in aqueous solution. *J. Chem. Theory Comput.*, 7(4):818–824, 2011.

[431] M. J. Krisch, R. D'Auria, M. A. Brown, D. J. Tobias, J. C. Hemminger, M. Ammann, D. E. Starr, and H. Bluhm. The effect of an organic surfactant on the liquid–vapor interface of an electrolyte solution. *J. Phys. Chem. C*, 111(36):13497–13509, 2007.

[432] H. Du, S. R. Wickramasinghe, and X. Qian. Specificity in cationic interaction with poly(N-isopropylacrylamide). *J. Phys. Chem. B*, 117(17):5090–5101, 2013.

[433] E. E. Bruce and N. F. A. van der Vegt. Molecular scale solvation in complex solutions. *J. Am. Chem. Soc.*, 141(33):12948–12956, 2019.

[434] E. E. Bruce, H. I. Okur, S. Stegmaier, C. I. Drexler, B. A. Rogers, N. F. A. van der Vegt, S. Roke, and P. S. Cremer. Molecular mechanism for the interactions of Hofmeister cations with macromolecules in aqueous solution. *J. Am. Chem. Soc.*, 142(45):19094–19100, 2020.

[435] P. Lo Nostro and B. W. Ninham. Editorial: Electrolytes and specific ion effects. New and old horizons. *Curr. Opin. Colloid Interface Sci.*, 23:A1–A5, 2016.

[436] L. Götte, K. M. Parry, W. Hua, D. Verreault, H. C. Allen, and D. J. Tobias. Solvent-shared ion pairs at the air–solution interface of magnesium chloride and sulfate solutions revealed by sum frequency spectroscopy and molecular dynamics simulations. *J. Phys. Chem. A*, 121 (34):6450–6459, 2017.

[437] Q. He, G. I. Vargas-Zúñiga, S. H. Kim, S. K. Kim, and J. L. Sessler. Macrocycles as ion pair receptors. *Chem. Rev.*, 119(17):9753–9835, 2019.

[438] R. G. Pearson. Hard and soft acids and bases. *J. Am. Chem. Soc.*, 85(22):3533–3539, 1963.

[439] J. Čeleda, S. Škramovsky, and J Žilkova. The metachores of polyvalent and associated electrolytes in aqueous solutions. *Collect. Czech. Chem. Commun.*, 49:1079–1089, 1984.

[440] A. A. Abramzon and R. D. Gaukhberg. Surface tension of salt solutions. *Russ. J. App. Chem*, 66(6):1139; Continued in 66 (7), 1315 and 66 (8), 1473., 1993.

[441] P. K. Weissenborn and R. J. Pugh. Surface tension of aqueous solutions of electrolytes: Relationship with ion hydration, oxygen solubility, and bubble coalescence. *J. Colloid Interface Sci.*, 184(2):550–563, 1996.

[442] Y. Marcus. Surface tension of aqueous electrolytes and ions. *J. Chem. Eng. Data*, 55(9): 3641–3644, 2010.

[443] B. Hess, C. Kutzner, D. van der Spoel, and E. Lindahl. GROMACS 4: Algorithms for highly efficient, load-balanced, and scalable molecular simulation. *J. Chem. Theory Comput.*, 4(3): 435–447, 2008.

[444] L. X. Dang. Mechanism and thermodynamics of ion selectivity in aqueous solutions of 18-Crown-6 Ether: A molecular dynamics study. *J. Am. Chem. Soc.*, 117(26):6954–6960, 1995.

[445] M. Boström, D. R. M. Williams, and B. W. Ninham. Surface tension of electrolytes: Specific ion effects explained by dispersion forces. *Langmuir*, 17(15):4475–4478, 2001.

[446] J. N. Brönsted. Studies on solubility. IV. The principle of the specific interaction of ions. *J. Am. Chem. Soc.*, 44(5):877–898, 1922.

[447] J. N. Brönsted. The individual thermodynamic properties of ions. *J. Am. Chem. Soc.*, 45(12): 2898–2910, 1923.

[448] A. W. Morris and J. P. Riley. The bromide/chlorinity and sulphate/chlorinity ratio in sea water. *Deep Sea Res. Oceanogr. Abstr.*, 13(4):699–705, 1966.

[449] B. S. Vo and D. C. Shallcross. Modeling solution phase behavior in multicomponent ion exchange equilibria involving H+, Na+, K+, Mg2+, and Ca2+ ions. *J. Chem. Eng. Data*, 50 (6):1995–2002, 2005.

[450] Q. Du, E. Freysz, and Y. R. Shen. Vibrational spectra of water molecules at quartz/water interfaces. *Phys. Rev. Lett.*, 72(2):238–241, 1994.

[451] G. L. Richmond. Molecular bonding and interactions at aqueous surfaces as probed by vibrational sum frequency spectroscopy. *Chem. Rev.*, 102(8):2693–2724, 2002.

[452] G. Kim, M. Gurau, J. Kim, and P. S. Cremer. Investigations of lysozyme adsorption at the air/water and quartz/water interfaces by vibrational sum frequency spectroscopy. *Langmuir*, 18(7):2807–2811, 2002.

[453] M. A. Knackstedt and B. W. Ninham. Correlations and thermodynamic coefficients in dilute asymmetric electrolyte solutions. *J. Phys. Chem.*, 100(4):1330–1335, 1996.

[454] L. Guldbrand and B. Jönsson. Electrical double layer forces. A Monte Carlo study. *J. Chem. Phys.*, 80(5):2221, 1984.

[455] R. Buchner, S. G. Capewell, G. Hefter, and P. M. May. Ion-pair and solvent relaxation processes in aqueous Na2SO4 solutions. *J. Phys. Chem. B*, 103(7):1185–1192, 1999.

[456] A. Eiberweiser and R. Buchner. Ion-pair or ion-cloud relaxation? On the origin of small-amplitude low-frequency relaxations of weakly associating aqueous electrolytes. *J. Mol. Liq.*, 176:52–59, 2012.

[457] W. Wachter, W. Kunz, R. Buchner, and G. Hefter. Is there an anionic Hofmeister effect on water dynamics? Dielectric spectroscopy of aqueous solutions of NaBr, NaI, NaNO3, NaClO4, and NaSCN. *J. Phys. Chem. A*, 109(39):8675–8683, 2005.

[458] M. M. Santos, J. R. F. Guedes de Carvalho, and R. A. Guedes do Carvalho. Determination of the association constant of NaSO4- with the sodium-selective electrode. *J. Solution Chem.*, 4(1):25–29, 1975.

[459] P. Luts, J. L. C. Vanhees, J. H. E Yperman, J. M. A. Mullens, and L. C. van Poucke. Potentiometric investigation of NaSO4- ion pair formation in NaClO4 medium. *J. Solution Chem.*, 21(4):375–382, 1992.

[460] U. Essmann, L. Perera, M. L. Berkowitz, T. Darden, H. Lee, and L. G. Pedersen. A smooth particle mesh Ewald method. *J. Chem. Phys.*, 103(19):8577–8593, 1995.

[461] S. I. Mamatkulov, K. F. Rinne, R. Buchner, R. R. Netz, and D. J. Bonthuis. Water-separated ion pairs cause the slow dielectric mode of magnesium sulfate solutions. *J. Chem. Phys.*, 148 (22):222812, 2018.

[462] W. R. Cannon, B. M. Pettitt, and J. A. McCammon. Sulfate anion in water: Model structural, thermodynamic, and dynamic properties. *J. Phys. Chem.*, 98(24):6225–6230, 1994.

[463] E. D. Risberg, L. Eriksson, J. Mink, L. G. M. Pettersson, M. Y. Skripkin, and M. Sandström. Sulfur X-ray absorption and vibrational spectroscopic study of sulfur dioxide , sulfite , and sulfonate solutions and of the Substituted sulfonate ions X3CSO3- (X=H, Cl, s). *Inorg. Chem.*, 46(20):8332–8348, 2007.

[464] T.-Y. Lin and S. N. Timasheff. Why do some organisms use a urea-methylamine mixture as osmolyte? Thermodynamic compensation of urea and trimethylamine N-oxide interactions with protein. *Biochemistry*, 33(42):12695–12701, 1994.

[465] A. Wang and D. W. Bolen. A naturally occurring protective system in urea-rich cells: mechanism of osmolyte protection of proteins against urea denaturation. *Biochemistry*, 36 (30):9101–9108, 1997.

[466] C. C. Mello and D. Barrick. Measuring the stability of partly folded proteins using TMAO. *Protein Sci.*, 12(7):1522–1529, 2003.

[467] L. M. F. Holthauzen and D. W. Bolen. Mixed osmolytes: The degree to which one osmolyteaffects the protein stabilizing ability of another. *Protein Sci.*, 16(2):293–298, 2006.

[468] S. Bharadwaj and N. F. A. van der Vegt. Does preferential adsorption drive cononsolvency? *Macromolecules*, 52(11):4131–4138, 2019.

[469] L. B. Sagle, Y. Zhang, V. A. Litosh, X. Chen, Y. Cho, and P. S. Cremer. Investigating the hydrogen-bonding model of urea denaturation. *J. Am. Chem. Soc.*, 131(26):9304–9310, 2009.

[470] J. Wang, B. Liu, G. Ru, J. Bai, and J. Feng. Effect of urea on phase transition of poly(N-isopropylacrylamide) and poly(N,N-diethylacrylamide) hydrogels: A clue for urea-induced denaturation. *Macromolecules*, 49(1):234–243, 2016.

[471] D. Mukherji, C. M. Marques, and K. Kremer. Polymer collapse in miscible good solvents is a generic phenomenon driven by preferential adsorption. *Nat. Commun.*, 5:4882, 2014.

[472] F. Rodríguez-Ropero, T. Hajari, and N. F. A. van der Vegt. Mechanism of polymer collapse in miscible good solvents. *J. Phys. Chem. B*, 119(51):15780–15788, 2015.

[473] C. Dalgicdir, F. Rodríguez-Ropero, and N. F. A. van der Vegt. Computational calorimetry of PNIPAM cononsolvency in water/methanol mixtures. *J. Phys. Chem. B*, 121(32):7741–7748, 2017.

[474] S. Bharadwaj, P. B. Sunil Kumar, S. Komura, and A. P. Deshpande. Kosmotropic effect leads to LCST decrease in thermoresponsive polymer solutions. *J. Chem. Phys.*, 148(8):084903, 2018.

[475] J. Wang, N. Wang, B. Liu, J. Bai, P. Gong, G. Ru, and J. Feng. Preferential adsorption of the additive is not a prerequisite for cononsolvency in water-rich mixtures. *Phys. Chem. Chem. Phys.*, 19(44):30097–30106, 2017.

[476] H. Yamauchi and Y. Maeda. LCST and UCST behavior of poly(N-isopropylacrylamide) in DMSO/water mixed solvents studied by IR and micro-Raman spectroscopy. *J. Phys. Chem. B*, 111(45):12964–12968, 2007.

[477] S. Cozzolino, R. Oliva, G. Graziano, and P. Del Vecchio. Counteraction of denaturant-induced protein unfolding is a general property of stabilizing agents. *Phys. Chem. Chem. Phys.*, 20(46):29389–29398, 2018.

[478] N. F. A. van der Vegt, D. Trzesniak, B. Kasumaj, and W. F. van Gunsteren. Energy–entropy compensation in the transfer of nonpolar solutes from water to cosolvent/water mixtures. *ChemPhysChem*, 5(1):144–147, 2004.

[479] M. Dijkstra, D. Frenkel, and J. P. Hansen. Phase separation in binary hard-core mixtures. *J. Chem. Phys.*, 101(4):3179–3189, 1994.

[480] S. K. Schnell, P. Englebienne, J.-M. Simon, P. Krüger, S. P. Balaji, S. Kjelstrup, D. Bedeaux, A. Bardow, and T. J. H. Vlugt. How to apply the Kirkwood–Buff theory to individual species in salt solutions. *Chem. Phys. Lett.*, 582:154–157, 2013.

[481] P. H. Yancey, M. E. Clark, S. C. Hand, R. D. Bowlus, and G. N. Somero. Living with water stress: Evolution of osmolyte systems. *Science*, 217(4566):1214–1222, 1982.

[482] D. R. Canchi and A. E. García. Cosolvent effects on protein stability. *Annu. Rev. Phys. Chem.*, 64:273–293, 2013.

[483] P. Ganguly, T. Hajari, J-E. Shea, and N. F. A. van der Vegt. Mutual exclusion of urea and trimethylamine N-oxide from amino acids in mixed solvent environment. *J. Phys. Chem. Lett.*, 6(4):581–585, 2015.

[484] P. Ganguly, P. Boserman, N. F. A. van der Vegt, and J.-E. Shea. Trimethylamine N-oxide counteracts urea denaturation by inhibiting protein-urea preferential interaction. *J. Am. Chem. Soc.*, 140(1):483–492, 2018.

[485] J. Hunger, N. Ottosson, K. Mazur, M. Bonn, and H. J. Bakker. Water-mediated interactions between trimethylamine-N-oxide and urea. *Phys. Chem. Chem. Phys.*, 17(1):298–306, 2015.

[486] W. J. Xie, S. Cha, J. Hunger, W. J. Xie, S. Cha, T. Ohto, W. Mizukami, and Y. Mao. Large hydrogen-bond mismatch between TMAO and urea promotes their hydrophobic association. *Chem*, 4(11):2615–2627, 2018.

[487] K. J. Tielrooij, N. Garcia-Araez, M. Bonn, and H. J. Bakker. Cooperativity in ion hydration. *Science*, 328(5981):1006–1009, 2010.

[488] B. J. Finlayson-Pitts. Reactions at surfaces in the atmosphere: Integration of experiments and theory as necessary (but not necessarily sufficient) for predicting the physical chemistry of aerosols. *Phys. Chem. Chem. Phys.*, 11(36):7760–7779, 2009.

[489] P. Perera, M. Wyche, Y. Loethen, and D. Ben-Amotz. Solute-induced perturbations of solvent-shell molecules observed using multivariate Raman curve resolution. *J. Am. Chem. Soc.*, 130(14):4576–4577, 2008.

[490] K. Mochizuki and D. Ben-Amotz. Hydration-shell transformation of thermosensitive aqueous polymers. *J. Phys. Chem. Lett.*, 8(7):1360–1364, 2017.

[491] N. Gomopoulos, C. Lütgebaucks, Q. Sun, C. Macias-Romero, and S. Roke. Label-free second harmonic and hyper rayleigh scattering with high efficiency. *Opt. Express*, 21(1):815–821, 2013.

[492] K. S. Pitzer. Thermodynamics of electrolytes. I. Theoretical basis and general equations. *J. Phys. Chem.*, 77(2):268–277, 1973.

[493] M. Kohagen, E. Pluhařová, P. E. Mason, and P. Jungwirth. Exploring ion–ion interactions in aqueous solutions by a combination of molecular dynamics and neutron scattering. *J. Phys. Chem. Lett.*, 6(9):1563–1567, 2015.

[494] J. C. Rasaiah and H. L. Friedman. Integral equation methods in the computation of equilibrium properties of ionic solutions. *J. Chem. Phys.*, 48(6):2742–2752, 1968.

[495] Y. Luo, W. Jiang, H. Yu, A. D. MacKerell Jr., and B. Roux. Simulation study of ion pairing in concentrated aqueous salt solutions with a polarizable force field. *Faraday Discuss.*, 160: 135–149, 2013.

[496] I. Kalcher and J. Dzubiella. Structure-thermodynamics relation of electrolyte solutions. *J. Chem. Phys.*, 130(13):134507, 2009.

[497] I. S. Joung and T. E. Cheatham. Molecular dynamics simulations of the dynamic and energetic properties of alkali and halide ions using water-model-specific ion parameters. *J. Phys. Chem. B*, 113(40):13279–13290, 2009.

[498] Y. Marcus and G. Hefter. Ion pairing. *Chem. Rev.*, 106(11):4585–4621, 2006.

[499] H. J. C. Berendsen, D. van der Spoel, and R. van Drunen. GROMACS: A message-passing parallel molecular dynamics implementation. *Comput. Phys. Commun.*, 91(1-3):43–56, 1995.

[500] C. I. Bayly, P. Cieplak, W. Cornell, and P. A. Kollman. A well-behaved electrostatic potential based method using charge restraints for deriving atomic charges: The RESP model. *J. Phys. Chem.*, 97(40):10269–10280, 1993.

[501] E. N. Brodskaya, A. P. Lyubartsev, and A. Laaksonen. Investigation of water clusters containing OH- and H3O+ ions in atmospheric conditions. A molecular dynamics simulation study. *J. Phys. Chem. B*, 106(25):6479–6487, 2002.

[502] E. N. Brodskaya, A. V. Egorov, A. P. Lyubartsev, and A. Laaksonen. Computer modeling of melting of ionized ice microcrystals. *J. Chem. Phys.*, 119(19):10237–10246, 2003.

[503] R. Zangi and J. B. F. N. Engberts. Physisorption of hydroxide ions from aqueous solution to a hydrophobic surface. *J. Am. Chem. Soc.*, 127(7):2272–2276, 2005.

[504] M. Bonomi, D. Branduardi, G. Bussi, C. Camilloni, D. Provasi, P. Raiteri, D. Donadio, F. Marinelli, F. Pietrucci, R. A. Broglia, and M. Parrinello. PLUMED: A portable plugin for free-energy calculations with molecular dynamics. *Comput. Phys. Commun.*, 180(10): 1961–1972, 2009.

[505] G. Scatchard and R. C. Breckenridge. Isotonic solutions. II. The chemical potential of water in aqueous solutions of potassium and sodium phosphates and arsenates at 25°. *J. Phys. Chem.*, 58(8):596–602, 1954.

[506] D. R. Lide. *Handbook of chemistry and physics*. CRC Press, Boca Raton, FL, 85 edition, 2004.

[507] P. Ganguly, P. Schravendijk, B. Hess, and N. F. A. van der Vegt. Ion pairing in aqueous electrolyte solutions with biologically relevant anions. *J. Phys. Chem. B*, 115(13):3734–3739, 2011.

[508] J. A. Dean. *Lange's handbook of chemistry*. McGraw-Hill, New York, 1992.

[509] P. E. Mason, J. M. Cruickshank, G. W. Neilson, and P. Buchanan. Neutron scattering studies on the hydration of phosphate ions in aqueous solutions of K3PO4, K2HPO4 and KH2PO4. *Phys. Chem. Chem. Phys.*, 5(20):4686–4690, 2003.

[510] W. W. Rudolph and G. Irmer. Raman and infrared spectroscopic investigations on aqueous alkali metal phosphate solutions and density functional theory calculations of phosphate – water clusters. *Appl. Spectrosc.*, 61(12):1312–1327, 2007.

[511] C. C. Pye and W. W. Rudolph. An ab initio, infrared, and Raman investigation of phosphate ion hydration. *J. Phys. Chem. A*, 107(41):8746–8755, 2003.

[512] C. Ebner, U. Onthong, and M. Probst. Computational study of hydrated phosphate anions. *J. Mol. Liq.*, 118(1-3):15–25, 2005.

[513] G. A. Krestov. *Thermodynamics of solvation: Solution and dissolution, ions and solvents, strucutres and energetics*. Ellis Horwood Ltd, New York, 1991.

[514] J. Dzubiella, M. Fyta, D. Horinek, I. Kalcher, R. R. Netz, and N. Schwierz. Ion-specificity: From solvation thermodynamics to molecular simulations and back. In Werner Kunz, editor, *Specif. Ion Eff.*, pages 231–265. World Scientific Publishing Co. Pte. Ltd., Singapore, 2010.

[515] A. B. Pribil, T. S. Hofer, B. R. Randolf, and B. M. Rode. Structure and dynamics of phosphate ion in aqueous solution: An ab initio QMCF MD study. *J. Comput. Chem.*, 29(14):2330–2334, 2008.

[516] F. Rodríguez-Ropero and N. F. A. van der Vegt. Direct osmolyte–macromolecule interactions confer entropic stability to folded states. *J. Phys. Chem. B*, 118(26):7327–7334, 2014.

[517] F. Rodríguez-Ropero and N. F. A. van der Vegt. On the urea induced hydrophobic collapse of a water soluble polymer. *Phys. Chem. Chem. Phys.*, 17(13):8491–8498, 2015.

[518] P. Ganguly, N. F. A. van der Vegt, and J.-E. Shea. Hydrophobic association in mixed urea–TMAO solutions. *J. Phys. Chem. Lett.*, 7(15):3052–3059, 2016.

[519] R. Buchner and G. Hefter. Interactions and dynamics in electrolyte solutions by dielectric spectroscopy. *Phys. Chem. Chem. Phys.*, 11(40):8984, 2009.